CENTRO INTERNACIONAL DE ESTUDOS
DE DOUTORAMENTO E AVANZADOS
DA USC (CIEDUS)

TESE DE DOUTORAMENTO

Modeling and Numerical Methods for the Study of Nonlinear Electromagnetic Problems

Marta Piñeiro Peón

ESCOLA DE DOUTORAMENTO INTERNACIONAL EN CIENCIAS E TECNOLOXÍA

PROGRAMA DE DOUTORAMENTO EN MÉTODOS MATEMÁTICOS E SIMULACIÓN NUMÉRICA EN ENXEÑARÍA E CIENCIAS APLICADAS

SANTIAGO DE COMPOSTELA

2018

USC
UNIVERSIDADE
DE SANTIAGO
DE COMPOSTELA

DECLARACIÓN DA AUTORA DA TESE

Modelling and Numerical Methods for the Study of Nonlinear Electromagnetic Problems

Dna. Marta Piñeiro Peón

Presento miña tese, seguindo o procedemento adecuado ao Regulamento, e declaro que:

A tese abarca os resultados da elaboración do meu traballo.

2) No seu caso, na tese se fai referencia as colaboracións que tivo este traballo.
3) A tese é a versión definitiva presentada para a súa defensa e coincide ca versión enviada en formato electrónico.
4) Confirmo que a tese non incorre en ningún tipo de plaxio de outros autores nin de traballos presentados por min para a obtención de outros títulos.

En Santiago de Compostela, 10 de abril de 2018

USC
UNIVERSIDADE
DE SANTIAGO
DE COMPOSTELA

AUTORIZACIÓN DA DIRECTORA DA TESE

Modelling and Numerical Methods for the Study of Nonlinear Electromagnetic Problems

Dna. María del Pilar Salgado Rodríguez

INFORMA:

Que a presente tese correspóndese co traballo realizado por Dna. ***Marta Piñeiro Peón****, baixo a miña dirección, e autorizo a súa presentación, considerando que reúne os requisitos esixidos no Regulamento de Estudos de Doutoramento da USC, e que como directora desta non incorre nas causas de abstención establecidas na Lei 40/2015.*

En Santiago de Compostela, 10 de abril de 2018

USC
UNIVERSIDADE
DE SANTIAGO
DE COMPOSTELA

USC
UNIVERSIDADE
DE SANTIAGO
DE COMPOSTELA

USC
UNIVERSIDADE
DE SANTIAGO
DE COMPOSTELA

Contents

USC
UNIVERSIDADE
DE SANTIAGO
DE COMPOSTELA

Preface

The purpose of this thesis is the mathematical study and numerical solution of a range of problems that arise in low-frequency electromagnetics, and their application to the simulation of industrial processes. More precisely, we deal with both eddy current and magnetostatic problems, sometimes coupling the distributed formulation (that is, in terms of partial differential equations) with a lumped one (i.e., in terms of ordinary differential equations) modelling electrical circuits. Our study is motivated by the need of characterizing, through mathematical modelling and numerical simulation, the electromagnetic phenomena that take place in several industrial processes, such as the magnetization and demagnetization of ferromagnetic pieces, induction heating or the operation of electrical machines, in order to be able to perform a subsequent optimization and optimal control.

This memoir is divided into two differentiated parts. In the first one, contributions are made to the study and numerical solution of eddy current models in three-dimensional and axisymmetric domains, considering both linear and nonlinear magnetic materials. In the second part, we approach the modelling and optimization of electrical machines in two-dimensional domains from multiple perspectives. In both cases we will face challenges related to the development of new models and algorithms, together with the mathematical and numerical analysis of partial differential equation problems that provide theoretical support to numerical techniques already present in the literature. We deal with these challenges after performing a review on the state of art of the models, which are detailed in each chapter separately. In what follows, we briefly describe the problems we will study in both parts, together with the organization of the memoir.

Part I

The eddy current model is obtained from the full Maxwell's system of equations by neglecting the displacement currents in Ampère's law. This problem arises very often in the numerical simulation of industrial processes: induction heating, non-destructive testing, electromagnetic forming, magnetic levitation …just to name a few. As a consequence, it has been subjected to thorough study during the last decades, mostly in the linear case (see, for example, [7, 102]). However, there have also been important advances in the mathematical and numerical analysis of transient nonlinear models, some of them even incorporating hysteresis effects (see, for instance, [107] and references therein).

In linear magnetic media, where the magnetic flux and the magnetic intensity fields are pro-

portional to each other, problems can be studied in the harmonic regime when the sources are sinusoidal. This is because, in this case, Maxwell's equations preserve this dependence with respect to time for all electromagnetic fields. In spite of being apparently simple, this linear model has given rise to a wide range of different formulations in the three-dimensional case (see, for instance, [7] for a quite comprehensive review). A particular case that has drawn the attention of the scientific community in the last years, and on which we will focus, is the one having conductors that are not strictly contained in the geometric domain, being often referred to as eddy current problem with *electric ports*. In particular, this model brings the possibility of coupling the distributed eddy current formulation with a lumped one modelling an electrical circuit managing the current supply.

The different strategies to formulate the harmonic eddy current problem arise from the desire of solving the problem in the most general topological setting at the lowest computational cost in terms of degrees of freedom. In this context, we will study the so-called $\boldsymbol{T}, \phi - \phi$ formulation, which combines a vector potential $\boldsymbol{T}$, defined only in the conducting domain, with a scalar potential ϕ supported in the whole domain. Moreover, the numerical discretization will be based on the finite element method; in particular, we will use edge elements for variable $\boldsymbol{T}$ and standard Lagrange elements for ϕ. This kind of formulation has been widely used by electrical engineers and is one of the most used in commercial software for the solution of three-dimensional eddy current problems. However, the existing literature related to its mathematical analysis in both the continuous and discrete cases is comparatively limited, and therefore it offers challenges from the mathematical and numerical analysis point of view.

Therefore, in Chapter 1, we will provide a theoretical support for the harmonic $\boldsymbol{T}, \phi - \phi$ formulation in bounded domains with electric ports. The sources will be given in terms of currents or voltage drops. Moreover, we will analyze two versions of this formulation, depending on the consideration or not of a gauge condition on the vector potential $\boldsymbol{T}$.

The results for the ungauged version of the $\boldsymbol{T}, \phi - \phi$ formulation have been published in

[26] A. Bermúdez, M. Piñeiro, R. Rodríguez, and P. Salgado. Analysis of an ungauged T, ϕ–ϕ formulation of the eddy current problem with currents and voltage excitations. *ESAIM: Math. Model. Numer. Anal.*, 51(6):2487–2509, 2017.

On the other hand, the occurrence either of sources that are not harmonic functions of time or of materials having a nonlinear magnetic behaviour, require the use of genuinely transient models. Additionally, the inclusion in the model of hysteresis effects turns out to be unavoidable for some industrial applications, such as the demagnetization of pieces. This fact leads to an extra difficulty, since under these circumstances the magnetic flux in the ferromagnetic pieces not only depends nonlinearly on the present magnetic intensity in it, but it depends also on its magnetic history.

There exist several methods to model the hysteresis phenomenon, such as the Stoner-Wohlfarth, the Jiles-Atherton, the Globus and the Preisach models (see, for instance, [68]). All of these models are halfway between simplifying the relation between the magnetic flux density and the magnetic field intensity to an univaluate function, and the micromagnetic methods, that consider the process at a microscopic level. In particular, it is usual to assume that processes are rate-

independent, which means that the magnetic flux does not depend on the speed of change of the magnetic field intensity with time.

Chapter 2 deals with the modelling and simulation of magnetization and demagnetization processes. The research on this topic was initiated in the master's thesis and was motivated by an INNTERCONNECTA research project developed for the company CIE-Galfor. In the framework of the PhD thesis, the main focus is to develop a numerical tool to compute the magnetic fields distribution during a non-destructive test called *magnetic particle inspection* (MPI), whose purpose is to detect near-surface cracks in ferromagnetic pieces. In this framework, a software simulating the whole process in the case of cylindrical pieces was created, including also the final demagnetization step. For this purpose, we will use the classical scalar Preisach model, which was first described in [84]. Moreover, we will restrict ourselves to the scalar case, in which both the magnetic flux and the magnetic field intensity have only one non-null component.

The main results appearing in this chapter have been published in

[20] A. Bermúdez, D. Gómez, M. Piñeiro, P. Salgado, and P. Venegas. Numerical simulation of magnetization and demagnetization processes. *IEEE Trans. Magn.*, 53(12):1–6, 2017.

Part II

In the last decades, in parallel with the fast development of computing capabilities, great efforts have been made to obtain realistic numerical models for several industrial processes. The solution to these models give very useful insights on the physical phenomena involved in the associated applications, leading to a better understanding and, most of the times, to an improvement of such processes. In particular, recent advances have resulted in efficient numerical solutions for electrical machines (for example, see [94, 97]), beyond the scope of the classical analytical methods, which are limited to homogeneous, linear and steady-state frameworks due to its magnetic circuit approach. In this way, numerical simulation plays an important role to optimize the design and operating conditions of electrical machines, preventing the building of unnecessary prototypes and allowing savings both in their construction and operation.

In the second part of the memoir, dedicated to the study of alternating current (AC) electrical motors, we focus on radial flux machines, which are characterized by the current density being parallel to the rotation axis, and thus having magnetic vector fields that live in the planes orthogonal to this direction. These machines can be classified in several ways, one of the most common being the consideration of two categories: synchronous and induction motors. The first group contains those devices whose rotation speed is related to the angular frequency of the input source in terms of its number of poles, and we focus on the subgroup having permanent magnets in either rotor or stator. In opposition, in induction machines, the magnetic field in rotor or stator is induced by the one in the other part, which contains the coils through which the current is externally supplied. This kind of motors have a rotation rate that is lower than the synchronous speed, the so-called *slip* being the quantity that defines the difference between them (see [35, 55]).

In synchronous machines, due to the fact that the imposed source current goes through stranded

conductors parallel to the rotation axis and that the ferromagnetic cores are laminated orthogonally to this direction, it is reasonable to assume that the electromagnetic fields can be approximated with a two-dimensional model defined in a cross-section transversal to the device. Moreover, the sources of the problem are the remanent flux density in permanent magnets, defined by vectors that lie in these cross-sections, and either the current or the voltage drop in conductors. Therefore, to model these machines, we will use a distributed transient magnetic formulation for the active zone, coupled with circuit equations relating currents and voltage drops in conductors.

In this way, in Chapter 3, we give a first step towards the analysis of the genuine physical problem, as we do not consider the motion of the machine, what would lead to a much more difficult problem. Furthermore, we will restrict ourselves to the case in which the sources in conductors are only given in terms of the potential drops along them. Thus, we will perform the mathematical and numerical analysis of an integro-differential problem coupling an elliptic partial differential equation with a circuit equation linking currents and voltage drops. Thus, the problem is as a nonlinear system of implicit ordinary differential equations in terms of the currents traversing the coils as unknowns. For the discretization, a backward-Euler scheme has been combined with a finite element method for the distributed part.

The results appearing in this chapter have been sent for publication

[27] A. Bermúdez, M. Piñeiro, and P. Salgado. Mathematical and Numerical Analysis of a Transient Magnetic Model with Voltage Drop Excitations. (Submitted).

Optimization and optimal control of electromagnetic industrial processes has been an active subject of study in the last few years, and, in particular, for electrical machines (see, for instance, [50, 90] and references therein). Indeed, this field offers great opportunities in the design of industrial processes, as it automatically retrieves the best option in terms of the chosen objectives and under the given restrictions. Therefore, it has been implemented for a wide range of applications within the electrical machine framework, such as the optimization design, minimization of losses, control of circuit variables for performance improvement, optimal speed control, …

In Chapter 4, we study an optimal control problem defined on a permanent magnet machine. In this occasion, we will take into account the rotation of the machine, but sources in the stator will be given in terms of the currents through the stranded conductors. As a consequence, we will not have circuit equations coupled to the distributed model, and we will have a transient magnetic model with time appearing as a parameter. The functional cost to minimize is the total power loss in the stator coils and two kind of restrictions are imposed: box-type constraints on the amplitudes on the stator currents and an inequality state constraint in order to guarantee that the resulting machine generates a large enough torque. Due to the low computational cost required for the optimization process to be viable, we have decided to approximate the constitutive magnetic law in the ferromagnetic cores by a linear one. The resulting control problem is studied from the mathematical and numerical analysis point of view, and some numerical results are shown for a toy model.

This problem was developed in collaboration with Professor Fredi Tröltzsch, during two research stays at Technische Universität Berlin. Moreover, a publication containing the main

results in this chapter is being prepared.

On the other hand, in the case of induction machines, we will focus on the ones having squirrel cage rotors. In this type of motors, the input source is given in the stator, and the rotor contains a set of embedded bars that are connected to each other on the end-rings at both sides of the machine. Therefore, in opposition to the synchronous case, now we are obliged to consider the eddy currents in the rotor to be able to model the device appropriately. However, if we consider a more involved circuit characterizing the whole squirrel-cage, in the distributed part we can still consider a two-dimensional model defined in a cross-section transversal to the device. Accordingly, the numerical simulation of these machines by using finite element methods involves the solution of a nonlinear system of partial differential equations coupled with circuit equations. This solution generally requires supplying initial conditions that, if chosen far from the physical ones, a very long CPU time is needed to reach the steady-state solution, which is the main goal in most cases.

Thus, in Chapter 5 we will present a novel and efficient methodology to reduce the transient part in finite element simulations, so that the steady-state regime is reached in the shortest time possible. For this purpose, we will develop a method that seeks good approximations for suitable initial currents in the rotor bars of a squirrel cage induction motor with sources in the stator given in terms of periodic currents. These initial currents are the result of solving an overdetermined problem with two unknowns in the least-square sense. The numerical results show important computational savings to reach the steady-state, in comparison with starting with null initial conditions, what validates the efficiency of the procedure.

The results appearing in this chapter have been sent for publication

[18] A. Bermúdez, D. Gómez, M. Piñeiro, and P. Salgado. Numerical Method for Accelerating the Steady State in an Induction Machine. (Submitted).

Additionally, we have applied for a Spanish patent

[19] A. Bermúdez, D. Gómez, M. Piñeiro, and P. Salgado. Procedimiento y producto de programa informático para acelerar el cálculo del estado estacionario de un motor de inducción de jaula de ardilla, Spanish Patent (request number P201830228).

USC
UNIVERSIDADE
DE SANTIAGO
DE COMPOSTELA

Part I

Eddy Current Problems Analysis

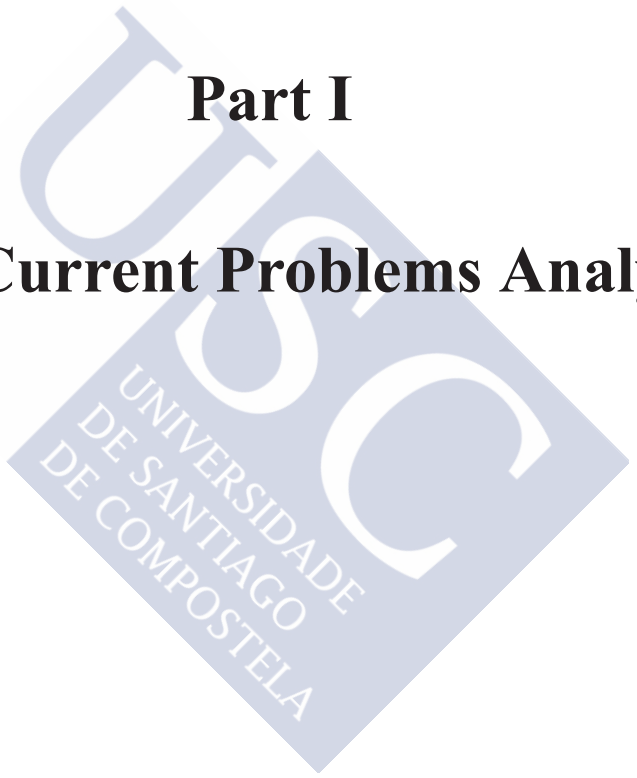

USC
UNIVERSIDADE
DE SANTIAGO
DE COMPOSTELA

Introduction

The modern theory that describes electromagnetic phenomena in the free space can be reduced to a set of four equations, known as *Maxwell's system of equations*, which reads

$$\begin{aligned} -\mu_0\varepsilon_0\frac{\partial \boldsymbol{E}}{\partial t} + \mathbf{curl}\,\boldsymbol{B} &= \mu_0\boldsymbol{J}, && \text{(Ampère's Law)}\\ \frac{\partial \boldsymbol{B}}{\partial t} + \mathbf{curl}\,\boldsymbol{E} &= \mathbf{0}, && \text{(Faraday's Law)}\\ \operatorname{div}\boldsymbol{B} &= 0, && \text{(Gauss' Magnetic Law)}\\ \varepsilon_0 \operatorname{div}\boldsymbol{E} &= \rho, && \text{(Gauss' Electric Law)} \end{aligned}$$

where we have used standard notation in electromagnetism: $\boldsymbol{E}$ is the electric intensity field, $\boldsymbol{B}$ is the magnetic flux density, ρ is the volume electric charge density, $\boldsymbol{J}$ is the current density, and μ_0, ε_0 are the magnetic permeability and the electric permittivity of the vacuum, respectively (see [53]). These equations are valid in the whole space $\mathbb{R}^3$ and for all time $t > 0$. The SI coherent units of the above fields, along with the values of constants μ_0 and ε_0, are given in Table I.1.

Furthermore, the so-called *continuity equation*, relating ρ and $\boldsymbol{J}$, can be deduced from the above system, reading

$$\frac{\partial \rho}{\partial t} + \operatorname{div}\boldsymbol{J} = 0.$$

In material regions, the development of physical processes essentially depends on their properties. In the framework of electromagnetic field theory, matter is considered as a continuum medium whose properties are described in terms of formal qualities such as the *electric permittivity*, the *magnetic permeability* and *electrical conductivity*, which are described below. Firstly, we detail *Maxwell's system of equations* in material regions, which reads

$$-\frac{\partial \boldsymbol{D}}{\partial t} + \mathbf{curl}\,\boldsymbol{H} = \boldsymbol{J}, \tag{I.1}$$

$$\frac{\partial \boldsymbol{B}}{\partial t} + \mathbf{curl}\,\boldsymbol{E} = \mathbf{0}, \tag{I.2}$$

$$\operatorname{div}\boldsymbol{B} = 0, \tag{I.3}$$

$$\operatorname{div}\boldsymbol{D} = \rho, \tag{I.4}$$

where $\boldsymbol{D}$ is the electric displacement and $\boldsymbol{H}$ is the magnetic intensity field. Again, the SI coherent units of the involved fields are given in Table I.1.

Maxwell's system of equations has to be completed with some complementary equations relating fundamental with auxiliary fields, that is, $\boldsymbol{E}$ and $\boldsymbol{B}$ with $\boldsymbol{D}$ and $\boldsymbol{H}$, respectively. Generally, the equations describing these relations are called *constitutive laws*, and read, in the most simple case (that is, for homogeneous, linear, isotropic media),

$$\boldsymbol{D} = \varepsilon\boldsymbol{E}, \tag{I.5}$$

$$\boldsymbol{B} = \mu\boldsymbol{H}, \tag{I.6}$$

Symbol	Units	Value
$\boldsymbol{E}$	N/C	
$\boldsymbol{D}$	C/m^2	
$\boldsymbol{B}$	T	
$\boldsymbol{H}$	A/m	
ρ	C/m^3	
$\boldsymbol{J}$	A/m^2	
μ_0	H/m	$4\pi \times 10^{-7}$
ε_0	C^2/(N·m^2)	$1/(36\pi \times 10^9)$

Table I.1: Electromagnetic units.

where ε and μ are constants called *electric permittivity* and *magnetic permeability*, respectively, having the same units as the corresponding constants in free space.

There are situations in which the hypothesis of materials being homogeneous, linear and isotropic is not valid, and therefore constitutive laws are not given by (I.5)–(I.6). Throughout the document, we will assume that the electric permittivity is given by a constant in each material region, but this will not be the case for the relation between $\boldsymbol{B}$ and $\boldsymbol{H}$. In general, concerning the magnetic constitutive relation, materials can be described as:

- Inhomogeneous. In opposition to homogeneous materials, the magnetic permeability μ depends on the space variable.

- Anisotropic. In opposition to isotropic materials, $\boldsymbol{H}$ and $\boldsymbol{B}$ are not parallel to each other, and therefore the magnetic permeability is represented by a second-order symmetric tensor. This happens when the medium presents different electromagnetic properties in each space direction.

- Nonlinear. In opposition to linear materials, $\boldsymbol{B}$ and $\boldsymbol{H}$ are related to each other by a magnetic constitutive law of the form $\boldsymbol{B} = \boldsymbol{\mathcal{B}}(\boldsymbol{H})$, where $\boldsymbol{\mathcal{B}}$ is, in general, a nonlinear vector law. This case comprises ferromagnetic materials, which show the hysteresis phenomenon, due to which the magnetic flux density $\boldsymbol{B}$ does not only depend on the magnetic intensity field at present time, but also on its past values. Moreover, the magnetic constitutive law for anhysteretic materials (that is, materials not presenting hysteresis) can be usually written as $\boldsymbol{B} = \mu(|\boldsymbol{H}|)\boldsymbol{H}$, with the magnetic permeability μ depending nonlinearly on the modulus of the magnetic intensity field.

Another relation is frequently added to Maxwell's equation, at the same level of the constitutive relations, linking the current density and the electric intensity field, which is known as *Ohm's law*. In the case of static media, this law reads

$$\boldsymbol{J} = \sigma \boldsymbol{E},$$

with σ the electrical conductivity, which is null in dielectrics and, in general, a nonlinear tensor depending on temperature, frequency, etc., in conductors. However, we will consider the conductivity to be a positive scalar field in conductors.

We finally notice that, since matter consists of atoms and molecules, the physical electromagnetic fields change very quickly in both space and time, due to the discrete nature of matter and to thermal oscillations. Therefore, Maxwell's equations and electromagnetic properties have to be understood as macroscopic averages of the physical ones.

In many applications, the involved physical phenomena do no require to solve the full Maxwell's system of equations, allowing us to introduce different simplified models. For instance, this happens in the case of slowly time-varying electromagnetic fields, where the displacement currents term, $\partial \boldsymbol{D}/\partial t$, can be neglected from Ampère's law (see [7]). The obtained model is known as *eddy current* or *magneto-quasistatic approximation*, and reads as follows:

$$\mathbf{curl}\, \boldsymbol{H} = \boldsymbol{J}, \tag{I.7}$$

$$\frac{\partial \boldsymbol{B}}{\partial t} + \mathbf{curl}\, \boldsymbol{E} = \boldsymbol{0}, \tag{I.8}$$

$$\operatorname{div} \boldsymbol{B} = 0. \tag{I.9}$$

We notice that, since we are not going to be interested in computing the electric field $\boldsymbol{E}$ in conductors, we have not considered equation (I.4).

It can be seen that this is a good approximation when the electromagnetic fields propagate almost instantaneously, that is, when the transmission-time is very slow with respect to the inverse of the angular frequency. Thus, these equations can be then used to model problems where the frequency is relatively low and any radiation effects can be neglected. Some authors have proved the validity of this approximation both in the hole space $\mathbb{R}^3$ and in bounded domains; see, for instance, [8] and Section 2.3 from [7]. This model is essential for the modelling and numerical simulation of several industrial processes, which include magnetization and demagnetization of ferromagnetic pieces, induction heating, electromagnetic forming, magnetic levitation, the operation of electrical machines,…

From equations (I.7) and (I.9), we can deduce the following interface conditions:

$$[\boldsymbol{H} \times \boldsymbol{n}]_{\mathcal{S}} = \boldsymbol{J}_{\mathcal{S}} \qquad \text{and} \qquad [\boldsymbol{B} \cdot \boldsymbol{n}]_{\mathcal{S}} = 0,$$

respectively, where $[\,\cdot\,]_{\mathcal{S}}$ denotes the jump across any surface $\mathcal{S}$ and $\boldsymbol{J}_{\mathcal{S}}$ is the surface current density that flows on $\mathcal{S}$. Moreover, since $\boldsymbol{J} = \boldsymbol{0}$ in dielectrics and, from (I.7), $\operatorname{div} \boldsymbol{J} = 0$, we deduce that $\boldsymbol{J} \cdot \boldsymbol{n} = 0$ on the interface between conducting and dielectric domains.

Additionally, many industrial applications involve time-periodic sources (for instance, when this source is an alternating current). In this situation, if we denote the source frequency by $f \neq 0$, and in the presence of linear isotropic materials, we could seek for time-harmonic solutions of

system (I.7)–(I.9), of the form:

$$\begin{aligned}
\boldsymbol{J}(\boldsymbol{x},t) &= \boldsymbol{\mathcal{J}}(\boldsymbol{x})\cos(\omega t+\phi) = \Re\left[\boldsymbol{\mathcal{J}}(\boldsymbol{x})e^{i\omega t}\right],\\
\boldsymbol{H}(\boldsymbol{x},t) &= \boldsymbol{\mathcal{H}}(\boldsymbol{x})\cos(\omega t+\phi) = \Re\left[\boldsymbol{\mathcal{H}}(\boldsymbol{x})e^{i\omega t}\right],\\
\boldsymbol{E}(\boldsymbol{x},t) &= \boldsymbol{\mathcal{E}}(\boldsymbol{x})\cos(\omega t+\phi) \ = \Re\left[\boldsymbol{\mathcal{E}}(\boldsymbol{x})e^{i\omega t}\right],
\end{aligned}$$

with $\omega = 2\pi f$ and $\boldsymbol{\mathcal{J}}(\boldsymbol{x}) := \boldsymbol{\mathcal{J}}(\boldsymbol{x})e^{i\phi}$, $\boldsymbol{\mathcal{E}}(\boldsymbol{x}) := \boldsymbol{\mathcal{E}}(\boldsymbol{x})e^{i\phi}$ and $\boldsymbol{\mathcal{H}}(\boldsymbol{x}) := \boldsymbol{\mathcal{H}}(\boldsymbol{x})e^{i\phi}$ complex-valued fields solution to the following time-independent system of equations:

$$\begin{aligned}
\operatorname{div}(\mu\boldsymbol{\mathcal{H}}) &= 0,\\
i\omega\mu\boldsymbol{\mathcal{H}} + \mathbf{curl}\,\boldsymbol{\mathcal{E}} &= \mathbf{0},\\
\mathbf{curl}\,\boldsymbol{\mathcal{H}} &= \boldsymbol{\mathcal{J}}.
\end{aligned}$$

We notice that the above system is usually called *time-harmonic eddy currents model* and that $\boldsymbol{\mathcal{J}}$, $\boldsymbol{\mathcal{E}}$ and $\boldsymbol{\mathcal{H}}$ are often known as *phasors* corresponding to the current density, electric intensity and magnetic intensity fields, respectively.

In this first part of the memoir, we will deal with both a time-harmonic eddy current formulation and a transient one. Firstly, in Chapter 1, we will focus on the mathematical and numerical analysis of a formulation for the time-harmonic eddy current problem in 3D bounded domains, combining a vector potential in conductors with a scalar one in the whole domain. We will restrict ourselves to the case with *electric ports*, in which sources are given on the domain boundary, either in terms of currents or voltage drops prescribed by external power generators. Then, in Chapter 2, we will address a nonlinear transient eddy current problem, including hysteresis effects, in order to perform the numerical simulation of magnetization and demagnetization processes. In this case, geometries will present cylindrical symmetry, and two main situations will be distinguished, depending on the current density living in, or being perpendicular to, the meridional section of the conducting domain. In the first case, it is usual to solve a problem defined only in the conducting part and written in terms of the magnetic field, while in the second one it is more common to use the so-called magnetic vector potential as it leads to a scalar problem (see [17, 21]).

Chapter 1

Analysis of a $\boldsymbol{T}$,ϕ–ϕ Formulation of the Eddy Current Problem with Currents and Voltage Excitations

1.1 Introduction

This chapter deals with the mathematical analysis of the so-called $\boldsymbol{T}, \phi - \phi$ formulation for solving time-harmonic eddy current problems defined in three-dimensional bounded domains containing both conducting and dielectric materials. This kind of problem often arises in electrical engineering in the numerical simulation of varied devices, such as electrical machines, metallurgical furnaces, non-destructive testing tools, etc., (see [7]). We will focus on the case in which some of the conducting subdomains are not strictly contained in the computational one, with sources given either in terms of the current intensities crossing their intersections with the outer boundary or in terms of the potential drops between them. This particular case is referred in the literature in different ways, such as the eddy current problem with *electric ports*, with *non-local boundary conditions* or *coupled with electrical circuits*. Thanks to its widespread applicability, this problem has been subjected to thorough study during the last decades, by using different unknowns and formulations. We refer the reader to Chapter 8 of [7], where we can find a quite comprehensive review of the most relevant formulations, along with the main results from a mathematical and numerical point of view. Additionally, we can cite [4, 23], more recent publications that analyse other relevant formulations of the eddy current problem with electric ports.

In this chapter we will focus on the well-known $\boldsymbol{T}, \phi - \phi$ formulation, which combines a vector potential $\boldsymbol{T}$, defined only in the conducting domain and discretised using edge elements, with a scalar potential ϕ supported in the whole domain and discretised by nodal elements. One great advantage of this methodology is the low computational effort needed for its solution because the only vector unknown, $\boldsymbol{T}$, has to be computed only in conductors, where there are generally far fewer degrees of freedom. Therefore, this kind of formulation is one of the most used in

commercial software for the solution of three-dimensional eddy current problems (e.g., Altair Flux® or ANSYS Maxwell®).

While the $\boldsymbol{T}, \phi - \phi$ formulation has been widely used by electrical engineers (see, for instance, [32, 34, 74, 108]), the existing literature related to its mathematical analysis in both the continuous and discrete cases is comparatively limited. In particular, the theoretical analysis usually covers a formulation with a gauge condition for the electrical vector potential and uses a nodal finite element for its approximation. In this framework, we refer the reader to Section 8.1.3 of [7], where a continuous formulation is studied, and to the papers [41, 60], which perform the analysis in the transient case. Also, a nodal ungauged transient formulation involving only volumic sources instead of boundary ones is analysed in [71] at a discrete level. However, the formulation implemented in commercial software is usually based on edge finite elements and, to the best of the authors' knowledge, a rigorous analysis for this case with electric ports has not yet been performed. To attain this goal, we will rest upon the uniqueness of the magnetic field, even though its decomposition in vector and scalar potentials may not be unique. In this way, we will first establish an equivalence between an ungauged $\boldsymbol{T}, \phi - \phi$ formulation of the problem and a slight variation of the magnetic field formulation analysed in [22]. This equivalence, proved at both continuous and discrete levels, will be the key to obtain the uniqueness of the magnetic field reconstructed from the scalar and vector potentials, and to obtain the convergence result for the discrete scheme. We notice that, from a computational point of view, the ungauged $\boldsymbol{T}, \phi - \phi$ formulation leads to an undetermined problem that requires an iterative method for finding a particular solution to it. On the other hand, we have also extended the theory to cover a gauged version of the problem, whose analysis cannot also be found in the present literature. The solution of this version of the formulation will be unique, and thus, if the problem is not too large it is possible to use a direct solver for its resolution. The techniques used to perform the mathematical and numerical analysis in this second stage will be the same as for the ungauged case.

Concerning the discretization of the problems, *edge* finite elements will be employed for the approximation of the vector potential and standard Lagrange finite elements for that of the scalar potential. A drawback of this formulation is that it requires the computation of a source field in the dielectric domain, the so-called *impressed vector potential*, which is not trivial if the dielectric domain is not simply connected. Based on the ideas introduced by Bíró and Preis in [34], we will compute this field by using the Biot-Savart law, what eliminates the necessity of using multivalued scalar potentials, even in the case of homologically non-trivial topologies. From the point of view of the mathematical analysis, this approach guarantees the convergence of the numerical method when sources are provided in terms of the currents crossing some parts of the boundary, but this is not the case if the potential drops are given. To overcome this theoretical difficulty, we also include a brief explanation of the procedure introduced in [5] for constructing the impressed vector potential by computing the so-called loop fields, which would be suitable to prove the convergence in all cases; see [6], where this idea is also exploited in the implementation of a magnetic field/scalar potential formulation.

The outline of this chapter is as follows: in Section 1.2 we present the eddy current model and recall a formulation to solve it presented in [22]; in Section 1.3, we derive the strong $\boldsymbol{T}, \phi - \phi$ formulation for the eddy current problem; in Sections 1.4 and 1.5, we perform the mathematical

and numerical analysis of this formulations, without imposing a gauge condition in the first case and with a Coulomb's gauge in the second, through its equivalence with the one studied in [22]; in Section 1.6, we introduce a numerical procedure to compute the impressed vector potential and, with this end, we derive an expression to evaluate the Biot-Savart field corresponding to a polygonal filament carrying a unit current intensity; finally, in Section 1.7, some numerical results are reported.

1.2 Eddy Current Model with Sources as Boundary Data

Eddy currents in linear, homogeneous and isotropic media are usually modeled by the low-frequency harmonic Maxwell's equations,

$$\mathbf{curl}\, \boldsymbol{H} = \boldsymbol{J}, \tag{1.1}$$

$$i\omega\mu\boldsymbol{H} + \mathbf{curl}\, \boldsymbol{E} = \boldsymbol{0}, \tag{1.2}$$

$$\mathrm{div}(\mu\boldsymbol{H}) = 0, \tag{1.3}$$

along with Ohm's law

$$\boldsymbol{J} = \sigma\boldsymbol{E}, \tag{1.4}$$

where we recall that $\boldsymbol{E}$, $\boldsymbol{H}$ and $\boldsymbol{J}$ are the phasors corresponding to the electric field, the magnetic field and the current density, respectively, $\omega \neq 0$ is the angular frequency (with $\omega = 2\pi f$, f being the current frequency), μ the magnetic permeability and σ the electrical conductivity. Note that the latter is non-null only in conducting media.

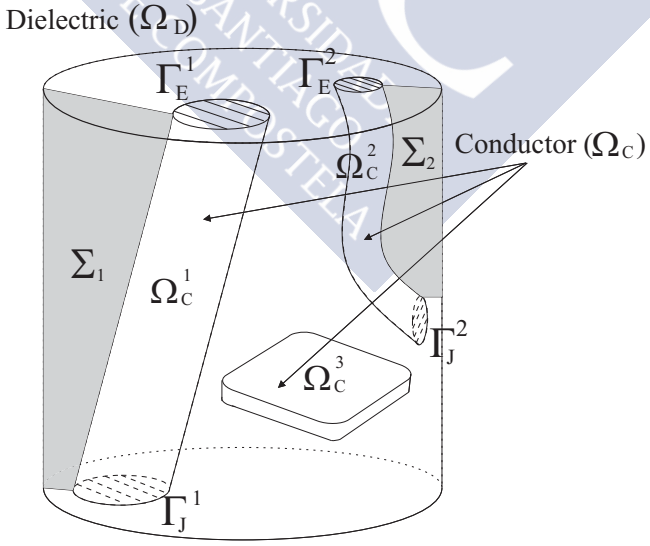

Figure 1.1: Sketch of the domain ($N = 2$, $M = 3$).

Although equations (1.1)–(1.4) concern the whole space, for computational purposes we restrict them to a simply connected three-dimensional bounded domain Ω with a connected boundary. This domain Ω consists of two parts, Ω_C and Ω_D, occupied by conductors and dielectrics, respectively (see Figure 1.1), and we assume that Ω_D is connected. Domains Ω, Ω_C and Ω_D are assumed

to have Lipschitz-continuous boundaries. We denote by Γ_{C}, Γ_{D} and Γ_{I} the open Lipschitz surfaces such that $\overline{\Gamma}_{\mathrm{C}} := \partial\Omega_{\mathrm{C}} \cap \partial\Omega$ is the outer boundary of the conductors, $\overline{\Gamma}_{\mathrm{D}} := \partial\Omega_{\mathrm{D}} \cap \partial\Omega$ that of the dielectrics and $\overline{\Gamma}_{\mathrm{I}} := \partial\Omega_{\mathrm{C}} \cap \partial\Omega_{\mathrm{D}}$ the interface between both domains. We also denote by $\boldsymbol{n}$ the outward unit normal vector to $\partial\Omega$, as well as other unit vectors normal to particular surfaces that will be deduced from the context.

The connected components of the conducting domain Ω_{C}^n, $n = 1, \ldots, M$, are supposed to be simply connected with connected boundaries. The first N connected components of the conducting domain, the so-called *inductors*, are assumed to intersect the boundary of Ω in such a way that the outer boundary of each of them, $\partial\Omega_{\mathrm{C}}^n \cap \partial\Omega$, has two disjoint connected components, both being the closure of non-zero measure open surfaces: the *current entrances* $\overline{\Gamma}_{\mathrm{J}}^n$ and the *current exits* $\overline{\Gamma}_{\mathrm{E}}^n$, where the conductor is connected to an alternating electric source. We denote $\Gamma_{\mathrm{J}} := \Gamma_{\mathrm{J}}^1 \cup \cdots \cup \Gamma_{\mathrm{J}}^N$, $\Gamma_{\mathrm{E}} := \Gamma_{\mathrm{E}}^1 \cup \cdots \cup \Gamma_{\mathrm{E}}^N$ and $\overline{\Gamma}_{\mathrm{I}}^n = \partial\Omega_{\mathrm{C}}^n \cap \partial\Omega_{\mathrm{D}}$, $n = 1, \ldots, N$. Furthermore, we assume that $\overline{\Gamma}_{\mathrm{J}}^n \cap \overline{\Gamma}_{\mathrm{J}}^m = \emptyset$ and $\overline{\Gamma}_{\mathrm{E}}^n \cap \overline{\Gamma}_{\mathrm{E}}^m = \emptyset$, $1 \leq m, n \leq N$, $m \neq n$, and $\overline{\Gamma}_{\mathrm{J}} \cap \overline{\Gamma}_{\mathrm{E}} = \emptyset$. The remaining connected components Ω_{C}^n, $n = N+1, \ldots, M$, are assumed to have their closure included in Ω, and will be referred to as *workpieces*.

As illustrated in Figure 1.1, we assume that for each inductor Ω_{C}^n, $n = 1, \ldots, N$, there exists a connected *cutting* surface $\Sigma_n \subset \Omega_{\mathrm{D}}$ such that $\partial\Sigma_n \subset \partial\Omega_{\mathrm{D}}$ and $\widetilde{\Omega}_{\mathrm{D}} := \Omega_{\mathrm{D}} \setminus \bigcup_{n=1}^N \Sigma_n$ is pseudo-Lipschitz and simply connected (see, for instance, [9]). We also assume that $\overline{\Sigma}_n \cap \overline{\Sigma}_m = \emptyset$ for $n \neq m$ and that the boundary of each current entrance surface, $\gamma_n := \partial\Gamma_{\mathrm{J}}^n$, is a simple closed curve. We denote the two faces of each Σ_n by Σ_n^- and Σ_n^+ and fix a unit normal $\boldsymbol{n}_n$ on Σ_n as the *outer* normal to $\Omega_{\mathrm{D}} \setminus \Sigma_n$ along Σ_n^+. We choose an orientation for each γ_n by taking its initial and end points on Σ_n^- and Σ_n^+, respectively. We denote by $\boldsymbol{\tau}_n$ the unit vector tangent to γ_n according with this orientation. Moreover, let us emphasise that the cutting surfaces Σ_n, $n = 1, \ldots, N$, will be only a theoretical tool to prove some of the following results. However, there is no need to construct such surfaces to apply the $\boldsymbol{T}, \phi - \phi$ formulation of the eddy current problem that we will introduce and analyse in this paper.

We assume that there exist constants $\underline{\mu}$, $\overline{\mu}$, $\underline{\sigma}$ and $\overline{\sigma}$ such that

$$
\begin{aligned}
&0 < \underline{\mu} \leq \mu(\boldsymbol{x}) \leq \overline{\mu} \quad \text{a.e. } \boldsymbol{x} \in \Omega, \\
&0 < \underline{\sigma} \leq \sigma(\boldsymbol{x}) \leq \overline{\sigma} \quad \text{a.e. } \boldsymbol{x} \in \Omega_{\mathrm{C}} \text{ and } \sigma \equiv 0 \text{ in } \Omega_{\mathrm{D}}.
\end{aligned}
$$

To solve equations (1.1)–(1.4) in a bounded domain, it is necessary to add suitable boundary conditions. We consider the following which will appear as natural boundary conditions of the weak formulation of the problem:

$$
\boldsymbol{E} \times \boldsymbol{n} = \boldsymbol{0} \qquad \text{on } \Gamma_{\mathrm{E}} \cup \Gamma_{\mathrm{J}}, \tag{1.5}
$$

$$
\mu \boldsymbol{H} \cdot \boldsymbol{n} = 0 \qquad \text{on } \partial\Omega. \tag{1.6}
$$

The former means that the electric current is normal to the entrance and exit surfaces, whereas the latter means that the magnetic field is tangential to the boundary. These boundary conditions have been proposed in [37]; we refer to [22] for further discussion about them.

Boundary condition (1.6) implies that the tangential component of the electric field $\boldsymbol{E}$ is a surface gradient. Indeed, after integrating $i\omega\mu\boldsymbol{H} \cdot \boldsymbol{n}$ on any surface S contained in $\partial\Omega$, by using (1.2)

and Stokes' theorem we obtain

$$0 = \int_S i\omega\mu \boldsymbol{H}\cdot\boldsymbol{n} = -\int_S \mathbf{curl}\,\boldsymbol{E}\cdot\boldsymbol{n} = -\int_{\partial S}\boldsymbol{E}\cdot\boldsymbol{\tau} = -\int_{\partial S}\boldsymbol{n}\times(\boldsymbol{E}\times\boldsymbol{n})\cdot\boldsymbol{\tau},$$

$\boldsymbol{\tau}$ being a unit vector tangent to ∂S. Therefore, since $\partial\Omega$ is simply connected, there exists a sufficiently smooth function V defined on $\partial\Omega$ up to a constant, such that V is a surface potential of the tangential component of $\boldsymbol{E}$; that is, $\boldsymbol{n}\times\boldsymbol{E}\times\boldsymbol{n} = -\,\mathbf{grad}_\tau V$ on $\partial\Omega$, where $\mathbf{grad}_\tau$ denotes the surface gradient. On the other hand, equation (1.5) implies that V must be constant on each connected component of Γ_{E} and Γ_{J}. Let V_{E}^n and V_{J}^n be complex numbers such that $V = V_{\mathrm{E}}^n$ on Γ_{E}^n and $V = V_{\mathrm{J}}^n$ on Γ_{J}^n, $n = 1,\dots,N$. The difference $\Delta V_n = V_{\mathrm{E}}^n - V_{\mathrm{J}}^n$ is the potential drop along conductor Ω_{C}^n.

Multiplying Faraday's law (1.2) by $\overline{\boldsymbol{H}}$, integrating over Ω and then applying a Green's formula along with equation (1.1), we obtain

$$\int_\Omega i\omega\mu|\boldsymbol{H}|^2 + \int_{\Omega_{\mathrm{C}}}\boldsymbol{E}\cdot\overline{\boldsymbol{J}} = \int_{\partial\Omega}(\boldsymbol{E}\times\boldsymbol{n})\cdot\overline{\boldsymbol{H}}.$$

Using that $\boldsymbol{n}\times\boldsymbol{E}\times\boldsymbol{n} = -\,\mathbf{grad}_\tau V$ on $\partial\Omega$, we write

$$\begin{aligned}\int_{\partial\Omega}(\boldsymbol{E}\times\boldsymbol{n})\cdot\overline{\boldsymbol{H}} = -\int_{\partial\Omega}(\mathbf{grad}_\tau V\times\boldsymbol{n})\cdot\overline{\boldsymbol{H}} &= -\int_{\partial\Omega}\mathbf{curl}_\tau V\cdot\overline{\boldsymbol{H}}\\ &= -\int_{\partial\Omega} V\,\mathrm{curl}_\tau\,\overline{\boldsymbol{H}} = -\int_{\partial\Omega} V\,\mathbf{curl}\,\overline{\boldsymbol{H}}\cdot\boldsymbol{n}, \quad (1.7)\end{aligned}$$

where $\mathbf{curl}_\tau$ and curl_τ denote the surface vector and scalar curls, respectively.

Now, since $\mathbf{curl}\,\boldsymbol{H} = \boldsymbol{J}$ and $\boldsymbol{J} = \boldsymbol{0}$ in Ω_{D},

$$\begin{aligned}\int_{\partial\Omega} V\,\mathbf{curl}\,\overline{\boldsymbol{H}}\cdot\boldsymbol{n} = \sum_{n=1}^N\left(V_{\mathrm{E}}^n\int_{\Gamma_{\mathrm{E}}^n}\mathbf{curl}\,\overline{\boldsymbol{H}}\cdot\boldsymbol{n} + V_{\mathrm{J}}^n\int_{\Gamma_{\mathrm{J}}^n}\mathbf{curl}\,\overline{\boldsymbol{H}}\cdot\boldsymbol{n}\right)\\ = -\sum_{n=1}^N\Delta V_n\int_{\Gamma_{\mathrm{J}}^n}\mathbf{curl}\,\overline{\boldsymbol{H}}\cdot\boldsymbol{n}, \quad (1.8)\end{aligned}$$

the last equality because, for each inductor,

$$0 = \int_{\Omega_{\mathrm{C}}^n}\mathrm{div}(\mathbf{curl}\,\overline{\boldsymbol{H}}) = \int_{\partial\Omega_{\mathrm{C}}^n}\mathbf{curl}\,\overline{\boldsymbol{H}}\cdot\boldsymbol{n} = \int_{\Gamma_{\mathrm{E}}^n}\mathbf{curl}\,\overline{\boldsymbol{H}}\cdot\boldsymbol{n} + \int_{\Gamma_{\mathrm{J}}^n}\mathbf{curl}\,\overline{\boldsymbol{H}}\cdot\boldsymbol{n}.$$

Then, from the above equations we derive the energy conservation law:

$$\int_\Omega i\omega\mu|\boldsymbol{H}|^2 + \int_{\Omega_{\mathrm{C}}}\boldsymbol{E}\cdot\overline{\boldsymbol{J}} = \sum_{n=1}^N\overline{I_n}\,\Delta V_n,$$

with $I_n := \int_{\Gamma_{\mathrm{J}}^n}\boldsymbol{J}\cdot\boldsymbol{n} = \int_{\Gamma_{\mathrm{J}}^n}\mathbf{curl}\,\boldsymbol{H}\cdot\boldsymbol{n}$ being the current intensity through conductor Ω_{C}^n, $n = 1,\dots,N$.

In order to consider sources provided by external circuits we have two possibilities: either the current intensity or the potential drop must be given for each inductor Ω_{C}^n, $n = 1,\dots,N$. We

assume that for $n = 1, \ldots, N_I$ ($0 \leq N_I \leq N$) the current intensity I_n crossing Γ_{J}^n is given, in which case the boundary condition reads

$$\int_{\Gamma_{\mathrm{J}}^n} \mathbf{curl}\, \boldsymbol{H} \cdot \boldsymbol{n} = I_n, \quad n = 1, \ldots, N_I, \tag{1.9}$$

and, for $n = N_I + 1, \ldots, N$, the potential drop ΔV_n between Γ_{J}^n and Γ_{E}^n is given, in which case the boundary condition reads

$$\boldsymbol{n} \times \boldsymbol{E} \times \boldsymbol{n} = -\,\mathbf{grad}_\tau\, V \quad \text{on } \partial\Omega, \quad \text{with } V|_{\Gamma_{\mathrm{E}}^n} - V|_{\Gamma_{\mathrm{J}}^n} = \Delta V_n, \quad n = N_I + 1, \ldots, N. \tag{1.10}$$

The system composed by equations (1.1)–(1.4) subjected to boundary conditions (1.5), (1.6), (1.9) and (1.10) is frequently known as the *eddy current problem with non-local boundary conditions*.

1.3 $\boldsymbol{T}, \phi - \phi$ Formulation of the Eddy Current Problem

Our first goal is to introduce some auxiliary unknowns that will be used to solve the previous set of equations. First of all, note that given a complex vector of currents $(I_n)_{n=1}^N \in \mathbb{C}^N$, there exists $\boldsymbol{T}_0 \in \mathrm{H}(\mathbf{curl}, \Omega)$ such that

$$\int_{\Gamma_{\mathrm{J}}^n} \mathbf{curl}\, \boldsymbol{T}_0 \cdot \boldsymbol{n} = I_n \quad \text{for } n = 1, \ldots, N,$$
$$\mathbf{curl}\, \boldsymbol{T}_0 = \boldsymbol{0} \quad \text{in } \Omega_{\mathrm{D}} \cup \left(\cup_{n=N+1}^{M} \Omega_{\mathrm{C}}^n \right).$$

Such $\boldsymbol{T}_0$ is usually called an *impressed vector potential*. An example is given by $\boldsymbol{T}_0(\boldsymbol{x}) = \sum_{n=1}^N I_n \boldsymbol{t}_{0,n}(\boldsymbol{x})$, with $\boldsymbol{t}_{0,n} \in \mathrm{H}(\mathbf{curl}, \Omega)$ satisfying

$$\int_{\Gamma_{\mathrm{J}}^n} \mathbf{curl}\, \boldsymbol{t}_{0,n} \cdot \boldsymbol{n} = 1, \tag{1.11}$$

$$\mathbf{curl}\, \boldsymbol{t}_{0,n} = \boldsymbol{0} \quad \text{in } \Omega \setminus \overline{\Omega_{\mathrm{C}}^n}, \tag{1.12}$$

for $n = 1, \ldots, N$. We will refer to these vector fields $\boldsymbol{t}_{0,n}$, $n = 1, \ldots, N$, as *normalised impressed vector potentials*. They can be defined in different ways (see, e.g., [32]).

From equations (1.1) and (1.4) we have that $\operatorname{div} \boldsymbol{J} = 0$ in Ω_{C} and $\boldsymbol{J} \cdot \boldsymbol{n} = 0$ on Γ_{I}. Therefore,

$$\begin{aligned} \operatorname{div} (\boldsymbol{J} - \mathbf{curl}\, \boldsymbol{T}_0) &= 0 \quad \text{in } \Omega_{\mathrm{C}}, \\ (\boldsymbol{J} - \mathbf{curl}\, \boldsymbol{T}_0) \cdot \boldsymbol{n} &= 0 \quad \text{on } \Gamma_{\mathrm{I}}, \\ \int_{\Gamma_{\mathrm{J}}^n} (\boldsymbol{J} - \mathbf{curl}\, \boldsymbol{T}_0) \cdot \boldsymbol{n} &= 0 \quad \text{for } n = 1, \ldots, N. \end{aligned}$$

Hence, it can be proved that for each connected component of the conducting domain Ω_{C}^n, $n = 1, \ldots, M$, there exists a vector field $\boldsymbol{T}^n$ supported in Ω_{C}^n such that

$$\begin{aligned} \mathbf{curl}\, \boldsymbol{T}^n &= \boldsymbol{J} - \mathbf{curl}\, \boldsymbol{T}_0 \quad \text{in } \Omega_{\mathrm{C}}^n, \\ \boldsymbol{T}^n \times \boldsymbol{n} &= \boldsymbol{0} \quad \text{on } \Gamma_{\mathrm{I}}^n \end{aligned}$$

(see, for example, Theorem 2.1 in [48]). Let $\widetilde{\boldsymbol{T}}^n$ be the extension by zero to Ω of $\boldsymbol{T}^n$, $n = 1, \ldots, M$. Let $\widetilde{\boldsymbol{T}} := \sum_{n=1}^{M} \widetilde{\boldsymbol{T}}^n$ and $\boldsymbol{T} := \widetilde{\boldsymbol{T}}|_{\Omega_{\mathrm{C}}}$. Then, $\boldsymbol{T}$ satisfies $\mathbf{curl}\, \boldsymbol{T} = \boldsymbol{J} - \mathbf{curl}\, \boldsymbol{T}_0$ in Ω_{C} and $\boldsymbol{T} \times \boldsymbol{n} = \boldsymbol{0}$ on Γ_{I}. Such a $\boldsymbol{T}$ is called a *current vector potential*.

Now, from (1.1), $\mathbf{curl}\, \boldsymbol{H} = \boldsymbol{J} = \mathbf{curl}\, \widetilde{\boldsymbol{T}} + \mathbf{curl}\, \boldsymbol{T}_0$, so that, since Ω is simply connected,

$$\boldsymbol{H} = \widetilde{\boldsymbol{T}} + \boldsymbol{T}_0 - \mathbf{grad}\, \phi \tag{1.13}$$

for some $\phi \in \mathrm{H}^1(\Omega)$; ϕ is usually called a *magnetic scalar potential*. Notice that such an $\boldsymbol{H}$ satisfies automatically the constraint $\mathbf{curl}\, \boldsymbol{H} = \boldsymbol{0}$ in Ω_{D}, which follows from (1.1) and (1.4).

Taking the previous decomposition into account, the time-harmonic eddy current problem (1.1)–(1.6) leads to:

$$i\omega\mu\,(\boldsymbol{T} + \boldsymbol{T}_0 - \mathbf{grad}\, \phi) + \mathbf{curl}\left(\frac{1}{\sigma}\,\mathbf{curl}(\boldsymbol{T} + \boldsymbol{T}_0)\right) = \boldsymbol{0} \quad \text{in } \Omega_{\mathrm{C}}, \tag{1.14}$$

$$\mathrm{div}\left(\mu(\widetilde{\boldsymbol{T}} + \boldsymbol{T}_0 - \mathbf{grad}\, \phi)\right) = 0 \quad \text{in } \Omega, \tag{1.15}$$

$$\left(\frac{1}{\sigma}\,\mathbf{curl}(\boldsymbol{T} + \boldsymbol{T}_0)\right) \times \boldsymbol{n} = \boldsymbol{0} \quad \text{on } \Gamma_{\mathrm{E}} \cup \Gamma_{\mathrm{J}}, \tag{1.16}$$

$$\mu(\widetilde{\boldsymbol{T}} + \boldsymbol{T}_0 - \mathbf{grad}\, \phi) \cdot \boldsymbol{n} = 0 \quad \text{on } \partial\Omega. \tag{1.17}$$

The above equations correspond to the strong $\boldsymbol{T}, \phi - \phi$ formulation of problem (1.1)–(1.4) subjected to boundary conditions (1.5), (1.6), (1.9) and (1.10) (see [34]). We will see in the next section that decomposition (1.13) is not unique, and therefore this is not a well-posed problem. Nevertheless, it is possible to add some requirements to the problem in order to guarantee that it will have only one solution (the usually called *gauge conditions*). One of these sets of conditions is the so-called *Coulomb's gauge*, which in this case reads:

$$\mathrm{div}\, \boldsymbol{T} = 0 \quad \text{in } \Omega_{\mathrm{C}}, \tag{1.18}$$

$$\boldsymbol{T} \cdot \boldsymbol{n} = 0 \quad \text{on } \Gamma_{\mathrm{E}} \cup \Gamma_{\mathrm{J}}. \tag{1.19}$$

We will dedicate the next two sections to perform the mathematical and numerical analysis of the weak versions of both the ungagued and gauged $\boldsymbol{T}, \phi - \phi$ formulations, that is, of (1.14)–(1.17) and (1.14)–(1.19), respectively.

1.4 Mathematical and Numerical Analysis of the Ungauged $\boldsymbol{T}, \phi - \phi$ Formulation

Our next goal is to introduce a weak formulation of problem (1.14)–(1.17). If we test (1.14) with a function $\boldsymbol{S} \in \mathrm{H}(\mathbf{curl}, \Omega_{\mathrm{C}})$ such that $\boldsymbol{S} \times \boldsymbol{n} = \boldsymbol{0}$ on Γ_{I}, using a Green's formula and (1.16), we

obtain

$$\int_{\Omega_{\rm C}} i\omega\mu\,(\boldsymbol{T}+\boldsymbol{T}_0-\mathbf{grad}\,\phi)\cdot\overline{\boldsymbol{S}}+\int_{\Omega_{\rm C}}\frac{1}{\sigma}\,\mathbf{curl}(\boldsymbol{T}+\boldsymbol{T}_0)\cdot\mathbf{curl}\,\overline{\boldsymbol{S}}$$
$$=-\int_{\partial\Omega_{\rm C}}\frac{1}{\sigma}\,\mathbf{curl}(\boldsymbol{T}+\boldsymbol{T}_0)\times\boldsymbol{n}\cdot\overline{\boldsymbol{S}}=-\int_{\Gamma_{\rm E}\cup\Gamma_{\rm J}}\frac{1}{\sigma}\,\mathbf{curl}(\boldsymbol{T}+\boldsymbol{T}_0)\times\boldsymbol{n}\cdot\overline{\boldsymbol{S}}$$
$$+\int_{\Gamma_{\rm I}}\frac{1}{\sigma}\,\mathbf{curl}(\boldsymbol{T}+\boldsymbol{T}_0)\cdot\overline{\boldsymbol{S}}\times\boldsymbol{n}=0.$$

Hence, using that $\boldsymbol{T}_0=\sum_{n=1}^{N}I_n\boldsymbol{t}_{0,n}$ we write

$$\int_{\Omega_{\rm C}} i\omega\mu(\boldsymbol{T}-\mathbf{grad}\,\phi)\cdot\overline{\boldsymbol{S}}+\int_{\Omega_{\rm C}}\frac{1}{\sigma}\,\mathbf{curl}\,\boldsymbol{T}\cdot\mathbf{curl}\,\overline{\boldsymbol{S}}$$
$$+\sum_{n=1}^{N}I_n\left(\int_{\Omega_{\rm C}} i\omega\mu\boldsymbol{t}_{0,n}\cdot\overline{\boldsymbol{S}}+\int_{\Omega_{\rm C}}\frac{1}{\sigma}\,\mathbf{curl}\,\boldsymbol{t}_{0,n}\cdot\mathbf{curl}\,\overline{\boldsymbol{S}}\right)=0. \quad (1.20)$$

On the other hand, multiplying (1.15) by $i\omega\overline{\psi}$ with $\psi\in\mathrm{H}^1(\Omega)$, using a Green's formula and taking (1.17) into account, we obtain

$$\int_{\Omega} i\omega\mu\left(\widetilde{\boldsymbol{T}}+\boldsymbol{T}_0-\mathbf{grad}\,\phi\right)\cdot\mathbf{grad}\,\overline{\psi}=0.$$

Then, for all $\psi\in\mathrm{H}^1(\Omega)$ we have that

$$\int_{\Omega} i\omega\mu\left(\widetilde{\boldsymbol{T}}-\mathbf{grad}\,\phi\right)\cdot\mathbf{grad}\,\overline{\psi}+\sum_{n=1}^{N}I_n\int_{\Omega} i\omega\mu\boldsymbol{t}_{0,n}\cdot\mathbf{grad}\,\overline{\psi}=0. \quad (1.21)$$

When all the sources are given in terms of the current intensities crossing the conducting subdomains, the problem to solve is (1.20)–(1.21). However, when there are conductors for which the potential drops are given, we need to derive some other equations to determine the corresponding current intensities. To this end, we multiply equation (1.2) by the conjugate of $\boldsymbol{t}_{0,m}$ and integrate over Ω for $m=N_I+1,\ldots,N$, to obtain

$$\int_{\Omega} i\omega\mu\boldsymbol{H}\cdot\bar{\boldsymbol{t}}_{0,m}+\int_{\Omega}\mathbf{curl}\,\boldsymbol{E}\cdot\bar{\boldsymbol{t}}_{0,m}=0.$$

Now, using a Green's formula and the fact that $\mathbf{curl}\,\bar{\boldsymbol{t}}_{0,m}=\boldsymbol{0}$ out of $\Omega_{\rm C}^m$, we have

$$\int_{\Omega}\mathbf{curl}\,\boldsymbol{E}\cdot\bar{\boldsymbol{t}}_{0,m}=\int_{\Omega_{\rm C}^m}\boldsymbol{E}\cdot\mathbf{curl}\,\bar{\boldsymbol{t}}_{0,m}-\int_{\partial\Omega}(\boldsymbol{E}\times\boldsymbol{n})\cdot\bar{\boldsymbol{t}}_{0,m}.$$

Proceeding as in (1.7)–(1.8) with the test function $\boldsymbol{t}_{0,m}$ instead of $\boldsymbol{H}$, it is easy to check that

$$\int_{\partial\Omega}(\boldsymbol{E}\times\boldsymbol{n})\cdot\bar{\boldsymbol{t}}_{0,m}=\Delta V_m.$$

Then, from the last three equations, (1.1) and (1.4) we obtain

$$\int_{\Omega} i\omega\mu\boldsymbol{H}\cdot\bar{\boldsymbol{t}}_{0,m}+\int_{\Omega_{\rm C}^m}\frac{1}{\sigma}\,\mathbf{curl}\,\boldsymbol{H}\cdot\mathbf{curl}\,\bar{\boldsymbol{t}}_{0,m}=\Delta V_m.$$

Thus, using again that $\boldsymbol{H} = \widetilde{\boldsymbol{T}} + \boldsymbol{T}_0 - \mathbf{grad}\,\phi$ and $\boldsymbol{T}_0 = \sum_{n=1}^{N} I_n \boldsymbol{t}_{0,n}$, we write for $m = N_I + 1, \ldots, N$

$$\int_\Omega i\omega\mu(\widetilde{\boldsymbol{T}} - \mathbf{grad}\,\phi)\cdot\overline{\boldsymbol{t}}_{0,m} + \int_{\Omega_{\mathrm{C}}^m}\frac{1}{\sigma}\,\mathbf{curl}\,\boldsymbol{T}\cdot\mathbf{curl}\,\overline{\boldsymbol{t}}_{0,m} + \sum_{n=1}^{N} I_n\int_\Omega i\omega\mu\boldsymbol{t}_{0,n}\cdot\overline{\boldsymbol{t}}_{0,m} + I_m\int_{\Omega_{\mathrm{C}}^m}\frac{1}{\sigma}|\,\mathbf{curl}\,\boldsymbol{t}_{0,m}|^2 = \Delta V_m. \quad (1.22)$$

We define the following closed subspace of $\mathrm{H}(\mathbf{curl},\Omega_{\mathrm{C}})$:

$$\boldsymbol{\mathcal{Y}} := \{\boldsymbol{S}\in\mathrm{H}(\mathbf{curl},\Omega_{\mathrm{C}})\ :\ \boldsymbol{S}\times\boldsymbol{n} = \mathbf{0}\ \text{on}\ \Gamma_{\mathrm{I}}\}\,.$$

Collecting equations (1.20)–(1.22), we derive the following formulation:

Problem 1.1. *Let $\boldsymbol{t}_{0,n}\in\mathrm{H}(\mathbf{curl},\Omega)$, $n = 1,\ldots,N$, satisfying (1.11)–(1.12). Given $I_n\in\mathbb{C}$, $n = 1,\ldots,N_I$, and $\Delta V_n\in\mathbb{C}$, $n = N_I+1,\ldots,N$, find $\boldsymbol{T}\in\boldsymbol{\mathcal{Y}}$, $\phi\in\mathrm{H}^1(\Omega)$ and $I_n\in\mathbb{C}$ for $n = N_I+1,\ldots,N$ such that*

$$\int_{\Omega_{\mathrm{C}}} i\omega\mu(\boldsymbol{T} - \mathbf{grad}\,\phi)\cdot\overline{\boldsymbol{S}} + \int_{\Omega_{\mathrm{C}}}\frac{1}{\sigma}\,\mathbf{curl}\,\boldsymbol{T}\cdot\mathbf{curl}\,\overline{\boldsymbol{S}} + \sum_{n=N_I+1}^{N} I_n\left(\int_{\Omega_{\mathrm{C}}} i\omega\mu\boldsymbol{t}_{0,n}\cdot\overline{\boldsymbol{S}} + \int_{\Omega_{\mathrm{C}}^n}\frac{1}{\sigma}\,\mathbf{curl}\,\boldsymbol{t}_{0,n}\cdot\mathbf{curl}\,\overline{\boldsymbol{S}}\right) = -\sum_{n=1}^{N_I} I_n\left(\int_{\Omega_{\mathrm{C}}} i\omega\mu\boldsymbol{t}_{0,n}\cdot\overline{\boldsymbol{S}} + \int_{\Omega_{\mathrm{C}}^n}\frac{1}{\sigma}\,\mathbf{curl}\,\boldsymbol{t}_{0,n}\cdot\mathbf{curl}\,\overline{\boldsymbol{S}}\right)\quad\forall\,\boldsymbol{S}\in\boldsymbol{\mathcal{Y}}, \quad (1.23)$$

$$-\int_{\Omega_{\mathrm{C}}} i\omega\mu\boldsymbol{T}\cdot\mathbf{grad}\,\overline{\psi} + \int_\Omega i\omega\mu\,\mathbf{grad}\,\phi\cdot\mathbf{grad}\,\overline{\psi} - \sum_{n=N_I+1}^{N} I_n\int_\Omega i\omega\mu\boldsymbol{t}_{0,n}\cdot\mathbf{grad}\,\overline{\psi} = \sum_{n=1}^{N_I} I_n\int_\Omega i\omega\mu\boldsymbol{t}_{0,n}\cdot\mathbf{grad}\,\overline{\psi}\quad\forall\,\psi\in\mathrm{H}^1(\Omega), \quad (1.24)$$

$$\left(\int_{\Omega_{\mathrm{C}}} i\omega\mu\boldsymbol{T}\cdot\overline{\boldsymbol{t}}_{0,m} - \int_\Omega i\omega\mu\,\mathbf{grad}\,\phi\cdot\overline{\boldsymbol{t}}_{0,m} + \int_{\Omega_{\mathrm{C}}^m}\frac{1}{\sigma}\,\mathbf{curl}\,\boldsymbol{T}\cdot\mathbf{curl}\,\overline{\boldsymbol{t}}_{0,m} + \sum_{n=N_I+1}^{N} I_n\int_\Omega i\omega\mu\boldsymbol{t}_{0,n}\cdot\overline{\boldsymbol{t}}_{0,m} + I_m\int_{\Omega_{\mathrm{C}}^m}\frac{1}{\sigma}|\,\mathbf{curl}\,\boldsymbol{t}_{0,m}|^2\right)\overline{K}_m = \Delta V_m\overline{K}_m - \left(\sum_{n=1}^{N_I} I_n\int_\Omega i\omega\mu\boldsymbol{t}_{0,n}\cdot\overline{\boldsymbol{t}}_{0,m}\right)\overline{K}_m\quad\forall\,K_m\in\mathbb{C},\quad m = N_I+1,\ldots,N. \quad (1.25)$$

This is the ungauged version of the well-known $\boldsymbol{T},\phi-\phi$ formulation of problem (1.1)–(1.4) subjected to boundary conditions (1.5), (1.6), (1.9) and (1.10). Let us notice that this problem is not well-posed; indeed, we will show in the following subsection that it has infinitely many solutions. Still, we will also show that any of these solutions allows us to solve our original problem.

1.4.1 Mathematical Analysis

Now, we recall the magnetic field formulation considered in [22] of the same eddy current problem that will be used to analyse the $\boldsymbol{T}, \phi - \phi$ formulation. To this end, we define

$$\boldsymbol{\mathcal{X}} := \{\boldsymbol{G} \in \mathrm{H}(\mathbf{curl}, \Omega) \,:\, \mathbf{curl}\, \boldsymbol{G} = \boldsymbol{0} \text{ in } \Omega_{\mathrm{D}}\}$$

and, given $\boldsymbol{K} \in \mathbb{C}^{N_I}$,

$$\boldsymbol{\mathcal{V}}(\boldsymbol{K}) := \left\{\boldsymbol{G} \in \boldsymbol{\mathcal{X}} \,:\, \int_{\Gamma_{\mathrm{J}}^n} \mathbf{curl}\, \boldsymbol{G} \cdot \boldsymbol{n} = K_n,\ n = 1, \ldots, N_I\right\},$$

which is a closed linear manifold of $\boldsymbol{\mathcal{X}}$.

Remark 1.2. *For all $\boldsymbol{G} \in \boldsymbol{\mathcal{X}}$, $\mathbf{curl}\, \boldsymbol{G} \cdot \boldsymbol{n} \in \mathrm{H}^{-1/2}(\partial\Omega)$ and $\mathbf{curl}\, \boldsymbol{G} \cdot \boldsymbol{n} = 0$ on Γ_{D}. Then, $\int_{\Gamma_{\mathrm{J}}^n} \mathbf{curl}\, \boldsymbol{G} \cdot \boldsymbol{n}$ is well defined. Indeed, let δ be any smooth function defined in $\partial\Omega$, such that $\delta = 1$ on Γ_{J}^n and $\delta = 0$ on Γ_{E} and on Γ_{J}^m, $m = 1, \ldots, N$, $m \neq n$. Then $\int_{\Gamma_{\mathrm{J}}^n} \mathbf{curl}\, \boldsymbol{G} \cdot \boldsymbol{n} := \langle \mathbf{curl}\, \boldsymbol{G} \cdot \boldsymbol{n}, \delta \rangle_{\mathrm{H}^{-1/2}(\partial\Omega) \times \mathrm{H}^{1/2}(\partial\Omega)}$ is well defined and its value does not depend on the particular choice of δ.*

The following magnetic field formulation is derived by using the same arguments from [22], where a similar problem but only with current intensity source terms has been considered.

Problem 1.3. *Given $I_n \in \mathbb{C}$, $n = 1, \ldots, N_I$, and $\Delta V_n \in \mathbb{C}$, $n = N_I + 1, \ldots, N$, find $\boldsymbol{H} \in \boldsymbol{\mathcal{V}}(\boldsymbol{I})$ such that*

$$\int_{\Omega} i\omega\mu \boldsymbol{H} \cdot \overline{\boldsymbol{G}} + \int_{\Omega_{\mathrm{C}}} \frac{1}{\sigma}\, \mathbf{curl}\, \boldsymbol{H} \cdot \mathbf{curl}\, \overline{\boldsymbol{G}} = \sum_{n=N_I+1}^{N} \Delta V_n \int_{\Gamma_{\mathrm{J}}^n} \mathbf{curl}\, \overline{\boldsymbol{G}} \cdot \boldsymbol{n} \quad \forall\, \boldsymbol{G} \in \boldsymbol{\mathcal{V}}(\boldsymbol{0}). \tag{1.26}$$

We have the following results:

Theorem 1.4. *Problem 1.3 has a unique solution.*

Proof. The result follows immediately from the fact that $\boldsymbol{\mathcal{V}}(\boldsymbol{I}) \neq \emptyset$ (see Lemma 2 in [22] or Section 3.2 in [24]), the $\boldsymbol{\mathcal{X}}$-ellipticity of the continuous sesquilinear form in the left hand side of (1.26) and the continuity of the linear functional $\boldsymbol{G} \longmapsto \sum_{n=N_I+1}^{N} \Delta V_n \int_{\Gamma_{\mathrm{J}}^n} \mathbf{curl}\, \overline{\boldsymbol{G}} \cdot \boldsymbol{n}$. □

Theorem 1.5. *Given $I_n \in \mathbb{C}$, $n = 1, \ldots, N_I$, and $\Delta V_n \in \mathbb{C}$, $n = N_I + 1, \ldots, N$, let $\boldsymbol{H} \in \boldsymbol{\mathcal{V}}(\boldsymbol{I})$ be the solution to Problem 1.3. Let $\boldsymbol{J} := \mathbf{curl}\, \boldsymbol{H}$ and $\boldsymbol{E} := \left(\frac{1}{\sigma}\boldsymbol{J}\right)|_{\Omega_{\mathrm{C}}}$. Then, the following equations hold true:*

$$i\omega\mu \boldsymbol{H} + \mathbf{curl}\, \boldsymbol{E} = \boldsymbol{0} \quad \text{in } \Omega_{\mathrm{C}}, \tag{1.27}$$

$$\mathrm{div}\,(\mu \boldsymbol{H}) = 0 \quad \text{in } \Omega, \tag{1.28}$$

$$\boldsymbol{J} = \boldsymbol{0} \quad \text{in } \Omega_{\mathrm{D}}, \tag{1.29}$$

$$\int_{\Gamma_{\mathrm{J}}^n} \mathbf{curl}\, \boldsymbol{H} \cdot \boldsymbol{n} = I_n \quad n = 1, \ldots, N_I, \tag{1.30}$$

$$\mu \boldsymbol{H} \cdot \boldsymbol{n} = 0 \quad \text{on } \partial\Omega, \tag{1.31}$$

$$\boldsymbol{E} \times \boldsymbol{n} = -\,\mathbf{grad}\, V_* \times \boldsymbol{n} \quad \text{in } \mathrm{H}_{00}^{-1/2}(\Gamma_{\mathrm{E}} \cup \Gamma_{\mathrm{J}})^3, \tag{1.32}$$

for some $V_* \in \mathrm{H}^1(\Omega_{\mathrm{C}})$ *constant on each connected component of* $\Gamma_{\mathrm{E}} \cup \Gamma_{\mathrm{J}}$ *and satisfying* $V_*|_{\Gamma_{\mathrm{E}}^n} - V_*|_{\Gamma_{\mathrm{J}}^n} = \Delta V_n$, $n = N_I + 1, \dots, N$. *Hence, in particular,*

$$\boldsymbol{E} \times \boldsymbol{n} = \boldsymbol{0} \quad \textit{on } \Gamma_{\mathrm{J}} \cup \Gamma_{\mathrm{E}}.$$

Proof. The proof is quite similar to that of Theorem 3.8 in [24]. For the sake of completeness, we include it here.
Given $\delta \in \mathcal{D}(\Omega)$, $\mathbf{grad}\,\delta \in \boldsymbol{\mathcal{V}}(\boldsymbol{0})$. Then, (1.26) yields

$$\int_{\Omega} i\omega\mu \boldsymbol{H} \cdot \mathbf{grad}\,\overline{\delta} = 0.$$

Consequently, (1.28) holds true.
Now, let $\boldsymbol{G} \in \mathcal{D}(\Omega)^3$ be such that $\operatorname{supp} \boldsymbol{G} \subset \Omega_{\mathrm{C}}$. Then, $\boldsymbol{G} \in \boldsymbol{\mathcal{V}}(\boldsymbol{0})$ too, and (1.26) yields

$$\int_{\Omega_{\mathrm{C}}} i\omega\mu \boldsymbol{H} \cdot \overline{\boldsymbol{G}} + \int_{\Omega_{\mathrm{C}}} \frac{1}{\sigma} \mathbf{curl}\,\boldsymbol{H} \cdot \mathbf{curl}\,\overline{\boldsymbol{G}} = 0.$$

Hence, $\boldsymbol{E} := \left(\frac{1}{\sigma} \mathbf{curl}\,\boldsymbol{H}\right)|_{\Omega_{\mathrm{C}}}$ satisfies (1.27).
Equation (1.29) follows from the definition of $\boldsymbol{J}$ and the fact that $\boldsymbol{H} \in \boldsymbol{\mathcal{X}}$, whereas equation (1.30) follows from the fact that $\boldsymbol{H} \in \boldsymbol{\mathcal{V}}(\boldsymbol{I})$.
To prove (1.31), notice that $\mu\boldsymbol{H} \in \mathrm{H}(\mathrm{div}, \Omega)$ because of (1.28). Then, $\mu\boldsymbol{H} \cdot \boldsymbol{n} \in \boldsymbol{H}^{-1/2}(\partial\Omega)$ and, given $\delta \in \mathrm{H}^1(\Omega)$, we have that

$$\langle \mu\boldsymbol{H} \cdot \boldsymbol{n}, \delta \rangle_{\partial\Omega} = \int_{\Omega} \mathrm{div}(\mu\boldsymbol{H})\overline{\delta} + \int_{\Omega} \mu\boldsymbol{H} \cdot \mathbf{grad}\,\overline{\delta} = 0,$$

the last equality because of (1.28) and (1.26), since $\mathbf{grad}\,\delta \in \boldsymbol{\mathcal{V}}(\boldsymbol{0})$. Then $\mu\boldsymbol{H} \cdot \boldsymbol{n} = 0$ in $\mathrm{H}^{-1/2}(\partial\Omega)$ and thus (1.31) holds true.
Finally, notice that $\boldsymbol{E} \in \mathrm{H}(\mathbf{curl}, \Omega_{\mathrm{C}})$ because of (1.27), and consequently $\boldsymbol{E} \times \boldsymbol{n} \in \mathrm{H}^{-1/2}(\partial\Omega_{\mathrm{C}})^3$. Hence, to prove (1.32), it is enough to show that there exists $V_* \in \mathrm{H}^1(\Omega_{\mathrm{C}})$ constant on each connected component of $\Gamma_{\mathrm{E}} \cup \Gamma_{\mathrm{J}}$, satisfying $V_*|_{\Gamma_{\mathrm{E}}^n} - V_*|_{\Gamma_{\mathrm{J}}^n} = \Delta V_n$, $n = N_I + 1, \dots, N$ and such that $\langle \boldsymbol{E} \times \boldsymbol{n}, \boldsymbol{v} \rangle_{\partial\Omega_{\mathrm{C}}} = -\langle \mathbf{grad}\, V_* \times \boldsymbol{n}, \boldsymbol{v} \rangle_{\partial\Omega_{\mathrm{C}}}$ for every $\boldsymbol{v} \in \mathrm{H}_{00}^{1/2}(\Gamma_{\mathrm{J}} \cup \Gamma_{\mathrm{E}})^3$.
Given one such $\boldsymbol{v}$, there exits $\boldsymbol{G} \in \mathrm{H}^1(\Omega)^3$ vanishing in Ω_{D} and such that $\boldsymbol{G}|_{\partial\Omega_{\mathrm{C}}} = \boldsymbol{v}$. Clearly, $\boldsymbol{G} \in \boldsymbol{\mathcal{X}}$. In what follows we prove that $\langle \mathbf{curl}\,\boldsymbol{G} \cdot \boldsymbol{n}, 1 \rangle_{\Gamma_{\mathrm{J}}^n} = 0$, $n = 1, \dots, N_I$. With this aim, let ζ_n be a smooth function defined in Ω such that $\zeta_n|_{\Gamma_{\mathrm{J}}^m} = \delta_{nm}$, $m = 1, \dots, N$, and $\zeta_n|_{\Gamma_{\mathrm{E}}} = 0$. Then, using a Green's formula and the fact that $\boldsymbol{G}$ vanishes in Ω_{D}, we obtain

$$\langle \mathbf{curl}\,\boldsymbol{G} \cdot \boldsymbol{n}, 1 \rangle_{\Gamma_{\mathrm{J}}^n} = \langle \mathbf{curl}\,\boldsymbol{G} \cdot \boldsymbol{n}, \zeta_n \rangle_{\partial\Omega} = \int_{\Omega_{\mathrm{C}}} \mathbf{curl}\,\boldsymbol{G} \cdot \mathbf{grad}\,\overline{\zeta}_n.$$

Moreover, since $\boldsymbol{G}|_{\Omega_{\mathrm{C}}} \in \mathrm{H}^1(\Omega_{\mathrm{C}})^3$ and $\mathbf{grad}\,\zeta_n|_{\Omega_{\mathrm{C}}} \in \mathrm{H}(\mathbf{curl}, \Omega_{\mathrm{C}})$, using a Green's formula,

$$\int_{\Omega_{\mathrm{C}}} \mathbf{curl}\,\boldsymbol{G} \cdot \mathbf{grad}\,\overline{\zeta}_n = \int_{\partial\Omega_{\mathrm{C}}} \mathbf{grad}\,\overline{\zeta}_n \times \boldsymbol{n} \cdot \overline{\boldsymbol{G}} = \int_{\Gamma_{\mathrm{J}}^n} \mathbf{grad}\,\overline{\zeta}_n \times \boldsymbol{n} \cdot \overline{\boldsymbol{G}} = 0,$$

the last equality because ζ_n is constant on Γ_{J}^n. Therefore, $\boldsymbol{G} \in \boldsymbol{\mathcal{V}}(\boldsymbol{0})$ and we can use it to test (1.26).

Since $\boldsymbol{G}$ is null outside Ω_{C} and $\boldsymbol{E} = \frac{1}{\sigma}\,\mathbf{curl}\,\boldsymbol{H}$ in Ω_{C}, using a Green's formula and (1.27) we obtain

$$\sum_{n=N_I+1}^{N} \Delta V_n \langle \mathbf{curl}\,\overline{\boldsymbol{G}}\cdot\boldsymbol{n}, 1\rangle_{\Gamma_{\mathrm{J}}^n} = \int_{\Omega_{\mathrm{C}}} i\omega\mu\boldsymbol{H}\cdot\overline{\boldsymbol{G}} + \int_{\Omega_{\mathrm{C}}} \boldsymbol{E}\cdot\mathbf{curl}\,\overline{\boldsymbol{G}}$$
$$= \langle \boldsymbol{E}\times\boldsymbol{n}, \boldsymbol{G}\rangle_{\partial\Omega_{\mathrm{C}}} = \langle \boldsymbol{E}\times\boldsymbol{n}, \boldsymbol{v}\rangle_{\partial\Omega_{\mathrm{C}}}.$$

On the other hand, for $n = N_I+1,\ldots,N$, let $\zeta_n \in \mathrm{H}^1(\Omega)$ be such that ζ_n vanishes in $\Omega_{\mathrm{C}}\setminus\Omega_{\mathrm{C}}^n$, $\zeta_n = 1$ on Γ_{J}^n and $\zeta_n = 0$ on Γ_{E}^n. If we define $V_* := \sum_{n=N_I+1}^{N}(-\Delta V_n)\,\overline{\zeta}_n|_{\Omega_{\mathrm{C}}} \in \mathrm{H}^1(\Omega_{\mathrm{C}})$, taking into account that $\boldsymbol{G}$ is null in Ω_{D} and applying Green's formulas, we obtain

$$\sum_{n=N_I+1}^{N} \Delta V_n \left\langle \mathbf{curl}\,\overline{\boldsymbol{G}}\cdot\boldsymbol{n}, 1\right\rangle_{\Gamma_{\mathrm{J}}^n} = \left\langle \mathbf{curl}\,\overline{\boldsymbol{G}}\cdot\boldsymbol{n}, \sum_{n=N_I+1}^{N}\overline{\Delta V_n}\zeta_n\right\rangle_{\partial\Omega}$$
$$= -\int_{\Omega_{\mathrm{C}}} \mathbf{curl}\,\overline{\boldsymbol{G}}\cdot\mathbf{grad}\,V_* = -\left\langle \mathbf{grad}\,V_*\times\boldsymbol{n}, \boldsymbol{v}\right\rangle_{\partial\Omega_{\mathrm{C}}}.$$

Thus, from the last two equations, we derive (1.32). □

Remark 1.6. *Let us notice that the current intensities through Γ_{J}^n, $n = N_I+1,\ldots,N$, can be computed from $\boldsymbol{H}$ as follows:*

$$I_n = \int_{\Gamma_{\mathrm{J}}^n} \mathbf{curl}\,\boldsymbol{H}\cdot\boldsymbol{n}, \qquad n = N_I+1,\ldots,N.$$

Our next goal is to prove that Problems 1.1 and 1.3 are equivalent, for what the following lemma will be the main tool. Here and thereafter, for any $\boldsymbol{S}\in\boldsymbol{\mathcal{Y}}$, $\widetilde{\boldsymbol{S}}$ will denote the extension of $\boldsymbol{S}$ by zero to Ω. Notice that $\widetilde{\boldsymbol{S}}\in\boldsymbol{\mathcal{X}}$.

Lemma 1.7. *Let $\boldsymbol{t}_{0,n}\in\mathrm{H}(\mathbf{curl},\Omega)$, $n=1,\ldots,N$, satisfying (1.11)–(1.12). Given $K_n\in\mathbb{C}$, $n=1,\ldots,N_I$, $\boldsymbol{G}\in\boldsymbol{\mathcal{V}}(\boldsymbol{K})$ if and only if there exist $\boldsymbol{S}\in\boldsymbol{\mathcal{Y}}$, $\psi\in\mathrm{H}^1(\Omega)$ and $K_n\in\mathbb{C}$, $n=N_I+1,\ldots,N$, such that $\boldsymbol{G} = \widetilde{\boldsymbol{S}} + \sum_{n=1}^{N} K_n\boldsymbol{t}_{0,n} - \mathbf{grad}\,\psi$. Moreover, in such a case, $K_n = \int_{\Gamma_{\mathrm{J}}^n}\mathbf{curl}\,\boldsymbol{G}\cdot\boldsymbol{n}$, $n=N_I+1,\ldots,N$.*

Proof. Given $\boldsymbol{G}\in\boldsymbol{\mathcal{V}}(\boldsymbol{K})$, let $K_n := \int_{\Gamma_{\mathrm{J}}^n}\mathbf{curl}\,\boldsymbol{G}\cdot\boldsymbol{n}$, $n=N_I+1,\ldots,N$, and $\widehat{\boldsymbol{G}} := \boldsymbol{G} - \sum_{n=1}^{N}K_n\boldsymbol{t}_{0,n}$. We have that $\widehat{\boldsymbol{G}}\in\mathrm{H}(\mathbf{curl},\Omega)$ and it satisfies

$$\begin{aligned}
\mathrm{div}(\mathbf{curl}\,\widehat{\boldsymbol{G}}) &= \boldsymbol{0} \quad && \text{in } \Omega,\\
\mathbf{curl}\,\widehat{\boldsymbol{G}}\cdot\boldsymbol{n} &= 0 \quad && \text{on } \Gamma_{\mathrm{I}},\\
\int_{\Gamma_{\mathrm{J}}^n}\mathbf{curl}\,\widehat{\boldsymbol{G}}\cdot\boldsymbol{n} &= 0 \quad && \text{for } n=1,\ldots,N.
\end{aligned}$$

The equations above allow us to use again Theorem 2.1 from [48] as in the derivation of the $\boldsymbol{T},\phi-\phi$ formulation to obtain $\boldsymbol{S}\in\boldsymbol{\mathcal{Y}}$ which satisfies

$$\begin{aligned}
\mathbf{curl}\,\boldsymbol{S} &= \mathbf{curl}\,\widehat{\boldsymbol{G}} \quad && \text{in } \Omega_{\mathrm{C}},\\
\boldsymbol{S}\times\boldsymbol{n} &= \boldsymbol{0} \quad && \text{on } \Gamma_{\mathrm{I}}.
\end{aligned}$$

Then, $\mathbf{curl}(\widehat{\boldsymbol{G}}-\widetilde{\boldsymbol{S}})=\mathbf{0}$ in Ω, so that, since Ω is simply connected, there exists $\psi\in\mathrm{H}^1(\Omega)$ such that $\widehat{\boldsymbol{G}}=\widetilde{\boldsymbol{S}}-\mathbf{grad}\,\psi$. Thus, $\boldsymbol{G}=\widehat{\boldsymbol{G}}+\sum_{n=1}^{N}K_n\boldsymbol{t}_{0,n}=\widetilde{\boldsymbol{S}}+\sum_{n=1}^{N}K_n\boldsymbol{t}_{0,n}-\mathbf{grad}\,\psi$ in Ω.
Conversely, let $\boldsymbol{G}=\widetilde{\boldsymbol{S}}+\sum_{n=1}^{N}K_n\boldsymbol{t}_{0,n}-\mathbf{grad}\,\psi$, with $\boldsymbol{S}\in\boldsymbol{\mathcal{Y}}$, $\psi\in\mathrm{H}^1(\Omega)$ and $K_n\in\mathbb{C}$, $n=N_I+1,\ldots,N$. Clearly $\boldsymbol{G}\in\mathrm{H}(\mathbf{curl},\Omega)$ and $\mathbf{curl}\,\boldsymbol{G}=\mathbf{0}$ in Ω_{D}, so that $\boldsymbol{G}\in\boldsymbol{\mathcal{X}}$.
Moreover, for $n=1,\ldots,N_I$, we have that

$$\int_{\Gamma_{\mathrm{J}}^n}\mathbf{curl}\,\boldsymbol{G}\cdot\boldsymbol{n}=\int_{\Gamma_{\mathrm{J}}^n}\mathbf{curl}\,\boldsymbol{S}\cdot\boldsymbol{n}+\sum_{m=1}^{N}K_m\int_{\Gamma_{\mathrm{J}}^n}\mathbf{curl}\,\boldsymbol{t}_{0,m}\cdot\boldsymbol{n}=\int_{\Gamma_{\mathrm{J}}^n}\mathbf{curl}\,\boldsymbol{S}\cdot\boldsymbol{n}+K_n.$$

Let $\delta\in\mathcal{C}^\infty(\overline{\Omega})$ be as in Remark 1.2. Then, using a Green's formula, the divergence theorem and Proposition 3.3 from [47], we have that

$$\begin{aligned}\int_{\Gamma_{\mathrm{J}}^n}\mathbf{curl}\,\boldsymbol{S}\cdot\boldsymbol{n}&:=\langle\mathbf{curl}\,\widetilde{\boldsymbol{S}}\cdot\boldsymbol{n},\delta\rangle_{\mathrm{H}^{-1/2}(\partial\Omega)\times\mathrm{H}^{1/2}(\partial\Omega)}\\&=\int_{\Omega}\mathbf{curl}\,\widetilde{\boldsymbol{S}}\cdot\mathbf{grad}\,\overline{\delta}=-\langle\widetilde{\boldsymbol{S}}\times\boldsymbol{n},\mathbf{grad}_\tau\,\delta\rangle_{\mathrm{H}^{-1/2}(\partial\Omega)^3\times\mathrm{H}^{1/2}(\partial\Omega)^3}\\&=-\langle\widetilde{\boldsymbol{S}}\times\boldsymbol{n},\mathbf{grad}_\tau\,\delta\rangle_{\mathrm{H}^{-1/2}(\Gamma_{\mathrm{D}})^3\times\mathrm{H}^{1/2}(\Gamma_{\mathrm{D}})^3}\\&\qquad-\langle\widetilde{\boldsymbol{S}}^n\times\boldsymbol{n},\mathbf{grad}_\tau\,\delta\rangle_{\mathrm{H}^{-1/2}(\Gamma_{\mathrm{E}}\cup\Gamma_{\mathrm{J}})^3\times\mathrm{H}^{1/2}(\Gamma_{\mathrm{E}}\cup\Gamma_{\mathrm{J}})^3}=0,\end{aligned}$$

where for the last equality we have used that $\widetilde{\boldsymbol{S}}=\mathbf{0}$ in Ω_{D} and δ is constant on each connected component of $\Gamma_{\mathrm{E}}\cup\Gamma_{\mathrm{J}}$ (see Remark 1.2). Hence, $K_n=\int_{\Gamma_{\mathrm{J}}^n}\mathbf{curl}\,\boldsymbol{G}\cdot\boldsymbol{n}$, $n=1,\ldots,N$, so that, in particular, $\boldsymbol{G}\in\boldsymbol{\mathcal{V}}(\boldsymbol{K})$. □

Taking the previous decomposition into account, we have that solving Problem 1.1 is equivalent to solving Problem 1.3. In fact, we have the following result:

Theorem 1.8. *Let $\boldsymbol{t}_{0,n}\in\mathrm{H}(\mathbf{curl},\Omega)$, $n=1,\ldots,N$, satisfying (1.11)–(1.12). Let $I_n\in\mathbb{C}$, $n=1,\ldots,N_I$, and $\Delta V_n\in\mathbb{C}$, $n=N_I+1,\ldots,N$. Any solution $(\boldsymbol{T},\phi,I_{N_I+1},\ldots,I_N)$ to Problem 1.1 leads to the unique magnetic field $\boldsymbol{H}:=\widetilde{\boldsymbol{T}}+\sum_{n=1}^{N}I_n\boldsymbol{t}_{0,n}-\mathbf{grad}\,\phi$ that solves Problem 1.3. Conversely, the solution $\boldsymbol{H}$ to Problem 1.3 can be written as $\boldsymbol{H}=\widetilde{\boldsymbol{T}}+\sum_{n=1}^{N}I_n\boldsymbol{t}_{0,n}-\mathbf{grad}\,\phi$, with $(\boldsymbol{T},\phi,I_{N_I+1},\ldots,I_N)$ being a solution to Problem 1.1.*

Proof. Let $(\boldsymbol{T},\phi,I_{N_I+1},\ldots,I_N)$ be a solution to Problem 1.1 and $\boldsymbol{H}:=\widetilde{\boldsymbol{T}}+\sum_{n=1}^{N}I_n\boldsymbol{t}_{0,n}-\mathbf{grad}\,\phi$. According to Lemma 1.7, $\boldsymbol{H}\in\boldsymbol{\mathcal{V}}(\boldsymbol{I})$. Let $\boldsymbol{G}\in\boldsymbol{\mathcal{V}}(\mathbf{0})$. We use Lemma 1.7 to write $\boldsymbol{G}=\widetilde{\boldsymbol{S}}+\sum_{n=N_I+1}^{N}K_n\boldsymbol{t}_{0,n}-\mathbf{grad}\,\psi$ with $\boldsymbol{S}\in\boldsymbol{\mathcal{Y}}$ and $\psi\in\mathrm{H}^1(\Omega)$. Hence, (1.26) follows by adding equalities (1.23), (1.24) and (1.25). Then, $\boldsymbol{H}$ is the solution to Problem 1.3.
Conversely, let $\boldsymbol{H}$ be the unique solution to Problem 1.3. According to Lemma 1.7, we write $\boldsymbol{H}=\widetilde{\boldsymbol{T}}+\sum_{n=1}^{N}I_n\boldsymbol{t}_{0,n}-\mathbf{grad}\,\phi$ with $\boldsymbol{T}\in\boldsymbol{\mathcal{Y}}$, $\phi\in\mathrm{H}^1(\Omega)$ and $I_n\in\mathbb{C}$, $n=N_I+1,\ldots,N$. Then, by substituting this expression in (1.26) and taking separately test functions $\boldsymbol{G}=\widetilde{\boldsymbol{S}}$ for $\boldsymbol{S}\in\boldsymbol{\mathcal{Y}}$, $\boldsymbol{G}=\mathbf{grad}\,\psi$ for $\psi\in\mathrm{H}^1(\Omega)$ and $\boldsymbol{G}=\boldsymbol{t}_{0,n}$, $n=N_I+1,\ldots,N$, we check that $(\boldsymbol{T},\phi,I_{N_I+1},\ldots,I_N)$ is a solution to Problem 1.1. □

Remark 1.9. *The decomposition $\boldsymbol{H}=\widetilde{\boldsymbol{T}}+\sum_{n=1}^{N}I_n\boldsymbol{t}_{0,n}-\mathbf{grad}\,\phi$ used in the above results is not unique. Therefore, Problem 1.1 is not well-posed since it has multiple solutions $(\boldsymbol{T},\phi,I_{N_I+1},\ldots,I_N)$; however, $\boldsymbol{H}:=\widetilde{\boldsymbol{T}}+\sum_{n=1}^{N}I_n\boldsymbol{t}_{0,n}-\mathbf{grad}\,\phi$ is uniquely determined for all of them. Furthermore, from the computational point of view, it could be interesting to obtain*

one particular solution to this underdetermined problem because, to do this, the more expensive vector unknown has to be computed only in conductors. Moreover, another advantage of the $\boldsymbol{T}, \phi - \phi$ *formulation with respect to an* $\boldsymbol{H}, \phi$ *formulation is that it does not involve a multivalued potential, what would require the construction of cutting surfaces.*

1.4.2 Finite Element Discretisation

In this section we will introduce a discretisation of Problem 1.1 and proceed as in the previous subsection for its analysis. In this subsection, we assume that Ω, Ω_{C} and Ω_{D} are Lipschitz polyhedra and consider regular tetrahedral meshes $\mathcal{T}_h$ of Ω such that each element $T \in \mathcal{T}_h$ is contained either in $\overline{\Omega}_{\mathrm{C}}$ or in $\overline{\Omega}_{\mathrm{D}}$ (h stands as usual for the corresponding mesh-size). Therefore, $\mathcal{T}_h(\Omega_{\mathrm{D}}) := \left\{T \in \mathcal{T}_h : \ T \subset \overline{\Omega}_{\mathrm{D}}\right\}$ and $\mathcal{T}_h(\Omega_{\mathrm{C}}) := \left\{T \in \mathcal{T}_h : \ T \subset \overline{\Omega}_{\mathrm{C}}\right\}$ are meshes of Ω_{D} and Ω_{C}, respectively.

We employ edge finite elements to approximate the current vector potential $\boldsymbol{T}$, more precisely, lowest-order Nédélec finite elements:

$$\boldsymbol{\mathcal{N}}_h(\Omega_{\mathrm{C}}) := \{\boldsymbol{G}_h \in \mathrm{H}(\mathbf{curl}, \Omega_{\mathrm{C}}) : \ \boldsymbol{G}_h|_T \in \boldsymbol{\mathcal{N}}(T) \ \forall T \in \mathcal{T}_h(\Omega_{\mathrm{C}})\},$$

where, for each tetrahedron T,

$$\boldsymbol{\mathcal{N}}(T) := \left\{\boldsymbol{G}_h \in \mathbb{P}_1^3(T) : \ \boldsymbol{G}_h(\boldsymbol{x}) = \mathbf{a} \times \boldsymbol{x} + \mathbf{b}, \ \mathbf{a}, \mathbf{b} \in \mathbb{C}^3, \ \boldsymbol{x} \in T\right\}.$$

For the magnetic potential ϕ we use standard finite elements:

$$\mathcal{L}_h(\Omega) := \left\{\psi_h \in \mathrm{H}^1(\Omega) : \ \psi_h|_T \in \mathbb{P}_1(T) \quad \forall T \in \mathcal{T}_h\right\},$$

We introduce the discrete subspace of $\boldsymbol{\mathcal{Y}}$,

$$\boldsymbol{\mathcal{Y}}_h := \{\boldsymbol{G}_h \in \boldsymbol{\mathcal{N}}_h(\Omega_{\mathrm{C}}) \ : \ \boldsymbol{G}_h \times \boldsymbol{n} = \mathbf{0} \text{ on } \Gamma_{\mathrm{I}}\},$$

We also introduce discrete normalised impressed vector potentials $\boldsymbol{t}_{0,n}^h \in \boldsymbol{\mathcal{N}}_h(\Omega)$, $n = 1, \ldots, N$, satisfying

$$\int_{\Gamma_{\mathrm{J}}^n} \mathbf{curl}\, \boldsymbol{t}_{0,n}^h \cdot \boldsymbol{n} = 1, \tag{1.33}$$

$$\mathbf{curl}\, \boldsymbol{t}_{0,n}^h = \mathbf{0} \quad \text{in } \overline{\Omega \setminus \Omega_{\mathrm{C}}^n} \tag{1.34}$$

and a discrete impressed vector potential $\boldsymbol{T}_0^h := \sum_{n=1}^N I_n \boldsymbol{t}_{0,n}^h \in \boldsymbol{\mathcal{N}}_h(\Omega)$. We describe in next section how such $\boldsymbol{t}_{0,n}^h$, $n = 1, \ldots, N$, can be computed in practice.

Then, the discretisation of Problem 1.1 reads as follows:

Problem 1.10. *Let* $\boldsymbol{t}_{0,n}^h \in \boldsymbol{\mathcal{N}}_h(\Omega)$, $n = 1, \ldots, N$, *satisfying (1.33)–(1.34). Given* $I_n \in \mathbb{C}$, $n = 1, \ldots, N_I$, *and* $\Delta V_n \in \mathbb{C}$, $n = N_I + 1, \ldots, N$, *find* $\boldsymbol{T}_h \in \boldsymbol{\mathcal{Y}}_h$, $\phi_h \in \mathcal{L}_h(\Omega)$ *and* $I_n^h \in \mathbb{C}$ *for*

$n = N_I + 1, \dots, N$ *such that*

$$\int_{\Omega_{\mathrm{C}}} i\omega\mu(\boldsymbol{T}_h - \mathbf{grad}\,\phi_h)\cdot\overline{\boldsymbol{S}}_h + \int_{\Omega_{\mathrm{C}}}\frac{1}{\sigma}\,\mathbf{curl}\,\boldsymbol{T}_h\cdot\mathbf{curl}\,\overline{\boldsymbol{S}}_h + \sum_{n=N_I+1}^{N} I_n^h\left(\int_{\Omega_{\mathrm{C}}} i\omega\mu\boldsymbol{t}_{0,n}^h\cdot\overline{\boldsymbol{S}}_h + \int_{\Omega_{\mathrm{C}}}\frac{1}{\sigma}\,\mathbf{curl}\,\boldsymbol{t}_{0,n}^h\cdot\mathbf{curl}\,\overline{\boldsymbol{S}}_h\right) = -\sum_{n=1}^{N_I} I_n\left(\int_{\Omega_{\mathrm{C}}} i\omega\mu\boldsymbol{t}_{0,n}^h\cdot\overline{\boldsymbol{S}}_h + \int_{\Omega_{\mathrm{C}}}\frac{1}{\sigma}\,\mathbf{curl}\,\boldsymbol{t}_{0,n}^h\cdot\mathbf{curl}\,\overline{\boldsymbol{S}}_h\right)\quad\forall\,\boldsymbol{S}_h\in\boldsymbol{\mathcal{Y}}_h,\quad(1.35)$$

$$-\int_{\Omega_{\mathrm{C}}} i\omega\mu\boldsymbol{T}_h\cdot\mathbf{grad}\,\overline{\psi}_h + \int_{\Omega} i\omega\mu\,\mathbf{grad}\,\phi_h\cdot\mathbf{grad}\,\overline{\psi}_h - \sum_{n=N_I+1}^{N} I_n^h\int_{\Omega} i\omega\mu\boldsymbol{t}_{0,n}^h\cdot\mathbf{grad}\,\overline{\psi}_h = \sum_{n=1}^{N_I} I_n\int_{\Omega} i\omega\mu\boldsymbol{t}_{0,n}^h\cdot\mathbf{grad}\,\overline{\psi}_h\quad\forall\,\psi_h\in\mathcal{L}_h(\Omega),\quad(1.36)$$

$$\left(\int_{\Omega_{\mathrm{C}}} i\omega\mu\boldsymbol{T}_h\cdot\bar{\boldsymbol{t}}_{0,m}^h - \int_{\Omega} i\omega\mu\,\mathbf{grad}\,\phi_h\cdot\bar{\boldsymbol{t}}_{0,m}^h + \int_{\Omega_{\mathrm{C}}^m}\frac{1}{\sigma}\,\mathbf{curl}\,\boldsymbol{T}_h\cdot\mathbf{curl}\,\bar{\boldsymbol{t}}_{0,m}^h + \sum_{n=N_I+1}^{N} I_n^h\int_{\Omega} i\omega\mu\boldsymbol{t}_{0,n}^h\cdot\bar{\boldsymbol{t}}_{0,m}^h + I_m^h\int_{\Omega_{\mathrm{C}}^m}\frac{1}{\sigma}|\,\mathbf{curl}\,\boldsymbol{t}_{0,m}^h|^2\right)\overline{K}_m = \Delta V_m\overline{K}_m - \left(\sum_{n=1}^{N_I} I_n\int_{\Omega} i\omega\mu\boldsymbol{t}_{0,n}^h\cdot\bar{\boldsymbol{t}}_{0,m}^h\right)\overline{K}_m\quad\forall\,K_m\in\mathbb{C},\quad m = N_I+1,\dots,N.\quad(1.37)$$

As in the continuous case, Problem 1.10 has infinitely many solutions, but any of them will be useful for our purpose.

Again, we will perform the mathematical analysis of the above problem by proving its equivalence with a discrete version of Problem 1.3. To this end, let us consider the following discrete subspaces:

$$\boldsymbol{\mathcal{X}}_h := \{\boldsymbol{G}_h\in\boldsymbol{\mathcal{N}}_h(\Omega)\,:\,\mathbf{curl}\,\boldsymbol{G}_h = \mathbf{0}\ \text{in}\ \Omega_{\mathrm{D}}\}\subset\boldsymbol{\mathcal{X}},$$
$$\boldsymbol{\mathcal{V}}_h(\boldsymbol{K}) := \left\{\boldsymbol{G}_h\in\boldsymbol{\mathcal{X}}_h\,:\,\int_{\Gamma_{\mathrm{J}}^n}\mathbf{curl}\,\boldsymbol{G}_h\cdot\boldsymbol{n} = K_n,\ n = 1,\dots,N_I\right\}\subset\boldsymbol{\mathcal{V}}(\boldsymbol{K}).$$

Then, Problem 1.3 is discretised as follows:

Problem 1.11. *Given* $I_n\in\mathbb{C}$, $n = 1,\dots,N_I$, *and* $\Delta V_n\in\mathbb{C}$, $n = N_I+1,\dots,N$, *find* $\boldsymbol{H}_h\in\boldsymbol{\mathcal{V}}_h(\boldsymbol{I})$ *such that*

$$\int_{\Omega} i\omega\mu\boldsymbol{H}_h\cdot\overline{\boldsymbol{G}}_h + \int_{\Omega_{\mathrm{C}}}\frac{1}{\sigma}\,\mathbf{curl}\,\boldsymbol{H}_h\cdot\mathbf{curl}\,\overline{\boldsymbol{G}}_h = \sum_{n=N_I+1}^{N}\Delta V_n\int_{\Gamma_{\mathrm{J}}^n}\mathbf{curl}\,\overline{\boldsymbol{G}}_h\cdot\boldsymbol{n}\quad\forall\,\boldsymbol{G}_h\in\boldsymbol{\mathcal{V}}_h(\mathbf{0}).\quad(1.38)$$

We have the following result.

Theorem 1.12. *Problem 1.11 has a unique solution $\boldsymbol{H}_h$. Moreover, if the solution to Problem 1.3 satisfies $\boldsymbol{H}|_{\Omega_{\mathrm{C}}} \in \mathrm{H}^r(\mathbf{curl}, \Omega_{\mathrm{C}})$ and $\boldsymbol{H}|_{\Omega_{\mathrm{D}}} \in \mathrm{H}^r(\Omega_{\mathrm{D}})^3$ with $r \in \left(\frac{1}{2}, 1\right]$, then the following error estimate holds*

$$\|\boldsymbol{H} - \boldsymbol{H}_h\|_{\mathrm{H}(\mathbf{curl},\Omega)} \leq Ch^r \left[\|\boldsymbol{H}\|_{\mathrm{H}^r(\mathbf{curl},\Omega_{\mathrm{C}})} + \|\boldsymbol{H}\|_{\mathrm{H}^r(\Omega_{\mathrm{D}})^3}\right],$$

where C is a strictly positive constant independent of h and $\boldsymbol{H}$.

Proof. Since the sesquilinear form in the left hand side of (1.38) is continuous and $\boldsymbol{\mathcal{X}}_h-$elliptic, the only thing to prove in order to obtain the well-posedness of Problem 1.11 is that $\boldsymbol{\mathcal{V}}_h(\boldsymbol{I}) \neq \emptyset$. This proof is very similar to the one appearing in Section 4 of [24], but we include it here for the sake of completeness. Indeed, for $n = 1, \ldots, N_I$, let $\widehat{\boldsymbol{H}}_h^n \in \boldsymbol{\mathcal{X}}_h$ be such that $\int_{\partial\Gamma_{\mathrm{J}}^j} \widehat{\boldsymbol{H}}_h^n \cdot \boldsymbol{\tau}_j = \delta_{jn}$ for $j = 1, \ldots, N$. In Remark 5.3 from [24], a basis of $\boldsymbol{\mathcal{X}}_h$ under our geometrical assumptions is given, from which such $\widehat{\boldsymbol{H}}_h^n$ are easy to construct. Then we define

$$\widehat{\boldsymbol{H}}_h := \sum_{n=1}^{N_I} I_n \widehat{\boldsymbol{H}}_h^n.$$

Hence,

$$\int_{\Gamma_{\mathrm{J}}^j} \mathbf{curl}\, \widehat{\boldsymbol{H}}_h \cdot \boldsymbol{n} = \int_{\partial\Gamma_{\mathrm{J}}^j} \widehat{\boldsymbol{H}}_h \cdot \boldsymbol{\tau}_j = \sum_{n=1}^{N_I} I_n \int_{\partial\Gamma_{\mathrm{J}}^j} \widehat{\boldsymbol{H}}_h^n \cdot \boldsymbol{\tau}_j = I_j.$$

Thus, $\widehat{\boldsymbol{H}}_h \in \boldsymbol{\mathcal{V}}(\boldsymbol{I})$.
On the other hand, concerning the error estimate, it follows from the ellipticity of the sesquilinear form, Céa's lemma and standard error estimates for edge elements. □

To the best of the authors' knowledge, the regularity of $\boldsymbol{H}$ assumed in the second part of Theorem 1.12 has not been proved. Indeed, as shown in Theorem 1.5, the solution $\boldsymbol{H}$ to Problem 1.3 satisfies $\mathrm{div}(\mu H) = 0$ in Ω and $\mu\boldsymbol{H} \cdot \boldsymbol{n} = 0$ on $\partial\Omega$. Therefore, when μ is constant in the whole domain Ω, according to [9, Proposition 3.7], $\boldsymbol{H} \in \mathrm{H}^r(\Omega)^3$ for some $r > 1/2$. However, even in this case, it is not known whether $\mathbf{curl}\, \boldsymbol{H} \in \mathrm{H}^r(\Omega_{\mathrm{C}})^3$.

The following characterization is the discrete analogue to Lemma 1.7.

Lemma 1.13. *Let $\boldsymbol{t}_{0,n}^h \in \boldsymbol{\mathcal{N}}_h(\Omega)$, $n = 1, \ldots, N$, satisfying (1.33)–(1.34). Given $K_n \in \mathbb{C}$, $n = 1, \ldots, N_I$, a discrete field $\boldsymbol{G}_h \in \boldsymbol{\mathcal{V}}_h(\boldsymbol{K})$ if and only if there exist $\boldsymbol{S}_h \in \boldsymbol{\mathcal{Y}}_h$, $\psi_h \in \mathcal{L}_h(\Omega)$ and $K_n^h \in \mathbb{C}$, $n = N_I+1, \ldots, N$, such that $\boldsymbol{G}_h = \widetilde{\boldsymbol{S}}_h + \sum_{n=1}^{N_I} K_n \boldsymbol{t}_{0,n}^h + \sum_{n=N_I+1}^{N} K_n^h \boldsymbol{t}_{0,n}^h - \mathbf{grad}\, \psi_h$. Moreover, $K_n^h = \int_{\Gamma_{\mathrm{J}}^n} \mathbf{curl}\, \boldsymbol{G}_h \cdot \boldsymbol{n}$, $n = N_I + 1, \ldots, N$.*

Proof. Given $\boldsymbol{G}_h \in \boldsymbol{\mathcal{V}}_h(\boldsymbol{K})$, let $K_n^h := \int_{\Gamma_{\mathrm{J}}^n} \mathbf{curl}\, \boldsymbol{G}_h \cdot \boldsymbol{n}$, $n = N_I + 1, \ldots, N$, and $\widehat{\boldsymbol{G}}_h := \boldsymbol{G}_h - \sum_{n=1}^{N_I} K_n \boldsymbol{t}_{0,n}^h - \sum_{n=N_I+1}^{N} K_n^h \boldsymbol{t}_{0,n}^h$. Then, $\widehat{\boldsymbol{G}}_h \in \boldsymbol{\mathcal{N}}_h(\Omega)$, $\mathbf{curl}\, \widehat{\boldsymbol{G}}_h = \boldsymbol{0}$ in Ω_{D} and $\int_{\Gamma_{\mathrm{J}}^n} \mathbf{curl}\, \widehat{\boldsymbol{G}}_h \cdot \boldsymbol{n} = 0$, $n = 1, \ldots, N$.

Let us recall that we denote $\widetilde{\Omega}_{\mathrm{D}} := \Omega_{\mathrm{D}} \setminus \bigcup_{n=1}^{N} \Sigma_n$ the simply connected domain obtained by removing the cut surfaces Σ_n, $n = 1, \ldots, N$, from Ω_{D}. We assume that surfaces Σ_n are polyhedral and the meshes are compatible with them in the sense that each Σ_n is a union of faces of tetrahedra $T \in \mathcal{T}_h$. Therefore, $\mathcal{T}_h(\Omega_{\mathrm{D}})$ can also be seen as a mesh of $\widetilde{\Omega}_{\mathrm{D}}$. Each function $\widehat{\psi} \in \mathrm{H}^1(\widetilde{\Omega}_{\mathrm{D}})$ has, in general, different traces on each side of Σ_n and we denote by

$$[\![\widehat{\psi}]\!]_{\Sigma_n} := \widehat{\psi}|_{\Sigma_n^-} - \widehat{\psi}|_{\Sigma_n^+}$$

the jump of $\widehat{\psi}$ through Σ_n along $\boldsymbol{n}_n$. Moreover, the gradient of $\widehat{\psi}$ in $\mathcal{D}'(\widetilde{\Omega}_{\mathrm{D}})$ can be extended to $\mathrm{L}^2(\Omega_{\mathrm{D}})^3$ and will be denoted by $\widetilde{\mathbf{grad}}\, \widehat{\psi}$.
Let us introduce the space:

$$\mathcal{L}_h(\widetilde{\Omega}_{\mathrm{D}}) := \left\{ \widehat{\psi}_h \in \mathrm{H}^1(\widetilde{\Omega}_{\mathrm{D}}) : \ \widehat{\psi}_h|_T \in \mathbb{P}_1(T) \quad \forall T \in \mathcal{T}_h(\Omega_{\mathrm{D}}) \right\},$$

and the subspace

$$\Theta_h := \left\{ \widehat{\psi}_h \in \mathcal{L}_h(\widetilde{\Omega}_{\mathrm{D}}) : \ [\![\widehat{\psi}_h]\!]_{\Sigma_n} = \text{constant}, n = 1, \ldots, N \right\}.$$

Since $\widehat{\boldsymbol{G}}_h|_{\Omega_{\mathrm{D}}} \in \boldsymbol{\mathcal{N}}_h(\Omega_{\mathrm{D}})$ is such that $\mathbf{curl}\, \widehat{\boldsymbol{G}}_h|_{\Omega_{\mathrm{D}}} = \mathbf{0}$, according to Lemma 5.5 from [29], there exists $\widehat{\psi}_h \in \Theta_h$ such that $\widehat{\boldsymbol{G}}_h|_{\Omega_{\mathrm{D}}} = -\widetilde{\mathbf{grad}}\, \widehat{\psi}_h$. Moreover, by using Stokes' theorem,

$$0 = \int_{\Gamma_{\mathrm{J}}^n} \mathbf{curl}\, \widehat{\boldsymbol{G}}_h \cdot \boldsymbol{n} = \int_{\gamma_n} \widehat{\boldsymbol{G}}_h \cdot \boldsymbol{\tau}_n = \int_{\gamma_n} \widetilde{\mathbf{grad}}\, \widehat{\psi}_h \cdot \boldsymbol{\tau}_n = [\![\widehat{\psi}_h]\!]_{\Sigma_n},$$

which implies that $\widehat{\psi}_h$ does not have jumps across the cut interfaces Σ_n, $n = 1, \ldots, N$, and hence $\widehat{\psi}_h \in \mathcal{L}_h(\Omega_{\mathrm{D}})$ and $\widehat{\boldsymbol{G}}_h|_{\Omega_{\mathrm{D}}} = -\mathbf{grad}\, \widehat{\psi}_h$. Let $\psi_h \in \mathcal{L}_h(\Omega)$ be any extension of $\widehat{\psi}_h$ to Ω and $\boldsymbol{S}_h := \widehat{\boldsymbol{G}}_h|_{\Omega_{\mathrm{C}}} + \mathbf{grad}\, \psi_h|_{\Omega_{\mathrm{C}}} \in \boldsymbol{\mathcal{N}}_h(\Omega_{\mathrm{C}})$. Since $\widehat{\boldsymbol{G}}_h = -\mathbf{grad}\, \psi_h$ in Ω_{D}, we have that $\widehat{\boldsymbol{G}}_h \times \boldsymbol{n} = -\mathbf{grad}\, \psi_h \times \boldsymbol{n}$ on Γ_{I}. Therefore,

$$\boldsymbol{S}_h \times \boldsymbol{n} = \widehat{\boldsymbol{G}}_h \times \boldsymbol{n} + \mathbf{grad}\, \psi_h \times \boldsymbol{n} = \mathbf{0} \quad \text{on } \Gamma_{\mathrm{I}}.$$

Then, $\boldsymbol{G}_h = \widetilde{\boldsymbol{S}}_h + \sum_{n=1}^{N_I} K_n \boldsymbol{t}_{0,n}^h + \sum_{n=N_I+1}^{N} K_n^h \boldsymbol{t}_{0,n}^h - \mathbf{grad}\, \psi_h$, with $\boldsymbol{S}_h \in \boldsymbol{\mathcal{Y}}_h$ and $\psi_h \in \mathcal{L}_h(\Omega)$. Conversely, let $\boldsymbol{G}_h = \widetilde{\boldsymbol{S}}_h + \sum_{n=1}^{N_I} K_n \boldsymbol{t}_{0,n}^h + \sum_{n=N_I+1}^{N} K_n^h \boldsymbol{t}_{0,n}^h - \mathbf{grad}\, \psi_h$ with $\boldsymbol{S}_h \in \boldsymbol{\mathcal{Y}}_h$, $\psi_h \in \mathcal{L}_h(\Omega)$ and $K_n \in \mathbb{C}$, $n = N_I + 1, \ldots, N$. Clearly, $\boldsymbol{G}_h \in \boldsymbol{\mathcal{X}}_h$. Moreover, since $\boldsymbol{S}_h \in \boldsymbol{\mathcal{Y}}_h$, by Stokes' theorem

$$\int_{\Gamma_{\mathrm{J}}^n} \mathbf{curl}\, \boldsymbol{S}_h \cdot \boldsymbol{n} = \int_{\gamma_n} \boldsymbol{S}_h \cdot \boldsymbol{\tau}_n = 0, \quad n = 1, \ldots, N.$$

Therefore,

$$\int_{\Gamma_{\mathrm{J}}^m} \mathbf{curl}\, \boldsymbol{G}_h \cdot \boldsymbol{n} = \sum_{n=1}^{N_I} K_n \int_{\Gamma_{\mathrm{J}}^m} \mathbf{curl}\, \boldsymbol{t}_{0,n}^h \cdot \boldsymbol{n} + \sum_{n=N_I+1}^{N} K_n^h \int_{\Gamma_{\mathrm{J}}^m} \mathbf{curl}\, \boldsymbol{t}_{0,n}^h \cdot \boldsymbol{n} = K_m, \quad m = 1, \ldots, N_I,$$

$$\int_{\Gamma_{\mathrm{J}}^m} \mathbf{curl}\, \boldsymbol{G}_h \cdot \boldsymbol{n} = \sum_{n=1}^{N_I} K_n \int_{\Gamma_{\mathrm{J}}^m} \mathbf{curl}\, \boldsymbol{t}_{0,n}^h \cdot \boldsymbol{n} + \sum_{n=N_I+1}^{N} K_n^h \int_{\Gamma_{\mathrm{J}}^m} \mathbf{curl}\, \boldsymbol{t}_{0,n}^h \cdot \boldsymbol{n} = K_m^h, \quad m = N_I + 1, \ldots, N.$$

Consequently, $\boldsymbol{G}_h \in \boldsymbol{\mathcal{V}}_h(\boldsymbol{K})$ and we finish the proof. □

Taking the previous decomposition into account, we conclude that solving Problem 1.10 is equivalent to solving Problem 1.11.

Theorem 1.14. *Let $\boldsymbol{t}_{0,n}^h \in \boldsymbol{\mathcal{N}}_h(\Omega)$, $n = 1, \ldots, N$, satisfying (1.33)–(1.34). Let $I_n \in \mathbb{C}$, $n = 1, \ldots, N_I$, and $\Delta V_n \in \mathbb{C}$, $n = N_I + 1, \ldots, N$. If $(\boldsymbol{T}_h, \phi_h, I_{N_I+1}^h, \ldots, I_N^h)$ is a solution to Problem 1.10, then $\boldsymbol{H}_h := \widetilde{\boldsymbol{T}}_h + \sum_{n=1}^{N_I} I_n \boldsymbol{t}_{0,n}^h + \sum_{n=N_I+1}^{N} I_n^h \boldsymbol{t}_{0,n}^h - \mathbf{grad}\, \phi_h$ solves Problem 1.11. Conversely, if $\boldsymbol{H}_h$ is the solution to Problem 1.11, then it can be written as $\boldsymbol{H}_h = \widetilde{\boldsymbol{T}}_h + \sum_{n=1}^{N_I} I_n \boldsymbol{t}_{0,n}^h + \sum_{n=N_I+1}^{N} I_n^h \boldsymbol{t}_{0,n}^h - \mathbf{grad}\, \phi_h$, with $(\boldsymbol{T}_h, \phi_h, I_{N_I+1}^h, \ldots, I_N^h)$ being a solution to Problem 1.10.*

Proof. Let $(\boldsymbol{T}_h, \phi_h, I_{N_I+1}^h, \ldots, I_N^h)$ be a solution to Problem 1.10 and

$$\boldsymbol{H}_h := \widetilde{\boldsymbol{T}}_h + \sum_{n=1}^{N_I} I_n \boldsymbol{t}_{0,n}^h + \sum_{n=N_I+1}^{N} I_n^h \boldsymbol{t}_{0,n}^h - \mathbf{grad}\, \phi_h.$$

According to Lemma 1.13, $\boldsymbol{H}_h \in \boldsymbol{\mathcal{V}}_h(\boldsymbol{I})$. Let $\boldsymbol{G}_h \in \boldsymbol{\mathcal{V}}_h(\boldsymbol{0})$. Using again Lemma 1.13, we have that there exist $\boldsymbol{S}_h \in \boldsymbol{\mathcal{Y}}_h$, $\psi_h \in \mathcal{L}_h(\Omega)$ and $K_n^h \in \mathbb{C}$, $n = N_I + 1, \ldots, N$ such that $\boldsymbol{G}_h = \widetilde{\boldsymbol{S}}_h + \sum_{n=N_I+1}^{N} K_n^h \boldsymbol{t}_{0,n}^h - \mathbf{grad}\, \psi_h$. Then, by testing equations (1.35), (1.36) and (1.37) with $\boldsymbol{S}_h$, ψ_h and $K_{N_I+1}^h, \ldots, K_N^h$, respectively, and adding the resulting equations, it is easy to check (1.38). Thus, $\boldsymbol{H}_h$ is the solution to Problem 1.11.
Conversely, let $\boldsymbol{H}_h$ be the solution to Problem 1.11. According to Lemma 1.13, there exist $\boldsymbol{T}_h \in \boldsymbol{\mathcal{Y}}_h$, $\phi_h \in \mathcal{L}_h(\Omega)$ and $I_n^h \in \mathbb{C}$, $n = N_I + 1, \ldots, N$, such that $\boldsymbol{H}_h = \widetilde{\boldsymbol{T}}_h + \sum_{n=1}^{N_I} I_n \boldsymbol{t}_{0,n}^h + \sum_{n=N_I+1}^{N} I_n^h \boldsymbol{t}_{0,n}^h - \mathbf{grad}\, \phi_h$. Moreover, $I_n^h = \int_{\Gamma_J^n} \mathbf{curl}\, \boldsymbol{H}_h \cdot \boldsymbol{n}$, $n = N_I + 1, \ldots, N$. Substituting $\boldsymbol{H}_h$ by this expression in (1.38) and testing the resulting equation successively with $\boldsymbol{G}_h = \widetilde{\boldsymbol{S}}_h$ for $\boldsymbol{S}_h \in \boldsymbol{\mathcal{Y}}_h$, $\boldsymbol{G}_h = \mathbf{grad}\, \psi_h$ for $\psi_h \in \mathcal{L}_h(\Omega)$ and $\boldsymbol{G}_h = \boldsymbol{t}_{0,m}^h$, $m = N_I + 1, \ldots, N$, we obtain equations (1.35), (1.36) and (1.37), respectively. Thus $(\boldsymbol{T}_h, \phi_h, I_{N_I+1}, \ldots, I_N)$ is a solution to Problem 1.10. □

Remark 1.15. *The decomposition of the solution to Problem 1.11, $\boldsymbol{H}_h = \widetilde{\boldsymbol{T}}_h + \sum_{n=1}^{N_I} I_n \boldsymbol{t}_{0,n}^h + \sum_{n=N_I+1}^{N} I_n^h \boldsymbol{t}_{0,n}^h - \mathbf{grad}\, \phi_h$, is not unique and, therefore, Problem 1.10 is not well posed. Actually, Problem 1.10 has infinitely many solutions, all of them leading to the same approximated magnetic field $\boldsymbol{H}_h$. In order to obtain a particular solution to this problem one could use an iterative method like biconjugate gradient, which is the one that we have used in our numerical tests.*

1.5 Mathematical Analysis and Numerical of the Gauged $\boldsymbol{T}, \phi - \phi$ Formulation

Now, we will deal with the $\boldsymbol{T}, \phi - \phi$ formulation incorporating gauge conditions (1.18)–(1.19). Similarly to the ungauged case, we introduce first the weak formulation of problem (1.14)–(1.19). For equations (1.14)–(1.17), we use the same arguments as in the previous section. On the other hand, if we test equation (1.18) with a function $\zeta \in \mathrm{H}^1(\Omega_C)$ such that $\zeta = 0$ on Γ_I,

using a Green's formula and (1.19) we obtain:

$$\int_{\Omega_{\mathrm{C}}} \boldsymbol{T} \cdot \mathbf{grad}\, \overline{\zeta} = 0.$$

Thus, defining

$$\mathcal{Z} := \{\zeta \in \mathrm{H}^1(\Omega_{\mathrm{C}}) \,:\, \zeta = 0 \text{ on } \Gamma_{\mathrm{I}}\},$$

equations (1.14)–(1.17), along with the gauge conditions (1.18)–(1.19), lead us to the following problem:

Problem 1.16. *Let $\boldsymbol{t}_{0,n} \in \mathrm{H}(\mathbf{curl}, \Omega)$, $n = 1, \ldots, N$, satisfying (1.11)–(1.12). Given $I_n \in \mathbb{C}$, $n = 1, \ldots, N_I$, and $\Delta V_n \in \mathbb{C}$, $n = N_I + 1, \ldots, N$, find $\boldsymbol{T} \in \boldsymbol{\mathcal{Y}}$, $\phi \in \mathrm{H}^1(\Omega)/\mathbb{C}$, $\xi \in \mathcal{Z}$ and $I_n \in \mathbb{C}$ for $n = N_I + 1, \ldots, N$ such that*

$$\begin{aligned}\int_{\Omega_{\mathrm{C}}} i\omega\mu(\boldsymbol{T} - \mathbf{grad}\,\phi) \cdot \overline{\boldsymbol{S}} + \int_{\Omega_{\mathrm{C}}} \frac{1}{\sigma} \mathbf{curl}\, \boldsymbol{T} \cdot \mathbf{curl}\, \overline{\boldsymbol{S}} + \sum_{n=N_I+1}^{N} I_n \left(\int_{\Omega_{\mathrm{C}}} i\omega\mu \boldsymbol{t}_{0,n} \cdot \overline{\boldsymbol{S}} \right.\\ \left. + \int_{\Omega_{\mathrm{C}}^n} \frac{1}{\sigma} \mathbf{curl}\, \boldsymbol{t}_{0,n} \cdot \mathbf{curl}\, \overline{\boldsymbol{S}} \right) + \int_{\Omega_{\mathrm{C}}} \mathbf{grad}\, \xi \cdot \overline{\boldsymbol{S}} = - \sum_{n=1}^{N_I} I_n \left(\int_{\Omega_{\mathrm{C}}} i\omega\mu \boldsymbol{t}_{0,n} \cdot \overline{\boldsymbol{S}} \right.\\ \left. + \int_{\Omega_{\mathrm{C}}^n} \frac{1}{\sigma} \mathbf{curl}\, \boldsymbol{t}_{0,n} \cdot \mathbf{curl}\, \overline{\boldsymbol{S}} \right) \quad \forall\, \boldsymbol{S} \in \boldsymbol{\mathcal{Y}}, \quad (1.39)\end{aligned}$$

$$\begin{aligned}- \int_{\Omega_{\mathrm{C}}} i\omega\mu \boldsymbol{T} \cdot \mathbf{grad}\, \overline{\psi} + \int_{\Omega} i\omega\mu\, \mathbf{grad}\, \phi \cdot \mathbf{grad}\, \overline{\psi} - \sum_{n=N_I+1}^{N} I_n \int_{\Omega} i\omega\mu \boldsymbol{t}_{0,n} \cdot \mathbf{grad}\, \overline{\psi}\\ = \sum_{n=1}^{N_I} I_n \int_{\Omega} i\omega\mu \boldsymbol{t}_{0,n} \cdot \mathbf{grad}\, \overline{\psi} \quad \forall\, \psi \in \mathrm{H}^1(\Omega)/\mathbb{C}, \quad (1.40)\end{aligned}$$

$$\int_{\Omega_{\mathrm{C}}} \boldsymbol{T} \cdot \mathbf{grad}\, \overline{\zeta} = 0 \quad \forall\, \zeta \in \mathcal{Z}, \quad (1.41)$$

$$\begin{aligned}\left(\int_{\Omega_{\mathrm{C}}} i\omega\mu \boldsymbol{T} \cdot \overline{\boldsymbol{t}}_{0,m} - \int_{\Omega} i\omega\mu\, \mathbf{grad}\, \phi \cdot \overline{\boldsymbol{t}}_{0,m} + \int_{\Omega_{\mathrm{C}}^m} \frac{1}{\sigma} \mathbf{curl}\, \boldsymbol{T} \cdot \mathbf{curl}\, \overline{\boldsymbol{t}}_{0,m} + \right.\\ \left. \sum_{n=N_I+1}^{N} I_n \int_{\Omega} i\omega\mu \boldsymbol{t}_{0,n} \cdot \overline{\boldsymbol{t}}_{0,m} + I_m \int_{\Omega_{\mathrm{C}}^m} \frac{1}{\sigma} |\mathbf{curl}\, \boldsymbol{t}_{0,m}|^2 \right) \overline{K}_m = \Delta V_m \overline{K}_m\\ - \left(\sum_{n=1}^{N_I} I_n \int_{\Omega} i\omega\mu \boldsymbol{t}_{0,n} \cdot \overline{\boldsymbol{t}}_{0,m} \right) \overline{K}_m \quad \forall\, K_m \in \mathbb{C}, \quad m = N_I + 1, \ldots, N. \quad (1.42)\end{aligned}$$

We notice that, in comparison with the ungauged $\boldsymbol{T}$,ϕ–ϕ formulation, the presence of the new equation (1.41) leads to the inclusion of a term in equation (t-phi:vfgauge) involving a Lagrange multiplier ξ. In this way, the system of equations associated to this problem is also symmetric, what is convenient from the computational point of view.

1.5.1 Mathematical Analysis

Now, we are going to state two results similar to Lemma 1.7 and Theorem 1.8 but for the gauged version of the $\boldsymbol{T}$,ϕ–ϕ formulation. Let

$$\widehat{\boldsymbol{\mathcal{Y}}} := \{\boldsymbol{S} \in \mathrm{H}(\mathbf{curl}, \Omega_{\mathrm{C}}) \cap \mathrm{H}(\mathrm{div}, \Omega_{\mathrm{C}}) \,:\, \mathrm{div}\, \boldsymbol{S} = 0 \text{ in } \Omega_{\mathrm{C}}, \\ \boldsymbol{S} \times \boldsymbol{n} = \boldsymbol{0} \text{ on } \Gamma_{\mathrm{I}} \text{ and } \boldsymbol{S} \cdot \boldsymbol{n} = \boldsymbol{0} \text{ on } \Gamma_{\mathrm{E}} \cup \Gamma_{\mathrm{J}}\}\,.$$

We have the following result:

Lemma 1.17. *Let $\boldsymbol{t}_{0,n} \in \mathrm{H}(\mathbf{curl}, \Omega)$, $n = 1, \ldots, N$, satisfying (1.11)–(1.12). Given $K_n \in \mathbb{C}$, $n = 1, \ldots, N_I$, and $\boldsymbol{G} \in \boldsymbol{\mathcal{V}}(\boldsymbol{K})$, there exist unique $\boldsymbol{S} \in \widehat{\boldsymbol{\mathcal{Y}}}$, $\psi \in \mathrm{H}^1(\Omega)/\mathbb{C}$ and $K_n \in \mathbb{C}$, $n = N_I + 1, \ldots, N$, such that $\boldsymbol{G} = \widetilde{\boldsymbol{S}} + \sum_{n=1}^{N} K_n \boldsymbol{t}_{0,n} - \mathbf{grad}\, \psi$.*

Proof. The proof is very similar to that of Theorem 1.7. Indeed, given $\boldsymbol{G} \in \boldsymbol{\mathcal{V}}(\boldsymbol{K})$, let $K_n := \int_{\Gamma_{\mathrm{J}}^n} \mathbf{curl}\, \boldsymbol{G} \cdot \boldsymbol{n}$, $n = N_I + 1, \ldots, N$, and $\widehat{\boldsymbol{G}} := \boldsymbol{G} - \sum_{n=1}^{N} K_n \boldsymbol{t}_{0,n}$. We have that $\widehat{\boldsymbol{G}} \in \mathrm{H}(\mathbf{curl}, \Omega)$ and it satisfies

$$\begin{aligned} \mathrm{div}(\mathbf{curl}\, \widehat{\boldsymbol{G}}) &= \boldsymbol{0} && \text{in } \Omega_{\mathrm{C}}, \\ \mathbf{curl}\, \widehat{\boldsymbol{G}} \cdot \boldsymbol{n} &= 0 && \text{on } \Gamma_{\mathrm{I}}\,, \\ \int_{\Gamma_{\mathrm{J}}^n} \mathbf{curl}\, \widehat{\boldsymbol{G}} \cdot \boldsymbol{n} &= 0 && \text{for } n = 1, \ldots, N. \end{aligned}$$

Using again Theorem 2.1 from [48], we deduce that there exists a unique $\boldsymbol{S} \in \mathrm{L}^2(\Omega_{\mathrm{C}})^3$ that satisfies

$$\begin{aligned} \mathbf{curl}\, \boldsymbol{S} &= \mathbf{curl}\, \widehat{\boldsymbol{G}} && \text{in } \Omega_{\mathrm{C}}, \\ \mathrm{div}\, \boldsymbol{S} &= 0 && \text{in } \Omega_{\mathrm{C}}, \\ \boldsymbol{S} \times \boldsymbol{n} &= \boldsymbol{0} && \text{on } \Gamma_{\mathrm{I}}\,, \\ \boldsymbol{S} \cdot \boldsymbol{n} &= 0 && \text{on } \Gamma_{\mathrm{E}} \cup \Gamma_{\mathrm{J}}. \end{aligned}$$

Moreover, $\mathbf{curl}(\widehat{\boldsymbol{G}} - \widetilde{\boldsymbol{S}}) = \boldsymbol{0}$ in Ω, so that, since Ω is simply connected, there exists $\psi \in \mathrm{H}^1(\Omega)$, unique up to a constant, such that $\widehat{\boldsymbol{G}} = \widetilde{\boldsymbol{S}} - \mathbf{grad}\, \psi$. Thus, $\boldsymbol{G} = \widehat{\boldsymbol{G}} + \sum_{n=1}^{N} K_n \boldsymbol{t}_{0,n} = \widetilde{\boldsymbol{S}} + \sum_{n=1}^{N} K_n \boldsymbol{t}_{0,n} - \mathbf{grad}\, \psi$ in Ω. □

Taking the previous decomposition into account, solving Problem 1.16 is equivalent to solving Problem 1.3. In fact, we have the following result:

Theorem 1.18. *Let $\boldsymbol{t}_{0,n} \in \mathrm{H}(\mathbf{curl}, \Omega)$, $n = 1, \ldots, N$, satisfying (1.11)–(1.12). Let $I_n \in \mathbb{C}$, $n = 1, \ldots, N_I$, and $\Delta V_n \in \mathbb{C}$, $n = N_I + 1, \ldots, N$. Any solution $(\boldsymbol{T}, \phi, \xi, I_{N_I+1}, \ldots, I_N)$ to Problem 1.16 leads to the unique magnetic field $\boldsymbol{H} := \widetilde{\boldsymbol{T}} + \sum_{n=1}^{N} I_n \boldsymbol{t}_{0,n} - \mathbf{grad}\, \phi$ that solves Problem 1.3. Conversely, the solution $\boldsymbol{H}$ to Problem 1.3 can be uniquely written as $\boldsymbol{H} = \widetilde{\boldsymbol{T}} + \sum_{n=1}^{N} I_n \boldsymbol{t}_{0,n} - \mathbf{grad}\, \phi$, with $(\boldsymbol{T}, \phi, 0, I_{N_I+1}, \ldots, I_N)$ being a solution to Problem 1.16. In particular, Problem 1.16 has a unique solution $(\boldsymbol{T}, \phi, \xi, I_{N_I+1}, \ldots, I_N)$, with ξ null in Ω_{C}.*

Proof. Let $\boldsymbol{t}_{0,n} \in \mathrm{H}(\mathbf{curl}, \Omega)$, $n = 1, \ldots, N$, satisfying (1.11)–(1.12). Let $I_n \in \mathbb{C}$, $n = 1, \ldots, N_I$, and $\Delta V_n \in \mathbb{C}$, $n = N_I + 1, \ldots, N$.
On the one hand, let $\boldsymbol{H}$ be the unique solution to Problem 1.3. According to Lemma 1.17, we write $\boldsymbol{H} = \widetilde{\boldsymbol{T}} + \sum_{n=1}^{N} I_n \boldsymbol{t}_{0,n} - \mathbf{grad}\, \phi$ with $\boldsymbol{T} \in \widehat{\boldsymbol{\mathcal{Y}}}$, $\phi \in \mathrm{H}^1(\Omega)$ and $I_n \in \mathbb{C}$, $n = N_I+1, \ldots, N$. Notice that, in particular, $\boldsymbol{T} \in \boldsymbol{\mathcal{Y}}$. Then, by substituting this expression in (1.26) and taking separately test functions $\boldsymbol{G} = \widetilde{\boldsymbol{S}}$ for $\boldsymbol{S} \in \boldsymbol{\mathcal{Y}}$, $\boldsymbol{G} = \mathbf{grad}\, \psi$ for $\psi \in \mathrm{H}^1(\Omega)$ and $\boldsymbol{G} = \boldsymbol{t}_{0,n}$, $n = N_I+1, \ldots, N$, we check that $(\boldsymbol{T}, \phi, 0, I_{N_I+1}, \ldots, I_N)$ satisfies equations (1.39), (1.40) and (1.42). Finally, since

$$\operatorname{div} \boldsymbol{T} = 0 \ \text{ in } \ \Omega_{\mathrm{C}} \qquad \text{and} \qquad \boldsymbol{T} \cdot \boldsymbol{n} = 0 \ \text{ on } \ \Gamma_{\mathrm{E}} \cup \Gamma_{\mathrm{J}},$$

we deduce that $\boldsymbol{T}$ satisfies equation (1.41). Therefore, $(\boldsymbol{T}, \phi, 0, I_{N_I+1}, \ldots, I_N)$ is a solution to Problem 1.16.
On the other hand, let $(\boldsymbol{T}, \phi, \xi, I_{N_I+1}, \ldots, I_N)$ be a solution to Problem 1.16. First, we will prove that $\xi = 0$ in Ω_{C}. Indeed, since ξ is zero on Γ_{I}, it is enough to show that $\mathbf{grad}\, \xi = \mathbf{0}$ in Ω_{C}. Since $\mathbf{grad}\, \xi \in \boldsymbol{\mathcal{Y}}$, we can take $\boldsymbol{S} = \mathbf{grad}\, \xi$ in (1.39), obtaining

$$\int_{\Omega_{\mathrm{C}}} i\omega\mu(\boldsymbol{T} - \mathbf{grad}\, \phi) \cdot \mathbf{grad}\, \overline{\xi} + \sum_{n=N_I+1}^{N} I_n \int_{\Omega_{\mathrm{C}}} i\omega\mu \boldsymbol{t}_{0,n} \cdot \mathbf{grad}\, \overline{\xi} + \int_{\Omega_{\mathrm{C}}} |\mathbf{grad}\, \xi|^2 = -\sum_{n=1}^{N_I} I_n \int_{\Omega_{\mathrm{C}}} i\omega\mu \boldsymbol{t}_{0,n} \cdot \mathbf{grad}\, \overline{\xi}.$$

On the other hand, we can also take $\psi = \widetilde{\xi}$ in (1.40), $\widetilde{\xi} \in \mathrm{H}^1(\Omega)$ being the extension by zero of ξ to Ω, and adding it to the above equation we obtain:

$$\int_{\Omega_{\mathrm{C}}} |\mathbf{grad}\, \xi|^2 = 0,$$

and therefore $\mathbf{grad}\, \xi = \mathbf{0}$ in $\mathrm{L}^2(\Omega_{\mathrm{C}})$. Then, $(\boldsymbol{T}, \phi, I_{N_I+1}, \ldots, I_N)$ is a solution to Problem 1.1. Let $\boldsymbol{H} := \widetilde{\boldsymbol{T}} + \sum_{n=1}^{N} I_n \boldsymbol{t}_{0,n} - \mathbf{grad}\, \phi$; according to Theorem 1.8, $\boldsymbol{H}$ is the solution to Problem 1.3. Moreover, taking $\zeta \in \mathcal{D}(\Omega_{\mathrm{C}})$ in (1.41) and using a Green's formula we deduce that $\operatorname{div} \boldsymbol{T} = 0$ in Ω_{C}. Furthermore, let $\iota \in \mathrm{H}_{00}^{1/2}(\Gamma_{\mathrm{E}} \cup \Gamma_{\mathrm{J}})$, $\widetilde{\iota}$ its extension by zero to $\partial\Omega_{\mathrm{C}}$ and $\zeta \in \mathcal{Z}$ such that $\zeta|_{\partial\Omega_{\mathrm{C}}} = \widetilde{\iota}$. If we take such a test function in (1.41) and use a Green's formula, we conclude that $\boldsymbol{T} \cdot \boldsymbol{n} = 0$ in $\mathrm{H}_{00}^{1/2}(\Gamma_{\mathrm{E}} \cup \Gamma_{\mathrm{J}})$. Therefore, $\boldsymbol{T} \in \widehat{\boldsymbol{\mathcal{Y}}}$, and following Lemma 1.17, we conclude that $(\boldsymbol{T}, \phi, 0, I_{N_I+1}, \ldots, I_N)$ is the only solution to Problem 1.16. □

1.5.2 Finite Element Discretisation

In this section we will introduce a discretisation of Problem 1.16 and proceed as in the previous subsection for its analysis. Similarly to the ungauged case, we assume in this subsection that Ω, Ω_{C} and Ω_{D} are Lipschitz polyhedra and consider regular tetrahedral meshes $\mathcal{T}_h$ of Ω such that each element $T \in \mathcal{T}_h$ is contained either in $\overline{\Omega}_{\mathrm{C}}$ or in $\overline{\Omega}_{\mathrm{D}}$.

Again, we employ lowest-order Nédélec finite finite elements to approximate the current vector potential $\boldsymbol{T}$, and standard finite elements for both the magnetic potential ϕ and the Lagrange

multiplier function ξ. We introduce the discrete subspace of $\mathcal{Z}$,

$$\mathcal{Z}_h := \{\zeta_h \in \mathcal{L}_h(\Omega_{\rm C}) \,:\, \zeta_h = 0 \text{ on } \Gamma_{\rm I}\}\,.$$

Therefore, the discretisation of Problem 1.16 reads as follows:

Problem 1.19. *Let $\boldsymbol{t}^h_{0,n} \in \boldsymbol{\mathcal{N}}_h(\Omega)$, $n = 1,\dots,N$, satisfying (1.33)–(1.34). Given $I_n \in \mathbb{C}$, $n = 1,\dots,N_I$, and $\Delta V_n \in \mathbb{C}$, $n = N_I+1,\dots,N$, find $\boldsymbol{T}_h \in \boldsymbol{\mathcal{Y}}_h$, $\phi_h \in \mathcal{L}_h(\Omega)/\mathbb{C}$, $\xi_h \in \mathcal{Z}_h$ and $I^h_n \in \mathbb{C}$ for $n = N_I+1,\dots,N$ such that*

$$\begin{aligned}\int_{\Omega_{\rm C}} i\omega\mu(\boldsymbol{T}_h - \mathbf{grad}\,\phi_h)\cdot\overline{\boldsymbol{S}}_h + \int_{\Omega_{\rm C}}\frac{1}{\sigma}\,\mathbf{curl}\,\boldsymbol{T}_h\cdot\mathbf{curl}\,\overline{\boldsymbol{S}}_h + \sum_{n=N_I+1}^{N} I^h_n\left(\int_{\Omega_{\rm C}} i\omega\mu\boldsymbol{t}^h_{0,n}\cdot\overline{\boldsymbol{S}}_h\right.\\ \left. + \int_{\Omega_{\rm C}}\frac{1}{\sigma}\,\mathbf{curl}\,\boldsymbol{t}^h_{0,n}\cdot\mathbf{curl}\,\overline{\boldsymbol{S}}_h\right) + \int_{\Omega_{\rm C}}\mathbf{grad}\,\xi_h\cdot\overline{\boldsymbol{S}}_h = -\sum_{n=1}^{N_I} I_n\left(\int_{\Omega_{\rm C}} i\omega\mu\boldsymbol{t}^h_{0,n}\cdot\overline{\boldsymbol{S}}_h\right.\\ \left. + \int_{\Omega_{\rm C}}\frac{1}{\sigma}\,\mathbf{curl}\,\boldsymbol{t}^h_{0,n}\cdot\mathbf{curl}\,\overline{\boldsymbol{S}}_h\right) \quad \forall\,\boldsymbol{S}_h \in \boldsymbol{\mathcal{Y}}_h, \quad (1.43)\end{aligned}$$

$$\begin{aligned}-\int_{\Omega_{\rm C}} i\omega\mu\boldsymbol{T}_h\cdot\mathbf{grad}\,\overline{\psi}_h + \int_{\Omega} i\omega\mu\,\mathbf{grad}\,\phi_h\cdot\mathbf{grad}\,\overline{\psi}_h - \sum_{n=N_I+1}^{N} I^h_n\int_{\Omega} i\omega\mu\boldsymbol{t}^h_{0,n}\cdot\mathbf{grad}\,\overline{\psi}_h\\ = \sum_{n=1}^{N_I} I_n\int_{\Omega} i\omega\mu\boldsymbol{t}^h_{0,n}\cdot\mathbf{grad}\,\overline{\psi}_h \quad \forall\,\psi_h \in \mathcal{L}_h(\Omega)/\mathbb{C}, \quad (1.44)\end{aligned}$$

$$\int_{\Omega_{\rm C}} \boldsymbol{T}_h\cdot\mathbf{grad}\,\overline{\zeta_h} = 0 \quad \forall\,\zeta_h \in \mathcal{Z}_h, \quad (1.45)$$

$$\begin{aligned}\left(\int_{\Omega_{\rm C}} i\omega\mu\boldsymbol{T}_h\cdot\overline{\boldsymbol{t}}^h_{0,m} - \int_{\Omega} i\omega\mu\,\mathbf{grad}\,\phi_h\cdot\overline{\boldsymbol{t}}^h_{0,m} + \int_{\Omega^m_{\rm C}}\frac{1}{\sigma}\,\mathbf{curl}\,\boldsymbol{T}_h\cdot\mathbf{curl}\,\overline{\boldsymbol{t}}^h_{0,m}\right.\\ \left. + \sum_{n=N_I+1}^{N} I^h_n\int_{\Omega} i\omega\mu\boldsymbol{t}^h_{0,n}\cdot\overline{\boldsymbol{t}}^h_{0,m} + I^h_m\int_{\Omega^m_{\rm C}}\frac{1}{\sigma}|\,\mathbf{curl}\,\boldsymbol{t}^h_{0,m}|^2\right)\overline{K}_m = \Delta V_m\overline{K}_m\\ - \left(\sum_{n=1}^{N_I} I_n\int_{\Omega} i\omega\mu\boldsymbol{t}^h_{0,n}\cdot\overline{\boldsymbol{t}}^h_{0,m}\right)\overline{K}_m \quad \forall\,K_m \in \mathbb{C}, \quad m = N_I+1,\dots,N. \quad (1.46)\end{aligned}$$

We will show this problem has a unique solution. Let

$$\widehat{\boldsymbol{\mathcal{Y}}}_h := \left\{\boldsymbol{G}_h \in \boldsymbol{\mathcal{N}}_h(\Omega_{\rm C}) \,:\, \int_{\Omega_{\rm C}} \boldsymbol{G}_h\cdot\mathbf{grad}\,\overline{\zeta}_h = 0\ \forall\zeta_h \in \mathcal{Z}_h, \quad \boldsymbol{G}_h\times\boldsymbol{n} = \boldsymbol{0} \text{ on } \Gamma_{\rm I}\right\}.$$

We have the following result:

Lemma 1.20. *Let $\boldsymbol{t}^h_{0,n} \in \boldsymbol{\mathcal{N}}_h(\Omega)$, $n = 1,\dots,N$, satisfying (1.33)–(1.34). Given $K_n \in \mathbb{C}$, $n = 1,\dots,N_I$, and a discrete field $\boldsymbol{G}_h \in \boldsymbol{\mathcal{V}}_h(\boldsymbol{K})$, there exist unique $\boldsymbol{S}_h \in \widehat{\boldsymbol{\mathcal{Y}}}_h$, $\psi_h \in \mathcal{L}_h(\Omega)/\mathbb{C}$ and $K^h_n \in \mathbb{C}$, $n = N_I+1,\dots,N$, such that $\boldsymbol{G}_h = \widetilde{\boldsymbol{S}}_h + \sum_{n=1}^{N_I} K_n\boldsymbol{t}^h_{0,n} + \sum_{n=N_I+1}^{N} K^h_n\boldsymbol{t}^h_{0,n} - \mathbf{grad}\,\psi_h$.*

Proof. Given $\boldsymbol{G}_h \in \boldsymbol{\mathcal{V}}_h(\boldsymbol{K})$, let $K_n^h := \int_{\Gamma_{\mathrm{J}}^n} \mathbf{curl}\, \boldsymbol{G}_h \cdot \boldsymbol{n}$, $n = N_I+1, \ldots, N$, and $\widehat{\boldsymbol{G}}_h := \boldsymbol{G}_h - \sum_{n=1}^{N_I} K_n \boldsymbol{t}_{0,n}^h - \sum_{n=N_I+1}^{N} K_n^h \boldsymbol{t}_{0,n}^h$. Then, $\widehat{\boldsymbol{G}}_h \in \boldsymbol{\mathcal{N}}_h(\Omega)$, $\mathbf{curl}\, \widehat{\boldsymbol{G}}_h = \boldsymbol{0}$ in Ω_{D} and $\int_{\Gamma_{\mathrm{J}}^n} \mathbf{curl}\, \widehat{\boldsymbol{G}}_h \cdot \boldsymbol{n} = 0$, $n = 1, \ldots, N$.
Following the same arguments as in Lemma 1.13, (in particular, using [29, Lemma 5.5]), there exists $\psi_h^D \in \mathcal{L}_h(\Omega_{\mathrm{D}})$, unique up to an additive constant, such that $\widehat{\boldsymbol{G}}_h|_{\Omega_{\mathrm{D}}} = -\,\mathbf{grad}\, \psi_h^D$. Let $\psi_h^C \in \mathcal{L}_h(\Omega_{\mathrm{C}})$ be the only solution to the problem:

Find $\psi_h^C \in \mathcal{L}_h(\Omega_{\mathrm{C}})$ such that $\psi_h^C = \psi_h^D$ on Γ_{I} and

$$\int_{\Omega_{\mathrm{C}}} \mathbf{grad}\, \psi_h^C \cdot \mathbf{grad}\, \overline{\varphi}_h = \int_{\Omega_{\mathrm{C}}} -\widehat{\boldsymbol{G}}_h \cdot \mathbf{grad}\, \overline{\varphi}_h \quad \forall\, \varphi_h \in \mathcal{Z}_h. \tag{1.47}$$

Let us define $\boldsymbol{S}_h := \widehat{\boldsymbol{G}}_h|_{\Omega_{\mathrm{C}}} + \mathbf{grad}\, \psi_h^C \in \boldsymbol{\mathcal{N}}_h(\Omega_{\mathrm{C}})$. Since $\widehat{\boldsymbol{G}}_h = -\,\mathbf{grad}\, \psi_h^D$ in Ω_{D}, we have that $\widehat{\boldsymbol{G}}_h \times \boldsymbol{n} = -\,\mathbf{grad}\, \psi_h^D \times \boldsymbol{n}$ on Γ_{I}. Therefore, since $\psi_h^C = \psi_h^D$ on Γ_{I},

$$\boldsymbol{S}_h \times \boldsymbol{n} = \widehat{\boldsymbol{G}}_h \times \boldsymbol{n} + \mathbf{grad}\, \psi_h^C \times \boldsymbol{n} = \boldsymbol{0} \quad \text{on } \Gamma_{\mathrm{I}}.$$

Then, $\boldsymbol{G}_h = \widetilde{\boldsymbol{S}}_h + \sum_{n=1}^{N_I} K_n \boldsymbol{t}_{0,n}^h + \sum_{n=N_I+1}^{N} K_n^h \boldsymbol{t}_{0,n}^h - \mathbf{grad}\, \psi_h$, with $\boldsymbol{S}_h \in \widehat{\boldsymbol{\mathcal{Y}}}_h$ and $\psi_h \in \mathcal{L}_h(\Omega)$ such that

$$\psi_h := \begin{cases} \psi_h^C & \text{in } \Omega_{\mathrm{C}}, \\ \psi_h^D & \text{in } \Omega_{\mathrm{D}}. \end{cases}$$

Notice that from the above construction we deduce that K_n^h, $n = N_I+1, \ldots, N$, and the degrees of freedom of $\boldsymbol{S}_h$ and ψ_h are unique. □

Taking the previous decomposition into account, solving Problem 1.19 is equivalent to solving Problem 1.11. In fact, we have the following result:

Theorem 1.21. *Let $\boldsymbol{t}_{0,n}^h \in \boldsymbol{\mathcal{N}}_h(\Omega)$, $n = 1, \ldots, N$, satisfying (1.33)–(1.34). Let $I_n \in \mathbb{C}$, $n = 1, \ldots, N_I$, and $\Delta V_n \in \mathbb{C}$, $n = N_I+1, \ldots, N$. If $(\boldsymbol{T}_h, \phi_h, I_{N_I+1}^h, \ldots, I_N^h)$ is a solution to Problem 1.19, then $\boldsymbol{H}_h := \widetilde{\boldsymbol{T}}_h + \sum_{n=1}^{N_I} I_n \boldsymbol{t}_{0,n}^h + \sum_{n=N_I+1}^{N} I_n^h \boldsymbol{t}_{0,n}^h - \mathbf{grad}\, \phi_h$ solves Problem 1.11. Conversely, if $\boldsymbol{H}_h$ is the solution to Problem 1.11, then it can be uniquely written as $\boldsymbol{H}_h = \widetilde{\boldsymbol{T}}_h + \sum_{n=1}^{N_I} I_n \boldsymbol{t}_{0,n}^h + \sum_{n=N_I+1}^{N} I_n^h \boldsymbol{t}_{0,n}^h - \mathbf{grad}\, \phi_h$, with $(\boldsymbol{T}_h, \phi_h, 0, I_{N_I+1}^h, \ldots, I_N^h)$ being a solution to Problem 1.19. In particular, Problem 1.19 has a unique solution $(\boldsymbol{T}_h, \phi_h, \xi_h, I_{N_I+1}^h, \ldots, I_N^h)$, with ξ_h null in Ω_{C}.*

Proof. Let $\boldsymbol{t}_{0,n}^h \in \boldsymbol{\mathcal{N}}_h(\Omega)$, $n = 1, \ldots, N$, satisfying (1.33)–(1.34). Let $I_n \in \mathbb{C}$, $n = 1, \ldots, N_I$, and $\Delta V_n \in \mathbb{C}$, $n = N_I+1, \ldots, N$.
On the one hand, let $\boldsymbol{H}_h$ be the unique solution to Problem 1.11. According to Lemma 1.20, we write

$$\boldsymbol{H}_h = \widetilde{\boldsymbol{T}}_h + \sum_{n=1}^{N_I} I_n \boldsymbol{t}_{0,n}^h + \sum_{n=N_I+1}^{N} I_n^h \boldsymbol{t}_{0,n}^h - \mathbf{grad}\, \phi_h$$

with $\boldsymbol{T}_h \in \widehat{\boldsymbol{\mathcal{Y}}}_h$, $\phi_h \in \mathcal{L}_h(\Omega)$ and $I_n^h \in \mathbb{C}$, $n = N_I+1, \ldots, N$. Notice that, in particular, $\boldsymbol{T}_h \in \boldsymbol{\mathcal{Y}}_h$. Then, by substituting this expression in (1.38) and taking separately test functions

$\boldsymbol{G}_h = \widetilde{\boldsymbol{S}}_h$ for $\boldsymbol{S}_h \in \boldsymbol{\mathcal{Y}}_h$, $\boldsymbol{G}_h = \mathbf{grad}\,\psi_h$ for $\psi_h \in \mathcal{L}_h(\Omega)$ and $\boldsymbol{G}_h = \boldsymbol{t}^h_{0,n}$, $n = N_I+1,\dots,N$, we check that $(\boldsymbol{T}_h, \phi_h, 0, I^h_{N_I+1},\dots,I^h_N)$ verifies equations (1.43), (1.44) and (1.46). Finally, we know from the construction of $\boldsymbol{T}_h$ in the above lemma that it verifies equation (1.45), and therefore we deduce that $(\boldsymbol{T}_h, \phi_h, 0, I_{N_I+1},\dots,I_N)$ is a solution to Problem 1.19.
On the other hand, let $(\boldsymbol{T}_h, \phi_h, \xi_h, I^h_{N_I+1},\dots,I^h_N)$ be a solution to Problem 1.19. Similarly to the continuous case, we can deduce that the Lagrange multiplier is such that $\xi_h \equiv 0$ in Ω_{C}. Therefore, $(\boldsymbol{T}_h, \phi_h, I^h_{N_I+1},\dots,I^h_N)$ is a solution to Problem 1.10. Let

$$\boldsymbol{H}_h := \widetilde{\boldsymbol{T}}_h + \sum_{n=1}^{N_I} I_n \boldsymbol{t}^h_{0,n} + \sum_{n=N_I+1}^{N} I^h_n \boldsymbol{t}^h_{0,n} - \mathbf{grad}\,\phi_h;$$

according to Theorem 1.14, $\boldsymbol{H}_h$ is the solution to Problem 1.11. Using again equation (1.45), we deduce that $\boldsymbol{T}_h \in \widehat{\boldsymbol{\mathcal{Y}}}_h$, and from the uniqueness of the decomposition in Lemma 1.20 we deduce that $(\boldsymbol{T}_h, \phi_h, 0, I^h_{N_I+1},\dots,I^h_N)$ is the only solution to Problem 1.19. □

The following result is an straightforward consequence of Theorem 1.14

Theorem 1.22. *Let $(\boldsymbol{T}, \phi, \xi, I_{N_I+1},\dots,I_N)$ and $(\boldsymbol{T}_h, \phi_h, \xi_h, I^h_{N_I+1},\dots,I^h_N)$ be solutions to Problems 1.16 and 1.19, respectively. Let $\boldsymbol{H} := \widetilde{\boldsymbol{T}} + \sum_{n=1}^{N} I_n \boldsymbol{t}_{0,n} - \mathbf{grad}\,\phi$ and $\boldsymbol{H}_h := \widetilde{\boldsymbol{T}}_h + \sum_{n=1}^{N_I} I_n \boldsymbol{t}^h_{0,n} + \sum_{n=N_I+1}^{N} I^h_n \boldsymbol{t}^h_{0,n} - \mathbf{grad}\,\phi_h$. If $\boldsymbol{H}|_{\Omega_{\mathrm{C}}} \in \mathrm{H}^r(\mathbf{curl}, \Omega_{\mathrm{C}})$ and $\boldsymbol{H}|_{\Omega_{\mathrm{D}}} \in \mathrm{H}^r(\Omega_{\mathrm{D}})^3$ with $r \in \left(\frac{1}{2}, 1\right]$, then*

$$\|\boldsymbol{H} - \boldsymbol{H}_h\|_{\mathrm{H}(\mathbf{curl},\Omega)} \leq C h^r \left[\|\boldsymbol{H}\|_{\mathrm{H}^r(\mathbf{curl},\Omega_{\mathrm{C}})} + \|\boldsymbol{H}\|_{\mathrm{H}^r(\Omega_{\mathrm{D}})^3}\right],$$

where C is a strictly positive constant independent of h and $\boldsymbol{H}$.

1.6 Computation of the Normalised Impressed Vector Potentials

The aim of this section is to introduce some numerical procedures to compute the discrete normalised impressed vector potential $\boldsymbol{t}^h_{0,n}$ that do not make use of cutting surfaces.

1.6.1 Using Biot-Savart Law

First, by following the ideas in [34], we propose a numerical method based on the Biot-Savart law. For each $n = 1,\dots,N$, let L_n be a polygonal filament (namely, a closed simple polygonal curve) going across Ω^n_{C} as shown in Figure 1.2. We assume that $L_n \cap \Omega^n_{\mathrm{C}}$ is made of edges of thetrahedra (as in Figure 1.2, again). Let $\boldsymbol{H}^n_{\mathrm{BS}}$ be the Biot-Savart field in Ω corresponding to L_n and carrying a unit current intensity:

$$\boldsymbol{H}^n_{\mathrm{BS}}(\boldsymbol{x}) := \frac{1}{4\pi} \int_{L_n} \boldsymbol{\tau}_{L_n} \times \frac{\boldsymbol{x} - \boldsymbol{x}'}{|\boldsymbol{x} - \boldsymbol{x}'|^3}\, d\boldsymbol{x}', \tag{1.48}$$

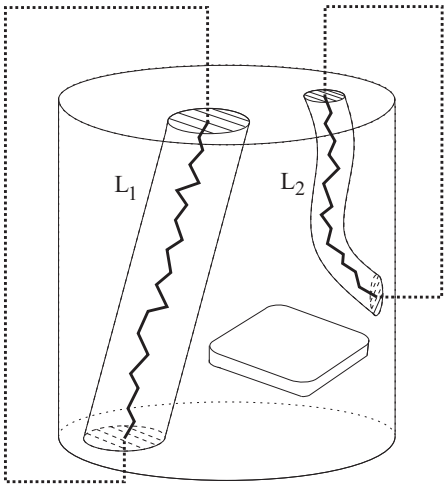

Figure 1.2: Current filaments for the domain in Figure 1.1.

where $\boldsymbol{\tau}_{L_n}$ is the unit vector tangent to L_n. It is easy to check that $\boldsymbol{H}^n_{\mathrm{BS}}$ has no singularities outside inductor Ω^n_{C}, since the current filament L_n does not intersect $\overline{\Omega \setminus \Omega^n_{\mathrm{C}}}$. In fact, since the integrand is infinitely smooth outside of L_n, it is immediate to check by differentiating under the integral sign that $\boldsymbol{H}^n_{\mathrm{BS}} \in \mathcal{C}^\infty(\overline{\Omega \setminus \Omega^n_{\mathrm{C}}})^3$. Then, we can take as discrete normalised impressed vector potential $\boldsymbol{t}^h_{0,n}$ the field in $\boldsymbol{\mathcal{N}}_h(\Omega)$ with its degrees of freedom defined for each edge ℓ of the mesh $\mathcal{T}_h$ as follows:

$$\int_\ell \boldsymbol{t}^h_{0,n} \cdot \boldsymbol{\tau}_\ell := \begin{cases} \int_\ell \boldsymbol{H}^n_{\mathrm{BS}} \cdot \boldsymbol{\tau}_\ell, & \text{if } \ell \subset \overline{\Omega \setminus \Omega^n_{\mathrm{C}}}, \\ 0, & \text{if } \ell \not\subset \overline{\Omega \setminus \Omega^n_{\mathrm{C}}}, \end{cases} \tag{1.49}$$

where $\boldsymbol{\tau}_\ell$ is the unit vector tangent to the edge ℓ. Therefore, $\boldsymbol{t}^h_{0,n}|_{\overline{\Omega\setminus\Omega^n_{\mathrm{C}}}}$ is the Nédélec interpolant of $\boldsymbol{H}^n_{\mathrm{BS}}|_{\overline{\Omega\setminus\Omega^n_{\mathrm{C}}}}$. Thus, since $\mathbf{curl}\, \boldsymbol{H}^n_{\mathrm{BS}} = \mathbf{0}$ in $\overline{\Omega \setminus \Omega^n_{\mathrm{C}}}$, we have that $\mathbf{curl}\, \boldsymbol{t}^h_{0,n} = \mathbf{0}$ in $\overline{\Omega \setminus \Omega^n_{\mathrm{C}}}$, too. On the other hand, since $\int_{\gamma_n} \boldsymbol{H}^n_{\mathrm{BS}} \cdot \boldsymbol{\tau}_n = 1$, we also have that $\int_{\gamma_n} \boldsymbol{t}^h_{0,n} \cdot \boldsymbol{\tau}_n = \int_{\gamma_n} \boldsymbol{H}^n_{\mathrm{BS}} \cdot \boldsymbol{\tau}_n = 1$. Thus, $\boldsymbol{t}^h_{0,n} \in \boldsymbol{\mathcal{N}}_h(\Omega)$ satisfies (1.33)–(1.34).

In order to compute (1.48) for $\boldsymbol{x} \in \overline{\Omega \setminus \Omega^n_{\mathrm{C}}}$, we add the contribution of each edge ℓ lying on the current filament L_n (note that this includes tehtrahedra edges as well as the segments out of Ω added to close the curve L_n; see Figure 1.2). Thus, we write

$$\boldsymbol{H}^n_{BS}(\boldsymbol{x}) = \sum_{\ell \subset L_n} \boldsymbol{H}^{n,\ell}_{BS}(\boldsymbol{x})$$

with

$$\begin{aligned} \boldsymbol{H}^{n,\ell}_{BS}(\boldsymbol{x}) := \frac{1}{4\pi} \int_\ell \boldsymbol{\tau}_{L_n} \times \frac{\boldsymbol{x} - \boldsymbol{x}'}{|\boldsymbol{x} - \boldsymbol{x}'|^3}\, d\boldsymbol{x}' &= \int_0^1 \frac{\boldsymbol{v}_\ell \times (\boldsymbol{x} - \boldsymbol{x}_{1,\ell} - s\boldsymbol{v}_\ell)}{|\boldsymbol{x} - \boldsymbol{x}_{1,\ell} - s\boldsymbol{v}_\ell|^3} ds \\ &= \frac{\boldsymbol{v}_\ell \times (\boldsymbol{x} - \boldsymbol{x}_{1,\ell})}{4\pi} \int_0^1 \frac{1}{|\boldsymbol{x} - \boldsymbol{x}_{1,\ell} - s\boldsymbol{v}_\ell|^3} ds, \end{aligned}$$

with $\boldsymbol{x}_{1,\ell}$, $\boldsymbol{x}_{2,\ell}$ the end-points of the edge ℓ and $\boldsymbol{v}_\ell := \boldsymbol{x}_{2,\ell} - \boldsymbol{x}_{1,\ell}$. If we denote by L_ℓ the straight line in $\mathbb{R}^3$ containing the edge ℓ, we notice that the integrand in the above expression is ill defined

if $\boldsymbol{x} \in \ell$ and that $\boldsymbol{H}_{BS}^{n,\ell}(\boldsymbol{x}) = \boldsymbol{0}$ for every $\boldsymbol{x} \in L_\ell \setminus \ell$. Let us define

$$\boldsymbol{a}_1 := \boldsymbol{x} - \boldsymbol{x}_{1,\ell} \qquad \text{and} \qquad \boldsymbol{a}_2 := \boldsymbol{x} - \boldsymbol{x}_{2,\ell}.$$

Then, it can be shown that the integral in the previous expression reduces to:

$$\boldsymbol{H}_{BS}^{n,\ell}(\boldsymbol{x}) = \begin{cases} \dfrac{(\boldsymbol{a}_1 - \boldsymbol{a}_2) \times \boldsymbol{a}_1}{4\pi} \dfrac{\boldsymbol{a}_2 \cdot (\boldsymbol{a}_1 - \boldsymbol{a}_2)\,|\boldsymbol{a}_1| - \boldsymbol{a}_1 \cdot (\boldsymbol{a}_1 - \boldsymbol{a}_2)\,|\boldsymbol{a}_2|}{|\boldsymbol{a}_1|\,|\boldsymbol{a}_2|\,|\boldsymbol{a}_1 \times \boldsymbol{a}_2|^2}, & \text{if } \boldsymbol{x} \notin L_\ell, \\ \boldsymbol{0}, & \text{if } \boldsymbol{x} \in L_\ell \setminus \ell. \end{cases} \tag{1.50}$$

Remark 1.23. *The above formula was developed following the ideas proposed by Urankar in [106], where he establishes an expression for the Biot-Savart field created by a straight current filament oriented in the $\boldsymbol{e}_z$ direction. Other alternatives can be found, for example, in [56] and the references therein.*

Even though (1.50) are analytical expressions to evaluate the integrals in (1.48), we compute numerically the integrals on the right hand side of (1.49) by means of the mid-point quadrature rule. In the next theorem we prove that the errors that arise from this numerical quadrature do not spoil the rate of convergence of the method in the case where all sources are given in terms of the current intensities.

Let $\widehat{\boldsymbol{t}}_{0,n}^h$ be the approximate discrete normalised impressed vector potential, obtained by using the mid-point rule for computing the integrals in (1.49); namely, $\widehat{\boldsymbol{t}}_{0,n}^h \in \boldsymbol{\mathcal{N}}_h(\Omega)$ and

$$\int_\ell \widehat{\boldsymbol{t}}_{0,n}^h \cdot \boldsymbol{\tau}_\ell := \begin{cases} \left(\boldsymbol{H}_{\mathrm{BS}}^n(\boldsymbol{x}_\ell) \cdot \boldsymbol{\tau}_\ell\right) |\ell|, & \text{if } \ell \subset \overline{\Omega \setminus \Omega_{\mathrm{C}}^n}, \\ 0, & \text{if } \ell \not\subset \overline{\Omega \setminus \Omega_{\mathrm{C}}^n}, \end{cases} \tag{1.51}$$

where $|\ell|$ denotes the length of the edge ℓ and $\boldsymbol{x}_\ell$ is its middle point. When $\widehat{\boldsymbol{t}}_{0,n}^h$ are used instead of $\boldsymbol{t}_{0,n}^h$ in Problem 1.10, we obtain an approximate discrete solution $(\widehat{\boldsymbol{T}}_h, \widehat{\phi}_h)$ instead of $(\boldsymbol{T}_h, \phi_h)$, from which we compute the approximate discrete magnetic field $\widehat{\boldsymbol{H}}_h := \widehat{\widetilde{\boldsymbol{T}}}_h + \sum_{n=1}^{N_I} I_n \widehat{\boldsymbol{t}}_{0,n}^h - \mathbf{grad}\, \widehat{\phi}_h$.

The following result shows that using the computed values $\widehat{\boldsymbol{H}}_h$ instead of the exact ones $\boldsymbol{H}_h$ does not deteriorate the order of convergence.

Theorem 1.24. *Let $\boldsymbol{H}_h$ and $\widehat{\boldsymbol{H}}_h$ be as defined above. Then, there exists a constant $C > 0$ such that*

$$\left\| \boldsymbol{H}_h - \widehat{\boldsymbol{H}}_h \right\|_{\mathrm{H}(\mathbf{curl},\Omega)} \leq Ch.$$

Proof. As shown in Theorem 1.14, $\boldsymbol{H}_h$ satisfies

$$\int_\Omega i\omega\mu \boldsymbol{H}_h \cdot \overline{\boldsymbol{G}}_h + \int_{\Omega_{\mathrm{C}}} \frac{1}{\sigma} \mathbf{curl}\, \boldsymbol{H}_h \cdot \mathbf{curl}\, \overline{\boldsymbol{G}}_h = 0 \quad \forall\, \boldsymbol{G}_h \in \boldsymbol{\mathcal{V}}_h(\boldsymbol{0}). \tag{1.52}$$

Notice that $\widehat{\boldsymbol{t}}_{0,n}^{\,h} \in \boldsymbol{\mathcal{N}}_h(\Omega)$ satisfy (1.34) but, in general,

$$\int_{\Gamma_{\mathrm{J}}^n} \mathbf{curl}\, \widehat{\boldsymbol{t}}_{0,n}^{\,h} \cdot \boldsymbol{n} \neq 1.$$

As a consequence, $\widehat{\boldsymbol{H}}_h$ is not a solution to Problem 1.11 because, in general, $\widehat{\boldsymbol{H}}_h \notin \boldsymbol{\mathcal{V}}_h(\boldsymbol{I})$. However, the same arguments used in the proof of Theorem 1.14 allow us to show that $\widehat{\boldsymbol{H}}_h$ satisfies the same equation:

$$\int_\Omega i\omega\mu \widehat{\boldsymbol{H}}_h \cdot \overline{\boldsymbol{G}}_h + \int_{\Omega_{\mathrm{C}}} \frac{1}{\sigma}\, \mathbf{curl}\, \widehat{\boldsymbol{H}}_h \cdot \mathbf{curl}\, \overline{\boldsymbol{G}}_h = 0 \quad \forall\, \boldsymbol{G}_h \in \boldsymbol{\mathcal{V}}_h(\mathbf{0}). \tag{1.53}$$

Let $\boldsymbol{F}_h := \widetilde{\boldsymbol{T}}_h - \mathbf{grad}\, \phi_h \in \boldsymbol{\mathcal{V}}_h(\mathbf{0})$ and $\widehat{\boldsymbol{F}}_h := \widehat{\widetilde{\boldsymbol{T}}}_h - \mathbf{grad}\, \widehat{\phi}_h \in \boldsymbol{\mathcal{V}}_h(\mathbf{0})$. Then, $\boldsymbol{H}_h = \boldsymbol{F}_h + \sum_{n=1}^{N_I} I_n \boldsymbol{t}_{0,n}^h$ and $\widehat{\boldsymbol{H}}_h = \widehat{\boldsymbol{F}}_h + \sum_{n=1}^{N_I} I_n \widehat{\boldsymbol{t}}_{0,n}^{\,h}$. Substituting these expressions into (1.52) and (1.53) and subtracting we obtain

$$\begin{aligned} &\int_\Omega i\omega\mu \Delta\boldsymbol{F}_h \cdot \overline{\boldsymbol{G}}_h + \int_{\Omega_{\mathrm{C}}} \frac{1}{\sigma}\, \mathbf{curl}\, \Delta\boldsymbol{F}_h \cdot \mathbf{curl}\, \overline{\boldsymbol{G}}_h \\ &+ \sum_{n=1}^{N_I} I_n \left(\int_{\Omega_{\mathrm{C}}} i\omega\mu \Delta\boldsymbol{t}_{0,n}^h \cdot \overline{\boldsymbol{G}}_h + \int_{\Omega_{\mathrm{C}}} \frac{1}{\sigma}\, \mathbf{curl}\, \Delta\boldsymbol{t}_{0,n}^h \cdot \mathbf{curl}\, \overline{\boldsymbol{G}}_h \right) = 0 \quad \forall\, \boldsymbol{G}_h \in \boldsymbol{\mathcal{V}}_h(\mathbf{0}), \end{aligned} \tag{1.54}$$

where $\Delta\boldsymbol{F}_h := \boldsymbol{F}_h - \widehat{\boldsymbol{F}}_h$ and $\Delta\boldsymbol{t}_{0,n}^h := \boldsymbol{t}_{0,n}^h - \widehat{\boldsymbol{t}}_{0,n}^{\,h}$. Since $a(\boldsymbol{F}_h, \boldsymbol{G}_h) := \int_\Omega i\omega\mu \boldsymbol{F}_h \cdot \overline{\boldsymbol{G}}_h + \int_{\Omega_{\mathrm{C}}} \frac{1}{\sigma}\, \mathbf{curl}\, \boldsymbol{F}_h \cdot \mathbf{curl}\, \overline{\boldsymbol{G}}_h$ is a continuous and elliptic bilinear form in $\boldsymbol{\mathcal{X}}_h \times \boldsymbol{\mathcal{X}}_h$ (see [22]), by taking $\boldsymbol{G}_h = \Delta\boldsymbol{F}_h$, we obtain

$$||\Delta\boldsymbol{F}_h||^2_{\mathrm{H}(\mathbf{curl},\Omega)} \leq C\, a(\Delta\boldsymbol{F}_h, \Delta\boldsymbol{F}_h) \leq C \sum_{n=1}^{N_I} |I_n|\, ||\Delta\boldsymbol{F}_h||_{\mathrm{H}(\mathbf{curl},\Omega)}\, ||\Delta\boldsymbol{t}_{0,n}^h||_{\mathrm{H}(\mathbf{curl},\Omega)},$$

and, then,

$$\begin{aligned} \left\| \boldsymbol{H}_h - \widehat{\boldsymbol{H}}_h \right\|_{\mathrm{H}(\mathbf{curl},\Omega)} &\leq ||\Delta\boldsymbol{F}_h||_{\mathrm{H}(\mathbf{curl},\Omega)} + \sum_{n=1}^{N_I} |I_n|\, ||\Delta\boldsymbol{t}_{0,n}^h||_{\mathrm{H}(\mathbf{curl},\Omega)} \\ &\leq C \sum_{n=1}^{N_I} |I_n|\, ||\Delta\boldsymbol{t}_{0,n}^h||_{\mathrm{H}(\mathbf{curl},\Omega)}. \end{aligned}$$

Let $\boldsymbol{\phi}_\ell$ be the basis function of the lowest-order Nédélec finite element space $\boldsymbol{\mathcal{N}}_h(\Omega)$ corresponding to the edge ℓ. Then,

$$\boldsymbol{t}_{0,n}^h = \sum_{\ell \subset \overline{\Omega \setminus \Omega_{\mathrm{C}}^n}} \left(\int_\ell \boldsymbol{H}_{\mathrm{BS}}^n \cdot \boldsymbol{\tau}_\ell \right) \boldsymbol{\phi}_\ell$$

and

$$\widehat{\boldsymbol{t}}_{0,n}^{\,h} = \sum_{\ell \subset \overline{\Omega \setminus \Omega_{\mathrm{C}}^n}} \left(\boldsymbol{H}_{\mathrm{BS}}^n(\boldsymbol{x}_\ell) \cdot \boldsymbol{\tau}_\ell |\ell| \right) \boldsymbol{\phi}_\ell,$$

$n = 1, \ldots, N$. Consequently, using the classical error formula for the mid-point rule leads to

$$||\Delta \boldsymbol{t}^h_{0,n}||_{\mathrm{L}^2(\Omega)^3} \leq \sum_{\ell \subset \overline{\Omega \setminus \Omega^n_{\mathrm{C}}}} \left| \int_\ell (\boldsymbol{H}_{\mathrm{BS}} - \boldsymbol{H}_{\mathrm{BS}}(\boldsymbol{x}_\ell)) \cdot \boldsymbol{\tau}_\ell \right| ||\boldsymbol{\phi}_\ell||_{\mathrm{L}^2(\Omega)^3}$$

$$\leq \sum_{\ell \subset \overline{\Omega \setminus \Omega^n_{\mathrm{C}}}} \frac{||\boldsymbol{H}_{\mathrm{BS}} \cdot \boldsymbol{\tau}_\ell||_{\mathrm{W}^{2,\infty}(\ell)} |\ell|^3}{24} ||\boldsymbol{\phi}_\ell||_{\mathrm{L}^2(\Omega)^3}$$

and, analogously,

$$||\operatorname{\mathbf{curl}} \Delta \boldsymbol{t}^h_{0,n}||_{\mathrm{L}^2(\Omega)^3} \leq \sum_{\ell \subset \overline{\Omega \setminus \Omega^n_{\mathrm{C}}}} \frac{||\boldsymbol{H}_{\mathrm{BS}} \cdot \boldsymbol{\tau}_\ell||_{\mathrm{W}^{2,\infty}(\ell)} |\ell|^3}{24} ||\operatorname{\mathbf{curl}} \boldsymbol{\phi}_\ell||_{\mathrm{L}^2(\Omega)^3},$$

Now, scaling arguments (see, for instance, [77]) and the regularity of the meshes lead to

$$||\boldsymbol{\phi}_\ell||_{\mathrm{L}^2(\Omega)^3} \leq \frac{C}{|\ell|} \qquad \text{and} \qquad ||\operatorname{\mathbf{curl}} \boldsymbol{\phi}_\ell||_{\mathrm{L}^2(\Omega)^3} \leq \frac{C}{|\ell|^2}.$$

Therefore,

$$||\Delta \boldsymbol{t}^h_{0,n}||_{\mathrm{L}^2(\Omega)^3} \leq Ch^2 \qquad \text{and} \qquad ||\operatorname{\mathbf{curl}} \Delta \boldsymbol{t}^h_{0,n}||_{\mathrm{L}^2(\Omega)^3} \leq Ch,$$

where C is a strictly positive constant independent of h. Then,

$$\left\| \boldsymbol{H}_h - \widehat{\boldsymbol{H}}_h \right\|_{\mathrm{H}(\mathbf{curl},\Omega)} \leq Ch.$$

□

Similarly, the conclusion of the above theorem can be extended to the case of Problem 1.19. However, for problems in which the potential drop is given as source data instead of the current intensity, the proof above is no longer valid. Nevertheless, we have numerically checked that this procedure for approximating the discrete normalised impressed vector potentials does not spoil the convergence rate.

1.6.2 Using Loop Fields

Alternatively to the strategy presented in the previous subsection, the procedure introduced in [5] to compute the so-called loop fields, (that is, the irrotational fields that cannot be expressed as gradients of single-valued scalar fields), allows constructing normalised impressed vector potentials that exactly meet conditions (1.33)–(1.34). This algorithm, like the previous one, does not make use of cutting surfaces, but is slightly more involved as it requires the use of some graph theory concepts. For completeness, we include here a brief description of the construction of a normalised impressed vector potential based on the one appearing in [5] and refer to this paper for further details.

First of all, we are going to introduce some definitions associated with graphs in the following remark.

Remark 1.25 (Graph theory concepts)**.** *A* graph $\mathfrak{G}$ *is an object consisting of two sets of elements: the so-called* vertices*,* $V(\mathfrak{G})$*, and the* edges*,* $E(\mathfrak{G})$*, along with a relation between them that associates each edge with two vertices, called its* ends*. Equivalently, one may think of the graph* $\mathfrak{G}$ *as the pair* $(V(\mathfrak{G}), E(\mathfrak{G}))$ *with*

$$E(\mathfrak{G}) \subset V(\mathfrak{G}) \times V(\mathfrak{G}).$$

A graph $\mathfrak{H}$ *is said to be a* subgraph *of graph* $\mathfrak{G}$ *if* $V(\mathfrak{H}) \subset V(\mathfrak{G})$ *and* $E(\mathfrak{H}) \subset E(\mathfrak{G})$*, each edge of* $\mathfrak{H}$ *having the same ends as an element of* $\mathfrak{H}$ *or* $\mathfrak{G}$*. A subgraph* $\mathfrak{H}$ *of* $\mathfrak{G}$ *is said to be a* spanning subgraph *if* $V(\mathfrak{H}) = V(\mathfrak{G})$*. See Figure 1.3 for an example on these concepts.*

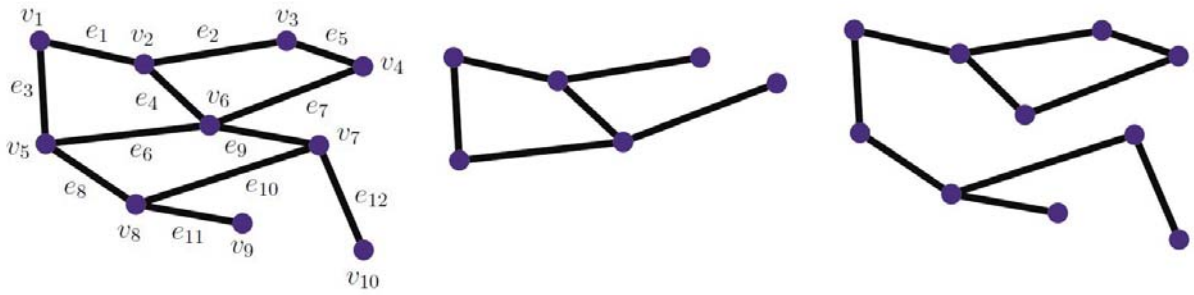

Figure 1.3: Example of a graph $\mathfrak{G}$ with vertices $V(\mathfrak{G}) = \{v_1, \ldots, v_{10}\}$ and edges $E(\mathfrak{G}) = \{e_1, \ldots, e_{12}\}$ (left). A subgraph of $\mathfrak{G}$ (center). A spanning subgraph of $\mathfrak{G}$ (right).

A walk *or* path *on a graph is an alternating sequence of vertices and edges, that contains at least one edge, no edge is used more than once and in which each edge is preceded and followed by its own end vertices. A* cycle *is a walk that starts and ends at the same vertex. A graph is* connected *if, for every two vertices, there is at least one walk between them; otherwise, we say that it is* disconnected*. See Figure 1.4 for an example on these concepts. In particular, all graphs contained in Figures 1.3 and 1.4 are connected.*

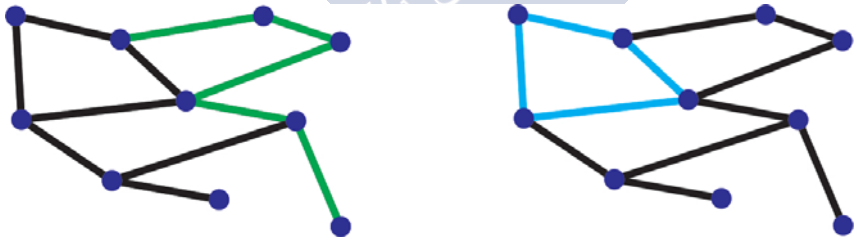

Figure 1.4: The subgraph in green is the walk $\{v_2, e_2, v_3, e_5, v_4, e_7, v_6, e_9, v_7, e_{12}, v_{10}\}$ on graph $\mathfrak{G}$ from Figure 1.3 (left). The subgraph in blue is the cycle $\{v_1, e_1, v_2, e_4, v_6, e_6, v_5, e_3, v_1\}$ (right) on graph $\mathfrak{G}$ from Figure 1.3.

A graph with no cycles is called a forest*, and a* tree *is a connected forest. Trees have the special property that every pair of its vertices is connected by a unique walk. A* spanning tree *of a graph is a spanning subgraph that is a tree, and therefore every two vertices are connected by exactly one walk. Sometimes it is convenient to label one vertex of a tree as special, being then called the* root *of the tree. Moreover, the tree with a fixed root is a* rooted tree*. In Figure 1.5 we show a spanning tree of graph* $\mathfrak{G}$ *appearing in Figure 1.3.*

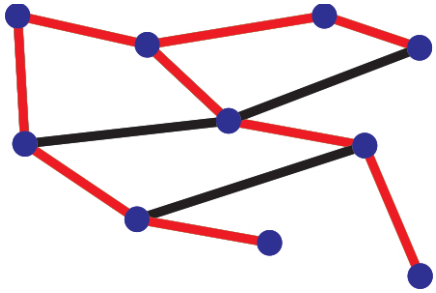

Figure 1.5: The subgraph in red is a spanning tree of graph $\mathfrak{G}$ from Figure 1.3.

If the edges of the graph $\mathfrak{G}$ are provided with an orientation, in such a way that for each of the edges we label one of its vertices as the initial and the other as the terminal, we call $\mathfrak{G}$ a directed graph *or* digraph *(see Figure 1.6–left). In a digraph, a* directed walk *is a walk in which an additional condition is imposed: the previous and following vertices of an edge have to be its start and end vertex, respectively (see Figure 1.6–right). Similarly, we can also extend the remaining above concepts to directed graphs, and we will sometimes drop the word "directed" from their name for the sake of simplicity.*

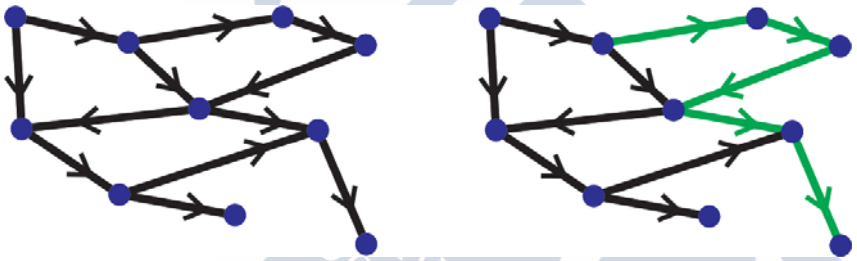

Figure 1.6: Example of a directed graph (left) and a directed walk defined on it (right).

Finally, we can assign each edge of a graph or directed graph $\mathfrak{G}$ a certain positive weight, obtaining a weighted (directed) graph. *In this way, we call a* minimum spanning tree *to a spanning tree in which the sum of the edges of the tree is minimal.*

In order to compute the loop field associated to an inductor Ω_{C}^n, we will consider the graph associated to the mesh of $\overline{\Omega \setminus \Omega_{\mathrm{C}}^n}$, considering the vertices and edges of this mesh as the corresponding ones of the graph. Moreover, we will assign each edge an orientation and a weight, in order to obtain a weighted directed graph. The orientation of the edges will be the one induced by the ordering of the mesh vertices, and their weight will be defined as the lengths of the corresponding mesh edges.

Let us denote by V and E the set of vertices and edges of the mesh

$$\mathcal{T}_h(\overline{\Omega \setminus \Omega_{\mathrm{C}}^n}) := \left\{ T \in \mathcal{T}_h : \, T \subset \overline{\Omega \setminus \Omega_{\mathrm{C}}^n} \right\},$$

respectively. Moreover, let $\mathcal{S}_h = (V, L)$ be a minimum spanning tree of the directed graph (V, E) and let v_1 be its root. Then, given a vertex $v \in V$, there exists a unique walk C_v that connects v_1 to v. Furthermore, given a walk C_v, let us denote by $-C_v$ the walk that connects v to v_1. Finally, given an edge $e \in E$, with initial and terminal vertices $v_{e,1}$ and $v_{e,2}$, respectively,

we define $D_e := C_{v_{e,1}} + e - C_{v_{e,2}}$ (see Figure 1.8). The Nédélec degrees of freedom of the normalised impressed vector potential can be computed as follows:

$$\int_\ell \boldsymbol{t}^h_{0,n} \cdot \boldsymbol{\tau}_\ell := \begin{cases} \mathrm{lk}(D_\ell, L_n), & \text{if } \ell \subset \overline{\Omega \setminus \Omega^n_{\mathrm{C}}}, \\ 0, & \text{if } \ell \not\subset \overline{\Omega \setminus \Omega^n_{\mathrm{C}}}, \end{cases}$$

where $\mathrm{lk}(D_\ell, L_n)$ is the so-called linking number of the oriented curves D_ℓ and L_n.

Remark 1.26. *According to [91], the linking number of two disjoint oriented curves γ and $\widetilde{\gamma}$ can be defined in up to eight different ways, all of them up-to-sign-equivalent. One of these definitions is the following:* $\mathrm{lk}(\gamma, \widetilde{\gamma})$ *is the number of times that γ winds around $\widetilde{\gamma}$ in the same direction (see Figure 1.7).*

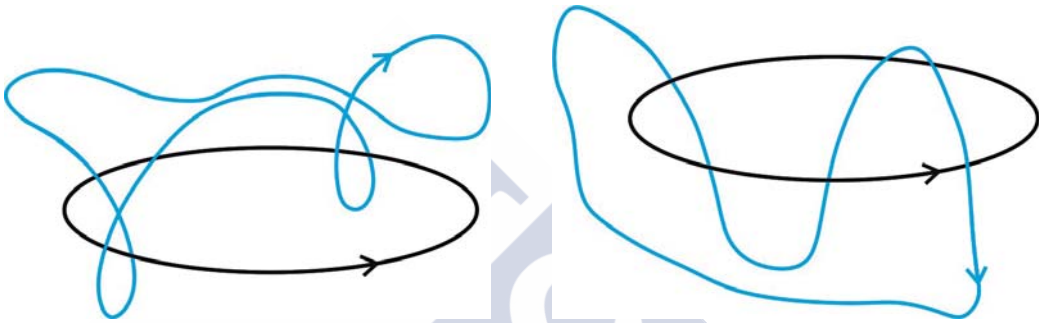

Figure 1.7: Examples of two oriented curves γ, in black, and $\widetilde{\gamma}$, in blue. The linking numbers are $\mathrm{lk}(\gamma, \widetilde{\gamma}) = 2$ (left) and $\mathrm{lk}(\gamma, \widetilde{\gamma}) = 0$ (right).

As shown in [5], the field $\boldsymbol{t}^h_{0,n}|_{\Omega \setminus \Omega^n_{\mathrm{C}}} \in \boldsymbol{\mathcal{N}}_h(\Omega \setminus \Omega^n_{\mathrm{C}})$ computed in this way is a loop field in $\mathcal{T}_h(\overline{\Omega \setminus \Omega^n_{\mathrm{C}}})$, and therefore it satisfies (1.33). Indeed, according to [5], the loop fields in a domain D are the solutions $\mathbf{Z}_h \in \boldsymbol{\mathcal{N}}_h(D)$ to the problem:

$$\mathbf{curl}\, \mathbf{Z}_h = \mathbf{0} \qquad \text{in } D, \tag{1.55}$$

$$\int_{\sigma_n} \mathbf{Z}_n \cdot \boldsymbol{\tau} = \kappa_n, \quad n = 1, \ldots, h_1, \tag{1.56}$$

$$\int_e \mathbf{Z}_h \cdot \boldsymbol{\tau} = 0 \qquad \forall e \in L_D, \tag{1.57}$$

where L_D is the set of edges of a spanning tree of the graph associated to a tetrahedral mesh of D, h_1 is the first Betti number of D, $\{[\sigma_n]\}_{n=1}^{h_1}$ is a basis of the first homology group of D, and $\kappa_n \in \mathbb{R}$, $n = 1, \ldots, h_1$, not all of them null. We notice that, when introducing the current filaments in Section 1.6.1, we are implicitly assuming that $\{[L_n]\}$ is a basis of the first homology group of $\mathbb{R}^3 \setminus \overline{\Omega \setminus \Omega^n_{\mathrm{C}}}$ (the first Betti number of $\mathbb{R}^3 \setminus \overline{\Omega \setminus \Omega^n_{\mathrm{C}}}$ is equal to one). Moreover, it is easy to see that $\boldsymbol{t}^h_{0,n}$ also verifies (1.34) since the current filaments verify $\mathrm{lk}(\partial\Gamma^n_{\mathrm{J}}, L_n) = 1$.

In order to compute this linking number we have used the algorithm described in [10]. We remark that calculating the linking number can be very costly even though we only have to do it for the edges e not belonging to $\mathcal{S}_h$ (since otherwise $C_{v_{e,1}} + e = C_{v_{e,2}}$ and D_ℓ degenerates). We refer to [5] for a more efficient algorithm to perform this computations.

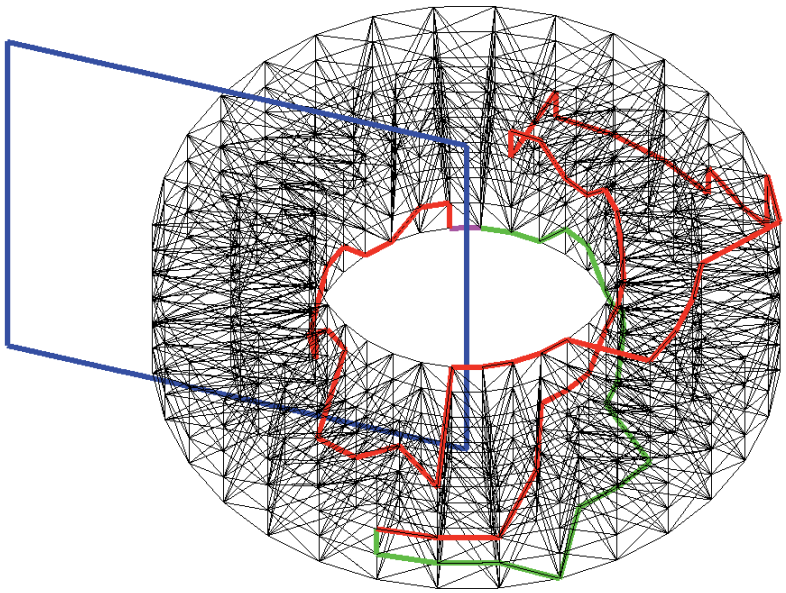

Figure 1.8: Current filament L_1 (blue), edge e (pink), walk $C_{v_{e,1}}$ (red) and walk $-C_{v_{e,2}}$ (green) with $\Omega_{\mathrm{D}} = \Omega \setminus \overline{\Omega_{\mathrm{C}}^1}$ a hollow cylinder.

1.7 Numerical Results

In this section we report some numerical results obtained with a MATLAB code which implements the numerical methods described above. In particular, since the linear system matrix arising from Problem 1.10 is complex non-Hermitian, we have used the command `bicg` to solve it, with a tolerance threshold of 10^{-8}. Let us remark that when this command is applied to an underdetermined linear system with a singular square matrix, it yields one particular solution. (Let us recall that obtaining one particular solution is enough, since any solution of this problem leads to the same magnetic field.) On the other hand, to solve Problem 1.19, we have used the *backslash* function.

First, we will study the convergence of the method by using an example with known analytical solution and only one connected component in the conducting part. Next, we will report the results for two examples having a domain with several connected components in the conducting domain.

1.7.1 Test with Analytical Solution

In this section we report the numerical results obtained for an academic test that confirm the results stated in the previous sections and the convergence of the proposed methodology.

We take as conducting domain a section of height $L = 0.5$ m of an infinite cylinder with radius $R = 0.5$ m, as shown in Figure 1.9 (left). This cylinder is composed by a conducting material

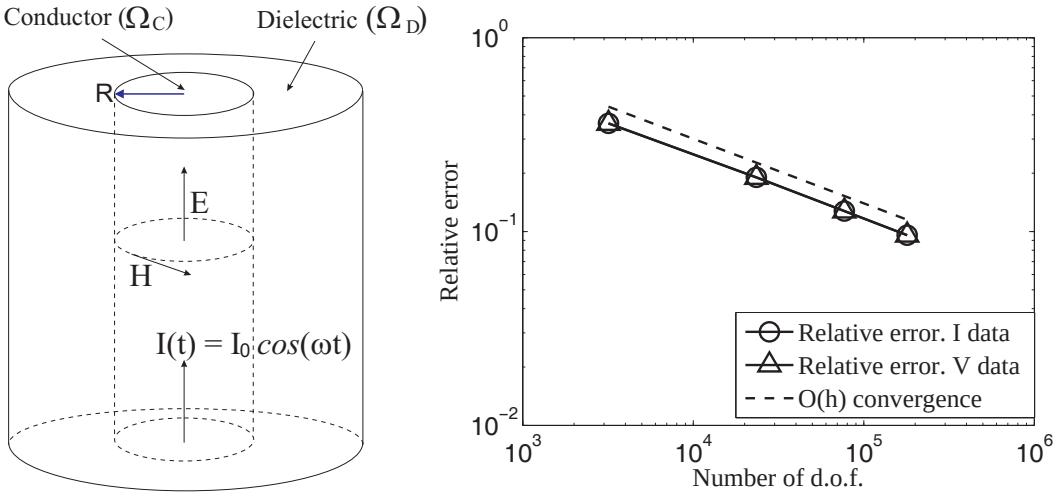

Figure 1.9: Infinite cylinder carrying an alternating current (left). Convergence order in $\mathrm{H}(\mathbf{curl}, \Omega)$ (right).

with electrical conductivity $\sigma = 151565.8\ (\Omega\mathrm{m})^{-1}$ and magnetic permeability $\mu = \mu_0 = 4\pi \times 10^{-7}\ \mathrm{Hm}^{-1}$, and it carries an alternating current $I(t) = I_0 \cos(\omega t)$, where $I_0 = 10^4$ A and $\omega = 2\pi f$, with $f = 50$ Hz, surrounded by dielectric material having an outer radius $R_\infty = 1$ m. We can obtain the analytical solution to the associated eddy current problem, which is (see [7], Section 8.1.5):

$$\boldsymbol{H}(\boldsymbol{x}) = \begin{cases} \dfrac{I_0 \mathcal{I}_1(\sqrt{i\omega\mu\sigma}\rho)}{2\pi R \mathcal{I}_1(\sqrt{i\omega\mu\sigma}R)} \boldsymbol{e}_\theta, & \text{if } \rho \leq R, \\ \dfrac{I_0}{2\pi\rho} \boldsymbol{e}_\theta, & \text{if } \rho > R, \end{cases}$$

where $\mathcal{I}_1$ is the modified Bessel function of the first kind and order 1, and $\rho = \sqrt{x_1^2 + x_2^2}$ and $\boldsymbol{e}_\theta := (-x_2, x_1, 0)/\rho$ are the radial coordinate and the angular unit vector in cylindrical coordinates, respectively. Notice that the solution to the problem does not depend on the values of L or R_∞ because the magnetic field $\boldsymbol{H}$ is independent of the z-coordinate and it exactly satisfies the boundary condition (1.6).

When comparing the numerical solution obtained from Problem 1.10 with the exact one, we obtain the error curves in Figure 1.9 (right), which show that an order of convergence $O(h)$ is clearly attained in this case, in agreement with the theoretical results. This test has been separately performed with current and potential drop as source data; the solutions showed the expected order of convergence with very similar relative errors with respect to the analytical solution, as it is deduced from the overlapping of the error curves in Figure 1.9 (right). In particular, for the case in which the potential drop is given, we have used the analytical expression (see again [7], Section 8.1.5):

$$\Delta V = \frac{\sqrt{i\omega\mu\sigma} L I_0}{2\pi\sigma R} \frac{\mathcal{I}_0(\sqrt{i\omega\mu\sigma}R)}{\mathcal{I}_1(\sqrt{i\omega\mu\sigma}R)} + i\omega\mu \frac{L I_0}{2\pi} \log\left(\frac{R_\infty}{R}\right),$$

where $\mathcal{I}_0$ is the modified Bessel function of the first kind and order 0. The conclusions are exactly the same for the fields obtained when solving Problem 1.19, and they are a particular solution

to the undetermined system arising from Problem 1.10. Moreover, the norm of the Lagrange multiplier function ξ is of order 10^{-16} with either current or potential drop as source data. Finally, we can compare the size of the linear system associated to the gauged and ungauged versions of the problem. In the case of the finer mesh, the first one has a total of 90609 degrees of freedom, while there are 82976 in the second case. Even though in this case the difference between the degrees of freedom is only of an 8%, situations with a greater time frequency require a much finer mesh in conductors in order to capture the so-called *skin effect*, leading to a greater difference between the two values.

1.7.2 Examples with Several Connected Components in the Conductor

In this section we report the results of two numerical tests with a topological setting closer to that appearing in applications, where the conducting domain usually comprises several connected components.

In the first example, *Test 1*, the proposed geometry consists of two cylindrical inductors, Ω_C^1 and Ω_C^2, with radius $R_c = 0.05$ m and height $h_c = 0.5$ m, and a parallelepipedic workpiece, Ω_C^3, with dimensions $h_w = 0.2$ m, $l_w = 0.2$ m and $w_w = 0.05$ m (see Figure 1.10). The distance between each inductor and the workpiece is 0.05 m. Both inductors have electrical conductivity $\sigma = 100\ (\Omega\text{m})^{-1}$ and vacuum magnetic permeability μ_0, while the workpiece has electrical conductivity $\sigma = 10^6\ (\Omega\text{m})^{-1}$ and vacuum magnetic permeability μ_0. The inductors are connected to an external current source and surrounded by a box of dielectric material of dimensions $w_D = 2.2$ m and $l_D = 2$ m (and with the same height as the inductors). The main goal is to compute the current density induced within the workpiece. The currents entering the inductors are $I_1 = I_2 = 10^3$ A, the frequency of the problem being $f = 50$ Hz.

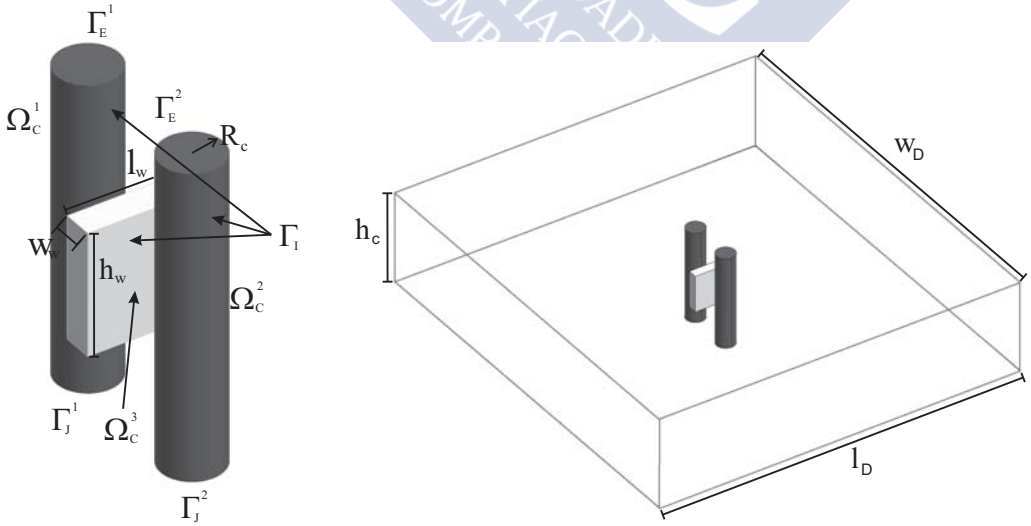

Figure 1.10: Geometrical setting for the conducting domain (left) and for the whole computational domain (right). Test 1.

In Figure 1.11 we show the complex modulus of the current density in the workpiece. Notice that the mesh was generated taking into account the *skin effect*, which usually appears in this

		Problem 1.10	Flux	Relative Error
Active Power (W)	Ω_{C}^1	$3.2105e5$	$3.1924e5$	0.5666%
$\int_{\Omega_{\mathrm{C}}^j} \frac{\lvert\boldsymbol{J}\rvert^2}{2\sigma}$, $j=1,2,3$	Ω_{C}^2	$3.2105e5$ W	$3.1955e5$ W	0.4691%
	Ω_{C}^3	0.0685 W	0.0632 W	6.6718%
Potential Drop (V)	ΔV_1	$642.1028 + 0.1574i$	$636.6797 + 0.1528i$	0.5666%
	ΔV_2	$642.1005 + 0.1572i$	$636.6760 + 0.1526i$	0.4691%

Table 1.1: Active power and potential drop comparison. Test 1.

kind of problems, making the current density in the workpiece to be highly concentrated near its boundary. This can be clearly seen in Figure 1.11.

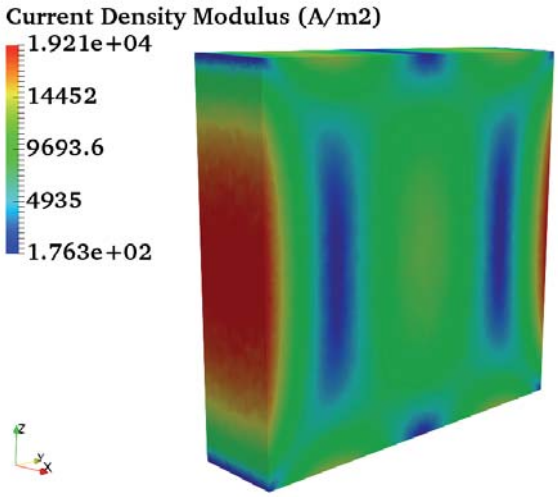

Figure 1.11: Current density modulus (A/m^2) in the workpiece Ω_{C}^3. Test 1.

In order to validate the method in this topological setting, we have compared the magnetic field obtained from the solution to Problem 1.10 and the solution to the same problem obtained with the commercial software Altair Flux®, which makes use of another variant of the $\boldsymbol{T}$,ϕ–ϕ with second order elements. This comparison is presented in terms of the active power in each connected component of the conducting domain and the potential drop in the inductors (see Tab. 1.1). Moreover, in Figure 1.12, we compare the value of the current density modulus along straight lines in the workpiece Ω_{C}^3 passing through the center of the piece in the z- and y-directions.

As it can be seen in Figure 1.12, the current density presents an important rate of change both along the z- and the y-directions in the workpiece. Anyway, the agreement between the values of the density computed with both methods can be clearly seen from this figure. Let us remark that this agreement is even better in the inductors, as is suggested by Table 1.1.

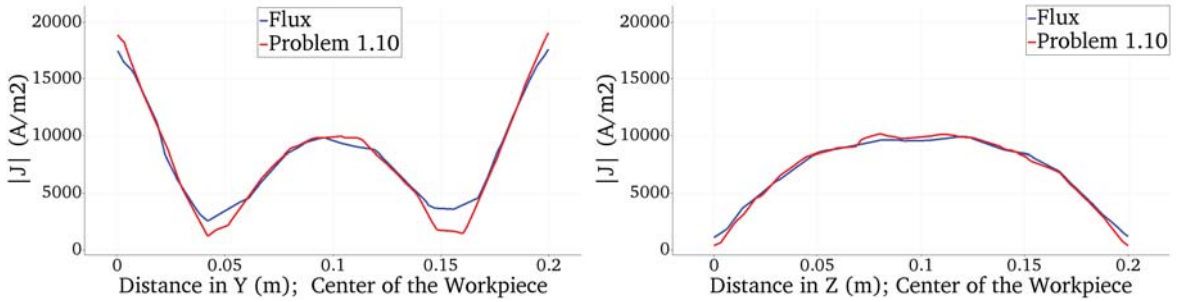

Figure 1.12: Current density modulus (A/m^2) comparison in the workpiece Ω_C^3 along different directions. Test 1.

On the other hand, we have considered a second example, *Test 2*, having a more involved geometry for the inductor, inspired in the configuration of an induction furnace (see [69]). As it can be seen in Figure 1.13, the conducting domain consists of a helical coil wounding around a cylindrical workpiece; the dielectric domain is just a parallelepipedic box of air surrounding the conductors. The workpiece is a cylinder of diameter 0.0035 m and it is 0.024 m high; the helical coil has a circular section of diameter 0.004 m, and it has a diameter of 0.016 m and a height of 0.026 m; the box measures $0.054 \times 0.054 \times 0.070$ m. All materials have the magnetic permeability of the vacuum, μ_0, while the electrical conductivity is equal to 58×10^6 $(\Omega\text{m})^{-1}$ for the helical conductor and 10^4 $(\Omega\text{m})^{-1}$ for the cylindrical one. The current that enters the inductor has an amplitude of 4×10^4 A, and the frequency of the problem is $f = 50$ Hz.

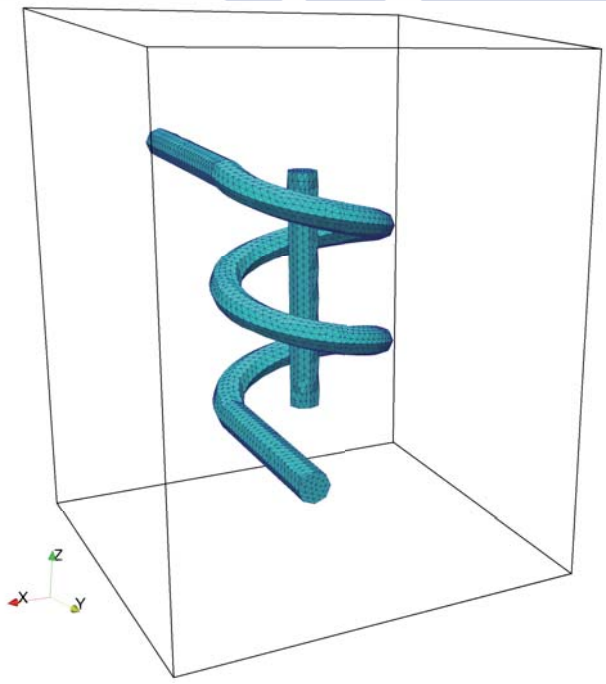

Figure 1.13: Geometrical setting for the conducting domain (blue) and dielectric domain (box). Test 2.

In Figure 1.14 we show the distribution of the normalised imposed vector potential $\boldsymbol{t}_0$ corresponding to the helical inductor, which is a real field. Moreover, Figure 1.15 shows the modulus of the magnetic field in the workpiece obtained from the solution to Problem 1.19.

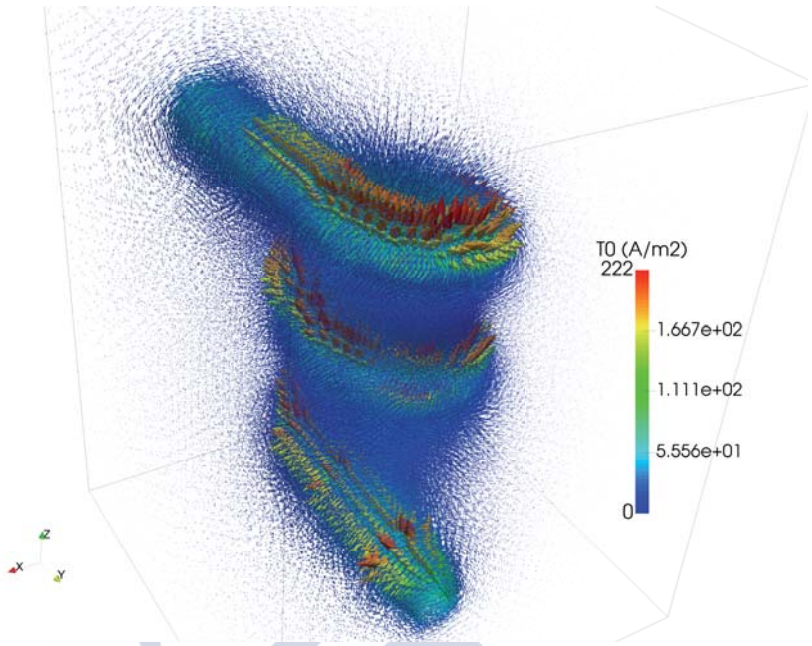

Figure 1.14: Normalised impressed vector potential $\boldsymbol{t}_0$. Test 2.

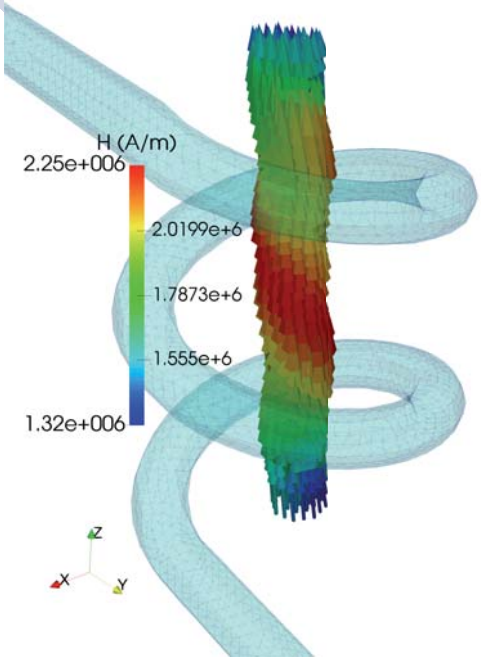

Figure 1.15: Complex modulus of the magnetic field (A/m) in the workpiece. Test 2.

USC
UNIVERSIDADE
DE SANTIAGO
DE COMPOSTELA

Chapter 2

Numerical Simulation of Magnetization and Demagnetization Processes

2.1 Introduction

Magnetic particle inspection (MPI) is a non–destructive testing (NDT) method that uses magnetization to detect surface breakings or near-surface defects in ferromagnetic pieces. Generally, the NDT methods use non-invasive techniques to determine the physical integrity of materials or structures. The physical basis of the MPI is as follows: when a ferromagnetic material is subjected to a magnetic field, the magnetic flux density accumulates in the interior of the specimen. Then, if a crack is present, the sudden change in the magnetic permeability of the medium results in an adjustment of the flux distribution to avoid the inhomogeneity. Therefore, the magnetic flux density increases in the surroundings of the breaking. As a consequence, if the magnetized piece is sprayed with fluorescent magnetic particles, these would concentrate at the defect region, which would become easily identified under ultraviolet light (see Figure 2.1). For more information on magnetic particle inspection, see [70] and references therein.

Since the objective of MPI is to reveal defects having any possible direction, and taking into account that the breakings are more easily detected when they are oriented perpendicularly to the magnetic field in the specimen, two kinds of magnetic field are usually established within the material: with circular and longitudinal orientation (see Figure 2.2).

On the other hand, magnetic moments of ferromagnetic materials have a strong tendency to align with external magnetic fields. Thus, these materials exhibit strong magnetic properties, whose effect remains even after the disappearance of the external field. Therefore, in most cases, pieces have to be demagnetized after the inspection, as residual magnetism could interfere with subsequent processing. While magnetic hysteresis could be neglected in the simulation of both magnetization steps (since the material is saturated to a great extent, see [66] and [110]), for the modeling of the demagnetization process, incorporating a hysteresis law is unavoidable. Generally, the existing literature on this topic focuses on the analysis of the magnetic field in terms

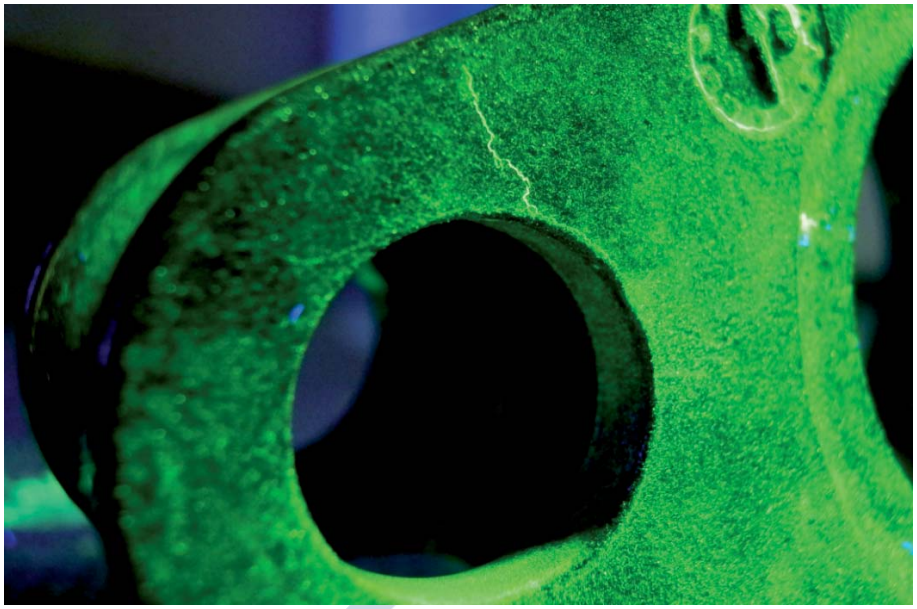

Figure 2.1: Surface breaking observed using MPI. From Wikimedia Commons under license CC-BY-SA-3.0.

of the contour and dimension of the defects and on the interplay between this magnetic field and the magnetic particles. In particular, the demagnetization stage that usually follows these processes is not considered, and hysteresis is not taken into account. To the authors' knowledge, the only exception to this practice can be found in [65]; in this publication, the author simulates a circular magnetization process, performed with a DC current and taking hysteresis into account in order to study the interaction between the remanent magnetic field and the magnetic particles close to the cracks.

Computer simulation has been proved to be very helpful in the study of all kinds of physical phenomena. In the particular case of MPI, the analysis of the numerical results when applying different current waveforms in various geometric configurations can lead to a better understanding of the technique and to an improvement of the inspection and demagnetization processes.

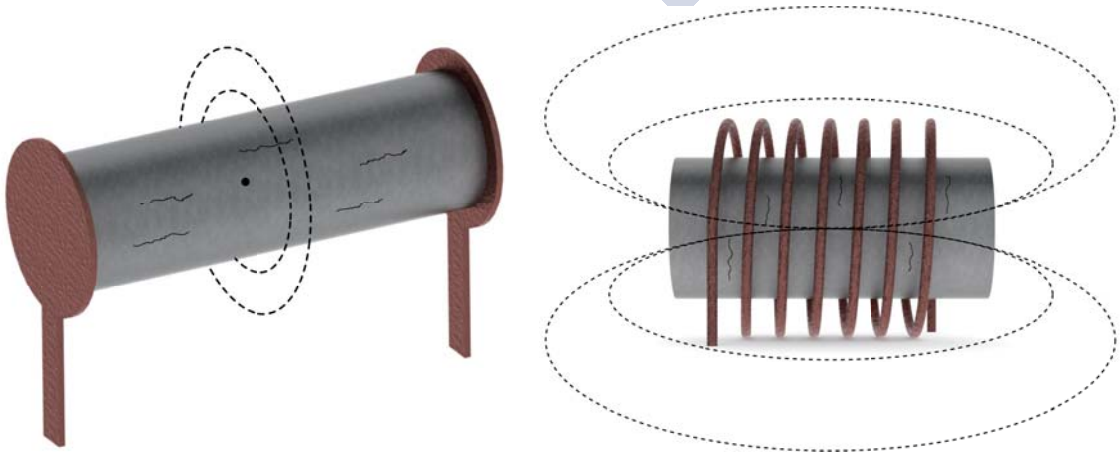

Figure 2.2: Field lines in circular magnetization (left) and longitudinal magnetization (right).

We refer the reader to [11] for a review on the finite element method applied to electromagnetic NDT.

The main contribution of this chapter is the simulation of the complete magnetization and demagnetization process involved in a MPI test by including the magnetic hysteresis. The outline of this chapter is as follows: in Section 2.2 we present the mathematical formulations used to simulate the different stages of the magnetic particle inspection process; Section 2.2.1 contains an explanation of the formulation for the circular magnetization and demagnetization steps, and in Section 2.2.2 the same description is performed for the longitudinal case; furthermore, Section 2.2.3 describes the model employed to simulate the magnetic hysteresis. Moreover, in Section 2.3 some comments are made on the numerical implementation of the models presented in Section 2.2. Finally, in Section 2.4 we present and analyze several numerical results, for the circular case in Section 2.4.1 and for the longitudinal one in Section 2.4.2.

2.2 Mathematical Models of Magnetization and Demagnetization

The electromagnetic models for both magnetization and demagnetization processes will be based on the eddy current model. More precisely, we will start from equations (I.7)–(I.9), completed with Ohm's law $\boldsymbol{J} = \sigma \boldsymbol{E}$ in conductors ($\sigma > 0$ being the electrical conductivity), $\boldsymbol{J} = \boldsymbol{0}$ in dielectrics and a suitable isotropic relation between $\boldsymbol{H}$ and $\boldsymbol{B}$, which will be detailed in Section 2.2.3.

The usual procedure followed in industry to perform a MPI test can be divided into three steps. First, the ferromagnetic piece is successively subjected to longitudinal and circular magnetization. Then, the demagnetization process takes place, which can be carried out inducing either a circular or a longitudinal field. Nevertheless, we will study the case in which the magnetization steps could be performed in any order.

From the physical point of view, if a circularly magnetized piece is subjected to a longitudinal magnetic field, the latter will erase the existing magnetization (as long as its amplitude is large enough) due to the change in the field direction (see [40]). Naturally, this would also happen if one subjects a longitudinally magnetized specimen to a circular magnetic field. Consequently, circular and longitudinal magnetizations/demagnetizations are considered to be independent processes and they will be modeled separately. We will only couple magnetization and demagnetization when the induced fields have the same direction.

2.2.1 Circular Model

The circular magnetization and demagnetization are performed by clamping the piece between two electrical contacts while the current is passed directly through the specimen, going from

one contact to the other (see Figure 2.2–left). To model it, we will consider that the conducting ferromagnetic pieces have cylindrical symmetry and that all fields are θ–independent. We will also assume that the current density traverses the piece along its axial direction and has the form $\boldsymbol{J}(\boldsymbol{x},t) \equiv J_z(\rho,z,t)\boldsymbol{e}_z$. As a consequence, from (I.8), Ohm's law and the isotropic property, we deduce that $\boldsymbol{H}(\boldsymbol{x},t) \equiv H_\theta(\rho,z,t)\boldsymbol{e}_\theta$. We will denote by $(\boldsymbol{e}_\rho,\boldsymbol{e}_\theta,\boldsymbol{e}_z)$ the orthonormal basis of the cylindrical coordinate system.

We highlight that, since we are only interested in the magnetic fields in the ferromagnetic piece, we will restrict ourselves to a problem defined in this domain. This is possible because, in this particular case, thanks to certain assumptions on the current density that are specified below, we are able to define suitable boundary conditions for H_θ in terms of the problem data, which will be the current $I(t)$ entering the piece through the contacts.

Taking (I.7), (I.8) and Ohm's law into account, we deduce the following equation in the conducting domain

$$\frac{\partial B_\theta}{\partial t}\boldsymbol{e}_\theta + \mathbf{curl}\left(\frac{1}{\sigma}\,\mathbf{curl}(H_\theta \boldsymbol{e}_\theta)\right) = \mathbf{0}. \tag{2.1}$$

On the other hand, we will assume that the current density enters perpendicularly to the contacts, that is, $\boldsymbol{J}\times\boldsymbol{n} = \mathbf{0}$ on these parts of the boundary, and that it is tangential to the rest of the boundary, i.e., $\boldsymbol{J}\cdot\boldsymbol{n} = 0$. Therefore, the current crossing the domain can be defined as

$$I(t) = \int_{\mathcal{S}_z} \boldsymbol{J}(\boldsymbol{x},t)\cdot\boldsymbol{n}(\boldsymbol{x}),$$

where $\mathcal{S}_z$ is any cross-section transversal to the axial direction. Taking (I.7) and Stokes' theorem into account, it follows that

$$I(t) = \int_{\partial\mathcal{S}_z} \boldsymbol{H}(\boldsymbol{x},t)\cdot\boldsymbol{\tau}(\boldsymbol{x}) = \int_0^{2\pi} H_\theta(R_{\mathcal{S}}(z),z,t)\, R_{\mathcal{S}}(z)\, d\theta,$$

where $R_{\mathcal{S}}(z)$ is the radius of cross-section $\mathcal{S}_z$ and $\boldsymbol{\tau}$ is the unit vector tangent to $\partial\mathcal{S}_z$ (see Figure 2.3). Then,

$$H_\theta(R_{\mathcal{S}}(z),z,t) = \frac{I(t)}{2\pi R_{\mathcal{S}}(z)} \tag{2.2}$$

for every $\mathcal{S}_z$.

Taking (2.1) and (2.2) into account and using the notation in Figure 2.4, the problem to solve is defined only in the meridional section Ω of the piece to inspect and reads

Problem 2.1. *Given current $I(t)$ and an initial magnetic intensity field H_0, find H_θ in $\Omega\times(t_0,T]$*

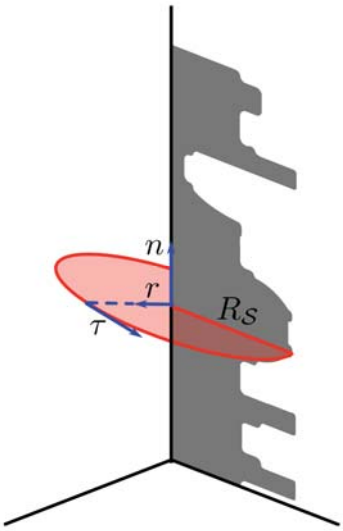

Figure 2.3: Cross-section $\mathcal{S}_z$ with unit tangent vector $\boldsymbol{\tau}$.

Figure 2.4: Computational domain. Circular magnetization.

such that

$$\frac{\partial \mathcal{B}(H_\theta,\xi)}{\partial t}\boldsymbol{e}_\theta + \mathbf{curl}\left(\frac{1}{\sigma}\,\mathbf{curl}(H_\theta \boldsymbol{e}_\theta)\right) = \mathbf{0} \quad \textit{in } \Omega \times (t_0,T], \tag{2.3}$$

$$H_\theta(0,z,t) = 0 \quad \textit{on } (0,L)\times(t_0,T], \tag{2.4}$$

$$H_\theta(R_{\mathcal{S}}(z),z,t) = \frac{I(t)}{2\pi R_{\mathcal{S}}(z)} \quad \textit{on } (0,L)\times(t_0,T], \tag{2.5}$$

$$\frac{\partial H_\theta}{\partial z}(\rho,z,t) = 0 \quad \textit{on } (\Gamma_1\cup\Gamma_2)\times(t_0,T], \tag{2.6}$$

$$H_\theta(\rho,z,t_0) = H_0(\rho,z) \quad \textit{in } \Omega. \tag{2.7}$$

In the above problem, where L is the piece length in the axial direction, $\mathcal{B}$ is the scalar hysteresis operator that defines the magnetic flux density in terms of the magnetic intensity field and ξ describes the initial magnetization state (see Section 2.2.3). We notice that H_θ has to be null on the symmetry axis in order to prevent nonphysical singularities, and that boundary condition (2.6) follows from the current density being entering perpendicularly to the contacts.

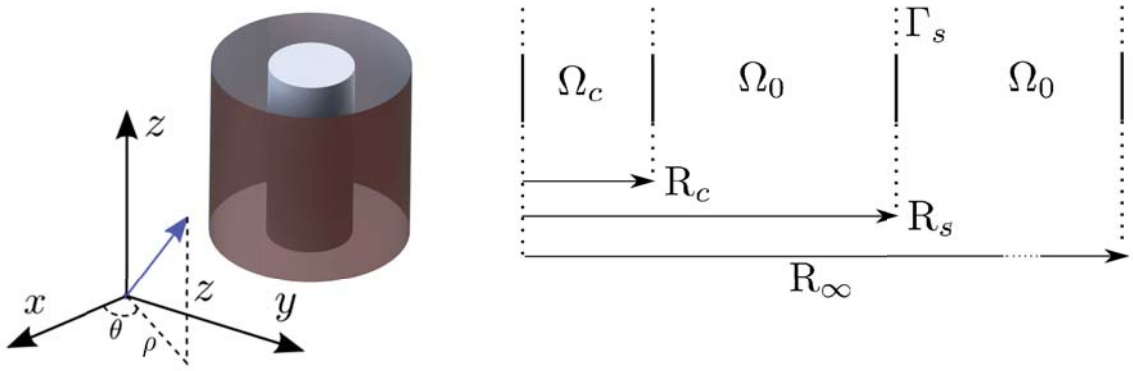

Figure 2.5: Geometric domain 3D (left) and meridional section (right). Longitudinal magnetization.

2.2.2 Longitudinal Model

In the longitudinal magnetization and demagnetization stages, the piece to be examined is located inside a conducting coil carrying an alternating current in the azimuthal direction (see Figure 2.2 – right). Thus, in order to consider pieces having cylindrical symmetry, it may seem convenient to replace the coil by several toroidal rings and to develop an axisymmetric model written in terms of the azimuthal component of the magnetic vector potential. However, in such a case the magnetic intensity and magnetic induction fields would be vectors, and then the inclusion of a vector hysteresis law would be unavoidable. Therefore, as a first step, we propose a simplified model for the analysis of the longitudinal case, which will be defined in a one dimensional domain and use a scalar hysteresis law. The key point for this simplification consists in assuming that the pieces are cylindrical and unbounded in the z-direction. Moreover, we approximate the coil by an infinitely thin conducting surface Γ_{S} carrying a surface current density $\boldsymbol{J}_{\mathrm{S}}(\boldsymbol{x},t) \equiv J_{\mathrm{S}}(\rho,t)\boldsymbol{e}_\theta$ (see Figure 2.5).

We will denote by Ω_c the piece to be inspected, with radius R_c, composed by a conducting ferromagnetic material with hysteresis effects, and by Ω_0 the air surrounding it. The air is artificially bounded in the ρ-direction, R_∞ being its outer radius. Finally, we call R_{S} the distance from the conducting surface to the symmetry axis.

The geometric considerations, along with the source direction, suggest that the fields are independent of the (θ, z) coordinates. Then, taking (I.7) and the source form into account, we deduce that $\boldsymbol{H}(\boldsymbol{x},t) \equiv H_z(\rho,t)\boldsymbol{e}_z$. Moreover, we assume that the material has an isotropic magnetic behavior which implies that $\boldsymbol{B}(\boldsymbol{x},t) \equiv B_z(\rho,t)\boldsymbol{e}_z$.

Gauss' magnetic law (I.9) leads to the existence of a magnetic vector potential $\boldsymbol{A}$ such that $\boldsymbol{B} = \mathbf{curl}\,\boldsymbol{A}$. This vector field is defined up to the gradient of a scalar field; in order to ensure uniqueness of the solution to the problem, we can impose a gauge condition such as $\mathrm{div}\,\boldsymbol{A} = 0$. Furthermore, in the considered case, it can be proved that $\boldsymbol{A}(\boldsymbol{x},t) \equiv A_\theta(\rho,t)\boldsymbol{e}_\theta$. Then, taking (I.7)–(I.8) and Ohm's law into account, and since domain Ω_c contains the symmetry axis, we can rewrite the problem as follows:

Problem 2.2. *Given the surface current density* $J_{\mathrm{S}}(t)$ *and an initial condition* A_0 *in* $(0, R_c)$*, find* A_θ *in* $(0, R_\infty) \times (t_0, T]$ *such that*

$$\sigma \frac{\partial A_\theta}{\partial t} - \frac{\partial}{\partial \rho}\left(\mathcal{B}^{-1}\left(\frac{1}{\rho}\frac{\partial}{\partial \rho}\left(\rho A_\theta\right), \xi\right)\right) = 0 \quad \textit{in } (0, R_c) \times (t_0, T], \tag{2.8}$$

$$\frac{\partial}{\partial \rho}\left(\frac{1}{\mu_0}\frac{1}{\rho}\frac{\partial}{\partial \rho}\left(\rho A_\theta\right)\right) = 0 \quad \textit{in } [(R_c, R_{\mathrm{S}}) \cup (R_{\mathrm{S}}, R_\infty)] \times (t_0, T], \tag{2.9}$$

$$\left[\frac{1}{\mu_0}\frac{1}{\rho}\frac{\partial}{\partial \rho}(\rho A_\theta)\right]_{\rho = R_{\mathrm{S}}} = J_{\mathrm{S}}(t) \quad \textit{on } \{R_{\mathrm{S}}\} \times (t_0, T], \tag{2.10}$$

$$A_\theta = 0 \quad \textit{on } \{0\} \times (t_0, T], \tag{2.11}$$

$$\frac{1}{\rho}\frac{\partial}{\partial \rho}(\rho A_\theta) = 0 \quad \textit{on } \{R_\infty\} \times (t_0, T], \tag{2.12}$$

$$A_\theta = A_0 \quad \textit{in } (0, R_c) \times \{t_0\}. \tag{2.13}$$

In the above problem, where $[\,\cdot\,]_{\rho = R_{\mathrm{S}}}$ denotes the jump across the surface $\rho = R_{\mathrm{S}}$ and μ_0 is the vacuum's magnetic permeability. Notice that the source is imposed by (2.10), i.e., by the jump of $\boldsymbol{H} \times \boldsymbol{n}$ at $\rho = R_{\mathrm{S}}$, which is equal to the surface current density $\boldsymbol{J}_{\mathrm{S}}$. An important advantage of this approximated model is that R_∞ can be taken as close to R_{S} as desired because, from Ampères law (I.7) in the air, the magnetic field $\boldsymbol{H}$ has to be null beyond the conducting surface, and thus the Neumann boundary condition (2.12) holds for any $\rho > R_{\mathrm{S}}$. Moreover, and similarly to the circular case, we have required A_θ to be null on the symmetry axis in order to avoid the appearance of nonphysical singularities in the solution.

2.2.3 Magnetic Hysteresis

The behavior of hysteretic materials is characterized by the dependance of the magnetic induction $\boldsymbol{B}$ at each point $\boldsymbol{x}$ not only on the value of the magnetic intensity $\boldsymbol{H}$ at present time but also on the so–called magnetic history. The latter, at a point $\boldsymbol{x}$, is simply the set of all past values of the magnetic intensity $\boldsymbol{H}$ at $\boldsymbol{x}$.

In both the circular and the longitudinal formulations, the magnetic intensity and induction fields only have one non–null component, in the $\boldsymbol{e}_z$ direction in the longitudinal case and in the $\boldsymbol{e}_\theta$ direction in the circular one. This allows us to use a scalar constitutive law for the nonlinear material. In order to simulate the magnetic hysteresis, we have chosen the well–known classical Preisach model (see [73]). This model characterizes soft ferromagnetic materials by means of a finite set of operators, called *hysteresis operators*, each one represented by a relay $\mathcal{R}_{\alpha\beta}$ depending on parameters α and β such that $\alpha < \beta$ (see Figure 2.6 for a particular example). Mathematically, a relay is defined in the following way:

$$\mathcal{R}_{\alpha\beta} : \mathcal{C}([t_0, T]; \mathbb{R}) \times \{-1, 1\} \longrightarrow L^\infty([t_0, T]; \mathbb{R})$$

$$(u, \xi) \longmapsto \mathcal{R}_{\alpha\beta}(u, \xi)(t) = \begin{cases} -1 & \text{if } u(t) \leq \alpha, \\ +1 & \text{if } u(t) \geq \beta, \\ \delta(u|_{[t_0,t]}, \xi) & \text{if } u(t) \in (\alpha, \beta), \end{cases}$$

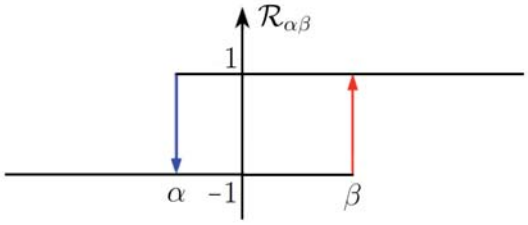

Figure 2.6: Relay operator $\mathcal{R}_{\alpha\beta}$.

where

$$\delta(u|_{[t_0,t]},\xi) = \begin{cases} -1 & \text{if} \quad t = t_0,\ \xi = -1, \\ -1 & \text{if} \quad t > t_0,\ \xi = -1,\ u(s) \in (\alpha,\beta)\,\forall s \in [t_0,t], \\ -1 & \text{if} \quad \exists\, q > t_0 \,/\, u(q) = \alpha, u(s) \in (-\infty,\beta)\,\forall s \in [q,t], \\ 1 & \text{if} \quad t = t_0,\ \xi = 1, \\ 1 & \text{if} \quad t > t_0,\ \xi = 1,\ u(s) \in (\alpha,\beta)\,\forall s \in [t_0,t], \\ 1 & \text{if} \quad \exists\, q > t_0 \,/\, u(q) = \beta, u(s) \in (\alpha,\infty)\,\forall s \in [q,t]. \end{cases}$$

Thus, for every point $\boldsymbol{x}$ in the ferromagnetic domain, the hysteresis operator is defined in the following way:

$$\mathcal{B}(u,\xi)(\boldsymbol{x},t) = \iint_{\alpha<\beta} \mathcal{R}_{\alpha\beta}(u(\boldsymbol{x},t),\xi(\boldsymbol{x}))\,\mu(\alpha,\beta)\,\mathrm{d}\alpha\,\mathrm{d}\beta,$$

where μ is a weight function of compact support that identifies the ferromagnetic material (called *Preisach function*) and ξ is a function that takes values in the set $\{-1,1\}$ and contains the information about the initial state of magnetization of every point of the ferromagnetic domain.

Preisach function μ is unique for every material but it can be approximated in different ways, for example, from experimental data or through analytical functions depending on different material parameters. For more information, see Chapter 5 in [107].

Thus, we will have that $B_z = \mathcal{B}(H_z,\xi)$ for longitudinal magnetization and $B_\theta = \mathcal{B}(H_\theta,\xi)$ for circular magnetization.

2.3 Implementation Issues

For numerical approximation, we propose a backward-Euler scheme for time-discretization. Due to the inclusion of hysteresis, the problems to be solved at each time step are nonlinear; therefore, we propose here to use the so-called Bermúdez-Moreno algorithm, a fixed point method introduced in [25] in an abstract framework. This procedure makes use of a multiplier that is updated in each iteration and is defined in terms of $\mathcal{B}$ and $\mathcal{B}^{-1}$ for the circular and longitudinal models, respectively. To use this algorithm, and following the same arguments as in Chapter 5 from [107], we define, for each point $\boldsymbol{x}$ in the ferromagnetic domain and each time step t_m, a *local* magnetic constitutive law relating the magnetic flux $\boldsymbol{B}(\boldsymbol{x},t_m)$ and the magnetic

intensity $\boldsymbol{H}(\boldsymbol{x}, t_m)$ in terms of the hysteresis operator $\mathcal{B}$ (or its inverse, $\mathcal{B}^{-1}$, depending on the formulation) and the values of $\boldsymbol{H}$ at points $\{(\boldsymbol{x}, t_k),\ k = 1, \dots, m-1\}$. Moreover, as it will be detailed later, an important advantage of this approach is that, although the multiplier is defined in terms of $\mathcal{B}^{-1}$ for the longitudinal model, the effective computation of the inverse of the hysteresis operator is not required.

Finally, we notice that we have only detailed here the semidiscretization in time for the sake of readability. However, we have used a finite element method for the space-discretization, and thus H_θ and A_θ were approximated by piecewise linear finite elements in the circular and longitudinal magnetization models, respectively.

2.3.1 Circular Model

Firstly, we take a uniform partition of the time interval $[t_0, T]$ with step size $\Delta t := (T - t_0)/M$, $\{t_m := t_0 + m\Delta t, m = 0, \dots, M\}$. In order to solve the problem for the circular magnetization, (2.3)–(2.7), we propose the following implicit scheme:

$m = 0$: We define $H_\theta^0 := H_0$ and $\mathcal{B}^0$ the nonlinear operator relating H_θ^0 and B_θ^0,

$$B_\theta^0(\rho, z) = \mathcal{B}^0\left(H_\theta^0\right)(\rho, z) = \mathcal{B}^0_{(\rho,z)}\left(H_\theta^0(\rho, z)\right), \quad (\rho, z) \in \Omega,$$

with $\mathcal{B}^0_{(\rho,z)} : \mathbb{R} \longrightarrow \mathbb{R}$, $\mathcal{B}^0_{(\rho,z)}(s) := \mathcal{B}(s, \xi)$, for all $s \in \mathbb{R}$.

$m \geq 1$: We define $B_\theta^{m-1} := \mathcal{B}^{m-1}(H_\theta^{m-1})$ and approximate $H_\theta(\rho, z, t_m) \approx H_\theta^m(\rho, z)$ in terms of the approximation at the previous time step H_θ^{m-1} as the solution to:

$$\begin{aligned}
\frac{1}{\Delta t}\mathcal{B}^m(H_\theta^m)\boldsymbol{e}_\theta + \mathbf{curl}\left(\frac{1}{\sigma}\mathbf{curl}(H_\theta^m \boldsymbol{e}_\theta)\right) &= \frac{1}{\Delta t}B_\theta^{m-1}\boldsymbol{e}_\theta \quad \text{in } \Omega,\\
H_\theta^m(0, z) &= 0 \quad \text{on } (0, L),\\
H_\theta^m(R_{\mathcal{S}}(z), z) &= \frac{I(t_m)}{2\pi R_{\mathcal{S}}(z)} \quad \text{on } (0, L),\\
\frac{\partial H_\theta^m}{\partial z}(\rho, z) &= 0 \quad \text{on } (\Gamma_1 \cup \Gamma_2),
\end{aligned}$$

where $\mathcal{B}^m$ represent the nonlinear operators relating H_θ^m and B_θ^m,

$$B_\theta^m(\rho, z) = \mathcal{B}^m\left(H_\theta^m\right)(\rho, z) = \mathcal{B}^m_{(\rho,z)}\left(H_\theta^m(\rho, z)\right), \quad (\rho, z) \in \Omega,\ m = 1, \dots, M,$$

with $\mathcal{B}^m_{(\rho,z)} : \mathbb{R} \longrightarrow \mathbb{R}$, $\mathcal{B}^m_{(\rho,z)}(s) := \mathcal{B}(u_m, \xi)$, with u_m the piecewise linear function such that $u_m(t_k) := H_\theta^k(\rho, z)$, $k = 0, \dots, m-1$, and $u(t_m) = s$, for all $s \in \mathbb{R}$.

On the other hand, as we have already mentioned, we will used the Bermúdez-Moreno algorithm to solve the nonlinearity. This approach requires the assumption that operators $\mathcal{B}^m_{(\rho,z)}$, $m = 0, \dots, M$, can be extended to maximal monotone operators, that is, they can be extended to unbounded operators $\widetilde{\mathcal{B}}^m_{(\rho,z)} : \mathbb{R} \longrightarrow \mathbb{R}$, $m = 0, \dots, M$, such that

$$\langle \widetilde{\mathcal{B}}^m_{(\rho,z)}(s), s\rangle \geq 0\ \forall\, s \in \mathbb{R} \quad \text{and} \quad id_{\mathbb{R}} + \widetilde{\mathcal{B}}^m_{(\rho,z)} \text{ is onto.}$$

These properties can be deduced, for instance, if $\mathcal{B}^m_{(\rho,z)}$, $(\rho,z)\in\Omega$, $m=0,\dots,M$, are strictly monotone operators in a bounded domain and constant elsewhere, the latter being a consequence of μ having compact support (see [107]).

In order to describe the algorithm to solve the nonlinearity, we will first introduce some definitions. For any operator $\mathcal{G}:\mathbb{R}\longrightarrow\mathbb{R}$ and any $\beta>0$, we define the associated operator $\mathcal{G}^\beta$ such that $\mathcal{G}^\beta(s)=\mathcal{G}(s)-\beta s$. Moreover, following [38], under the previous assumption, we can define $\mathcal{J}^\beta_\lambda\left[\mathcal{B}^m_{(\rho,z)}\right]$ for $\lambda\in(0,1/\beta)$, $(\rho,z)\in\Omega$ and $m=0,\dots,M$,

$$\mathcal{J}^\beta_\lambda\left[\mathcal{B}^m_{(\rho,z)}\right]:=\left(id_{\mathbb{R}}+\lambda\left(\mathcal{B}^m_{(\rho,z)}\right)^\beta\right)^{-1},$$

the so-called *resolvent operator* of $\left(\mathcal{B}^m_{(\rho,z)}\right)^\beta$. It is easy to see that

$$\mathcal{J}^\beta_\lambda\left[\mathcal{B}^m_{(\rho,z)}\right](s)=\mathcal{J}^0_{\frac{\lambda}{1-\lambda\beta}}\left[\mathcal{B}^m_{(\rho,z)}\right]\left(\frac{s}{1-\lambda\beta}\right),\quad s\in\mathbb{R}.$$

Moreover, we can also define $\left(\mathcal{B}^m_{(\rho,z)}\right)^\beta_\lambda$ for $\lambda\in(0,1/\beta)$, $(\rho,z)\in\Omega$ and $m=0,\dots,M$,

$$\left(\mathcal{B}^m_{(\rho,z)}\right)^\beta_\lambda:=\frac{1}{\lambda}\left(id_{\mathbb{R}}-\mathcal{J}^\beta_\lambda\left[\mathcal{B}^m_{(\rho,z)}\right]\right),$$

the so-called *Yosida regularization* of $\left(\mathcal{B}^m_{(\rho,z)}\right)^\beta$.

Therefore, for the circular model, we introduce a multiplier $p^m_c(\rho,z)$, $m=1,\dots,M$, $(\rho,z)\in\Omega$, such that

$$p^m_c(\rho,z)=\mathcal{B}^m_{(\rho,z)}(H^m_\theta(\rho,z))-\beta_c(\rho,z)H^m_\theta(\rho,z),$$

for any given $\beta_c(\rho,z)>0$. It can be proved that (see [25]), for every $\lambda_c\in(0,1/\beta_c(\rho,z))$,

$$p^m_c(\rho,z)=(\mathcal{B}^m)^{\beta_c}_{\lambda_c}\left(H^m_\theta(\rho,z)+\lambda_c\,p^m_c(\rho,z)\right). \tag{2.14}$$

This equality, combined with the described time discretization, is the base of the fixed point iterations. Therefore, we propose the following algorithm to solve problem (2.3)–(2.7):

$m=0:$ We define $H^0_\theta:=H_0$ and $\mathcal{B}^0$ the nonlinear operator relating H^0_θ and B^0_θ,

$$B^0_\theta(\rho,z)=\mathcal{B}^0\left(H^0_\theta\right)(\rho,z)=\mathcal{B}^0_{(\rho,z)}\left(H^0_\theta(\rho,z)\right),\quad(\rho,z)\in\Omega,$$

with $\mathcal{B}^0_{(\rho,z)}:\mathbb{R}\longrightarrow\mathbb{R}$, $\mathcal{B}^0_{(\rho,z)}(s):=\mathcal{B}(s,\xi)$, for all $s\in\mathbb{R}$.

$m=1:$ We define $B^0_\theta:=\mathcal{B}^0(H^0_\theta)$, $p^{1,0}_c=0$ and approximate $H_\theta(\rho,z,t_1)\approx H^1_\theta(\rho,z)$ performing the following iterations on $s\geq1$ until convergence:

i) $H_\theta^{1,s}$ is the solution to the linear problem

$$\begin{aligned}\frac{1}{\Delta t}\beta_c H_\theta^{1,s}\boldsymbol{e}_\theta + \mathbf{curl}\left(\frac{1}{\sigma}\,\mathbf{curl}(H_\theta^{1,s}\boldsymbol{e}_\theta)\right)&\\ = \frac{1}{\Delta t}B_\theta^0\boldsymbol{e}_\theta - \frac{1}{\Delta t}p_c^{1,s-1} &\quad \text{in } \Omega,\\ H_\theta^{1,s}(0,z) = 0 &\quad \text{on } (0,L),\\ H_\theta^{1,s}(R_{\mathcal{S}}(z),z) = \frac{I(t_1)}{2\pi R_{\mathcal{S}}(z)} &\quad \text{on } (0,L),\\ \frac{\partial H_\theta^{1,s}}{\partial z}(\rho,z) = 0 &\quad \text{on } (\Gamma_1\cup\Gamma_2)\,.\end{aligned}$$

ii) $p_c^{1,s} = (\mathcal{B}^1)_{\lambda_c}^{\beta_c}\left(H_\theta^{1,s} + \lambda_c\, p_c^{1,s-1}\right)$ in Ω.

$m \geq 2$: We define $B_\theta^{m-1} := \mathcal{B}^{m-1}(H_\theta^{m-1})$, $p_c^{m,0} = p_c^{m-1}$ and approximate $H_\theta(\rho,z,t_m) \approx H_\theta^m(\rho,z)$ performing the following iterations on $s \geq 1$ until convergence:

i) $H_\theta^{m,s}$ is the solution to the linear problem

$$\begin{aligned}\frac{1}{\Delta t}\beta_c H_\theta^{m,s}\boldsymbol{e}_\theta + \mathbf{curl}\left(\frac{1}{\sigma}\,\mathbf{curl}(H_\theta^{m,s}\boldsymbol{e}_\theta)\right)&\\ = \frac{1}{\Delta t}B_\theta^{m-1}\boldsymbol{e}_\theta - \frac{1}{\Delta t}p_c^{m,s-1} &\quad \text{in } \Omega,\\ H_\theta^{m,s}(0,z) = 0 &\quad \text{on } (0,L),\\ H_\theta^{m,s}(R_{\mathcal{S}}(z),z) = \frac{I(t_m)}{2\pi R_{\mathcal{S}}(z)} &\quad \text{on } (0,L),\\ \frac{\partial H_\theta^{m,s}}{\partial z}(\rho,z) = 0 &\quad \text{on } (\Gamma_1\cup\Gamma_2)\,.\end{aligned}$$

ii) $p_c^{m,s} = (\mathcal{B}^m)_{\lambda_c}^{\beta_c}\,(H_\theta^{m,s} + \lambda_c\, p_c^{m,s-1})$ in Ω.

In order to compute $p_c^{m,s}(\rho,z)$, we solve the nonlinear system

$$\begin{aligned}u = \mathcal{J}_{\lambda_c}^{\beta_c}\left[\mathcal{B}_{(\rho,z)}^m\right]\left(H_\theta^{m,s}(\rho,z) + \lambda_c\, p_c^{m,s-1}(\rho,z)\right)&\\ = \mathcal{J}^0_{\frac{\lambda_c}{1-\lambda_c\beta_c}}\left[\mathcal{B}_{(\rho,z)}^m\right]\left(\frac{H_\theta^{m,s}(\rho,z) + \lambda_c\, p_c^{m,s-1}(\rho,z)}{1-\lambda_c\beta_c}\right)&\\ \Leftrightarrow u + \frac{\lambda_c}{1-\lambda_c\beta_c}\mathcal{B}_{(\rho,z)}^m(u) = \frac{H_\theta^{m,s}(\rho,z) + \lambda_c\, p_c^{m,s-1}(\rho,z)}{1-\lambda_c\beta_c}, &\quad u\in\mathbb{R}.\end{aligned}$$

For this, we approximate $\mathcal{B}_{(\rho,z)}^m$ by a continuous piecewise linear operator and solve the resulting piecewise linear system of equations.

The convergence of the proposed iterative method has been proved in [25] for $\lambda_c\beta_c \leq \frac{1}{2}$, and its performance depends on the choice of these parameters. For the implementation, we have

chosen the parameters in the following way:

$$\beta_c(\rho, z) := \frac{\sum_{i=1}^{n_{bh}} b_i(\rho, z)}{\sum_{i=1}^{n_{bh}} h_i},$$

where $\{h_i, i = 1, \ldots, n_{bh}\}$ is a given discretization of the interval $[0, H_{sat}] \subset \mathbb{R}$, H_{sat} depending on the magnetic properties of the ferromagnetic material, and $b_i(\rho, z) := \mathcal{B}^0_{(\rho,z)}(h_i)$, $i = 1, \ldots, n_{bh}$. Also, we have defined $\lambda_c(\rho, z) := 1/(2\beta_c(\rho, z))$. We reference Section 6.3 in [16] for other ways of choosing these parameters.

Finally, we notice that, for the spatial discretization of p_c^m, $m = 1, \ldots, M$, we have used standard first order Lagrange finite elements.

2.3.2 Longitudinal Model

In a similar way, for the longitudinal magnetization problem, (2.8)–(2.13), we propose:

$m = 0$: We define $A_\theta^0 := A_0$ in $(0, R_c)$ and, similarly to the circular case, $(\mathcal{B}^0)^{-1}$ the nonlinear operator relating $B_z^0 := (1/\rho)\left(\partial\left(\rho A_\theta^0\right)/(\partial\rho)\right)$ and H_z^0,

$$H_z^0(\rho) = \left(\mathcal{B}^0\right)^{-1}\left(B_z^0\right)(\rho) = \left(\mathcal{B}_\rho^0\right)^{-1}\left(B_z^0(\rho)\right), \quad \rho \in (0, R_c),$$

with $\mathcal{B}_\rho^0 : \mathbb{R} \longrightarrow \mathbb{R}$, $\mathcal{B}_\rho^0(s) := \mathcal{B}(s, \xi)$, for all $s \in \mathbb{R}$.

$m \geq 1$: We define

$$H_z^{m-1}(\rho) := \left(\mathcal{B}_\rho^{m-1}\right)^{-1}\left(\frac{1}{\rho}\frac{\partial\left(\rho A_\theta^{m-1}\right)}{\partial\rho}\right)$$

and approximate $A_\theta(\rho, t_m) \approx A_\theta^m(\rho)$ in terms of the approximation at the previous time step A_θ^{m-1} in $(0, R_c)$ as the solution to:

$$\begin{aligned}
\sigma\frac{1}{\Delta t}A_\theta^m - \frac{\partial}{\partial\rho}\left(\left(\mathcal{B}^m\right)^{-1}\left(\frac{1}{\rho}\frac{\partial}{\partial\rho}\left(\rho A_\theta^m\right)\right)\right) &= \sigma\frac{1}{\Delta t}A_\theta^{m-1} \quad \text{in } (0, R_c),\\
\frac{\partial}{\partial\rho}\left(\frac{1}{\mu_0}\frac{1}{\rho}\frac{\partial}{\partial\rho}\left(\rho A_\theta^m\right)\right) &= 0 \quad \text{in } (R_c, R_\infty)\setminus\{R_S\},\\
\left[\frac{1}{\mu_0}\frac{1}{\rho}\frac{\partial}{\partial\rho}(\rho A_\theta^m)\right]_{\rho=R_S} &= J_S(t_m),\\
A_\theta^m &= 0 \quad \text{on } \rho = 0,\\
\frac{1}{\rho}\frac{\partial}{\partial\rho}(\rho A_\theta^m) &= 0 \quad \text{on } \rho = R_\infty,
\end{aligned}$$

where $(\mathcal{B}^m)^{-1}$ represent the nonlinear operators relating B_z^m and H_z^m,

$$H_z^m(\rho) = (\mathcal{B}^m)^{-1}(B_z^m)(\rho) = \left(\mathcal{B}_\rho^m\right)^{-1}\left(\frac{1}{\rho}\frac{\partial(\rho A_\theta^m)}{(\partial\rho)}\right), \quad \rho \in (0, R_c),\ m = 1, \dots, M,$$

with $\mathcal{B}_\rho^m : \mathbb{R} \longrightarrow \mathbb{R}$, $\mathcal{B}_\rho^m(s) := \mathcal{B}(u_m, \xi)$, with u_m the piecewise linear function such that $u_m(t_k) := H_z^k(\rho)$, $k = 0, \dots, m-1$, and $u(t_m) = s$ for all $s \in \mathbb{R}$.

On the other hand, for the longitudinal case, the multiplier is defined as:

$$p_\ell^m(\rho) := \left(\mathcal{B}_\rho^m\right)^{-1}(B_z(\rho)) - \beta_\ell B_z(\rho),$$

for any given $\beta_\ell > 0$, $\rho \in (0, R_c)$, $m = 1, \dots, M$. Again, we assume that operators $\mathcal{B}_\rho^m$, $\rho \in (0, R_c)$, $m = 1, \dots, M$, can be extended to maximal monotone operators. We notice that, following [89], this assumption guarantees that the same is true for operators $\left(\mathcal{B}_\rho^m\right)^{-1}$, $\rho \in (0, R_c)$, $m = 0, \dots, M$. Then, similarly to the circular case, it can be proved that

$$p_\ell^m(\rho) = \left(\left(\mathcal{B}_\rho^m\right)^{-1}\right)_{\lambda_\ell}^{\beta_\ell}(B_z(\rho) + \lambda_\ell p_\ell^m(\rho)).$$

Moreover, following [89],

$$\left(\left(\mathcal{B}_\rho^m\right)^{-1}\right)_{\lambda_\ell}^{\beta_\ell}(B_z(\rho)) = \frac{1}{1-\beta_\ell\lambda_\ell}\left(\left(\mathcal{B}_\rho^m\right)^{-1}\right)_{\frac{\lambda_\ell}{1-\beta_\ell\lambda_\ell}}^{0}\left(\frac{B_z(\rho)}{1-\beta_\ell\lambda_\ell}\right) - \frac{\beta_\ell}{1-\beta_\ell\lambda_\ell}B_z(\rho)$$
$$= \frac{1}{1-\beta_\ell\lambda_\ell}\mathcal{J}_{\frac{1-\beta_\ell\lambda_\ell}{\lambda_\ell}}^0\left[\mathcal{B}_\rho^m\right]\left(\frac{B_z(\rho)}{\lambda_\ell}\right) - \frac{\beta_\ell}{1-\beta_\ell\lambda_\ell}B_z(\rho).$$

Therefore, since $B_z = (1/\rho)\,\partial(\rho A_\theta)/\partial\rho$,

$$p_\ell(\rho) = \frac{1}{1-\beta_\ell\lambda_\ell}\mathcal{J}_{\frac{1-\beta_\ell\lambda_\ell}{\lambda_\ell}}^0\left[\mathcal{B}_\rho^m\right]\left(\frac{1}{\lambda_\ell\rho}\frac{\partial}{\partial\rho}(\rho A_\theta(\rho)) + p_\ell(\rho)\right)$$
$$- \frac{\beta_\ell}{1-\beta_\ell\lambda_\ell}\left(\frac{1}{\rho}\frac{\partial}{\partial\rho}(\rho A_\theta(\rho)) + \lambda p_\ell(\rho)\right), \quad (2.15)$$

for every $\lambda_\ell \in (0, 1/\beta_\ell)$. In particular, by using this equality, $p_\ell(\rho)$ is updated using operators $\mathcal{B}_\rho^m$ instead of $\left(\mathcal{B}_\rho^m\right)^{-1}$. Thus, combining (2.15) with the time discretization, we propose the following fixed-point-type algorithm to solve problem (2.8)–(2.13):

$m = 0$: We define $A_\theta^0 := A_0$ in $(0, R_c)$ and $(\mathcal{B}^0)^{-1}$ the nonlinear operator relating B_z^0 and H_z^0,

$$H_z^0(\rho) = \left(\mathcal{B}^0\right)^{-1}\left(B_z^0\right)(\rho) = \left(\mathcal{B}_\rho^0\right)^{-1}\left(B_z^0(\rho)\right), \quad \rho \in (0, R_c),$$

with $\mathcal{B}_\rho^0 : \mathbb{R} \longrightarrow \mathbb{R}$, $\mathcal{B}_\rho^0(s) := \mathcal{B}(s, \xi)$, for all $s \in \mathbb{R}$.

$m = 1$: We define $p_\ell^{1,0} := 0$ and approximate $A_\theta(\rho, t_1) \approx A_\theta^1(\rho)$ performing the following iterations on $s \geq 1$ until convergence:

i) $A_\theta^{1,s}$ is the solution to the linear problem

$$\begin{aligned}
\sigma \frac{1}{\Delta t} A_\theta^{1,s} - \frac{\partial}{\partial \rho}\left(\beta_\ell \left(\frac{1}{\rho}\frac{\partial}{\partial \rho}\left(\rho A_\theta^{1,s}\right)\right)\right) & \\
= \sigma \frac{1}{\Delta t} A_\theta^0 + \frac{\partial}{\partial \rho} p_\ell^{1,s-1} & \quad \text{in } (0, R_c), \\
\frac{\partial}{\partial \rho}\left(\frac{1}{\mu_0}\frac{1}{\rho}\frac{\partial}{\partial \rho}\left(\rho A_\theta^{1,s}\right)\right) = 0 & \quad \text{in } (R_c, R_\infty) \setminus \{R_{\mathrm{S}}\}, \\
\left[\frac{1}{\mu_0}\frac{1}{\rho}\frac{\partial}{\partial \rho}(\rho A_\theta^{1,s})\right]_{\rho = R_{\mathrm{S}}} = J_{\mathrm{S}}(t_1), & \\
A_\theta^{1,s} = 0 & \quad \text{on } \rho = 0, \\
\frac{1}{\rho}\frac{\partial}{\partial \rho}(\rho A_\theta^{1m,s}) = 0 & \quad \text{on } \rho = R_\infty.
\end{aligned}$$

ii) We update the multiplier with expression (2.15)

$$\begin{aligned}
p_\ell^{1,s} = \frac{1}{1 - \beta_\ell \lambda_\ell} \mathcal{J}^0_{\frac{1-\beta_\ell\lambda_\ell}{\lambda_\ell}}\left[\mathcal{B}^1\right]\left(\frac{1}{\lambda_\ell \rho}\frac{\partial}{\partial \rho}(\rho A_\theta^{1,s}) + p_\ell^{1,s-1}\right) & \\
- \frac{\beta_\ell}{1 - \beta_\ell \lambda_\ell}\left(\frac{1}{\rho}\frac{\partial}{\partial \rho}(\rho A_\theta^{1,s}) + \lambda_\ell p_\ell^{1,s-1}\right) & \quad \text{in } (0, R_c).
\end{aligned}$$

$m \geq 2$: We define $p_\ell^{m,0} := p_\ell^{m-1}$ and approximate $A_\theta(\rho, t_m) \approx A_\theta^m$ performing the following iterations on $s \geq 1$ until convergence:

i) $A_\theta^{m,s}$ is the solution to the linear problem

$$\begin{aligned}
\sigma \frac{1}{\Delta t} A_\theta^{m,s} - \frac{\partial}{\partial \rho}\left(\beta_\ell \left(\frac{1}{\rho}\frac{\partial}{\partial \rho}\left(\rho A_\theta^{m,s}\right)\right)\right) & \\
= \sigma \frac{1}{\Delta t} A_\theta^{m-1} + \frac{\partial}{\partial \rho} p_\ell^{m,s-1} & \quad \text{in } (0, R_c), \\
\frac{\partial}{\partial \rho}\left(\frac{1}{\mu_0}\frac{1}{\rho}\frac{\partial}{\partial \rho}\left(\rho A_\theta^{m,s}\right)\right) = 0 & \quad \text{in } (R_c, R_\infty) \setminus \{R_{\mathrm{S}}\}, \\
\left[\frac{1}{\mu_0}\frac{1}{\rho}\frac{\partial}{\partial \rho}(\rho A_\theta^{m,s})\right]_{\rho = R_{\mathrm{S}}} = J_{\mathrm{S}}(t_m), & \\
A_\theta^{m,s} = 0 & \quad \text{on } \rho = 0, \\
\frac{1}{\rho}\frac{\partial}{\partial \rho}(\rho A_\theta^{m,s}) = 0 & \quad \text{on } \rho = R_\infty.
\end{aligned}$$

ii) We update the multiplier with expression (2.15)

$$\begin{aligned}
p_\ell^{m,s} = \frac{1}{1 - \beta_\ell \lambda_\ell} \mathcal{J}^0_{\frac{1-\beta_\ell\lambda_\ell}{\lambda_\ell}}\left[\mathcal{B}^m\right]\left(\frac{1}{\lambda_\ell \rho}\frac{\partial}{\partial \rho}(\rho A_\theta^{m,s}) + p_\ell^{m,s-1}\right) & \\
- \frac{\beta_\ell}{1 - \beta_\ell \lambda_\ell}\left(\frac{1}{\rho}\frac{\partial}{\partial \rho}(\rho A_\theta^{m,s}) + \lambda_\ell p_\ell^{m,s-1}\right) & \quad \text{in } (0, R_c).
\end{aligned}$$

In order to compute $p_\ell^{m,s}$, we solve the nonlinear system

$$u = \mathcal{J}^0_{\frac{1-\beta_\ell\lambda_\ell}{\lambda_\ell}}\left[\mathcal{B}_\rho^m\right]\left(\frac{1}{\lambda_\ell\rho}\frac{\partial}{\partial\rho}(\rho A_\theta^{m,s}(\rho)) + p_\ell^{m,s-1}(\rho)\right)$$
$$\Leftrightarrow u + \frac{1-\beta_\ell\lambda_\ell}{\lambda_\ell}\mathcal{B}_\rho^m(u) = \frac{1}{\lambda_\ell\rho}\frac{\partial}{\partial\rho}(\rho A_\theta^{m,s}(\rho)) + p_\ell^{m,s-1}(\rho), \quad u \in \mathbb{R}.$$

As for the circular case, we approximate $\mathcal{B}_\rho^m$ by a continuous piecewise linear operator and solve the resulting piecewise linear system of equations.

Moreover, in the step $m = 0$, we approximate $\mathcal{B}_\rho^0$ by a continuous piecewise linear operator. Additionally, and similarly to the circular case, we have chosen

$$\beta_\ell(\rho) := \frac{\sum_{i=1}^{n_{bh}} b_i(\rho)}{\sum_{i=1}^{n_{bh}} h_i},$$

where $\{h_i, i = 1, \ldots, n_{bh}\}$ is a given discretization of the interval $[0, H_{sat}] \subset \mathbb{R}$, H_{sat} depending on the magnetic properties of the ferromagnetic material, and $b_i(\rho) := \mathcal{B}_\rho^0(h_i)$, $i = 1, \ldots, n_{bh}$. Also, we have defined $\lambda_\ell(\rho) := 1/(2\beta_c(\rho))$.

Finally, we notice that, for the spatial discretization of p_ℓ^m, $m = 1, \ldots, M$, we have used standard zero-order Lagrange finite elements.

2.4 Numerical Results

As we mentioned in Section 2.2, we have simulated various processes corresponding to a magnetic particle inspection procedure, considering separately the cases in which the electromagnetic field has circular and longitudinal direction. Thus, we have successively solved a circular magnetization and demagnetization for different demagnetizing waveforms, and also several longitudinal magnetization and demagnetization processes. In order to numerically illustrate the results presented in the previous sections, we have considered a ferromagnetic material characterized by the major hysteresis loop (and initial magnetization curve) depicted in Figure 2.7. This curves where obtained using an artificial weight function μ (see Section 2.2.3); in particular, they do not correspond to any real material, although the qualitative behavior is the same.

Concerning the magnetization stages, all of them have been performed with a pure sinusoidal current waveform. Conversely, demagnetization is generally accomplished by subjecting the pieces to a magnetic field, initially equal to or greater than the one used for magnetization, and having a sinusoidal dependance on time, modulated by a decreasing function fading to zero (see [70]). To achieve this waveform for $\boldsymbol{H}$, a source with a similar behavior was used, obeying the general expression

$$J_S(R_S, t) = J_{S,0}\,\frac{T-t}{T-\widehat{t}_0}\,\sin(2\pi f_{demag}\,t), \quad t \in \left[\widehat{t}_0, T\right],$$

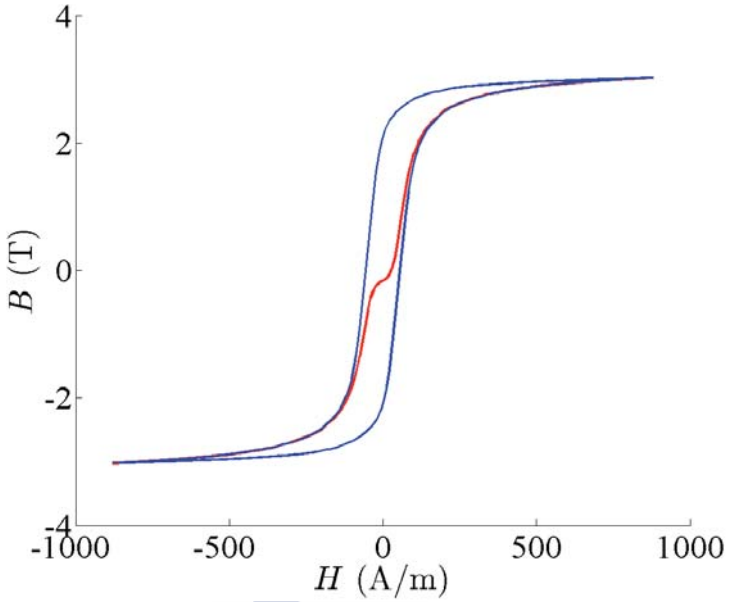

Figure 2.7: Initial magnetization curve (red). Major hysteresis loop (blue).

in the longitudinal case, and a similar one for $I(t)$ in the circular case. However, in Section 2.4.2 we will show that the magnetic field waveform is distorted as it penetrates into the piece (in the particular case of a longitudinal demagnetization), what causes the demagnetization process to be rather intricate. In Figure 2.8 an example of the aforementioned source signals used for the demagnetization stage are shown for $\widehat{t}_0 = 0.04$ s, $J_{\mathrm{S},0} = 2 \times 10^5$ A/m, $f_{demag} = 1$ Hz but different final time $T \in \{12.04, 36.04, 72.04, 144.04\}$ s. For each of these final times, we define the number of cycles $N := (T - \widehat{t}_0) f_{demag}$ required for the input signal to vanish.

Finally, we notice that all numerical simulations have been performed with an initially demagnetized piece, and therefore the initial fields, H_θ^0 for the circular case and A_θ^0 for the longitudinal one, were chosen to be identically null.

2.4.1 Circular Model

Concerning the simulation of circular magnetization stages, we have employed the same signal for all of them. In Figure 2.9–top we can see the $\theta-$component of the remanent flux density after these processes. It can be seen that the field is almost constant until it reaches the boundary, where a strong variation occurs. This variation is due to the skin effect, being stronger as the boundary approaches the symmetry axis of the piece. Moreover, in Figure 2.9–bottom, the value of this field on the three lines marked in Figure 2.9–top is plotted as a function of the $\rho-$coordinate.

Regarding circular demagnetization, in Figure 2.10 we show the $\theta-$component of the remanent flux density in the piece sketched in Figure 2.4 at $z = 0.2$ m after different processes of magnetization–demagnetization, with the demagnetizing source having a frequency of 1 Hz

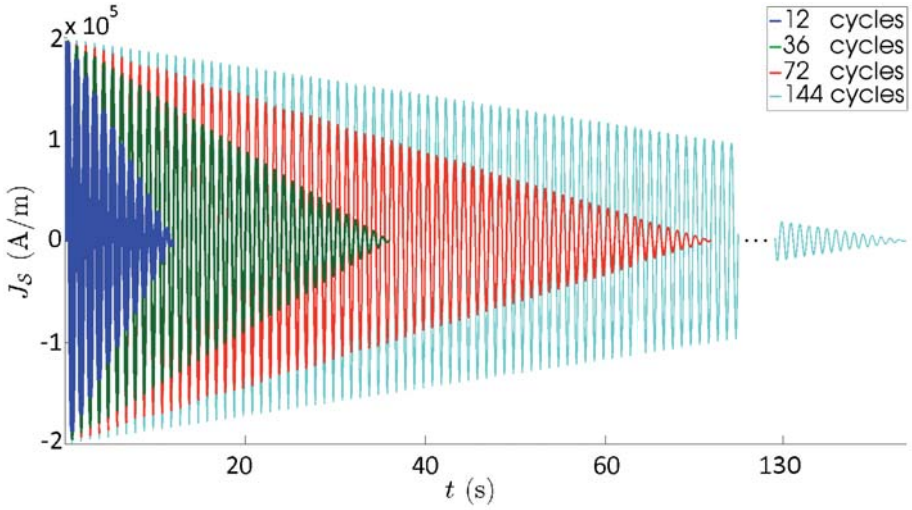

Figure 2.8: Demagnetizing source.

and for a different number of cycles (see Figure 2.8). Moreover, in Figure 2.11 we show the $\theta-$component of the remanent flux density in the same piece, at $z = 0.2$ m, with the demagnetizing source having two different frequencies: 1 Hz and 6 Hz. We observe that when we apply two demagnetizing signals having the same number of cycles, both of them achieve similar remanent flux densities at the surface of the piece, but with the one at 1 Hz the specimen is more efficiently demagnetized.

2.4.2 Longitudinal Model

Regarding the longitudinal simulations, in Figure 2.12 we show the magnetic field dependance on time at some points along the piece during the demagnetization stage. We observe that, although for values of ρ close to R_c the magnetic field mimics the source waveform, this property is lost as we get closer to the center of the specimen.

Furthermore, in Figure 2.14 and 2.15 we show the $z-$component of the remanent flux density in a cylindrical piece after different magnetization–demagnetization processes. Similar to the circular case, the magnetization stages were the same for all of them (see Figure 2.13 for the remanent flux density after this step), while the demagnetization part was performed with a different number of cycles or changing the frequency (see Figure 2.14 and 2.15, respectively).

Figure 2.14 shows that if we apply different sources at the same frequency, a greater number of source cycles results in a better demagnetization. On the other hand, in Figure 2.15 we can compare the remanent flux density when considering a 1 Hz source and a 6 Hz one. We observe that, even though the 1 Hz current achieves a better demagnetization in the interior of the piece, the remanent flux density on the surface is notably closer to zero with the 6 Hz source. Still, with the 6 Hz source complete demagnetization is not achieved in the interior of the piece.

The numerical results shown in this section 2.4 help us to become familiar with the inspection

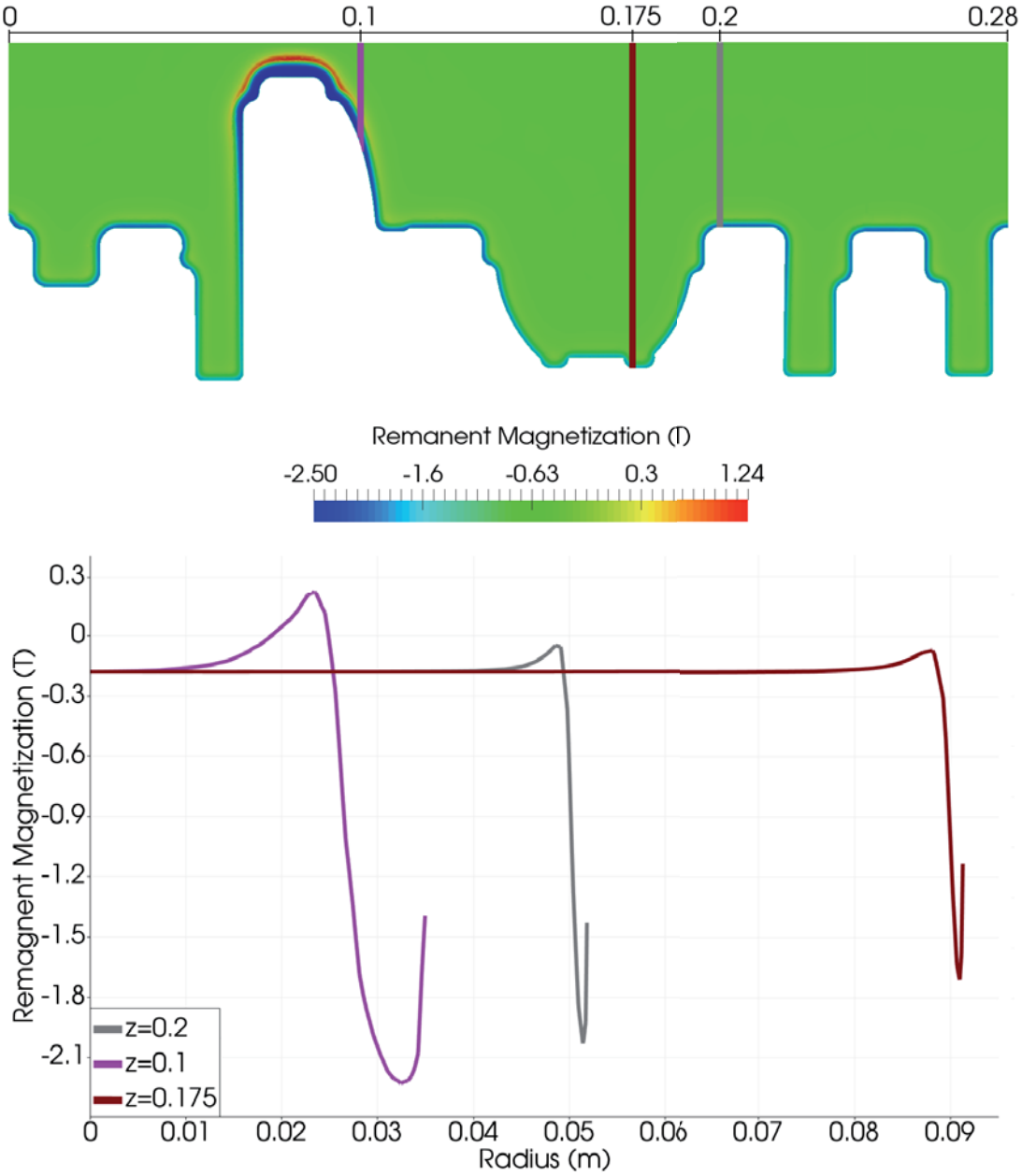

Figure 2.9: Remanent flux density ($\theta-$component) after circular magnetization at $z = 0.1$ m, $z = 0.175$ m and $z = 0.2$ m.

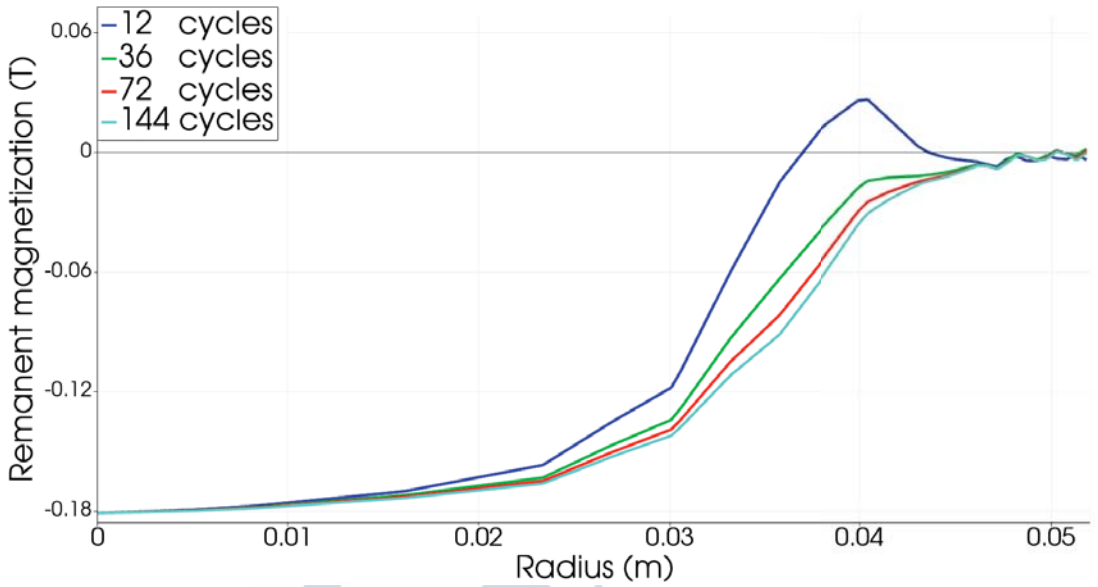

Figure 2.10: Remanent flux density ($\theta-$component) vs. radius in the cylindrical piece at $z = 0.2$ m. Circular demagnetization. Number of cycles comparison.

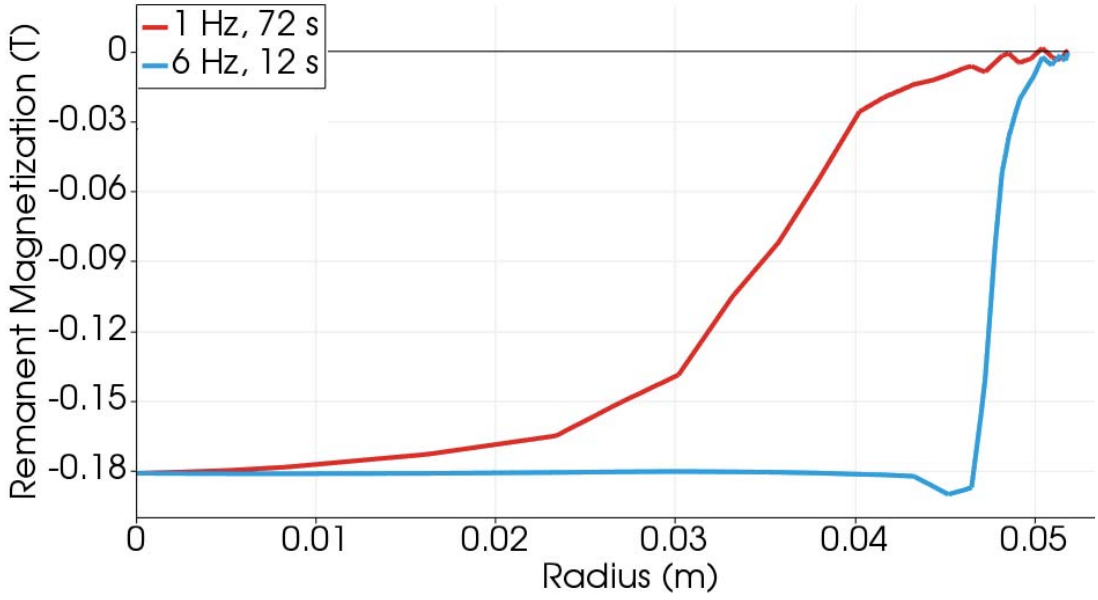

Figure 2.11: Remanent flux density ($\theta-$component) vs. radius in the cylindrical piece at $z = 0.2$ m. Circular demagnetization. Frequency comparison.

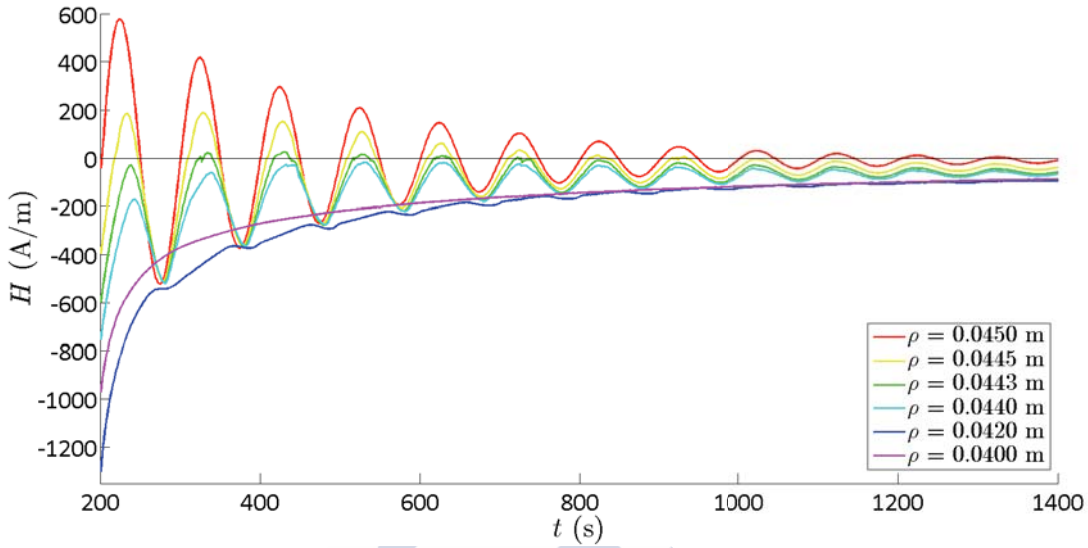

Figure 2.12: Magnetic field intensity H_z for different points along the piece during the longitudinal demagnetization process.

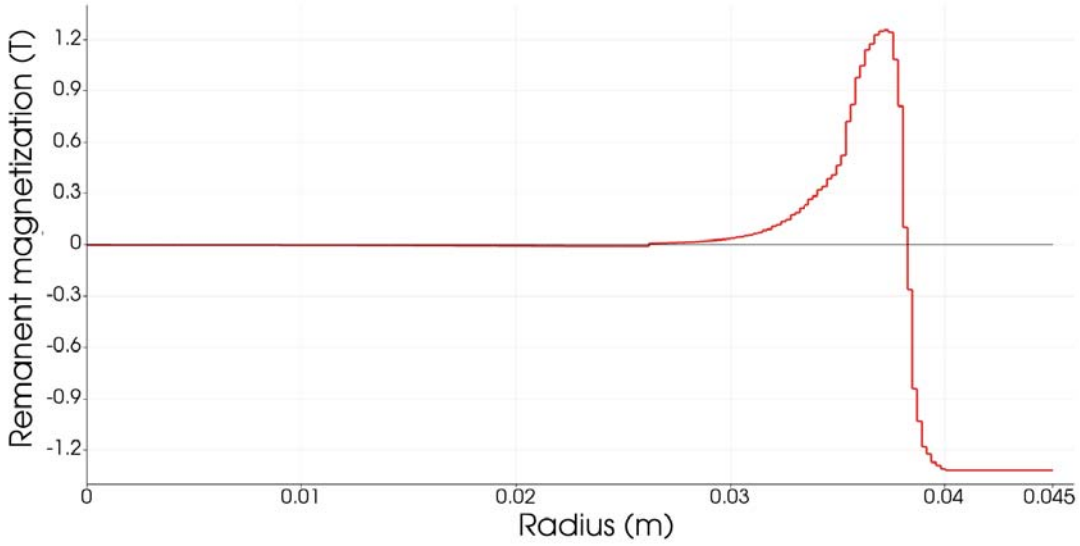

Figure 2.13: Remanent flux density ($z-$component) after longitudinal magnetization.

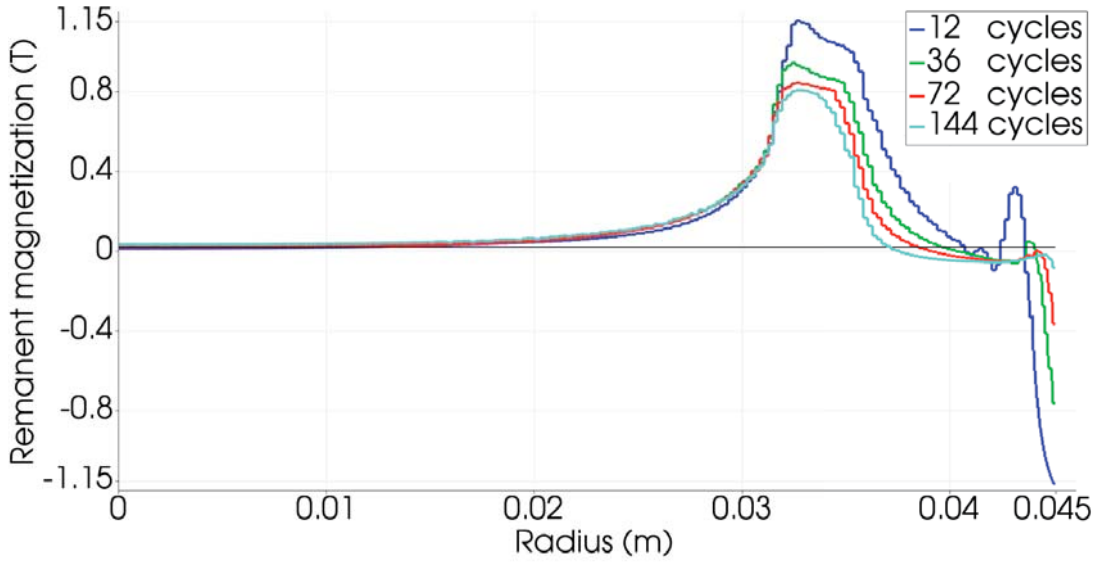

Figure 2.14: Remanent flux density ($z-$component) vs. radius in the cylindrical piece. Longitudinal demagnetization. Number of cycles comparison.

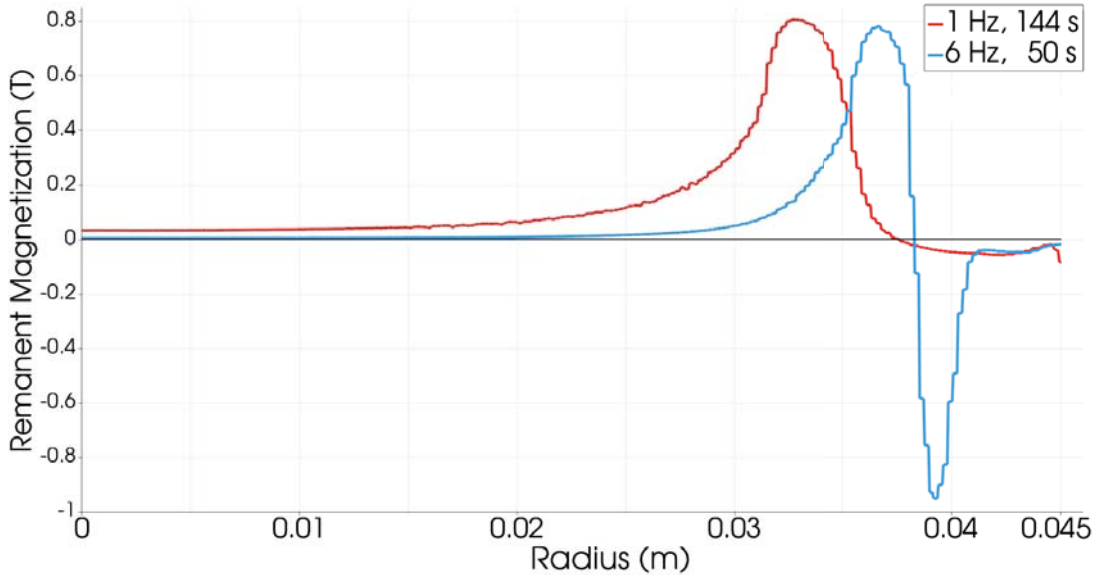

Figure 2.15: Remanent flux density ($z-$component) vs. radius in the cylindrical piece. Longitudinal demagnetization. Frequency comparison.

procedure as they give useful information on which are the most important source parameters for a successful demagnetization.

In Figure 2.13 and 2.9 we can see the remanent flux density after the longitudinal and circular magnetization processes, respectively. We observe that greater values are obtained in the circular case, in which the skin effect is also more noticeable.

Concerning the demagnetization step, as a general conclusion we can say that the results suggest that circular demagnetization should be used to obtain better results. Comparing Figure 2.10 with Figure 2.14, we can see that in the circular case, and except for the case of 12 cycles, there is not such a big dependance of the remanent flux density on the number of cycles as in the longitudinal case. Furthermore, lower values of the remanent flux density are achieved with circular demagnetization, even though in this case greater values result from the magnetization process.

USC
UNIVERSIDADE
DE SANTIAGO
DE COMPOSTELA

USC
UNIVERSIDADE
DE SANTIAGO
DE COMPOSTELA

Part II

Contributions to Electrical Machine Modeling

USC
UNIVERSIDADE
DE SANTIAGO
DE COMPOSTELA

Introduction

The generic term *electrical machine* makes reference to any device that converts electrical into mechanical energy or vice versa. Most electrical machines can carry out both tasks, even though each of them is designed to efficiently perform a particular one, as they are usually subjected to different operating requirements. When a machine is intended to generate mechanical from electrical power it is called *motor*, and the name *generator* is used if it converts mechanical energy into electrical one. Electrical transformers, which are used to change the voltage of an alternating current, are sometimes included into the category of electrical machine, but we are not going to consider them here. Moreover, we are only going to refer to electrical motors, keeping in mind that the main operating principles, characteristics and many other considerations apply to generators as well in a symmetrical fashion.

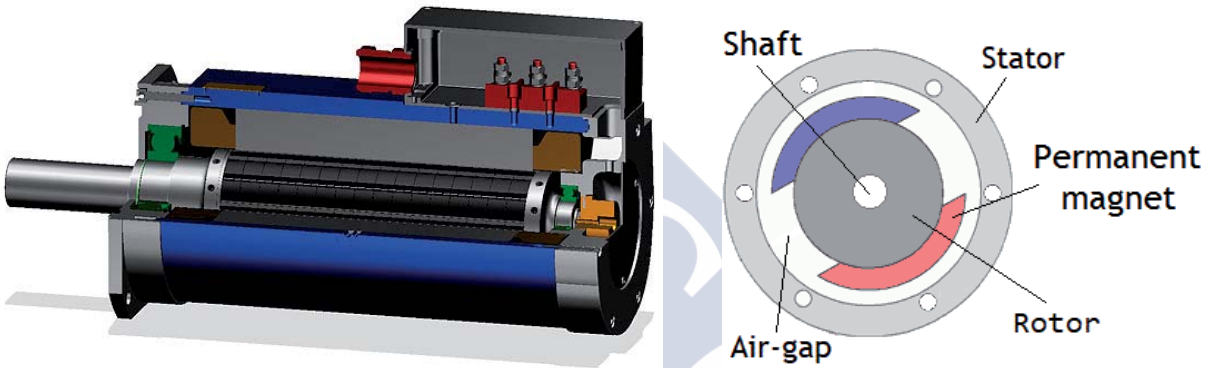

Figure II.1: PMS motor (left) and cross-section draft (right). From Wikimedia Commons under license CC-BY-SA-3.0.

Most electric motors operate by means of the interaction between the magnetic field created by an external source and the internal electromagnetic field. Besides, in order to produce mechanical energy, all motors have a moving part, which usually either oscillates linearly or rotates around a given axis. We are going to focus on the latter, which generally have cylindrical shape with two main parts separated by an *air-gap*: a *stator*, which remains still, and a *rotor*, which rotates about the so-called *shaft*, transmitting the mechanical energy to the load (see Figure II.1). Moreover, and independently of their moving direction, electrical machines can be classified into AC and DC, depending on wether they are fed by means of an alternating or a direct current, respectively. We are going to concentrate on radial-flux AC machines, characterized by the magnetic flux within the air-gap flowing in the radial direction with respect to the shaft, in opposition to axial or transversal-flux machines. On the other hand, concerning AC machines in general, there are two major classes, *synchronous* and *induction* machines. There are two main differences between them

- the nature of the source of the magnetic field in the rotor, and
- the relation between the rotation speed and the magnetic frequency of the currents in the stator.

Concerning the former aspect, most synchronous motors have active sources in both stator and rotor (except, for instance, reluctance motors), while the magnetic field in the rotor of induction

machines is induced from the one in the stator, either in a supplementary rotor winding or in a *squirrel cage* (see Figure II.2). Regarding the rotation angular speed, in synchronous machines it is equal to the so-called *synchronous speed*, which is defined in terms of the frequency of the stator sources and the number of poles of the machine, while induction motors rotate at a lower rate. In this part of the memoir, we will consider two types of electric motors: permanent magnet synchronous (PMS) and induction motors with squirrel-cage rotors.

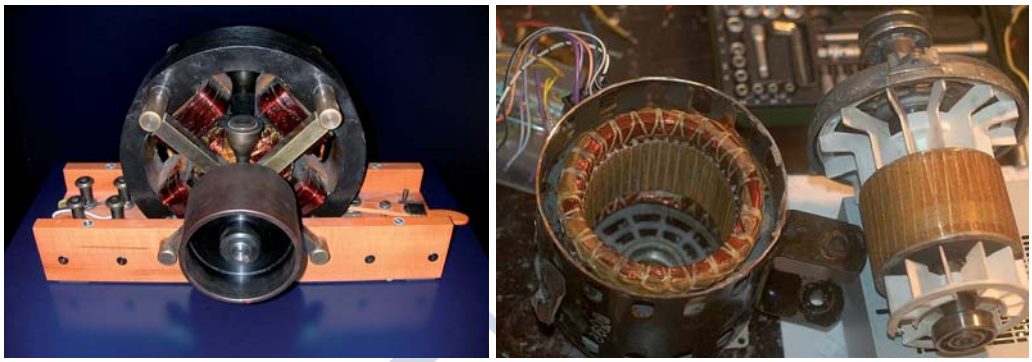

Figure II.2: Wound induction machine (left) and squirrel-cage induction machine (right). From Wikimedia Commons under license CC-BY-SA-3.0.

On the one hand, PMS motors are synchronous because they have active sources in both stator and rotor, coils in the first case and permanent magnets in the other (see Figure II.1). A *permanent magnet* is an object made of a ferromagnetic material that is *magnetized*, that is, that produces its own magnetic field. This property makes them suitable to replace windings in electrical machines under certain circumstances. Among the different ferromagnetic materials (such as iron, nickel, rare-earth metals,…), those suitable for permanent magnets are the so-called *hard*, which tend to stay magnetized as they have wide hysteresis-loops (see Figure II.3). For electromagnetic modelling purposes, permanent magnets are often characterised by the linear constitutive law

$$\boldsymbol{B} = \mu_0 \mu_r \boldsymbol{H} + \boldsymbol{B}^r,$$

where the scalar value μ_r is the relative magnetic permeability, and $\boldsymbol{B}^r$ is called the magnet *remanent flux density*. Depending on the geometrical arrangement of the permanent magnets in the rotor, PMS machines can be classified in several ways, among which we can find *surface magnet*, *interior magnet* or *flux concentrating* machines. For more information on permanent magnet motors we refer to [63].

Finally, in the last chapter we will deal with a squirrel cage induction motor, characterized by a rotor consisting in conducting bars inserted through the stack of insulated laminations, electrically shortened at each extremity by the end-rings, producing a cage-like structure. In this kind of machines, the speed difference between the physical rotor and the stator magnetic field causes the current induction in the conducting rotor bars; if the rotor moves at synchronous speed, rotor bars would be static with respect to the stator magnetic field, and thus no current would be induced.

Numerical simulation is an essential tool in the design of electrical machines, as it prevents the building of unnecessary prototypes and significantly reduces both cost and time to obtain new

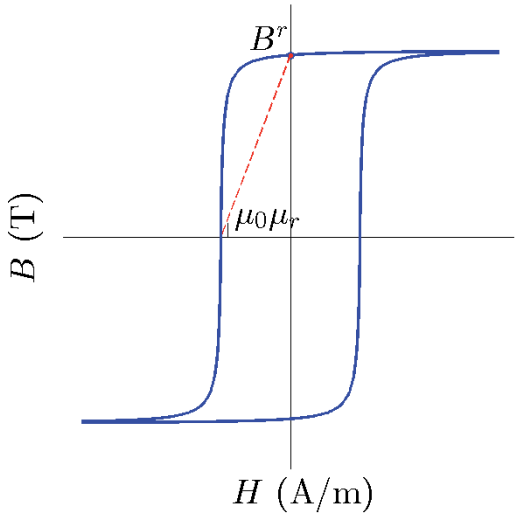

Figure II.3: Hysteresis loop of hard material.

configurations. In particular, the numerical simulation of electrical machines by using finite element methods generally requires the solution of a nonlinear system of partial differential equations derived from Maxwell's equations, eventually coupled with thermal and/or electrical circuit equations (see [92, 94, 116] and references therein). In the following chapters, we will focus on the electromagnetic aspect.

Figure II.4: Lamination detail. Derivative of *E-Twow Electric Motor* by Kaspars Dambis under license CC-BY-2.0.

The electromagnetic model of electrical machines is often based on describing the active zone of the motor as a 2D distributed nonlinear transient magnetic or eddy current problem. Indeed, in order to reduce electromagnetic losses, the magnetic cores of electrical machines are usually laminated media consisting of a large number of stacked steel sheets, which are orthogonal to the direction of the currents traversing the stator coil sides (see Figures II.4 and II.5). Considering the high number of sheets and their small thickness (usually less than one millimetre), solving a three-dimensional model would require considering a very fine mesh, leading to very high computational costs. As a consequence, the usual simulation model consists in an electromagnetic problem defined on a cross-section of the machine, while the end regions of the stator

windings and some other elements (for instance, the squirrel cage end-rings of induction motors) are modeled by circuit elements; in this way, the distributed 2D model will be coupled with a lumped one (see, for instance, [93]). On the other hand, the interplay between the magnetic fields in stator and rotor gives rise to a force that causes the latter to rotate around the machine axis. Therefore, the result is a transient problem defined in a moving geometry with prescribed speed.

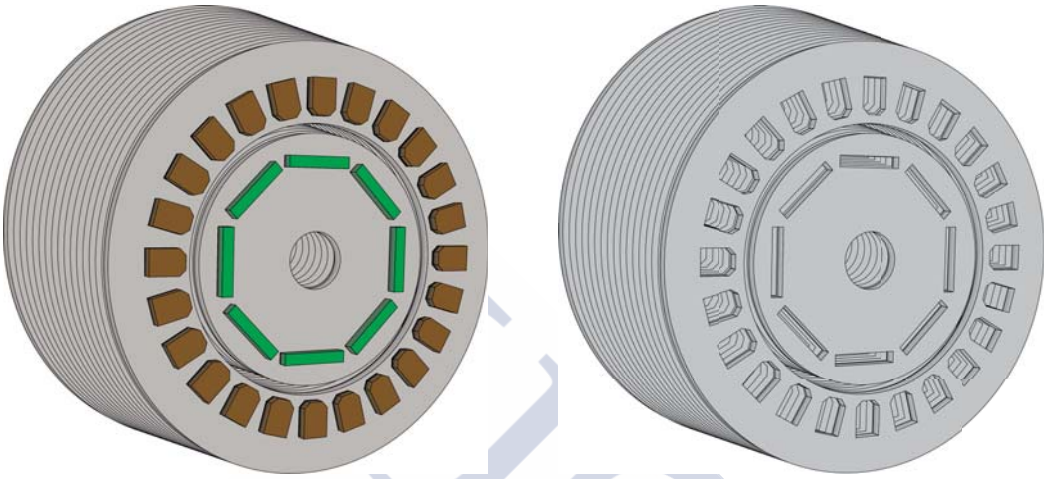

Figure II.5: Permanent magnet synchronous motor active zone (left) and lamination detail (right).

In the remainder of the thesis, we will study several problems related to electrical machines. First of all, we will state a 2D transient magnetic problem that arises in the mathematical modeling of laminated magnetic media and, in particular, of electrical machines. After this, we will briefly describe the problems addressed in this part of the thesis.

A Two-Dimensional Transient Magnetic Model

Let us start recalling that eddy currents are usually modelled by the low-frequency Maxwell's system of equations:

$$\begin{aligned} \mathbf{curl}\, \boldsymbol{H} &= \boldsymbol{J}, \\ \frac{\partial \boldsymbol{B}}{\partial t} + \mathbf{curl}\, \boldsymbol{E} &= \mathbf{0}, \\ \operatorname{div} \boldsymbol{B} &= 0, \end{aligned}$$

along with Ohm's law in stationary conductors

$$\boldsymbol{J} = \sigma \boldsymbol{E},$$

where $\boldsymbol{H}$ is the magnetic field, $\boldsymbol{B}$ is the magnetic flux density, $\boldsymbol{E}$ is the electric field, $\boldsymbol{J}$ is the current density (which is null in dielectrics) and $\sigma > 0$ is the electrical conductivity in

conductors. This model will be completed later with the corresponding constitutive laws relating $\boldsymbol{H}$ and $\boldsymbol{B}$.

Let us assume that the current density $\boldsymbol{J}$ has non-null component only in the z space direction and that this component does not depend on z, i.e., $\boldsymbol{J} = J_z \boldsymbol{e}_z$, with $J_z = J_z(x, y, t)$. We also assume that the geometry and the magnetic field $\boldsymbol{H}$ are invariant along the $z-$direction, and that all materials are magnetically isotropic. In this case, under an appropriate decay of fields at infinity (see [102]), the magnetic field $\boldsymbol{H}$, and then the magnetic induction $\boldsymbol{B}$, have only components on the $xy-$plane and both are independent of z, namely,

$$\boldsymbol{H} = H_x(x, y, t)\boldsymbol{e}_x + H_y(x, y, t)\boldsymbol{e}_y, \quad \boldsymbol{B} = B_x(x, y, t)\boldsymbol{e}_x + B_y(x, y, t)\boldsymbol{e}_y.$$

Since we are interested in using a finite element method for the numerical solution, we will restrict ourselves to a bounded domain. Thus, let us consider a 2D convex bounded domain Ω, with Lipschitz continuous boundary, containing a cross-section transversal to the device. Thus, let us assume that Ω is composed of the following open subsets

- a magnetically linear subdomain Ω_0,
- non-magnetic connected conductors Ω_n, $n = 1, \ldots, N_c$,
- a permanent magnet region $\Omega_{\rm pm}$ and
- a nonlinear ferromagnetic core $\Omega_{\rm nl}$.

We notice that, for the moment, we will not take motion into account. Moreover, we further assume that the boundaries of the conductors, $\partial\Omega_n$, $n = 1, \ldots, N_c$, are mutually disjoint and do not touch the boundary of Ω, and also that the same is true for the boundaries of the connected components of the permanent magnet region. We notice that all parts of the domain are non-conducting except for the non-magnetic conductors, which support the current density $\boldsymbol{J}$. Moreover, we will use the notation $\Omega_{\rm c} := \bigcup_{n=1}^{N_c} \Omega_n$.

In this framework, vector fields $\boldsymbol{H}$ and $\boldsymbol{B}$ are linked by the constitutive relations:

$$\begin{aligned} \boldsymbol{H} &= \nu_0 \boldsymbol{B} && \text{in } \Omega_0 \cup \Omega_{\rm c}, \\ \boldsymbol{H} &= \nu_{\rm pm}\boldsymbol{B} - \nu_{\rm pm}\boldsymbol{B}^r && \text{in } \Omega_{\rm pm}, \\ \boldsymbol{H} &= \widetilde{\nu}(|\boldsymbol{B}|)\boldsymbol{B} && \text{in } \Omega_{\rm nl}, \end{aligned}$$

where ν_0 is the vacuum magnetic reluctivity, $\boldsymbol{B}^r$ is the remanent flux density in the permanent magnets and $\nu_{\rm pm} : \Omega_{\rm pm} \longrightarrow \mathbb{R}^+$ is the magnetic reluctivity in the permanent magnets. In principle, both the magnetically linear subdomain and the nonlinear core subdomain may have several parts with different magnetic reluctivities. However, for the sake of simplicity, we have assumed there is only one for each of these two subdomains and that the magnetic reluctivity of the linear one is that of the vacuum, ν_0. We assume that $\boldsymbol{B}^r$ has only components on the $xy-$plane and both are independent of the $z-$coordinate and that $\nu_{\rm pm} \in \mathrm{L}^\infty(\Omega_{\rm pm})$. Furhtermore, we define the global magnetic reluctivity function $\nu : \Omega \times \mathbb{R}_0^+ \longrightarrow \mathbb{R}^+$ as

$$\nu(\boldsymbol{x}; s) := \begin{cases} \nu_0 & \text{if } \boldsymbol{x} \in \Omega_0 \cup \Omega_{\rm c}, \\ \nu_{\rm pm}(\boldsymbol{x}) & \text{if } \boldsymbol{x} \in \Omega_{\rm pm}, \\ \widetilde{\nu}(s) & \text{if } \boldsymbol{x} \in \Omega_{\rm nl}. \end{cases}$$

Let us make the following assumptions on the nonlinear reluctivity $\widetilde{\nu} : \mathbb{R}_0^+ \longrightarrow \mathbb{R}^+$,

$$\exists\, \nu_1, \nu_2 > 0 \,:\, \nu_1 \leq \widetilde{\nu}(s) \leq \nu_2 \quad \text{a.e. in } \mathbb{R}_0^+, \tag{II.1}$$

$$\exists\, M_{\widetilde{\nu}} > 0 \,:\, |\widetilde{\nu}(p)p - \widetilde{\nu}(q)q| \leq M_{\widetilde{\nu}}|p-q| \quad \forall\, p, q \in \mathbb{R}_0^+, \tag{II.2}$$

$$\exists\, \alpha_{\widetilde{\nu}} > 0 \,:\, (\widetilde{\nu}(p)p - \widetilde{\nu}(q)q)(p-q) \geq \alpha_{\widetilde{\nu}}|p-q|^2 \quad \forall\, p, q \in \mathbb{R}_0^+. \tag{II.3}$$

Therefore, we seek $\boldsymbol{H} \in \mathrm{H}(\mathbf{curl}, \Omega)$, $\boldsymbol{B} \in \mathrm{H}(\mathrm{div}, \Omega)$ and $\boldsymbol{E} \in \mathrm{H}(\mathbf{curl}, \Omega_{\mathrm{C}})$ such that

$$\mathbf{curl}\, \boldsymbol{H} = \boldsymbol{J} \quad \text{in } \Omega, \tag{II.4}$$

$$\frac{\partial \boldsymbol{B}}{\partial t} + \mathbf{curl}\, \boldsymbol{E} = \boldsymbol{0} \quad \text{in } \Omega_{\mathrm{C}}, \tag{II.5}$$

$$\mathrm{div}\, \boldsymbol{B} = 0 \quad \text{in } \Omega, \tag{II.6}$$

$$\boldsymbol{H} = \nu(\cdot, |\boldsymbol{B}|)\boldsymbol{B} \quad \text{in } \Omega, \tag{II.7}$$

$$\boldsymbol{J} = \sigma \boldsymbol{E} \quad \text{in } \Omega_{\mathrm{C}}, \tag{II.8}$$

$$\boldsymbol{B} \cdot \boldsymbol{n} = 0 \quad \text{on } \partial\Omega, \tag{II.9}$$

where the boundary condition means there is no magnetic flux through the boundary. We notice that, since we are not interested in obtaining the electric field $\boldsymbol{E}$ in dielectrics, Faraday's and Ohm's law, (II.5) and (II.8), respectively, have only been considered in the conducting domain Ω_{C}, where $\sigma > 0$.

In order to solve the described two-dimensional model, it is convenient to introduce a magnetic vector potential because it leads to solving a scalar problem instead of a vector one. Since $\boldsymbol{B}$ is divergence-free, there exists a so-called magnetic vector potential $\boldsymbol{A}$ such that $\boldsymbol{B} = \mathbf{curl}\, \boldsymbol{A}$. Under the assumptions above, we can choose a magnetic vector potential that does not depend on z and does not have either x or y components, i.e., $\boldsymbol{A} = A_z(x, y, t)\boldsymbol{e}_z$ (see, for instance, [36]).

Concerning the sources, we will suppose that all conductors are stranded, which makes it possible to assume that the current density is uniform and given by

$$J_{z,n}(t) = \frac{I_n(t)}{\mathrm{meas}(\Omega_n)}, \quad n = 1, \ldots, N_c,$$

where $I_n(t)$ denotes the total current across Ω_n at time t. Actually, for each conductor, we will see later that these sources can be given in terms of either the current or the potential drop per unit length in the z-direction.

Thus, in terms of $A = A_z$, if the currents were known for all conductors, the transient magnetic model (II.4)–(II.8) reads:

$$\begin{aligned}
-\,\mathrm{div}(\nu_0\, \mathbf{grad}\, A) &= 0 && \text{in } \Omega_0,\\
-\,\mathrm{div}(\nu_0\, \mathbf{grad}\, A) &= \frac{I_n(t)}{\mathrm{meas}(\Omega_n)} && \text{in } \Omega_n, n = 1, \ldots, N_c,\\
-\,\mathrm{div}(\nu_{\mathrm{pm}}\, \mathbf{grad}\, A) &= -\,\mathrm{div}\left(\nu_{\mathrm{pm}}\, (\boldsymbol{B}^r)^{\perp}\right) && \text{in } \Omega_{\mathrm{pm}},\\
-\,\mathrm{div}(\widetilde{\nu}(|\mathbf{grad}\, A|)\, \mathbf{grad}\, A) &= 0 && \text{in } \Omega_{\mathrm{nl}},
\end{aligned}$$

$$[\nu(\cdot;|\mathbf{grad}\, A|)\,\mathbf{grad}\, A\cdot\boldsymbol{n}]_\Gamma = \begin{cases} \nu_{\rm pm}\,(\boldsymbol{B}^r)^\perp\cdot\boldsymbol{n}, & \text{if } \Gamma\subset\partial\Omega_{\rm pm},\\ 0, & \text{otherwise,}\end{cases}$$

where $[\,\cdot\,]_\Gamma$ denotes the jump across any interface Γ, $(\boldsymbol{B}^r)^\perp := -B^r_y\boldsymbol{e}_x + B^r_x\boldsymbol{e}_y$ and $\boldsymbol{n}$ is a unit normal vector to interface Γ. Moreover, on the boundary $\partial\Omega$, we will consider the homogeneous Dirichlet boundary condition $A=0$, which guarantees (II.9).

Remark II.1. *Notice that the jump discontinuity in the above problem follows from the transmission condition $[\boldsymbol{H}\times\boldsymbol{n}]_\Gamma = \boldsymbol{0}$, which, at the same time, follows directly from the regularity of $\boldsymbol{H}$, as long as there are no surface currents on Γ.*

Next, we will see how to include some sources in terms of the potential drops per unit length in our formulation. Therefore, let us assume that we have N_V conductors with potential drop per unit length as source data, and $N_I = N_c - N_V$ conductors in which we impose the current. For the sake of simplicity, we will assume that the electrical conductivity σ is constant for all conductors, but otherwise the development below can be applied with no significant change (see [16]). Taking into account Faraday's law in the conducting domain (II.5), we deduce that there exist N_c scalar potentials V_n, $n=1,\dots,N_c$, unique up to a constant, such that

$$\frac{\partial\boldsymbol{A}}{\partial t} + \boldsymbol{E} = -\mathbf{grad}\, V_n \quad \text{in } \Omega_n, \quad n=1,\dots,N_c.$$

Taking into account the assumptions on $\boldsymbol{J}$ and Ohm's law (II.8), we deduce that $\boldsymbol{E}$ in conductors has non-null component only in the z space direction which is, furthermore, spatially constant in each Ω_n, $n=1,\dots,N_c$. Moreover, since $\boldsymbol{A} = A\boldsymbol{e}_z$, we have $-\mathbf{grad}\, V_n = -\dfrac{\partial V_n}{\partial z}\boldsymbol{e}_z$ in each Ω_n, $n=1,\dots,N_c$. As a consequence, the above equation reduces to

$$\frac{\partial A}{\partial t} + E_z = -C_n(t) \quad \text{in } \Omega_n, \quad n=1,\dots,N_c, \tag{II.10}$$

where $C_n(t) := (\partial V_n/\partial z)(t)$ is the potential drop per unit length along direction z in conductor Ω_n, $n=1,\dots,N_c$. Multiplying (II.10) by the electrical conductivity, integrating on each Ω_n, $n=1,\dots,N_V$, and taking Ohm's law into account we deduce

$$\frac{d}{dt}\int_{\Omega_n}\sigma A(x,y,t)\,dxdy + I_n(t) = -C_n(t)\sigma\,\mathrm{meas}(\Omega_n), \quad n=1,\dots,N_V. \tag{II.11}$$

Thus, if currents and voltage drops are given in conductors, the strong formulation for the transient magnetic model is the following:

Problem II.2. *Given $(C_1(t),\dots,C_{N_V}(t))^{\rm T}$, $(I_{N_V+1}(t),\dots,I_{N_V+N_I}(t))^{\rm T}$, $\boldsymbol{B}^r(x,y)$ and a vector of initial currents $\vec{I}_0\in\mathbb{R}^{N_V}$, find $A(x,y;t)$ and $(I_1(t),\dots,I_{N_I}(t))^{\rm T}$ for every $t\in[0,T]$*

satisfying $(I_1(0), \dots, I_{N_V}(0))^{\mathrm{T}} = \vec{I}_0$*,*

$$-\operatorname{div}(\nu_0 \,\mathbf{grad}\, A) = 0 \quad \textit{in } \Omega_0, \tag{II.12}$$

$$-\operatorname{div}(\nu_0 \,\mathbf{grad}\, A) = \frac{I_n(t)}{\operatorname{meas}(\Omega_n)} \quad \textit{in } \Omega_n, n = 1, \dots, N_V + N_I, \tag{II.13}$$

$$-\operatorname{div}(\nu_{\mathrm{pm}} \,\mathbf{grad}\, A) = -\operatorname{div}\left(\nu_{\mathrm{pm}} \,(\boldsymbol{B}^r)^{\perp}\right) \quad \textit{in } \Omega_{\mathrm{pm}}, \tag{II.14}$$

$$-\operatorname{div}(\tilde{\nu}(|\mathbf{grad}\, A|) \,\mathbf{grad}\, A) = 0 \quad \textit{in } \Omega_{\mathrm{nl}}, \tag{II.15}$$

$$[\nu(\cdot; |\mathbf{grad}\, A|) \,\mathbf{grad}\, A \cdot \boldsymbol{n}]_{\Gamma} = \begin{cases} \nu_{\mathrm{pm}} \,(\boldsymbol{B}^r)^{\perp} \cdot \boldsymbol{n}, & \textit{if } \Gamma \subset \partial\Omega_{\mathrm{pm}}, \\ 0, & \textit{otherwise}, \end{cases} \tag{II.16}$$

$$A = 0 \quad \textit{on } \partial\Omega, \tag{II.17}$$

and, for every $t \in (0, T]$*,*

$$\frac{d}{dt} \int_{\Omega_n} \sigma A(x, y, t) + I_n(t) = -C_n(t) \sigma \operatorname{meas}(\Omega_n), \quad n = 1, \dots, N_V. \tag{II.18}$$

In the next three chapters, we will start from this formulation to consider several problems from different perspectives. Firstly, in Chapter 3, we will study this problem with sources given in terms of the remanent fluxes in permanent magnets and the potential drop per unit length in each conductor, (that is, in the case $N_I = 0$). In particular, we will focus on showing that the continuous problem is well-posed and obtaining an error estimate for a finite element discretization. Then, in Chapter 4, we will define and study an optimal control problem related to Problem II.2, in the case $N_V = 0$, in which we will minimise the losses in a permanent magnet synchronous motor (PMSM), while we guarantee the generation of a certain minimum torque. In opposition to the other chapters in this part, we will restrict ourselves to the linear case, and we will study the problem from a mathematical and numerical analysis point of view. Finally, in Chapter 5, we will couple Problem II.2, (without permanent magnets), with some circuit equations and incorporate motion to be able to model an induction motor. We will use this model as the starting point for developing a methodology that seeks good approximations for the initial currents in the rotor bars of a squirrel-cage induction motor, allowing us to reach the steady-state of the machine in the shortest possible simulation time, avoiding the otherwise long transient state. For this purpose, we will make some simplifications to the improved formulation, in order to define a minimization problem that will provide us with the sought initial currents.

Chapter 3

Mathematical and Numerical Analysis of a Circuit Coupling Problem

3.1 Introduction

The objective of this chapter is the mathematical and numerical analysis of a nonlinear transient magnetic model defined in a two-dimensional domain, with sources given in terms of the potential drops in conductors and the remanent fluxes of permanent magnets. This model arises, for instance, in the simulation of electrical machines and, in particular, of permanent magnet synchronous motors (PMSM). In this kind of devices, the magnetic core is usually laminated orthogonally to the direction of the currents traversing the coils. Moreover, eddy current losses are often neglected in permanent magnets, so that these regions are modelled as non-conducting; eventually, a posteriori formulas could be used to estimate such losses (see, for instance, [105, 117]).

As we have mentioned in the introduction to this part of the thesis, both of the above simplifications allow us to build a 2D transient magnetic model in a cross section of the device, the stator coils being the only conducting part. These coils are generally composed by stranded wires carrying a uniformly distributed current density. The mathematical model used to simulate these conductors strongly depends on the kind of the imposed source. Indeed, as it can be seen in Problem II.2, if the source data are given in terms of the current traversing the wires, the problem reduces to solving a nonlinear magnetostatic problem at each time step, and thus time appears as a parameter. However, in the case where the potential drops are given, the distributed magnetostatic model has to be coupled with a circuit equation, equation (3.7), linking currents and voltage drops. In this chapter, we focus on this last case because the model offers challenges from a mathematical and numerical point of view, as detailed below.

Here, we give a first step towards the analysis of the genuine physical problem, as we do not consider the motion of the machine, what would lead to a much more difficult problem; see, for instance, [39] for a case incorporating also induction effects. Our mathematical model will

be obtained from the low-frequency approximation of Maxwell's equations, without taking any eddy current effects into consideration. Therefore, we will deal with an integro-differential problem coupling an elliptic partial differential equation, written in terms of the magnetic vector potential, with the circuit equations relating currents and voltage drops in stranded conductors. The partial differential equations are nonlinear due to the presence of ferromagnetic materials in the cores which usually have a strongly nonlinear magnetic behavior.

In the literature, we can find several references dealing with the analysis of low-frequency electromagnetic models coupled with circuit equations. For example, in [95], the authors study the well-posedness of a three-dimensional field/circuit nonlinear problem in the presence of eddy currents and provide error estimates for time discretization. In [80], the authors deal with a 3D field/circuit linear model, focusing only on the continuous formulation. Alternatively, field/circuit models also fit in the framework of differential algebraic systems of equations (DAE), usually when using finite integration techniques for the spatial discretization; see, for instance, [13, 15]. Finally, we also highlight the results presented in [72], where we can find a study of some classes of differential algebraic systems of equations in an abstract framework, in particular covering the case of systems of DAE coupled with partial differential equations (PDE). However, the absence of eddy currents in our problem leads to a system of elliptic partial differential equations coupled with a vector ordinary differential equation in terms of time, what suggests the use of different techniques to perform the mathematical and numerical analysis.

As discussed above, we focus on a model that does not consider eddy current effects. In the introduction of this part of the document, we obtained an integro-differential problem arising from the coupling of the Maxwell's system of equations with the circuit equations relating currents and voltage drops in stranded conductors. To perform its mathematical analysis, it will be written as a nonlinear system of implicit ordinary differential equations in terms of the currents traversing the coils, which are functions of time. The operator defining this system expresses the so-called flux linkages per unit length in the coils, in terms of the currents traversing them, via the resolution of some 2D magnetostatic problems. The properties of this operator are deduced directly from results already existing in the literature (specifically, those appearing in [59, 82]). To perform the numerical approximation of the continuous problem we propose an Euler-implicit scheme for the ODE, combined with a finite element method for the approximation of the involved distributed operator. Some convergence results are obtained for this numerical scheme. However, for the numerical implementation, we use the alternative approach proposed in [16] which consists in eliminating the unknown currents from the system by means of the circuit equations. This idea is also exploited in the theoretical analysis of the eddy current model performed in [80]. As a consequence, we need to prove an equivalence result between the implemented scheme and the discrete problem theoretically analysed.

The chapter is organized as follows. In Section 3.2 we obtain the weak formulation associated to Problem II.2, with $N_I = 0$, and express the problem as a system of implicit ODE; moreover, we perform its mathematical analysis in the continuous case. In Section 3.3 we introduce the finite element discretization of the magnetostatics problem involved in the definition of the ODE operator. In Section 3.4 we propose an implicit Euler scheme for the discretization of the system of ODE and prove an error estimate for its solution. In Section 3.5 we prove the equivalence

between the analysed problem and the implemented one. Finally, in Section 3.6, we show some numerical examples to illustrate the obtained convergence results.

3.2 Mathematical Analysis of the Continuous Problem

As we have mentioned in the introduction, in this chapter we are going to study Problem II.2, from the point of view of the mathematical and numerical analysis, in the case in which the source data in conductors are given in terms of the potential drops per unit length. Therefore, in this section, we will have $N_I = 0$ and $N_c = N_V$, and thus Problem II.2 reduces to:

Problem 3.1. *Given* $\vec{C}(t)^{\mathrm{T}} \in \mathcal{C}([0,T])^{N_c}$, $\vec{I}_0 \in \mathbb{R}^{N_c}$ *and* $\boldsymbol{B}^r \in \mathrm{L}^2(\Omega_{pm})^3$, *find* $A(t) \in \mathrm{H}^1_0(\Omega)$ *for every* $t \in [0,T]$ *and* $\vec{I}(t) \in \mathcal{C}^{0,1}([0,T])^{N_c}$ *satisfying* $\vec{I}(0) = \vec{I}_0$,

$$-\operatorname{div}(\nu_0 \,\mathbf{grad}\, A) = 0 \quad \textit{in } \Omega_0, \tag{3.1}$$

$$-\operatorname{div}(\nu_0 \,\mathbf{grad}\, A) = \frac{I_n(t)}{\operatorname{meas}(\Omega_n)} \quad \textit{in } \Omega_n, n = 1, \ldots, N_c, \tag{3.2}$$

$$-\operatorname{div}(\nu_{\mathrm{pm}} \,\mathbf{grad}\, A) = -\operatorname{div}\left(\nu_{\mathrm{pm}} \left(\boldsymbol{B}^r\right)^{\perp}\right) \quad \textit{in } \Omega_{\mathrm{pm}}, \tag{3.3}$$

$$-\operatorname{div}(\widetilde{\nu}(|\mathbf{grad}\, A|)\,\mathbf{grad}\, A) = 0 \quad \textit{in } \Omega_{\mathrm{nl}}, \tag{3.4}$$

$$[\nu(\cdot;|\mathbf{grad}\, A|)\,\mathbf{grad}\, A \cdot \boldsymbol{n}]_{\Gamma} = \begin{cases} \nu_{\mathrm{pm}} \left(\boldsymbol{B}^r\right)^{\perp} \cdot \boldsymbol{n}, & \textit{if } \Gamma \subset \partial\Omega_{\mathrm{pm}}, \\ 0, & \textit{otherwise}, \end{cases} \tag{3.5}$$

$$A = 0 \quad \textit{on } \partial\Omega, \tag{3.6}$$

and, for every $t \in (0,T]$,

$$\frac{d}{dt}\int_{\Omega_n} \sigma A(x,y,t) + I_n(t) = -C_n(t)\sigma \operatorname{meas}(\Omega_n), \quad n = 1, \ldots, N_c. \tag{3.7}$$

3.2.1 Weak Formulation for the Transient Magnetic Problem

Firstly, we will obtain the weak formulation corresponding to (3.1)–(3.6). To this aim, we multiply (3.1)–(3.4) by a sufficiently smooth test function W such that $W = 0$ on $\partial\Omega$, obtaining, after suitable integrations,

$$-\int_{\Omega_0} \operatorname{div}(\nu_0 \mathbf{grad}\, A) W = 0, \tag{3.8}$$

$$-\int_{\Omega_n} \operatorname{div}(\nu_0 \mathbf{grad}\, A) W = \int_{\Omega_n} \frac{I_n(t)}{\operatorname{meas}(\Omega_n)} W, \quad n = 1, \ldots, N_c, \tag{3.9}$$

$$-\int_{\Omega_{\mathrm{pm}}} \operatorname{div}(\nu_{\mathrm{pm}} \mathbf{grad}\, A) W = -\int_{\Omega_{\mathrm{pm}}} \operatorname{div}\left(\nu_{\mathrm{pm}} \left(\boldsymbol{B}^r\right)^{\perp}\right) W, \tag{3.10}$$

$$-\int_{\Omega_{\mathrm{nl}}} \operatorname{div}(\widetilde{\nu}(|\mathbf{grad}\, A|) \mathbf{grad}\, A) W = 0. \tag{3.11}$$

Using integration by parts on the left-hand sides of (3.8)–(3.11) we obtain

$$-\int_{\mathcal{U}} \operatorname{div}(\nu(\boldsymbol{x};|\mathbf{grad}\, A|)\mathbf{grad}\, A)W = \int_{\mathcal{U}} \nu(\boldsymbol{x};|\mathbf{grad}\, A|)\mathbf{grad}\, A\cdot \mathbf{grad}\, W - \int_{\partial\mathcal{U}} \nu(\boldsymbol{x};|\mathbf{grad}\, A|)\mathbf{grad}\, A\cdot \boldsymbol{n}\, W,$$

with $\mathcal{U}$ the subdomains of Ω, that is, Ω_0, Ω_{c}, Ω_{pm} and Ω_{nl}. On the other hand, concerning the right-hand side of (3.10),

$$-\int_{\Omega_{\mathrm{pm}}} \operatorname{div}\left(\nu_{\mathrm{pm}}\left(\boldsymbol{B}^r\right)^{\perp}\right) W = \int_{\Omega_{\mathrm{pm}}} \nu_{\mathrm{pm}}\left(\boldsymbol{B}^r\right)^{\perp}\cdot \mathbf{grad}\, W - \int_{\partial\Omega_{\mathrm{pm}}} \nu_{\mathrm{pm}}\left(\boldsymbol{B}^r\right)^{\perp}\cdot \boldsymbol{n}\, W.$$

Thus, summing up equations (3.8)-(3.11) and taking the interface and boundary conditions into account,

$$\int_{\Omega} \nu(\boldsymbol{x};|\mathbf{grad}\, A(\boldsymbol{x},t)|)\mathbf{grad}\, A(\boldsymbol{x},t)\cdot \mathbf{grad}\, W(\boldsymbol{x}) = \sum_{n=1}^{N_c}\int_{\Omega_n} \frac{I_n(t)}{\operatorname{meas}(\Omega_n)} W(\boldsymbol{x}) + \int_{\Omega_{\mathrm{pm}}} \nu_{\mathrm{pm}}(\boldsymbol{x})\left(\boldsymbol{B}^r\right)^{\perp}(\boldsymbol{x})\cdot \mathbf{grad}\, W(\boldsymbol{x}).$$

Then, the variational formulation associated to the eddy currents problem in terms of the $z-$component of the magnetic vector potential is:

Problem 3.2. *Given $\vec{C}(t)^{\mathrm{T}} \in \mathcal{C}([0,T])^{N_c}$, $\vec{I}_0 \in \mathbb{R}^{N_c}$ and $\boldsymbol{B}^r \in \mathrm{L}^2\left(\Omega_{pm}\right)^3$, find $A(t) \in \mathrm{H}_0^1(\Omega)$ for every $t \in [0,T]$ and $\vec{I}(t) \in \mathcal{C}^{0,1}([0,T])^{N_c}$ satisfying $\vec{I}(0) = \vec{I}_0$,*

$$\int_{\Omega} \nu(\boldsymbol{x};|\mathbf{grad}\, A(\boldsymbol{x},t)|)\mathbf{grad}\, A(\boldsymbol{x},t)\cdot \mathbf{grad}\, W(\boldsymbol{x}) = \sum_{n=1}^{N_c}\int_{\Omega_n} \frac{I_n(t)}{\operatorname{meas}(\Omega_n)} W(\boldsymbol{x}) + \int_{\Omega_{\mathrm{pm}}} \nu_{\mathrm{pm}}(\boldsymbol{x})\left(\boldsymbol{B}^r\right)^{\perp}(\boldsymbol{x})\cdot \mathbf{grad}\, W(\boldsymbol{x}),$$

for every $W \in \mathrm{H}_0^1(\Omega)$ and $t \in [0,T]$, and

$$\frac{d}{dt}\int_{\Omega_n} \sigma A(t) + I_n(t) = -C_n(t)\sigma \operatorname{meas}(\Omega_n), \quad n = 1,\ldots,N_c \quad \textit{in } (0,T].$$

In the next section, we will write Problem 3.2 as a nonlinear implicit system of ordinary differential equations in order to prove that it is well-posed.

3.2.2 Transient Magnetic Problem as a System of ODE

Let $\vec{\mathcal{F}} : \mathbb{R}^{N_c} \longrightarrow \mathbb{R}^{N_c}$ be the nonlinear operator defined as

$$\vec{\mathcal{F}}\left(\vec{I}\right) := \left(\int_{\Omega_1} \sigma A, \ldots, \int_{\Omega_{N_c}} \sigma A\right)^{\mathrm{T}} \in \mathbb{R}^{N_c},$$

with A the solution of the nonlinear magnetostatic problem:

Problem 3.3. *Given* $\vec{I} \in \mathbb{R}^{N_c}$ *and* $\boldsymbol{B}^r \in \mathrm{L}^2\left(\Omega_{pm}\right)^3$*, find* $A \in \mathrm{H}_0^1(\Omega)$ *such that*

$$\int_\Omega \nu(\boldsymbol{x}; |\mathbf{grad}\, A(\boldsymbol{x})|)\, \mathbf{grad}\, A(\boldsymbol{x}) \cdot \mathbf{grad}\, W(\boldsymbol{x}) = \sum_{n=1}^{N_c} \int_{\Omega_n} \frac{I_n}{\operatorname{meas}(\Omega_n)} W(\boldsymbol{x}) + \int_{\Omega_{\mathrm{pm}}} \nu_{\mathrm{pm}}(\boldsymbol{x})\, (\boldsymbol{B}^r)^\perp(\boldsymbol{x}) \cdot \mathbf{grad}\, W(\boldsymbol{x}),$$

for every $W \in \mathrm{H}_0^1(\Omega)$.

Let us notice that the integrals characterising the components of $\vec{\mathcal{F}}$ are related to the so-called *flux linkages* per unit length since the latter are defined, for conductor Ω_n, $n = 1, \ldots, N_c$, as

$$\frac{1}{\sigma \operatorname{meas}(\Omega_n)} \int_{\Omega_n} \sigma A.$$

Theorem 3.4. *Problem 3.3 has a unique solution.*

Proof. The proof of this theorem follows directly from the results presented in [59, 82].

Indeed, let $b : \mathrm{H}_0^1(\Omega) \times \mathrm{H}_0^1(\Omega) \longrightarrow \mathbb{R}$ be the function given by

$$p(A, W) := \int_\Omega \nu(\cdot; |\mathbf{grad}\, A|)\, \mathbf{grad}\, A \cdot \mathbf{grad}\, W,$$

with the associated operator $\mathcal{P} : \mathrm{H}_0^1(\Omega) \longrightarrow \mathrm{H}^{-1}(\Omega)$ defined by

$$\langle \mathcal{P}(A), W \rangle = \int_\Omega \nu(\cdot; |\mathbf{grad}\, A|)\, \mathbf{grad}\, A \cdot \mathbf{grad}\, W$$

for every $W \in \mathrm{H}_0^1(\Omega)$. Under conditions (II.1)–(II.3), operator $\mathcal{P}$ is strongly monotone and Lipschitz continuous, with constants $\alpha = \alpha_{\widetilde{\nu}}$ and $M = 3M_{\widetilde{\nu}}$, respectively (see [82]).

Concerning the right-hand side, since functions $(I_n / \operatorname{meas}(\Omega_n))\, \chi_{\Omega_n}$ belong to $\mathrm{L}^2(\Omega)$ for $n = 1, \ldots, N_c$, (χ_K being the indicator function of set K), and $\boldsymbol{B}^r \in \mathrm{L}^2\left(\Omega_{pm}\right)^3$, then the operator associated to the right-hand side is in $\mathrm{H}^{-1}(\Omega)$. □

From this theorem, we deduce that operator $\vec{\mathcal{F}}$ is well defined, and therefore we can rewrite Problem 3.2 as

Problem 3.5. *Given* $\vec{C}(t) \in \mathcal{C}([0,T])^{N_c}$ *and* $\vec{I}_0 \in \mathbb{R}^{N_c}$*, find* $\vec{I}(t) \in \mathcal{C}^{0,1}([0,T])^{N_c}$ *such that* $\vec{I}(0) = \vec{I}_0$ *and*

$$\frac{d}{dt}\vec{\mathcal{F}}\left(\vec{I}(t)\right) + \vec{I}(t) = -\left(C_1(t)\sigma \operatorname{meas}(\Omega_1), \ldots, C_{N_c}(t)\sigma \operatorname{meas}(\Omega_{N_c})\right)^{\mathrm{T}} \quad \textit{in } (0,T].$$

Remark 3.6. *We notice that, due to the definition of operator* $\vec{\mathcal{F}}$*, it is obvious that Problems 3.2 and 3.5 are equivalent.*

Theorem 3.7. *Operator $\vec{\mathcal{F}}$ is strongly monotone and globally Lipschitz continuous in $\mathbb{R}^{N_c}$ with respective constants C_{SM} and C_L to be defined below.*

Proof. Let $\vec{I}^1, \vec{I}^2 \in \mathbb{R}^{N_c}$ be given and $A_1, A_2 \in \mathrm{H}_0^1(\Omega)$ be the associated solutions to Problem 3.3, respectively. Then, $\mathcal{F}_n\left(\vec{I}^j\right) = \int_{\Omega_n} \sigma A_j$ for $j = 1, 2$ and $n = 1, \ldots, N_c$.

Let us consider the inner product in $\mathbb{R}^{N_c}$ defined as follows

$$\vec{K}^1 * \vec{K}^2 := \sum_{n=1}^{N_c} \frac{K_n^1 K_n^2}{\sigma \operatorname{meas}(\Omega_n)},$$

with $\|\cdot\|_*$ the associated norm.

First, we will prove that $\vec{\mathcal{F}}$ is strongly monotone:

$$\begin{aligned}
&\langle \mathcal{P}(A_1) - \mathcal{P}(A_2), A_1 - A_2\rangle = \langle \mathcal{P}(A_1), A_1 - A_2\rangle - \langle \mathcal{P}(A_2), A_1 - A_2\rangle \\
&= \int_\Omega \nu(\boldsymbol{x}; |\mathbf{grad}\, A_1|)\mathbf{grad}\, A_1 \cdot \mathbf{grad}\,(A_1 - A_2) - \int_\Omega \nu(\boldsymbol{x}; |\mathbf{grad}\, A_2|)\mathbf{grad}\, A_2 \cdot \mathbf{grad}\,(A_1 - A_2) \\
&\qquad = \sum_{n=1}^{N_c} \int_{\Omega_n} \frac{I_n^1 - I_n^2}{\operatorname{meas}(\Omega_n)}(A_1 - A_2) = \sum_{n=1}^{N_c} \frac{I_n^1 - I_n^2}{\sigma \operatorname{meas}(\Omega_n)} \int_{\Omega_n} \sigma(A_1 - A_2) \\
&\qquad\qquad = \left(\vec{I}^1 - \vec{I}^2\right) * \left(\vec{\mathcal{F}}\left(\vec{I}^1\right) - \vec{\mathcal{F}}\left(\vec{I}^2\right)\right).
\end{aligned}$$

Since $\mathcal{P}$ is strongly monotone with constant α,

$$\alpha ||A_1 - A_2||^2_{\mathrm{H}^1(\Omega)} \leq \langle \mathcal{P}(A_1) - \mathcal{P}(A_2), A_1 - A_2\rangle = \left(\vec{I}^1 - \vec{I}^2\right) * \left(\vec{\mathcal{F}}\left(\vec{I}^1\right) - \vec{\mathcal{F}}\left(\vec{I}^2\right)\right), \tag{3.12}$$

and then, in particular, $\vec{\mathcal{F}}$ is strictly monotone, that is,

$$\left(\vec{\mathcal{F}}\left(\vec{I}^1\right) - \vec{\mathcal{F}}\left(\vec{I}^2\right)\right) * \left(\vec{I}^1 - \vec{I}^2\right) > 0 \quad \forall\, \vec{I}^1, \vec{I}^2 \in \mathbb{R}^{N_c}, \vec{I}^1 \neq \vec{I}^2.$$

Now, taking $W \in \mathrm{H}_0^1(\Omega)$ such that

$$\int_{\Omega_n} \sigma W = I_n^1 - I_n^2,\ n = 1, \ldots, N_c, \qquad \text{and} \qquad ||W||_{\mathrm{H}^1(\Omega)} \leq C \left\|\vec{I}^1 - \vec{I}^2\right\|_* \tag{3.13}$$

for some $C > 0$ independent of $\vec{I}^1, \vec{I}^2$, we get

$$\begin{aligned}
&\langle \mathcal{P}(A_1) - \mathcal{P}(A_2), W\rangle = \langle \mathcal{P}(A_1), W\rangle - \langle \mathcal{P}(A_2), W\rangle \\
&\quad = \int_\Omega \nu(\boldsymbol{x}; |\mathbf{grad}\, A_1|)\mathbf{grad}\, A_1 \cdot \mathbf{grad}\, W - \int_\Omega \nu(\boldsymbol{x}; |\mathbf{grad}\, A_2|)\mathbf{grad}\, A_2 \cdot \mathbf{grad}\, W \\
&\qquad = \sum_{n=1}^{N_c} \int_{\Omega_n} \frac{I_n^1 - I_n^2}{\operatorname{meas}(\Omega_n)} W = \sum_{n=1}^{N_c} \frac{I_n^1 - I_n^2}{\sigma \operatorname{meas}(\Omega_n)} \int_{\Omega_n} \sigma W = \left\|\vec{I}^1 - \vec{I}^2\right\|_*^2.
\end{aligned}$$

Thus, taking into account that $\mathcal{P}$ is Lipschitz continuous,

$$\left\|\vec{I}^1-\vec{I}^2\right\|_*^2=\langle\mathcal{P}(A_1)-\mathcal{P}(A_2),W\rangle\leq||\mathcal{P}(A_1)-\mathcal{P}(A_2)||_{\mathrm{H}^{-1}(\Omega)}||W||_{\mathrm{H}^1(\Omega)}$$
$$\leq M||A_1-A_2||_{\mathrm{H}^1(\Omega)}||W||_{\mathrm{H}^1(\Omega)}\leq MC||A_1-A_2||_{\mathrm{H}^1(\Omega)}\left\|\vec{I}^1-\vec{I}^2\right\|_*.$$

Let us define $C_{SM}:=\alpha/M^2C^2$. Replacing in (3.12) we get

$$C_{SM}\left\|\vec{I}^1-\vec{I}^2\right\|_*^2\leq\alpha||A_1-A_2||^2_{\mathrm{H}^1(\Omega)}\leq\left(\vec{I}^1-\vec{I}^2\right)*\left(\vec{\mathcal{F}}\left(\vec{I}^1\right)-\vec{\mathcal{F}}\left(\vec{I}^2\right)\right),$$

and then $\vec{\mathcal{F}}$ is a strongly monotone operator globally in $\mathbb{R}^{N_c}$.

We notice that we can take $W\in\mathrm{H}^1_0(\Omega)$ verifying (3.13). Indeed, let $\widetilde{\Omega}:=\Omega\setminus\Omega_c$, $c_n:=(I_n^1-I_n^2)/\operatorname{meas}(\Omega_n)$, $n=1,\ldots,N_c$, and $g_n\in\mathrm{H}^{1/2}(\partial\Omega_n)$ with $g_n(\boldsymbol{x})=c_n$ for every $\boldsymbol{x}\in\partial\Omega_n$, $n=1,\ldots,N_c$. Then,

$$\int_{\Omega_n}\sigma c_n=I_n^1-I_n^2.$$

Moreover, let us consider the following Dirichlet problem:

$$\begin{cases}\text{Given } g_n\in\mathrm{H}^{1/2}(\partial\Omega_n),\ n=1,\ldots,N_c,\text{ find }\widetilde{W}\in\mathrm{H}^1_0(\widetilde{\Omega})\text{ such that}\\ \qquad -\Delta\widetilde{W}=0\quad\text{in }\widetilde{\Omega},\\ \qquad\widetilde{W}=g_n\quad\text{on }\partial\Omega_n,\ n=1,\ldots,N_c.\end{cases}$$

This problem is well-defined and

$$\left\|\widetilde{W}\right\|_{\mathrm{H}^1(\widetilde{\Omega})}\leq C\left\|\vec{I}^1-\vec{I}^2\right\|_*,$$

with C independent of $\vec{I}^1,\vec{I}^2$. We can define $W\in\mathrm{H}^1_0(\Omega)$ by

$$W:=\begin{cases}\widetilde{W} & \text{in }\widetilde{\Omega},\\ c_n & \text{in }\Omega_n,\ n=1,\ldots,N_c.\end{cases}$$

Now, we will show that $\vec{\mathcal{F}}$ is Lipschitz continuous. Indeed,

$$\left\|\vec{\mathcal{F}}\left(\vec{I}^1\right)-\vec{\mathcal{F}}\left(\vec{I}^2\right)\right\|_*=\left(\sum_{n=1}^{N_c}\frac{\left(\mathcal{F}_n\left(\vec{I}^1\right)-\mathcal{F}_n\left(\vec{I}^2\right)\right)^2}{\sigma\operatorname{meas}(\Omega_n)}\right)^{1/2}$$
$$=\left(\sum_{n=1}^{N_c}\frac{1}{\sigma\operatorname{meas}(\Omega_n)}\left(\int_{\Omega_n}\sigma(A_1-A_2)\right)^2\right)^{1/2}$$
$$=\left\|\left(\int_{\Omega_1}\sigma(A_1-A_2),\ldots,\int_{\Omega_{N_c}}\sigma(A_1-A_2)\right)^{\mathrm{T}}\right\|_*.$$

Since

$$\left(\int_{\Omega_n}\sigma(A_1-A_2)\right)^2 \leq \sigma^2||A_1-A_2||^2_{\mathrm{L}^1(\Omega_n)} \leq \sigma^2\,\mathrm{meas}(\Omega_n)||A_1-A_2||^2_{\mathrm{L}^2(\Omega_n)^2} \leq \sigma^2\,\mathrm{meas}(\Omega_n)||A_1-A_2||^2_{\mathrm{H}^1(\Omega_n)}$$

then, for every $n=1,\ldots,N_c$,

$$\left\|\vec{\mathcal{F}}\left(\vec{I}^1\right)-\vec{\mathcal{F}}\left(\vec{I}^2\right)\right\|_* = \left\|\left(\int_{\Omega_1}\sigma(A_1-A_2),\ldots,\int_{\Omega_{N_c}}\sigma(A_1-A_2)\right)^{\mathrm{T}}\right\|_* \leq \left(\sum_{n=1}^{N_c}\sigma||A_1-A_2||^2_{\mathrm{H}^1(\Omega_n)}\right)^{1/2} \leq C_1||A_1-A_2||_{\mathrm{H}^1(\Omega)}.$$

Finally, since

$$||A_1-A_2||^2_{\mathrm{H}^1(\Omega)} \leq \frac{1}{\alpha}\left(\vec{I}^1-\vec{I}^2\right)*\left(\vec{\mathcal{F}}\left(\vec{I}^1\right)-\vec{\mathcal{F}}\left(\vec{I}^2\right)\right) \leq \frac{1}{\alpha}\left\|\vec{I}^1-\vec{I}^2\right\|_*\left\|\vec{\mathcal{F}}\left(\vec{I}^1\right)-\vec{\mathcal{F}}\left(\vec{I}^2\right)\right\|_* \leq \frac{C_1}{\alpha}\left\|\vec{I}^1-\vec{I}^2\right\|_*||A_1-A_2||_{\mathrm{H}^1(\Omega)},$$

we conclude that

$$\left\|\vec{\mathcal{F}}\left(\vec{I}^1\right)-\vec{\mathcal{F}}\left(\vec{I}^2\right)\right\|_* \leq C_L||\vec{I}^1-\vec{I}^2||_*,$$

with $C_L := C_1^2/\alpha$, and therefore $\vec{\mathcal{F}}$ is Lipschitz continuous globally in $\mathbb{R}^{N_c}$. □

From the last theorem, applying a result by E. H. Zarantonello (see [114], Theorem 25.B), we deduce that

Corollary 3.8. *$\vec{\mathcal{F}}$ is invertible and its inverse $\vec{\mathcal{F}}^{-1}$ is Lipschitz continuous with Lipschitz constant equal to $1/C_{SM}$.*

This result allows us to rewrite Problem 3.5 in the following way:

Problem 3.9. *Given $\vec{C}(t)\in\mathcal{C}([0,T])^{N_c}$ and $\vec{I}_0\in\mathbb{R}^{N_c}$, find $\vec{I}(t)\in\mathcal{C}^{0,1}([0,T])^{N_c}$ such that $\vec{I}(0)=\vec{I}_0$ and*

$$\frac{d}{dt}\vec{L}(t)+\vec{\mathcal{F}}^{-1}\left(\vec{L}(t)\right) = -\left(C_1(t)\sigma\,\mathrm{meas}(\Omega_1),\ldots,C_{N_c}(t)\sigma\,\mathrm{meas}(\Omega_{N_c})\right)^{\mathrm{T}} \quad \text{in } (0,T],$$

with $\vec{L}(t)=\vec{\mathcal{F}}\left(\vec{I}(t)\right)$ for every $t\in[0,T]$.

Remark 3.10. *Problems 3.5 and 3.9 can be defined with lower regularity assumptions on the source data $\vec{C}(t)$. For instance, if $\vec{C}(t)$ is Lebesgue-measurable in $[0,T]$ and $\left|\vec{C}(t)\right|$ is bounded by a Lebesgue integrable function, both problems have a unique absolutely continuous solution, $\vec{I}(t)\in AC([0,T])^{N_c}$, fulfilling the differential equation almost everywhere in $[0,T]$. Furthermore, most of the results presented in this paper can also be proved under these assumptions.*

Theorem 3.11. *Problem 3.5 has a unique solution* $\vec{I}(t) \in \mathcal{C}^{0,1}([0,T])^{N_c}$ *such that*

$$\left\|\vec{I}(t)\right\| \leq \left\|\vec{I}_0\right\| + \frac{T}{C_{SM}} \left(\left\|\vec{I}_0\right\| + \sigma \max_{n=1,\dots,N_c} \{\text{meas}(\Omega_n)\} \left\|\vec{C}\right\|_{\text{L}^2(0,T)} \right) e^{T/C_{SM}}$$

for every $t \in [0,T]$.

Proof. Since $\vec{\mathcal{F}}^{-1}$ is globally Lipschitz continuous in $\mathbb{R}^{N_c}$, from Theorem 2.15 in [12] we conclude that Problem 3.9 has a unique solution $\vec{I} = \vec{\mathcal{F}}^{-1}\left(\vec{L}\right)$, with $\vec{L} \in \mathcal{C}^1([0,T])^{N_c}$. Therefore, Problem 3.5 has a unique solution $\vec{I} \in \mathcal{C}^{0,1}([0,T])^{N_c}$.

Moreover, integrating the equation appearing in Problem 3.9 in $(0,t)$,

$$\vec{L}(t) - \vec{L}(0) = -\int_0^t \left(\vec{\mathcal{F}}^{-1}\left(\vec{L}(s)\right) + (C_1(s)\sigma\,\text{meas}(\Omega_1), \dots, C_{N_c}(s)\sigma\,\text{meas}(\Omega_{N_c}))^{\text{T}} \right) ds$$

for every $t \in [0,T]$. Thus,

$$\begin{aligned}
\left\|\vec{L}(t) - \vec{L}(0)\right\| &\leq \int_0^t \left\|\vec{\mathcal{F}}^{-1}\left(\vec{L}(s)\right)\right\| ds \\
&\quad + \int_0^t \left\|(C_1(s)\sigma\,\text{meas}(\Omega_1), \dots, C_{N_c}(s)\sigma\,\text{meas}(\Omega_{N_c}))^{\text{T}}\right\| ds \\
&\leq \int_0^t \left\|\vec{\mathcal{F}}^{-1}\left(\vec{L}(s)\right) - \vec{\mathcal{F}}^{-1}\left(\vec{L}(0)\right)\right\| ds + T\left(\sigma \max_{n=1,\dots,N_c} \{\text{meas}(\Omega_n)\} \left\|\vec{C}\right\|_{\text{L}^2(0,T)} + \left\|\vec{I}_0\right\|\right) \\
&\leq \int_0^t \frac{1}{C_{SM}} \left\|\vec{L}(s) - \vec{L}(0)\right\| ds + T\left(\sigma \max_{n=1,\dots,N_c} \{\text{meas}(\Omega_n)\} \left\|\vec{C}\right\|_{\text{L}^2(0,T)} + \left\|\vec{I}_0\right\|\right).
\end{aligned}$$

Then, taking Gronwall's inequality into account (see, for instance, [85], Lemma 1.4.1),

$$\left\|\vec{L}(t) - \vec{L}(0)\right\| \leq T\left(\sigma \max_{n=1,\dots,N_c} \{\text{meas}(\Omega_n)\} \left\|\vec{C}\right\|_{\text{L}^2(0,T)} + \left\|\vec{I}_0\right\|\right) e^{T/C_{SM}}.$$

Now, since $\vec{I}(t) = \vec{\mathcal{F}}^{-1}\left(\vec{L}(t)\right)$,

$$\begin{aligned}
\left\|\vec{I}(t)\right\| - \left\|\vec{I}_0\right\| \leq \left\|\vec{I}(t) - \vec{I}_0\right\| &= \left\|\vec{\mathcal{F}}^{-1}\left(\vec{L}(t)\right) - \vec{\mathcal{F}}^{-1}\left(\vec{L}(0)\right)\right\| \leq \frac{1}{C_{SM}} \left\|\vec{L}(t) - \vec{L}(0)\right\| \\
&\leq \frac{T}{C_{SM}} \left(\sigma \max_{n=1,\dots,N_c} \{\text{meas}(\Omega_n)\} \left\|\vec{C}\right\|_{\text{L}^2(0,T)} + \left\|\vec{I}_0\right\|\right) e^{T/C_{SM}}.
\end{aligned}$$

□

The next theorem shows that the solution of the weak problem is also the solution of the strong one.

Theorem 3.12. *Let* $A(t) \in \text{H}_0^1(\Omega)$ *and* $\vec{I}(t) \in \mathbb{R}^{N_c}$, $t \in [0,T]$, *be the solution to Problem 3.2. Let* $\boldsymbol{B} := \mathbf{curl}(A\boldsymbol{e}_z)$ *and*

$$\boldsymbol{H} := \begin{cases} \nu_{\text{pm}}(\boldsymbol{B} - \boldsymbol{B}^r) & \text{in } \Omega_{\text{pm}}, \\ \nu(\cdot, |\boldsymbol{B}|)\boldsymbol{B} & \text{otherwise.} \end{cases}$$

The following equations hold true:

$$\mathbf{curl}\,\boldsymbol{H} = \frac{I_n(t)}{\operatorname{meas}(\Omega_n)}\boldsymbol{e}_z \quad \text{in } \Omega_n \times [0,T], n = 1,\dots,N_c \tag{3.14}$$

$$\mathbf{curl}\,\boldsymbol{H} = \mathbf{0} \quad \text{in } (\Omega_0 \cup \Omega_{\mathrm{pm}} \cup \Omega_{\mathrm{nl}}) \times [0,T], \tag{3.15}$$

$$\operatorname{div}\boldsymbol{B} = 0 \quad \text{in } \Omega \times [0,T], \tag{3.16}$$

$$\boldsymbol{B}\cdot\boldsymbol{n} = 0 \quad \text{on } \partial\Omega \times [0,T]. \tag{3.17}$$

Proof. Conditions (3.16) and (3.17) follow from the definition of $\boldsymbol{B}$ and the fact that Ω is simply connected.

Taking $W \in \mathcal{D}(\Omega) \subset \mathrm{H}_0^1(\Omega)$ for any $t \in [0,T]$,

$$\begin{aligned}\int_\Omega \nu(\cdot;|\mathbf{grad}\,A(t)|)\,\mathbf{grad}\,A(t)\cdot\mathbf{grad}\,W &= \int_\Omega \nu(\cdot;|\,\mathbf{curl}(A(t)\boldsymbol{e}_z)|)\;\mathbf{curl}(A(t)\boldsymbol{e}_z)\cdot\mathbf{curl}(W\boldsymbol{e}_z)\\ &= \int_{\Omega_n}\frac{I_n(t)}{\operatorname{meas}(\Omega_n)}W + \int_{\Omega_{\mathrm{pm}}}\nu_{\mathrm{pm}}\,(\boldsymbol{B}^r)^\perp\cdot\mathbf{grad}\,W\\ &= \int_{\Omega_n}\frac{I_n(t)}{\operatorname{meas}(\Omega_n)}W + \int_{\Omega_{\mathrm{pm}}}\nu_{\mathrm{pm}}\boldsymbol{B}^r\cdot\mathbf{curl}(W\boldsymbol{e}_z).\end{aligned}$$

Therefore, from the definition of $\boldsymbol{H}$:

$$\int_\Omega \boldsymbol{H}\cdot\mathbf{curl}(W\boldsymbol{e}_z) = \int_{\Omega_n}\frac{I_n(t)}{\operatorname{meas}(\Omega_n)}W$$

for every $t \in [0,T]$. Then, since $(I_n(t)/\operatorname{meas}(\Omega_n))\chi_{\Omega_n} \in \mathrm{L}^2(\Omega)$, $n = 1,\dots,N_c$, $t \in [0,T]$, $\boldsymbol{H} \in \boldsymbol{H}(\mathbf{curl},\Omega)$, and (3.14), (3.15) hold in $\mathrm{L}^2(\Omega_n)^3$, $n = 1,\dots,N_c$, and $\mathrm{L}^2(\Omega_0\cup\Omega_{\mathrm{pm}}\cup\Omega_{\mathrm{nl}})^3$, respectively, for every $t \in [0,T]$. □

3.3 Discretization of the ODE Operator

In this section we define an operator $\vec{\mathcal{F}}_h$ that will be constructed as an approximation of the ODE operator $\vec{\mathcal{F}}$. This new operator $\vec{\mathcal{F}}_h$ will be used in the next sections to introduce a numerical scheme.

To this end, in the sequel we will assume that Ω along with all its subdomains Ω_0, Ω_{c}, Ω_{pm} and Ω_{nl}, are Lipschitz polygons and consider regular triangular meshes $\mathcal{T}_h$ of Ω such that each element $T \in \mathcal{T}_h$ is contained in the closure of one of its subdomains (h stands, as usual, for the corresponding mesh-size). Therefore, $\mathcal{T}_h(\mathcal{U}) := \left\{T \in \mathcal{T}_h :\ T \subset \overline{\mathcal{U}}\right\}$ are meshes of $\overline{\mathcal{U}}$, for any $\mathcal{U}$ subdomain of Ω.

Moreover, let $\mathcal{L}_h(\Omega)$ be the space of standard piecewise linear finite elements on $\mathcal{T}_h$:

$$\mathcal{L}_h(\Omega) := \left\{ \psi_h \in \mathrm{H}^1(\Omega) \,:\, \psi_h|_T \in \mathbb{P}_1(T) \quad \forall T \in \mathcal{T}_h \right\},$$

and $\mathcal{L}_h^0(\Omega)$ the subespace

$$\mathcal{L}_h^0(\Omega) := \left\{ \psi_h \in \mathcal{L}_h(\Omega) \,:\, \psi_h|_{\partial\Omega} = 0 \right\}.$$

Let us define the nonlinear operator $\vec{\mathcal{F}}_h : \mathbb{R}^{N_c} \longrightarrow \mathbb{R}^{N_c}$ given by

$$\vec{\mathcal{F}}_h\left(\vec{I}\right) := \left(\int_{\Omega_1} \sigma A_h, \ldots, \int_{\Omega_{N_c}} \sigma A_h \right)^{\mathrm{T}} \in \mathbb{R}^{N_c},$$

with A_h being the solution of the discrete nonlinear magnetostatic problem:

Problem 3.13. *Given $\vec{I} \in \mathbb{R}^{N_c}$ and $\boldsymbol{B}^r \in \mathrm{L}^2\left(\Omega_{pm}\right)^3$, find $A_h \in \mathcal{L}_h^0(\Omega)$ such that*

$$\int_\Omega \nu(\boldsymbol{x}; |\mathbf{grad}\, A_h|)\, \mathbf{grad}\, A_h \cdot \mathbf{grad}\, W_h = \sum_{n=1}^{N_c} \int_{\Omega_n} \frac{I_n}{\mathrm{meas}(\Omega_n)} W_h + \int_{\Omega_{\mathrm{pm}}} \nu_{\mathrm{pm}} \left(\boldsymbol{B}^r\right)^\perp \cdot \mathbf{grad}\, W_h,$$

for every $W_h \in \mathcal{L}_h^0(\Omega)$.

Remark 3.14. *Since $\mathcal{L}_h^0(\Omega) \subset \mathrm{H}_0^1(\Omega)$ for every $h > 0$, Problem 3.13 has a unique solution and then operator $\vec{\mathcal{F}}_h$ is well-defined in $\mathbb{R}^{N_c}$.*

Theorem 3.15. *Operator $\vec{\mathcal{F}}_h$ is strongly monotone and Lipschitz continuous globally in $\mathbb{R}^{N_c}$ and uniformly for $h > 0$. Then, $\vec{\mathcal{F}}_h$ is invertible and its inverse $\vec{\mathcal{F}}_h^{-1}$ is Lipschitz continuous globally in $\mathbb{R}^{N_c}$ for every $h > 0$, with Lipschitz constant independent of h.*

Proof. Let $\vec{I}^1, \vec{I}^2 \in \mathbb{R}^{N_c}$ be given and $A_h^1, A_h^2 \in \mathcal{L}_h^0(\Omega)$ be the associated solutions to Problem 3.13, respectively. Then, $\mathcal{F}_{h,n}\left(\vec{I}^j\right) = \int_{\Omega_n} \sigma A_h^j$ for $j = 1, 2$ and $n = 1, \ldots, N_c$. In order to prove the desired properties of $\vec{\mathcal{F}}_h$, the same steps as in Theorem 3.7 can be followed, replacing fields $A_1, A_2 \in \mathrm{H}_0^1(\Omega)$ with $A_h^1, A_h^2 \in \mathcal{L}_h^0(\Omega)$. Moreover, it can be shown that we can take $W_h \in \mathcal{L}_h^0(\Omega)$ such that

$$\int_{\Omega_n} \sigma W_h = I_n^1 - I_n^2,\ n = 1, \ldots, N_c, \qquad \text{and} \qquad ||W_h||_{\mathrm{H}^1(\Omega)} \leq C \left\| \vec{I}^1 - \vec{I}^2 \right\|_*,$$

with $C > 0$ independent of h. Indeed, let $\widetilde{\Omega} := \Omega \setminus \Omega_c$, $c_n := (I_n^1 - I_n^2)/\,\mathrm{meas}(\Omega_n)$, $n = 1, \ldots, N_c$, and $g_n \in \mathrm{H}^{1/2}(\partial\Omega_n)$, $g_n(\boldsymbol{x}) = c_n$ for every $\boldsymbol{x} \in \partial\Omega_n$, $n = 1, \ldots, N_c$. Then,

$$\int_{\Omega_n} \sigma c_n = I_n^1 - I_n^2.$$

Furthermore, let us consider the following weak problem:

$$\begin{cases} \text{Given } g_n \in \mathrm{H}^{1/2}(\partial\Omega_n),\ n=1,\dots,N_c, \text{ find } \widetilde{W}_h \in \mathcal{L}_h(\widetilde{\Omega}) \text{ such that } \widetilde{W}_h|_{\partial\Omega_n} = g_n, \\ n=1,\dots,N_c,\ \widetilde{W}_h|_{\partial\Omega} = 0 \text{ and} \\ \\ \displaystyle\int_{\widetilde{\Omega}} \mathbf{grad}\,\widetilde{W}_h \cdot \mathbf{grad}\, V_h = 0 \\ \\ \text{for every } V_h \in \mathcal{L}_h^0(\widetilde{\Omega}). \end{cases}$$

This problem is well-defined and

$$\left\|\widetilde{W}_h\right\|_{\mathrm{H}^1(\widetilde{\Omega})} \leq C \left\|\vec{I}^1 - \vec{I}^2\right\|_*,$$

with C independent of $\vec{I}^1, \vec{I}^2$ and $h > 0$. We can define $W_h \in \mathcal{L}_h^0(\Omega)$ by

$$W_h := \begin{cases} \widetilde{W}_h & \text{in } \widetilde{\Omega}, \\ c_n & \text{in } \Omega_n,\ n=1,\dots,N_c. \end{cases}$$

By applying Zarantonello's theorem cited above, we deduce from last theorem that $\vec{\mathcal{F}}_h$ is invertible and that its inverse $\vec{\mathcal{F}}_h^{-1}$ is Lipschitz continuous with Lipschitz constant independent of $h > 0$. □

Then, we can define the semidiscrete versions of Problems 3.5 and 3.9 in the following way:

Problem 3.16. *Given $\vec{C}(t) \in \mathcal{C}([0,T])^{N_c}$ and $\vec{I}_0 \in \mathbb{R}^{N_c}$, find $\vec{I}_h(t) \in \mathcal{C}^{0,1}([0,T])^{N_c}$ such that $\vec{I}_h(0) = \vec{I}_0$ and*

$$\frac{d}{dt}\vec{\mathcal{F}}_h\left(\vec{I}_h(t)\right) + \vec{I}_h(t) = -\left(C_1(t)\sigma\,\mathrm{meas}(\Omega_1), \dots, C_{N_c}(t)\sigma\,\mathrm{meas}(\Omega_{N_c})\right)^{\mathrm{T}} \quad \text{in } (0,T].$$

Problem 3.17. *Given $\vec{C}(t) \in \mathcal{C}([0,T])^{N_c}$ and $\vec{I}_0 \in \mathbb{R}^{N_c}$, find $\vec{I}_h(t) \in \mathcal{C}^{0,1}([0,T])^{N_c}$ such that $\vec{I}_h(0) = \vec{I}_0$ and*

$$\frac{d}{dt}\vec{L}_h(t) + \vec{\mathcal{F}}_h^{-1}\left(\vec{L}_h(t)\right) = -\left(C_1(t)\sigma\,\mathrm{meas}(\Omega_1), \dots, C_{N_c}(t)\sigma\,\mathrm{meas}(\Omega_{N_c})\right)^{\mathrm{T}} \quad \text{in } (0,T],$$

with $\vec{L}_h(t) = \vec{\mathcal{F}}_h\left(\vec{I}_h(t)\right)$ for every $t \in [0,T]$.

Theorem 3.18. *Let $A(t) \in \mathrm{H}_0^1(\Omega)$ and $A_h(t) \in \mathcal{L}_h^0(\Omega)$ be the solutions to Problems 3.3 and 3.13, respectively, with data $\vec{I}(t)$. If $\vec{I}$ and $\vec{I}_h$ are the solutions to Problems 3.5 and 3.16, then,*

$$\left\|\vec{I} - \vec{I}_h\right\|_{\mathrm{L}^2(0,T)} \leq C\left(||A - A_h||_{\mathrm{L}^2\left(0,T;\,\mathrm{L}^2\left(\cup_{n=1}^{N_c}\Omega_n\right)\right)} + T||A(0) - A_h(0)||_{\mathrm{L}^2\left(\cup_{n=1}^{N_c}\Omega_n\right)}\right). \quad (3.18)$$

Proof. Subtracting Problems 3.5 and 3.16 we obtain

$$\begin{cases} \dfrac{d}{dt}\left(\vec{\mathcal{F}}\left(\vec{I}\right) - \vec{\mathcal{F}}_h(\vec{I}_h)\right) + \left(\vec{I}(t) - \vec{I}_h(t)\right) = \vec{0}, \\ \left(\vec{I}(0) - \vec{I}_h(0)\right) = \vec{0}. \end{cases}$$

Now, integrating in time in $(0,t)$

$$\left(\vec{\mathcal{F}}\left(\vec{I}(t)\right)-\vec{\mathcal{F}}_h\left(\vec{I}_h(t)\right)\right)+\int_0^t\left(\vec{I}(s)-\vec{I}_h(s)\right)\,ds=\vec{\mathcal{F}}\left(\vec{I}_0\right)-\vec{\mathcal{F}}_h\left(\vec{I}_0\right),$$

for $t\in(0,T]$, and multiplying by $\left(\vec{I}(t)-\vec{I}_h(t)\right)$, we deduce

$$\left\langle\vec{\mathcal{F}}\left(\vec{I}(t)\right)-\vec{\mathcal{F}}_h\left(\vec{I}_h(t)\right),\vec{I}(t)-\vec{I}_h(t)\right\rangle+\left\langle\int_0^t\left(\vec{I}(s)-\vec{I}_h(s)\right)\,ds,\vec{I}(t)-\vec{I}_h(t)\right\rangle$$
$$=\left\langle\vec{\mathcal{F}}\left(\vec{I}_0\right)-\vec{\mathcal{F}}_h\left(\vec{I}_0\right),\vec{I}(t)-\vec{I}_h(t)\right\rangle,\quad(3.19)$$

for every $t\in[0,T]$. We notice that the second term in the left-hand side of (3.19) satisfies

$$\left\langle\int_0^t\left(\vec{I}(s)-\vec{I}_h(s)\right)\,ds,\vec{I}(t)-\vec{I}_h(t)\right\rangle=\frac{1}{2}\frac{d}{dt}\left\|\int_0^t\left(\vec{I}(s)-\vec{I}_h(s)\right)\,ds\right\|^2.$$

Hence, if we add and subtract the term $\vec{\mathcal{F}}_h\left(\vec{I}(t)\right)$ in the first term of the left-hand side of (3.19), we get

$$\frac{1}{2}\frac{d}{dt}\left\|\int_0^t\left(\vec{I}(s)-\vec{I}_h(s)\right)\,ds\right\|^2+\left\langle\vec{\mathcal{F}}_h\left(\vec{I}(t)\right)-\vec{\mathcal{F}}_h\left(\vec{I}_h(t)\right),\vec{I}(t)-\vec{I}_h(t)\right\rangle$$
$$=-\left\langle\vec{\mathcal{F}}\left(\vec{I}(t)\right)-\vec{\mathcal{F}}_h\left(\vec{I}(t)\right),\vec{I}(t)-\vec{I}_h(t)\right\rangle$$
$$+\left\langle\vec{\mathcal{F}}\left(\vec{I}_0\right)-\vec{\mathcal{F}}_h\left(\vec{I}_0\right),\vec{I}(t)-\vec{I}_h(t)\right\rangle,\quad(3.20)$$

for every $t\in[0,T]$.

Integrating (3.20) in $[0,T]$,

$$\frac{1}{2}\left\|\int_0^T\left(\vec{I}(t)-\vec{I}_h(t)\right)\,dt\right\|^2+\int_0^T\left\langle\vec{\mathcal{F}}_h\left(\vec{I}(t)\right)-\vec{\mathcal{F}}_h\left(\vec{I}_h(t)\right),\vec{I}(t)-\vec{I}_h(t)\right\rangle\,dt$$
$$=-\int_0^T\left\langle\vec{\mathcal{F}}\left(\vec{I}(t)\right)-\vec{\mathcal{F}}_h\left(\vec{I}(t)\right),\vec{I}(t)-\vec{I}_h(t)\right\rangle\,dt$$
$$+\int_0^T\left\langle\vec{\mathcal{F}}\left(\vec{I}_0\right)-\vec{\mathcal{F}}_h\left(\vec{I}_0\right),\vec{I}(t)-\vec{I}_h(t)\right\rangle\,dt.\quad(3.21)$$

Moreover, since $\vec{\mathcal{F}}_h$ is a strongly monotone operator globally in $\mathbb{R}^{N_c}$ (and uniformly in $[0,T]$),

$$C\int_0^T\left\|\vec{I}(t)-\vec{I}_h(t)\right\|^2\,dt\le\int_0^T\left\langle\vec{\mathcal{F}}_h\left(\vec{I}(t)\right)-\vec{\mathcal{F}}_h\left(\vec{I}_h(t)\right),\vec{I}(t)-\vec{I}_h(t)\right\rangle\,dt$$
$$\Rightarrow\left\|\vec{I}-\vec{I}_h\right\|^2_{\mathrm{L}^2(0,T)}\le C\int_0^T\left\langle\vec{\mathcal{F}}_h\left(\vec{I}(t)\right)-\vec{\mathcal{F}}_h\left(\vec{I}_h(t)\right),\vec{I}(t)-\vec{I}_h(t)\right\rangle\,dt.$$

Thus, from (3.21) we get

$$\begin{aligned}\left\|\vec{I}-\vec{I}_h\right\|^2_{\mathrm{L}^2(0,T)} &\leq C\int_0^T \left|\left\langle \vec{\mathcal{F}}\left(\vec{I}(t)\right)-\vec{\mathcal{F}}_h\left(\vec{I}(t)\right),\vec{I}(t)-\vec{I}_h(t)\right\rangle\right| dt\\ &\quad + C\int_0^T \left|\left\langle \vec{\mathcal{F}}\left(\vec{I}_0\right)-\vec{\mathcal{F}}_h\left(\vec{I}_0\right),\vec{I}(t)-\vec{I}_h(t)\right\rangle\right| dt\\ &\leq C\int_0^T \left\|\vec{\mathcal{F}}\left(\vec{I}(t)\right)-\vec{\mathcal{F}}_h\left(\vec{I}(t)\right)\right\| \left\|\vec{I}(t)-\vec{I}_h(t)\right\| dt\\ &\quad + C\int_0^T \left\|\vec{\mathcal{F}}\left(\vec{I}_0\right)-\vec{\mathcal{F}}_h\left(\vec{I}_0\right)\right\| \left\|\vec{I}(t)-\vec{I}_h(t)\right\| dt\\ &\leq C\left\|\vec{I}-\vec{I}_h\right\|_{\mathrm{L}^2(0,T)}\left(\left\|\vec{\mathcal{F}}\left(\vec{I}\right)-\vec{\mathcal{F}}_h\left(\vec{I}\right)\right\|_{\mathrm{L}^2(0,T)}+T\left\|\vec{\mathcal{F}}\left(\vec{I}_0\right)-\vec{\mathcal{F}}_h\left(\vec{I}_0\right)\right\|\right). \quad (3.22)\end{aligned}$$

Then, taking into account the definitions of $\vec{\mathcal{F}}$ and $\vec{\mathcal{F}}_h$, we have

$$\left\|\vec{\mathcal{F}}\left(\vec{I}(t)\right)-\vec{\mathcal{F}}_h\left(\vec{I}(t)\right)\right\| \leq C\left\|A(t)-A_h(t)\right\|_{\mathrm{L}^2\left(\cup_{n=1}^{N_c}\Omega_n\right)}, \quad (3.23)$$

with $C>0$ independent of $h>0$, and finally,

$$\left\|\vec{I}-\vec{I}_h\right\|_{\mathrm{L}^2(0,T)} \leq C\left(\left\|A-A_h\right\|_{\mathrm{L}^2\left(0,T;\,\mathrm{L}^2\left(\cup_{n=1}^{N_c}\Omega_n\right)\right)}+T\left\|A(0)-A_h(0)\right\|_{\mathrm{L}^2\left(\cup_{n=1}^{N_c}\Omega_n\right)}\right).$$

□

Remark 3.19. *We notice that the error estimate obtained in Theorem 3.18 means that the convergence order of the solution to Problem 3.16 towards to the one of Problem 3.5 in* $\mathrm{L}^2(0,T)$ *is going to be determined by the spatial error made when approximating Problem 3.3 by Problem 3.13 in the* $\mathrm{L}^2\left(\cup_{n=1}^{N_c}\Omega_n\right)$*-norm. In Section 3.6, we will see that the numerical results seem to suggest that the optimal convergence order is* $O(h^2)$*. However, to the authors' knowledge, this can only be theoretically obtained under quite strong regularity assumptions (see [1, 111]). Therefore, we have chosen to work with a more reasonable set of hypotheses, leading to a sub-optimal error estimate for* $\left\|\vec{I}-\vec{I}_h\right\|_{\mathrm{L}^2(0,T)}$*. In particular, we will bound the expressions in (3.23) with the* $\mathrm{H}^1\left(\cup_{n=1}^{N_c}\Omega_n\right)$*-norm of the difference between the continuous and the discrete magnetic vector potentials.*

Consequently, we are going to give a set of sufficient conditions that will allow us to express the error estimate in terms of the problem data.

Assumptions 3.20. *Let* $A(t)\in \mathrm{H}^1_0(\Omega)$ *and* $A_h(t)\in\mathcal{L}^0_h(\Omega)$ *be the solutions to Problems 3.3 and 3.13, respectively, with data* $\vec{I}(t)$*. Let us assume*

(H1) the boundaries of Ω_n*,* $n=1,\ldots,N_c$*, are piecewise of class* $\mathcal{C}^3$*,*

(H2) the interfaces between all subdomains of Ω *are Lipschitz-continuous,*

(H3) there exists $\varepsilon\in(0,1]$ *such that* $A(t)|_{\Omega_n}\in \mathrm{H}^{1+\varepsilon}(\Omega_n)$*,* $n=1,\ldots,N_c$*, and*

$$||A(t)||_{\mathrm{H}^{1+\varepsilon}(\Omega_n)} \leq C\left(\left\|\vec{I}(t)\right\|+||\boldsymbol{B}^r||_{\mathrm{L}^2(\Omega_{pm})^3}\right),$$

where $C>0$ *depends only on* Ω_n*,* $n=1,\ldots,N_c$*.*

Corollary 3.21. *Under Assumptions (H1) to (H3), if $\vec{I}$ and $\vec{I}_h$ are the solutions to Problems 3.5 and 3.16, then,*

$$\left\|\vec{I}-\vec{I}_h\right\|_{\mathrm{L}^2(0,T)} \leq Ch^{\varepsilon}\left(||\boldsymbol{B}^r||_{\mathrm{L}^2(\Omega_{pm})^3}+\left\|\vec{I}_0\right\|+\left\|\vec{C}\right\|_{\mathrm{L}^2(0,T)}\right), \tag{3.24}$$

with $C>0$ independent of h.

Proof. Notice that, under conditions *(H1)−(H3)*, following [59] and [115], we have

$$||A(t)-A_h(t)||_{\mathrm{H}^1(\Omega_n)} \leq Ch^{\varepsilon}||A(t)||_{\mathrm{H}^{1+\varepsilon}(\Omega_n)},$$

$n=1,\ldots,N_c$, with $A(t)\in \mathrm{H}^1_0(\Omega)$ and $A_h(t)\in\mathcal{L}^0_h(\Omega)$ being the solutions to Problems 3.3 and 3.13, with data $\vec{I}(t)$, respectively, and C a constant independent of h. Therefore, taking into account Theorem 3.11, we have the following approximation result:

$$\begin{aligned}||A(t)-A_h(t)||_{\mathrm{L}^2\left(\cup_{n=1}^{N_c}\Omega_n\right)} &\leq C||A(t)-A_h(t)||_{\mathrm{H}^1\left(\cup_{n=1}^{N_c}\Omega_n\right)}\\ &\leq Ch^{\varepsilon}\left(\left\|\vec{I}(t)\right\|+||\boldsymbol{B}^r||_{\mathrm{L}^2(\Omega_{pm})^3}\right) \leq Ch^{\varepsilon}\left(\left\|\vec{I}_0\right\|+||\boldsymbol{B}^r||_{\mathrm{L}^2(\Omega_{pm})^3}+\left\|\vec{C}\right\|_{\mathrm{L}^2(0,T)}\right),\end{aligned}$$

with $C>0$ independent of $h>0$. Thus, using Theorem 3.18, we conclude

$$\left\|\vec{I}-\vec{I}_h\right\|_{\mathrm{L}^2(0,T)} \leq Ch^{\varepsilon}\left(||\boldsymbol{B}^r||_{\mathrm{L}^2(\Omega_{pm})^3}+\left\|\vec{I}_0\right\|+\left\|\vec{C}\right\|_{\mathrm{L}^2(0,T)}\right).$$

□

3.4 Numerical Analysis of a Fully Discrete Problem

In this section we propose a numerical scheme to approximate the solution to Problem 3.5.

Let us consider a uniform partition $\{t_m := m\Delta t, m=0,\ldots,M\}$ of $[0,T]$ with step size $\Delta t := T/M$. Then, the fully-discrete version of Problem 3.5 reads as follows:

Problem 3.22. *Given $\vec{C}(t)\in\mathcal{C}([0,T])^{N_c}$ and $\vec{I}_0\in\mathbb{R}^{N_c}$, find $\vec{I}_h^m\in\mathbb{R}^{N_c}$, $m=0,\ldots,M$, such that $\vec{I}_h^0=\vec{I}_0$ and*

$$\begin{aligned}\vec{\mathcal{F}}_h\left(\vec{I}_h^m\right)+\Delta t\,\vec{I}_h^m &= \vec{\mathcal{F}}_h\left(\vec{I}_h^{m-1}\right)\\ &\quad-\Delta t\left(C_1(t_m)\sigma\,\mathrm{meas}(\Omega_1),\ldots,C_{N_c}(t_m)\sigma\,\mathrm{meas}(\Omega_{N_c})\right)^{\mathrm{T}}, m=1,\ldots,M,\end{aligned} \tag{3.25}$$

being $\vec{\mathcal{F}}_h$ the nonlinear operator defined in Section 3.3.

3.4.1 Well-Posedness of the Fully Discrete Problem

In order to prove the following theorem we will make use again of Zarantonello's theorem.

Theorem 3.23. *Problem 3.22 has a unique solution.*

Proof. Let us define the nonlinear operators $\vec{\mathcal{G}}_{h,\Delta t} : \mathbb{R}^{N_c} \longrightarrow \mathbb{R}^{N_c}$,

$$\vec{\mathcal{G}}_{h,\Delta t}\left(\vec{K}\right) := \vec{\mathcal{F}}_h\left(\vec{K}\right) + \Delta t\, \vec{K}, \quad h, \Delta t > 0.$$

Since $\vec{\mathcal{F}}_h$ is strongly monotone and Lipschitz continuous globally in $\mathbb{R}^{N_c}$ with constants C_{SM} and C_L, respectively, we deduce that $\vec{\mathcal{G}}_{h,\Delta t}$ are strongly monotone and Lipschitz continuous globally in $\mathbb{R}^{N_c}$ with constants $(C_{SM} + \Delta t)$ and $(C_L + \Delta t)$, respectively. Therefore, proceeding by induction over m, and using again the theorem by Zarantonello cited in Section 3.2, we conclude the proof. □

3.4.2 Error Estimate

For any function $\vec{f} \in \mathcal{C}([0,T])^{N_c}$, let us define $\vec{f}_{\Delta t}$ the piecewise constant approximation of $\vec{f}$

$$\vec{f}_{\Delta t}(t) := \begin{cases} \vec{f}(0) & \text{for } t = 0, \\ \vec{f}(t_m) & \text{for } t \in (t_{m-1}, t_m],\ m = 1, \ldots, M. \end{cases}$$

Remark 3.24. *If $\vec{f} \in \mathcal{C}^{0,1}([0,T])$ with Lipschitz constant $L_{\vec{f}}$, then*

$$\begin{aligned} \left\|\vec{f} - \vec{f}_{\Delta t}\right\|^2_{\mathrm{L}^2(0,T)} &= \sum_{m=1}^{M} \int_{t_{m-1}}^{t_m} \left\|\vec{f}(t) - \vec{f}(t_m)\right\|^2 dt \\ &\leq \sum_{m=1}^{M} \int_{t_{m-1}}^{t_m} L^2_{\vec{f}} (t - t_m)^2\, dt = L^2_{\vec{f}} \sum_{m=1}^{M} \left[\frac{(t-t_m)^3}{3}\right]_{t_{m-1}}^{t_m} \\ &= \frac{L^2_{\vec{f}}}{3} \sum_{m=1}^{M} \Delta t^3 = \frac{L^2_{\vec{f}}\, T}{3} \Delta t^2 \end{aligned}$$

We have the following result:

Theorem 3.25. *Under Assumptions (H1) to (H3), if $\vec{C}(t) \in \mathcal{C}^{0,1}([0,T])^{N_c}$ then the solutions to Problems 3.5 and 3.22, $\vec{I}$ and $\{\vec{I}_h^m\}_{m=0}^M$, respectively, satisfy*

$$\begin{aligned} &\left(\sum_{m=1}^{M} \Delta t \left\|\vec{I}(t_m) - \vec{I}_h^m\right\|^2\right)^{1/2} \\ &\qquad \leq C\left(\Delta t\, (L_{\vec{I}} + L_{\vec{C}}) + h^{\varepsilon}\left(\left\|\vec{I}_0\right\|^2 + ||\boldsymbol{B}^r||^2_{\mathrm{L}^2(\Omega_{pm})^3} + \left\|\vec{C}\right\|^2_{\mathrm{L}^2(0,T)}\right)\right), \end{aligned} \tag{3.26}$$

with $L_{\vec{I}}$ and $L_{\vec{C}}$ the Lipschitz constants of mappings $\vec{I}$ and $\vec{C}$, respectively, and $C > 0$ is independent of Δt.

Proof. Let us denote $\vec{g} : [0,T] \longrightarrow \mathbb{R}^{N_c}$, the mapping

$$\vec{g}(t) := -\left(C_1(t)\sigma \operatorname{meas}(\Omega_1), \ldots, C_{N_c}(t)\sigma \operatorname{meas}(\Omega_{N_c})\right)^{\mathrm{T}}.$$

Firstly, integrating the equation appearing in Problem 3.5 between 0 and t_k, we obtain

$$\vec{\mathcal{F}}\left(\vec{I}(t_k)\right) - \vec{\mathcal{F}}\left(\vec{I}_0\right) + \int_0^{t_k} \vec{I}(t)\,dt = \int_0^{t_k} \vec{g}(t)\,dt. \tag{3.27}$$

On the other hand, summing up equations (3.25) for $m = 1, \ldots, k$,

$$\vec{\mathcal{F}}_h\left(\vec{I}_h^k\right) + \Delta t \sum_{m=1}^{k} \vec{I}_h^m = \vec{\mathcal{F}}_h\left(\vec{I}_0\right) + \Delta t \sum_{m=1}^{k} \vec{g}(t_m) = \vec{\mathcal{F}}_h\left(\vec{I}_0\right) + \int_0^{t_k} \vec{g}_{\Delta t}(t)\,dt. \tag{3.28}$$

Subtracting equations (3.27) and (3.28) and adding and subtracting the term $\int_0^{t_k} \vec{I}_{\Delta t}(t)\,dt$,

$$\begin{aligned}\vec{\mathcal{F}}\left(\vec{I}(t_k)\right) - \vec{\mathcal{F}}_h\left(\vec{I}_h^k\right) + \Delta t \sum_{m=1}^{k} \left(\vec{I}(t_m) - \vec{I}_h^m\right) \\ = \vec{\mathcal{F}}\left(\vec{I}_0\right) - \vec{\mathcal{F}}_h\left(\vec{I}_0\right) + \int_0^{t_k} \vec{I}_{\Delta t}(t) - \vec{I}(t)\,dt + \int_0^{t_k} \vec{g}(t) - \vec{g}_{\Delta t}(t)\,dt.\end{aligned}$$

Multiplying the above expression by $\left(\vec{I}(t_k) - \vec{I}_h^k\right)$ and adding and subtracting the term $\vec{\mathcal{F}}_h\left(\vec{I}(t_k)\right)$ we get

$$\begin{aligned}&\left\langle \vec{\mathcal{F}}_h\left(\vec{I}(t_k)\right) - \vec{\mathcal{F}}_h\left(\vec{I}_h^k\right), \vec{I}(t_k) - \vec{I}_h^k \right\rangle + \Delta t \left\langle \sum_{m=1}^{k} \vec{I}(t_m) - \vec{I}_h^m, \vec{I}(t_k) - \vec{I}_h^k \right\rangle \\ &\quad = -\left\langle \vec{\mathcal{F}}\left(\vec{I}(t_k)\right) - \vec{\mathcal{F}}_h\left(\vec{I}(t_k)\right), \vec{I}(t_k) - \vec{I}_h^k \right\rangle + \left\langle \vec{\mathcal{F}}\left(\vec{I}_0\right) - \vec{\mathcal{F}}_h\left(\vec{I}_0\right), \vec{I}(t_k) - \vec{I}_h^k \right\rangle \\ &\qquad + \left\langle \int_0^{t_k} \vec{I}_{\Delta t}(t) - \vec{I}(t)\,dt, \vec{I}(t_k) - \vec{I}_h^k \right\rangle + \left\langle \int_0^{t_k} \vec{g}(t) - \vec{g}_{\Delta t}(t)\,dt, \vec{I}(t_k) - \vec{I}_h^k \right\rangle.\end{aligned}$$

Now, taking the strong monotonicity of $\vec{\mathcal{F}}_h$ into account, we have

$$\begin{aligned}&C_{SM} \left\| \vec{I}(t_k) - \vec{I}_h^k \right\|^2 + \Delta t \left\langle \sum_{m=1}^{k} \vec{I}(t_m) - \vec{I}_h^m, \vec{I}(t_k) - \vec{I}_h^k \right\rangle \\ &\quad \leq -\left\langle \vec{\mathcal{F}}\left(\vec{I}(t_k)\right) - \vec{\mathcal{F}}_h\left(\vec{I}(t_k)\right), \vec{I}(t_k) - \vec{I}_h^k \right\rangle + \left\langle \vec{\mathcal{F}}\left(\vec{I}_0\right) - \vec{\mathcal{F}}_h\left(\vec{I}_0\right), \vec{I}(t_k) - \vec{I}_h^k \right\rangle \\ &\qquad + \left\langle \int_0^{t_k} \vec{I}_{\Delta t}(t) - \vec{I}(t)\,dt, \vec{I}(t_k) - \vec{I}_h^k \right\rangle + \left\langle \int_0^{t_k} \vec{g}(t) - \vec{g}_{\Delta t}(t)\,dt, \vec{I}(t_k) - \vec{I}_h^k \right\rangle.\end{aligned}$$

Multiplying the above expression by Δt and summing up for $k = 1, \ldots, \ell$, we get

$$\begin{aligned}&C_{SM} \sum_{k=1}^{\ell} \Delta t \left\| \vec{I}(t_k) - \vec{I}_h^k \right\|^2 + (\Delta t)^2 \sum_{k=1}^{\ell} \left\langle \sum_{m=1}^{k} \left(\vec{I}(t_m) - \vec{I}_h^m\right), \vec{I}(t_k) - \vec{I}_h^k \right\rangle \\ &\leq -\Delta t \sum_{k=1}^{\ell} \left\langle \vec{\mathcal{F}}\left(\vec{I}(t_k)\right) - \vec{\mathcal{F}}_h\left(\vec{I}(t_k)\right), \vec{I}(t_k) - \vec{I}_h^k \right\rangle + \Delta t \sum_{k=1}^{\ell} \left\langle \vec{\mathcal{F}}\left(\vec{I}_0\right) - \vec{\mathcal{F}}_h\left(\vec{I}_0\right), \vec{I}(t_k) - \vec{I}_h^k \right\rangle \\ &\quad + \Delta t \sum_{k=1}^{\ell} \left\langle \int_0^{t_k} \vec{I}_{\Delta t}(t) - \vec{I}(t)\,dt, \vec{I}(t_k) - \vec{I}_h^k \right\rangle + \Delta t \sum_{k=1}^{\ell} \left\langle \int_0^{t_k} \vec{g}(t) - \vec{g}_{\Delta t}(t)\,dt, \vec{I}(t_k) - \vec{I}_h^k \right\rangle\end{aligned} \tag{3.29}$$

for every $\ell = 1, \dots, M$.

Now, we are going to discuss every term in (3.29) separately. Firstly, concerning the second term on the left-hand side, taking into account that $2\langle u, u-v\rangle = ||u||^2 + ||u-v||^2 - ||v||^2$ and writing

$$\vec{I}(t_k) - \vec{I}_h^k = \sum_{m=1}^{k} \left(\vec{I}(t_m) - \vec{I}_h^m\right) - \sum_{m=1}^{k-1} \left(\vec{I}(t_m) - \vec{I}_h^m\right),$$

we get

$$\begin{aligned}
&(\Delta t)^2 \sum_{k=1}^{\ell} \left\langle \sum_{m=1}^{k} \left(\vec{I}(t_m) - \vec{I}_h^m\right), \vec{I}(t_k) - \vec{I}_h^k \right\rangle \\
&= \frac{1}{2} \sum_{k=1}^{\ell} \left\{ \left\| \Delta t \sum_{m=1}^{k} \left(\vec{I}(t_m) - \vec{I}_h^m\right) \right\|^2 + \left\| \Delta t \left(\vec{I}(t_k) - \vec{I}_h^k\right) \right\|^2 - \left\| \Delta t \sum_{m=1}^{k-1} \left(\vec{I}(t_m) - \vec{I}_h^m\right) \right\|^2 \right\} \\
&= \frac{1}{2} \left\{ \sum_{k=1}^{\ell} \left\| \Delta t \left(\vec{I}(t_k) - \vec{I}_h^k\right) \right\|^2 + \left\| \Delta t \sum_{k=1}^{\ell} \left(\vec{I}(t_k) - \vec{I}_h^k\right) \right\|^2 \right\} \\
&\geq \frac{1}{2} \left\| \Delta t \sum_{k=1}^{\ell} \left(\vec{I}(t_k) - \vec{I}_h^k\right) \right\|^2 . \qquad (3.30)
\end{aligned}$$

On the other hand, concerning the first term on the right-hand side of (3.29), and using Young's inequality for each $k = 1, \dots, \ell$, we obtain

$$\begin{aligned}
&\Delta t \sum_{k=1}^{\ell} \left\langle \vec{\mathcal{F}}\left(\vec{I}(t_k)\right) - \vec{\mathcal{F}}_h\left(\vec{I}(t_k)\right), \vec{I}(t_k) - \vec{I}_h^k \right\rangle \\
&\qquad \leq \sum_{k=1}^{\ell} \Delta t \, \frac{\varepsilon_1}{2} \left\| \vec{\mathcal{F}}\left(\vec{I}(t_k)\right) - \vec{\mathcal{F}}_h\left(\vec{I}(t_k)\right) \right\|^2 + \sum_{k=1}^{\ell} \Delta t \, \frac{1}{2\varepsilon_1} \left\| \vec{I}(t_k) - \vec{I}_h^k \right\|^2 ,
\end{aligned}$$

for every $\varepsilon_1 > 0$. Following the same argument as in Section 3.3, from Assumptions $(H1)$ to $(H3)$ we conclude that

$$\begin{aligned}
&\Delta t \sum_{k=1}^{\ell} \left\langle \vec{\mathcal{F}}\left(\vec{I}(t_k)\right) - \vec{\mathcal{F}}_h\left(\vec{I}(t_k)\right), \vec{I}(t_k) - \vec{I}_h^k \right\rangle \\
&\qquad \leq C h^{2\varepsilon} \ell \Delta t \, \frac{\varepsilon_1}{2} \left(\left\| \vec{I}_0 \right\|^2 + ||\boldsymbol{B}^r||^2_{\mathrm{L}^2(\Omega_{pm})^3} + \|\vec{g}\,\|^2_{\mathrm{L}^2(0,T)} \right) \\
&\qquad\qquad + \frac{1}{2\varepsilon_1} \sum_{k=1}^{\ell} \Delta t \left\| \vec{I}(t_k) - \vec{I}_h^k \right\|^2 \\
&\qquad \leq C h^{2\varepsilon} T \frac{\varepsilon_1}{2} \left(\left\| \vec{I}_0 \right\|^2 + ||\boldsymbol{B}^r||^2_{\mathrm{L}^2(\Omega_{pm})^3} + \|\vec{g}\,\|^2_{\mathrm{L}^2(0,T)} \right) \\
&\qquad\qquad + \frac{1}{2\varepsilon_1} \sum_{k=1}^{\ell} \Delta t \left\| \vec{I}(t_k) - \vec{I}_h^k \right\|^2 . \qquad (3.31)
\end{aligned}$$

Similarly, for the second term on the right-hand side of (3.29) we have

$$\begin{aligned}
&\Delta t \sum_{k=1}^{\ell} \left\langle \vec{\mathcal{F}}\left(\vec{I}_0\right) - \vec{\mathcal{F}}_h\left(\vec{I}_0\right), \vec{I}(t_k) - \vec{I}_h^k \right\rangle \\
&\qquad = \left\langle \vec{\mathcal{F}}\left(\vec{I}_0\right) - \vec{\mathcal{F}}_h\left(\vec{I}_0\right), \Delta t \sum_{k=1}^{\ell} \left(\vec{I}(t_k) - \vec{I}_h^k\right) \right\rangle \\
&\qquad \leq \frac{\varepsilon_2}{2} \left\| \vec{\mathcal{F}}\left(\vec{I}_0\right) - \vec{\mathcal{F}}_h\left(\vec{I}_0\right) \right\|^2 + \frac{1}{2\varepsilon_2} \left\| \Delta t \sum_{k=1}^{\ell} \left(\vec{I}(t_k) - \vec{I}_h^k\right) \right\|^2 \\
&\qquad \leq C h^{2\varepsilon} \frac{\varepsilon_2}{2} \left(\left\| \vec{I}_0 \right\|^2 + ||\boldsymbol{B}^r||^2_{\mathrm{L}^2(\Omega_{pm})^3} \right) + \frac{1}{2\varepsilon_2} \left\| \Delta t \sum_{k=1}^{\ell} \left(\vec{I}(t_k) - \vec{I}_h^k\right) \right\|^2 . \quad (3.32)
\end{aligned}$$

Moreover, regarding the third term on the right-hand side of (3.29), writing again

$$\vec{I}(t_k) - \vec{I}_h^k = \sum_{m=1}^{k} \left(\vec{I}(t_m) - \vec{I}_h^m\right) - \sum_{m=1}^{k-1} \left(\vec{I}(t_m) - \vec{I}_h^m\right),$$

and using summation by parts, we obtain

$$\begin{aligned}
&\Delta t \sum_{k=1}^{\ell} \left\langle \int_0^{t_k} \vec{I}_{\Delta t}(t) - \vec{I}(t)\, dt, \vec{I}(t_k) - \vec{I}_h^k \right\rangle \\
&\qquad = \left\langle \int_0^{t_\ell} \vec{I}_{\Delta t}(t) - \vec{I}(t)\, dt, \Delta t \sum_{k=1}^{\ell} \left(\vec{I}(t_k) - \vec{I}_h^k\right) \right\rangle \\
&\qquad\quad - \sum_{k=1}^{\ell-1} \left\langle \int_{t_k}^{t_{k+1}} \vec{I}_{\Delta t}(t) - \vec{I}(t)\, dt, \Delta t \sum_{m=1}^{k} \left(\vec{I}(t_m) - \vec{I}_h^m\right) \right\rangle . \quad (3.33)
\end{aligned}$$

Using Young's inequality in the first term of (3.33), we deduce

$$\begin{aligned}
&\left\langle \int_0^{t_\ell} \vec{I}_{\Delta t}(t) - \vec{I}(t)\, dt, \Delta t \sum_{k=1}^{\ell} \left(\vec{I}(t_k) - \vec{I}_h^k\right) \right\rangle \\
&\qquad \leq \frac{\varepsilon_3}{2} \left\| \int_0^{t_\ell} \vec{I}_{\Delta t}(t) - \vec{I}(t)\, dt \right\|^2 + \frac{1}{2\varepsilon_3} \left\| \Delta t \sum_{k=1}^{\ell} \left(\vec{I}(t_k) - \vec{I}_h^k\right) \right\|^2 \\
&\qquad \leq \frac{\varepsilon_3 t_\ell}{2} \left\| \vec{I}_{\Delta t} - \vec{I} \right\|^2_{\mathrm{L}^2(0,t_\ell)} + \frac{1}{2\varepsilon_3} \left\| \Delta t \sum_{k=1}^{\ell} \left(\vec{I}(t_k) - \vec{I}_h^k\right) \right\|^2 \\
&\qquad \leq \frac{\varepsilon_3 T}{2} \left\| \vec{I}_{\Delta t} - \vec{I} \right\|^2_{\mathrm{L}^2(0,T)} + \frac{1}{2\varepsilon_3} \left\| \Delta t \sum_{k=1}^{\ell} \left(\vec{I}(t_k) - \vec{I}_h^k\right) \right\|^2 ,
\end{aligned}$$

for every $\varepsilon_3 > 0$. Concerning the second term in (3.33), we have

$$\begin{aligned}
&\sum_{k=1}^{\ell-1} \left\langle \int_{t_k}^{t_{k+1}} \vec{I}_{\Delta t}(t) - \vec{I}(t)\, dt, \Delta t \sum_{m=1}^{k} \left(\vec{I}(t_m) - \vec{I}_h^m\right) \right\rangle \\
&\qquad \leq \sum_{k=1}^{\ell-1} \left\| \int_{t_k}^{t_{k+1}} \vec{I}_{\Delta t}(t) - \vec{I}(t)\, dt \right\| \left\| \Delta t \sum_{m=1}^{k} \left(\vec{I}(t_m) - \vec{I}_h^m\right) \right\| \\
&\qquad \leq \sum_{k=1}^{\ell-1} \left\| \vec{I}_{\Delta t} - \vec{I} \right\|_{\mathrm{L}^2(t_k,t_{k+1})} \sqrt{\Delta t} \left\| \Delta t \sum_{m=1}^{k} \left(\vec{I}(t_m) - \vec{I}_h^m\right) \right\| \\
&\qquad \leq \sum_{k=1}^{\ell-1} \frac{\beta_1}{2} \left\| \vec{I}_{\Delta t} - \vec{I} \right\|^2_{\mathrm{L}^2(t_k,t_{k+1})} + \Delta t \sum_{k=1}^{\ell-1} \frac{1}{2\beta_1} \left\| \Delta t \sum_{m=1}^{k} \left(\vec{I}(t_m) - \vec{I}_h^m\right) \right\|^2 \\
&\qquad \leq \frac{\beta_1}{2} \left\| \vec{I}_{\Delta t} - \vec{I} \right\|^2_{\mathrm{L}^2(0,T)} + \Delta t \sum_{k=1}^{\ell-1} \frac{1}{2\beta_1} \left\| \Delta t \sum_{m=1}^{k} \left(\vec{I}(t_m) - \vec{I}_h^m\right) \right\|^2, \quad (3.34)
\end{aligned}$$

for every $\beta_1 > 0$.

Finally, we can bound analogously the fourth term on the right-hand side of (3.29), obtaining

$$\begin{aligned}
&\Delta t \sum_{k=1}^{\ell} \left\langle \int_0^{t_k} \vec{g}(t) - \vec{g}_{\Delta t}(t)\, dt, \vec{I}(t_k) - \vec{I}_h^k \right\rangle \\
&\qquad \leq \left(\frac{\varepsilon_4 T + \beta_2}{2}\right) \|\vec{g} - \vec{g}_{\Delta t}\|^2_{\mathrm{L}^2(0,T)} + \frac{1}{2\varepsilon_4} \left\| \Delta t \sum_{k=1}^{\ell} \left(\vec{I}(t_k) - \vec{I}_h^k\right) \right\|^2 \\
&\qquad\qquad + \Delta t \sum_{k=1}^{\ell-1} \frac{1}{2\beta_2} \left\| \Delta t \sum_{m=1}^{k} \left(\vec{I}(t_m) - \vec{I}_h^m\right) \right\|^2, \quad (3.35)
\end{aligned}$$

for every $\varepsilon_4, \beta_2 > 0$.

Using (3.30)–(3.35) in (3.29) we conclude

$$\begin{aligned}
&C_{SM} \sum_{k=1}^{\ell} \Delta t \left\| \vec{I}(t_k) - \vec{I}_h^k \right\|^2 + \frac{1}{2} \left\| \Delta t \sum_{k=1}^{\ell} \left(\vec{I}(t_k) - \vec{I}_h^k\right) \right\|^2 \\
&\qquad \leq \frac{\varepsilon_3 T + \beta_1}{2} \left\| \vec{I}_{\Delta t} - \vec{I} \right\|^2_{\mathrm{L}^2(0,T)} + \frac{\varepsilon_4 T + \alpha_2}{2} \|\vec{g} - \vec{g}_{\Delta t}\|^2_{\mathrm{L}^2(0,T)} \\
&\qquad\qquad + \left(\frac{1}{2\varepsilon_2} + \frac{1}{2\varepsilon_3} + \frac{1}{2\varepsilon_4}\right) \left\| \Delta t \sum_{k=1}^{\ell} \left(\vec{I}(t_k) - \vec{I}_h^k\right) \right\|^2 \\
&\quad + \frac{1}{2\varepsilon_1} \sum_{k=1}^{\ell} \Delta t \left\| \vec{I}(t_k) - \vec{I}_h^k \right\|^2 + h^{2\varepsilon} \left(\frac{C_1\varepsilon_2 + C_2 T \varepsilon_1}{2}\right) \left(\left\| \vec{I}_0 \right\|^2 + ||\boldsymbol{B}^r||^2_{\mathrm{L}^2(\Omega_{pm})^3} \right) \\
&\qquad + h^{2\varepsilon} \frac{C_2 \varepsilon_1 T}{2} \|\vec{g}\|^2_{\mathrm{L}^2(0,T)} + \Delta t \left(\frac{1}{2\beta_1} + \frac{1}{2\beta_2}\right) \sum_{k=1}^{\ell-1} \left\| \Delta t \sum_{m=1}^{k} \left(\vec{I}(t_m) - \vec{I}_h^m\right) \right\|^2,
\end{aligned}$$

for every $\varepsilon_1, \varepsilon_2, \varepsilon_3, \varepsilon_4, \beta_1, \beta_2 > 0$ and $\ell = 1, \ldots, M$, and then,

$$\begin{aligned}\left(C_{SM} - \frac{1}{2\varepsilon_1}\right) \sum_{k=1}^{\ell} \Delta t \left\|\vec{I}(t_k) - \vec{I}_h^k\right\|^2 \\ + \left(\frac{1}{2} - \frac{1}{2\varepsilon_2} - \frac{1}{2\varepsilon_3} - \frac{1}{2\varepsilon_4}\right) \left\|\Delta t \sum_{k=1}^{\ell} \left(\vec{I}(t_k) - \vec{I}_h^k\right)\right\|^2 \\ \leq \frac{\varepsilon_3 T + \beta_1}{2} \left\|\vec{I}_{\Delta t} - \vec{I}\right\|^2_{\mathrm{L}^2(0,T)} + \frac{\varepsilon_4 T + \alpha_2}{2} \|\vec{g} - \vec{g}_{\Delta t}\|^2_{\mathrm{L}^2(0,T)} \\ + h^{2\varepsilon} \left(\frac{C_1\varepsilon_2 + C_2 T \varepsilon_1}{2}\right) \left(\left\|\vec{I}_0\right\|^2 + ||\boldsymbol{B}^r||^2_{\mathrm{L}^2(\Omega_{pm})^3}\right) \\ + h^{2\varepsilon} \frac{C_2 \varepsilon_1 T}{2} \|\vec{g}\|^2_{\mathrm{L}^2(0,T)} + \Delta t \left(\frac{1}{2\beta_1} + \frac{1}{2\beta_2}\right) \sum_{k=1}^{\ell-1} \left\|\Delta t \sum_{m=1}^{k} \left(\vec{I}(t_m) - \vec{I}_h^m\right)\right\|^2.\end{aligned}$$

Thus, taking $\varepsilon_1 > 1/2C_{SM} > 0$, $\varepsilon_2 = \varepsilon_3 = \varepsilon_4 = 3\varepsilon_1/((1 - C_{SM})\varepsilon_1 + 1) > 0$ and $\beta_1 = \beta_2 = 2\varepsilon_1/(2C_{SM}\varepsilon_1 - 1) > 0$,

$$\begin{aligned}\sum_{k=1}^{\ell} \Delta t \left\|\left(\vec{I}(t_k) - \vec{I}_h^k\right)\right\|^2 + \left\|\Delta t \sum_{k=1}^{\ell} \vec{I}(t_k) - \vec{I}_h^k\right\|^2 \leq C \left(\left\|\vec{I}_{\Delta t} - \vec{I}\right\|^2_{\mathrm{L}^2(0,T)} + \|\vec{g} - \vec{g}_{\Delta t}\|^2_{\mathrm{L}^2(0,T)}\right) \\ + Ch^{2\varepsilon} \left(\left\|\vec{I}_0\right\|^2 + ||\boldsymbol{B}^r||^2_{\mathrm{L}^2(\Omega_{pm})^3} + \|\vec{g}\|^2_{\mathrm{L}^2(0,T)}\right) + \Delta t \sum_{k=1}^{\ell-1} \left\|\Delta t \sum_{m=1}^{k} \left(\vec{I}(t_k) - \vec{I}_h^k\right)\right\|^2.\end{aligned}$$

Now, using the discrete Gronwall inequality (see Lemma 1.4.2 in [85]), we conclude

$$\begin{aligned}\sum_{k=1}^{M} \Delta t \left\|\vec{I}(t_k) - \vec{I}_h^k\right\|^2 \leq \sum_{k=1}^{M} \Delta t \left\|\vec{I}(t_k) - \vec{I}_h^k\right\|^2 + \left\|\Delta t \sum_{k=1}^{M} \left(\vec{I}(t_k) - \vec{I}_h^k\right)\right\|^2 \\ \leq C \left(\left\|\vec{I}_{\Delta t} - \vec{I}\right\|^2_{\mathrm{L}^2(0,T)} + \|\vec{g} - \vec{g}_{\Delta t}\|^2_{\mathrm{L}^2(0,T)} \right. \\ \left. + h^{2\varepsilon} \left(\left\|\vec{I}_0\right\|^2 + ||\boldsymbol{B}^r||^2_{\mathrm{L}^2(\Omega_{pm})^3} + \|\vec{g}\|^2_{\mathrm{L}^2(0,T)}\right)\right).\end{aligned}$$

□

3.5 An Equivalence Result between Two Fully Discrete Schemes

In the last section we have analysed the numerical convergence for Problem 3.22. However, following [16], we have implemented a different numerical scheme for the same problem. In this section, we will prove the equivalence between the two discretizations.

Thus, let us consider the following discrete problem, which is the one used for the implementation:

Problem 3.26. *Given $\vec{C}(t) \in \mathcal{C}([0,T])^{N_c}$, $\vec{I}_0 \in \mathbb{R}^{N_c}$ and $\boldsymbol{B}^r \in \mathrm{L}^2(\Omega_{pm})^3$, find $A_h^m \in \mathcal{L}_h^0(\Omega)$, $m = 1, \ldots, M$, such that*

$$\int_\Omega \nu(\cdot; |\mathbf{grad}\, A_h^m|)\, \mathbf{grad}\, A_h^m \cdot \mathbf{grad}\, W_h + \frac{1}{\Delta t} \sum_{n=1}^{N_c} \int_{\Omega_n} \left(\int_{\Omega_n} \sigma A_h^m \right) \frac{1}{\mathrm{meas}(\Omega_n)} W_h$$
$$= \frac{1}{\Delta t} \sum_{n=1}^{N_c} \int_{\Omega_n} \left(\int_{\Omega_n} \sigma A_h^{m-1} \right) \frac{1}{\mathrm{meas}(\Omega_n)} W_h - \sum_{n=1}^{N_c} \int_{\Omega_n} \sigma C_n(t_m) W_h$$
$$+ \int_{\Omega_{\mathrm{pm}}} \nu_{\mathrm{pm}} (\boldsymbol{B}^r)^\perp \cdot \mathbf{grad}\, W_h,$$

for every $W_h \in \mathcal{L}_h^0(\Omega)$, with $A_h^0 \in \mathcal{L}_h^0(\Omega)$ the solution to the weak formulation

$$\int_\Omega \nu(\cdot; |\mathbf{grad}\, A_h^0|)\, \mathbf{grad}\, A_h^0 \cdot \mathbf{grad}\, W_h$$
$$= \sum_{n=1}^{N_c} \int_{\Omega_n} \frac{I_{0,n}}{\mathrm{meas}(\Omega_n)} W_h + \int_{\Omega_{\mathrm{pm}}} \nu_{\mathrm{pm}} (\boldsymbol{B}^r)^\perp \cdot \mathbf{grad}\, W_h,$$

for every $W_h \in \mathcal{L}_h^0(\Omega)$.

Theorem 3.27. *Let $\vec{I}_h^m \in \mathbb{R}^{N_c}$, $m = 0, \ldots, M$, be the solution to Problem 3.22 and $A_h^m \in \mathcal{L}_h^0(\Omega)$, $m = 1, \ldots, M$, defined as the solution to Problem 3.13. Then, $A_h^m \in \mathcal{L}_h^0(\Omega)$, $m = 1, \ldots, M$, are a solution to Problem 3.26.*

Proof. Since Problem 3.13 has a unique solution, we deduce that

$$\mathcal{F}_{h,n}\left(\vec{I}_h^m\right) = \int_{\Omega_n} \sigma A_h^m, \quad n = 1, \ldots, N_c,\ m = 1, \ldots, M.$$

Furthermore, since $\vec{I}_h^m$, $m = 0, \ldots, M$, is the solution to Problem 3.22,

$$I_{h,n}^m = -\frac{1}{\Delta t} \mathcal{F}_{h,n}\left(\vec{I}_h^m\right) + \frac{1}{\Delta t} \mathcal{F}_{h,n}\left(\vec{I}_h^{m-1}\right) - C_n(t_m)\sigma\, \mathrm{meas}(\Omega_n)$$
$$= -\frac{1}{\Delta t} \int_{\Omega_n} \sigma A_h^m + \frac{1}{\Delta t} \int_{\Omega_n} \sigma A_h^{m-1} - C_n(t_m)\sigma\, \mathrm{meas}(\Omega_n)$$

for $n = 1, \ldots, N_c$, $m = 1, \ldots, M$. Replacing these expressions in Problem 3.13 we conclude

$$\int_\Omega \nu(\cdot; |\mathbf{grad}\, A_h^m|)\, \mathbf{grad}\, A_h^m \cdot \mathbf{grad}\, W_h + \frac{1}{\Delta t} \sum_{n=1}^{N_c} \int_{\Omega_n} \left(\int_{\Omega_n} \sigma A_h^m \right) \frac{1}{\mathrm{meas}(\Omega_n)} W_h$$
$$= \frac{1}{\Delta t} \sum_{n=1}^{N_c} \int_{\Omega_n} \left(\int_{\Omega_n} \sigma A_h^{m-1} \right) \frac{1}{\mathrm{meas}(\Omega_n)} W_h - \sum_{n=1}^{N_c} \int_{\Omega_n} \sigma C_n(t_m) W_h$$
$$+ \int_{\Omega_{\mathrm{pm}}} \nu_{\mathrm{pm}} (\boldsymbol{B}^r)^\perp \cdot \mathbf{grad}\, W_h,$$

for every $W_h \in \mathcal{L}_h^0(\Omega)$, with $A_h^0 \in \mathcal{L}_h^0(\Omega)$ the solution to

$$\int_\Omega \nu(\cdot; |\mathbf{grad}\, A_h^0|)\, \mathbf{grad}\, A_h^0 \cdot \mathbf{grad}\, W_h$$
$$= \sum_{n=1}^{N_c} \int_{\Omega_n} \frac{I_{0,n}}{\mathrm{meas}(\Omega_n)} W_h + \int_{\Omega_{\mathrm{pm}}} \nu_{\mathrm{pm}} (\boldsymbol{B}^r)^\perp \cdot \mathbf{grad}\, W_h,$$

for every $W_h \in \mathcal{L}_h^0(\Omega)$. Thus, $A_h^m \in \mathcal{L}_h^0(\Omega)$, $m = 1, \ldots, M$, are a solution to Problem 3.26. □

Theorem 3.28. *Let $A_h^m \in \mathcal{L}_h^0(\Omega)$, $m = 1, \dots, M$, be a solution to Problem 3.26. Let us define $\vec{I}_h^0 := \vec{I}_0$ and $\vec{I}_h^m \in \mathbb{R}^{N_c}$, $m = 1, \dots, M$, such that*

$$I_{h,n}^m := -\frac{1}{\Delta t}\int_{\Omega_n} \sigma A_h^m + \frac{1}{\Delta t}\int_{\Omega_n} \sigma A_h^{m-1} - C_n(t_m)\sigma \operatorname{meas}(\Omega_n), \quad n = 1, \dots, N_c. \tag{3.36}$$

Then, $\vec{I}_h^m$, $m = 0, \dots, M$, are the solution to Problem 3.22.

Proof. Let $\widetilde{A}_h^m \in \mathcal{L}_h^0(\Omega)$, $m = 0, \dots, M$, be the solution to Problem 3.13 with the currents defined in (3.36). In particular, $\widetilde{A}_h^0 = A_h^0$. Furthermore, taking the definitions of $\vec{I}_h^m$, $m = 0, \dots, M$, into account, fields $\widetilde{A}_h^m \in \mathcal{L}_h^0(\Omega)$, $m = 1, \dots, M$, are also the solutions to the following problems:

$$\begin{aligned}\int_\Omega \nu\left(\cdot; \left|\mathbf{grad}\, \widetilde{A}_h^m\right|\right) \mathbf{grad}\, \widetilde{A}_h^m \cdot \mathbf{grad}\, W_h + \frac{1}{\Delta t}\sum_{n=1}^{N_c}\int_{\Omega_n}\left(\int_{\Omega_n}\sigma A_h^m\right)\frac{1}{\operatorname{meas}(\Omega_n)}W_h \\ = \frac{1}{\Delta t}\sum_{n=1}^{N_c}\int_{\Omega_n}\left(\int_{\Omega_n}\sigma A_h^{m-1}\right)\frac{1}{\operatorname{meas}(\Omega_n)}W_h - \sum_{n=1}^{N_c}\int_{\Omega_n}\sigma C_n(t_m) W_h \\ + \int_{\Omega_{\mathrm{pm}}} \nu_{\mathrm{pm}}\left(\boldsymbol{B}^r\right)^\perp \cdot \mathbf{grad}\, W_h,\end{aligned}$$

for every $W_h \in \mathcal{L}_h^0(\Omega)$. By subtracting to the above equalities those in Problem 3.26, we deduce that

$$\int_\Omega \left(\nu\left(\cdot; \left|\mathbf{grad}\, \widetilde{A}_h^m\right|\right) \mathbf{grad}\, \widetilde{A}_h^m - \nu(\cdot; |\mathbf{grad}\, A_h^m|)\, \mathbf{grad}\, A_h^m\right) \cdot \mathbf{grad}\, W_h = 0$$

for every $W_h \in \mathcal{L}_h^0(\Omega)$, $m = 1, \dots, M$. Since $\mathcal{L}_h^0(\Omega) \subset \mathrm{H}_0^1(\Omega)$, we can rewrite the last equality in the following way:

$$\left\langle \mathcal{P}\left(\widetilde{A}_h^m\right) - \mathcal{P}(A_h^m), W_h \right\rangle = 0$$

for every $W_h \in \mathcal{L}_h^0(\Omega)$, $m = 1, \dots, M$. In particular, taking $W_h = \widetilde{A}_h^m - A_h^m$, and since operator $\mathcal{P}$ is strongly monotone, we obtain

$$0 = \left\langle \mathcal{P}\left(\widetilde{A}_h^m\right) - \mathcal{P}(A_h^m), \widetilde{A}_h^m - A_h^m \right\rangle \geq M \left\| \widetilde{A}_h^m - A_h^m \right\|_{\mathrm{H}^1(\Omega)}^2,$$

and therefore $\widetilde{A}_h^m = A_h^m$ for $m = 1, \dots, M$. Finally, taking the definition of $\vec{\mathcal{F}}_h$ into account, we have,

$$\mathcal{F}_{h,n}\left(\vec{I}_h^m\right) = \int_{\Omega_n} \sigma \widetilde{A}_h^m = \int_{\Omega_n} \sigma A_h^m, \quad n = 1, \dots, N_c,\ m = 1, \dots, M,$$

and then

$$\vec{\mathcal{F}}_h\left(\vec{I}_h^m\right) + \Delta t\, \vec{I}_h^m = \vec{\mathcal{F}}_h\left(\vec{I}_h^{m-1}\right) - \left(C_1(t_m)\sigma \operatorname{meas}(\Omega_1), \dots, C_{N_c}(t_m)\sigma \operatorname{meas}(\Omega_{N_c})\right)^{\mathrm{T}},$$

$m = 1, \dots, M$. Hence $\vec{I}_h^m$ are the solution to Problem 3.22. □

Remark 3.29. *In Theorems 3.27 and 3.28, we have seen that given a solution to Problem 3.26 we can compute the corresponding solution to Problem 3.22, and vice versa. Moreover, from the proof of the last theorem it can be deduced that Problem 3.26 has a unique solution. Indeed, given two solutions* $A_h^{m,1}, A_h^{m,2} \in \mathcal{L}_h^0(\Omega)$, $m = 1, \ldots, M$, *to Problem 3.26, let* $\vec{I}_h^{m,1}, \vec{I}_h^{m,2} \in \mathbb{R}^{N_c}$, $m = 0, \ldots, M$, *be the corresponding solutions to Problem 3.22, built as indicated in Theorem 3.28. Moreover, let* $\widetilde{A}_h^{m,1}, \widetilde{A}_h^{m,2} \in \mathcal{L}_h^0(\Omega)$, $m = 1, \ldots, M$, *be the solutions to Problem 3.13 corresponding to these currents. In the above proof, we have seen that* $\widetilde{A}_h^{m,1} = A_h^{m,1}$ *and* $\widetilde{A}_h^{m,2} = A_h^{m,2}$. *Therefore, since Problem 3.22 is well-posed,* $\vec{I}_h^{m,1} = \vec{I}_h^{m,2}$, $m = 1, \ldots, M$. *Consequently,* $\widetilde{A}_h^{m,1} = \widetilde{A}_h^{m,2}$, *and thus* $A_h^{m,1} = A_h^{m,2}$, $m = 1, \ldots, M$.

3.6 Numerical Results

In this section we report some numerical results obtained from a Fortran code that solves Problem 3.26. At each time step, the nonlinearity is solved by means of the fixed-point algorithm proposed in [16]. Since we have proved in the previous section that Problem 3.26 is equivalent to the original one, this code will allow us to confirm the convergence result stated in Theorem 3.25. To this end, we have solved an academic problem built from the analytical test presented in [30] for a linear case. In our setting, we consider sources given in terms of time-dependent voltage drops per unit length and replace the linear material with a permanent magnet and a nonlinear core. Moreover, we have also solved a test inspired in another one appearing in [33].

3.6.1 Academic Test

In Figure 3.1 we show the problem domain Ω that includes the cross sections of two coaxial copper wires, Ω_1 and Ω_2, separated by a permanent magnet, $\Omega_{\rm pm}$, and a ferromagnetic core, $\Omega_{\rm nl}$. We assume that the core and the magnet are non-conducting, and that the copper domains carry a uniformly distributed current density, i.e., they are stranded conductors.

Let us consider a cylindrical coordinate system (ρ, θ, z), with $\boldsymbol{e}_\rho$, $\boldsymbol{e}_\theta$ and $\boldsymbol{e}_z$ the corresponding local orthonormal basis. We assume that the z axis is orthogonal to the domain at point O. To apply the 2D transient magnetic model analysed in this paper, we suppose that the current density of the sources is uniform in each of them and orthogonal to the computational domain. More precisely,

$$\boldsymbol{J} = J_z(\rho, t)\boldsymbol{e}_z = \begin{cases} \dfrac{I(t)}{\pi R_1^2}\boldsymbol{e}_z & \text{in } (0, R_1) \times [0, T], \\ \boldsymbol{0} & \text{in } (R_1, R_3) \times [0, T], \\ -\dfrac{I(t)}{\pi(R_4^2 - R_3^2)}\boldsymbol{e}_z & \text{in } (R_3, R_4) \times [0, T]. \end{cases}$$

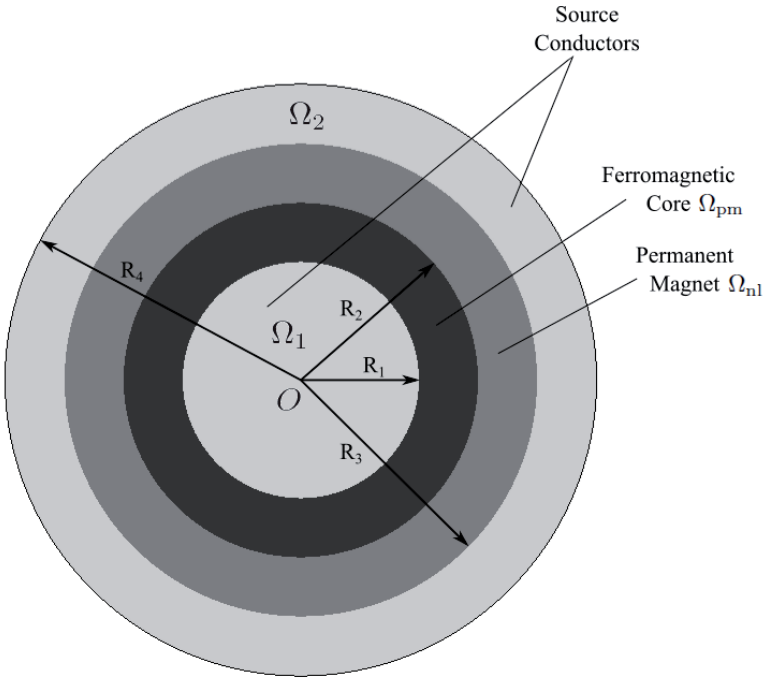

Figure 3.1: Sketch of domain Ω.

In this case, if the magnetic constitutive law in the permanent magnet is of the form $\boldsymbol{H} = \nu_{pm}\boldsymbol{B} - \nu_{pm}\boldsymbol{B}^r$ with a remanent flux $\boldsymbol{B}^r = B^r\boldsymbol{e}_\theta$, $B^r \in \mathbb{R}$, then all fields are independent of the azimuthal variable and the solution to the magnetostatic problem

$$\begin{aligned} \mathbf{curl}\,\boldsymbol{H} &= \boldsymbol{J} \quad \text{in } \Omega, \\ \operatorname{div}\boldsymbol{B} &= 0 \quad \text{in } \Omega, \\ \boldsymbol{B}\cdot\boldsymbol{n} &= 0 \quad \text{on } \partial\Omega, \end{aligned}$$

is

$$\boldsymbol{H} = H_\theta(\rho,t)\boldsymbol{e}_\theta = \begin{cases} \dfrac{\rho I(t)}{2\pi R_1^2}\boldsymbol{e}_\theta & \text{in } (0,R_1)\times[0,T], \\ \dfrac{I(t)}{2\pi\rho}\boldsymbol{e}_\theta & \text{in } (R_1,R_3)\times[0,T], \\ I(t)\left(\dfrac{1}{2\pi\rho} - \dfrac{(R_3^2-\rho^2)}{2\pi(R_4^2-R_3^2)\rho}\right)\boldsymbol{e}_\theta & \text{in } (R_3,R_4)\times[0,T]. \end{cases}$$

In the ferromagnetic core, we will consider the nonlinear constitutive magnetic law given by

$$B_\theta = \mu_0 H_\theta + \frac{2J_s}{\pi}\operatorname{atan}\left(\frac{\pi(\mu_r-1)\mu_0|H_\theta|}{2J_s}\right). \tag{3.37}$$

The positive part of the corresponding nonlinear BH curve is shown in Figure 3.2, for the values of the parameters used in the numerical simulations. We notice that, from Corollary 2.2 in [82], it can be seen that the corresponding nonlinear reluctivity function satisfies (II.1)–(II.3).

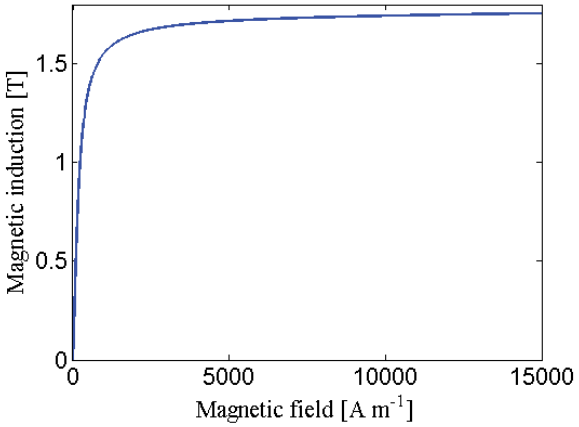

Figure 3.2: BH curve of the ferromagnetic core.

Following the same arguments as in [16], and using the notation

$$\gamma := \frac{(\mu_r - 1)\mu_0}{4J_s},$$

the expression of the solution to the magnetostatic problem (3.1)–(3.6) can be obtained integrating (3.37) in space:

In $(0, R_1) \times [0, T]$,

$$A(\rho,t) = \frac{I(t)}{2\pi\nu_0}\left\{-\frac{\rho^2}{2R_1^2} + \ln\left(\frac{R_2}{R_1}\right) + \frac{\nu_0}{\nu_{pm}}\ln\left(\frac{R_3}{R_2}\right) + \frac{R_4^2}{R_4^2 - R_3^2}\ln\left(\frac{R_4}{R_3}\right)\right\}$$
$$+ \frac{2J_s}{\pi}\left\{R_2\mathrm{atan}\left(\frac{\gamma I(t)}{R_2}\right) - R_1\mathrm{atan}\left(\frac{\gamma I(t)}{R_1}\right)\right.$$
$$\left. + \frac{\gamma I(t)}{2}\ln\left(\frac{\gamma^2 I(t)^2 + R_2^2}{\gamma^2 I(t)^2 + R_1^2}\right)\right\} + B^r(R_3 - R_2).$$

In $(R_1, R_2) \times [0, T]$,

$$A(\rho,t) = \frac{I(t)}{2\pi\nu_0}\left\{-\frac{1}{2} + \ln\left(\frac{R_2}{\rho}\right) + \frac{\nu_0}{\nu_{pm}}\ln\left(\frac{R_3}{R_2}\right) + \frac{R_4^2}{R_4^2 - R_3^2}\ln\left(\frac{R_4}{R_3}\right)\right\}$$
$$+ \frac{2J_s}{\pi}\left\{R_2\mathrm{atan}\left(\frac{\gamma I(t)}{R_2}\right) - \rho\,\mathrm{atan}\left(\frac{\gamma I(t)}{\rho}\right)\right.$$
$$\left. + \frac{\gamma I(t)}{2}\ln\left(\frac{\gamma^2 I(t)^2 + R_2^2}{\gamma^2 I(t)^2 + \rho^2}\right)\right\} + B^r(R_3 - R_2).$$

In $(R_2, R_3) \times [0, T]$,

$$A(\rho,t) = \frac{I(t)}{2\pi\nu_0}\left\{-\frac{1}{2} + \frac{\nu_0}{\nu_{pm}}\ln\left(\frac{R_3}{\rho}\right) + \frac{R_4^2}{R_4^2 - R_3^2}\ln\left(\frac{R_4}{R_3}\right)\right\} + B^r(R_3 - \rho).$$

In $(R_3, R_4) \times [0, T]$,

$$A(\rho, t) = \frac{I(t)}{2\pi\nu_0} \left\{ \frac{\rho^2 - R_4^2}{2(R_4^2 - R_3^2)} + \frac{R_4^2}{R_4^2 - R_3^2} \ln\left(\frac{R_4}{\rho}\right) \right\}.$$

We notice that, in particular, $A(R_4, t) = 0$ for every $t \in [0, T]$. This property allows us to have a conductor, Ω_2, that touches the boundary of the whole domain. Indeed, if we had considered a domain Ω_0 representing the air surrounding the device, the solution A would be identically zero there.

Finally, thanks to equation (3.7) the potential drops per unit length in Ω_1 and Ω_2 corresponding to these vector potential and currents can be analytically computed as

$$C_n(t) = -\frac{1}{\sigma \operatorname{meas}(\Omega_n)} \left(\frac{d}{dt} \int_{\Omega_n} \sigma A(t) + (-1)^n I(t) \right), \quad n = 1, 2.$$

After some straightforward computations we get

$$C_1(t) = \frac{I'(t)}{8\pi\nu_0} - \frac{I'(t)}{2\pi\nu_0} \left\{ \ln\left(\frac{R_2}{R_1}\right) + \frac{\nu_0}{\nu_{pm}} \ln\left(\frac{R_3}{R_2}\right) + \frac{R_4^2}{R_4^2 - R_3^2} \ln\left(\frac{R_4}{R_3}\right) \right\}$$
$$- \frac{J_s \gamma I'(t)}{\pi} \ln\left(\frac{\gamma^2 I(t)^2 + R_2^2}{\gamma^2 I(t)^2 + R_1^2}\right) - \frac{I(t)}{\sigma\pi R_1^2},$$

$$C_2(t) = \frac{I'(t)}{\pi(R_4^2 - R_3^2)^2 \nu_0} \left\{ \frac{R_3^2 R_4^2}{2} \ln\left(\frac{R_4}{R_3}\right) - \frac{R_4^4 - R_3^4}{8} \right\} + \frac{I(t)}{\sigma\pi(R_4^2 - R_3^2)}.$$

For the numerical computations, we have used the geometrical data $R_1 = 0.5$ m, $R_2 = 0.75$ m, $R_3 = 1$ m and $R_4 = 1.25$ m. Moreover, the copper coils electrical conductivity σ is equal to 5.7×10^7 (Ohm m)$^{-1}$ and the magnetic reluctivity of the vacuum, $\nu_0 = \frac{1}{4\pi} \times 10^7$ H^{-1} m; the material of the permanent magnet is characterised by $\nu_{pm} = 0.95\nu_0$ and the remanent flux density $\boldsymbol{B}^r = B^r \boldsymbol{e}_\theta$ by $B^r = 1.3$ T. Moreover, we have considered $\mu_0 = \frac{1}{\nu_0}$, $\mu_r = 5000$ and $J_s = 1.75$ T in the nonlinear material law of the ferromagnetic core. The considered source in the coils is the potential drop per unit length obtained for a current $I(t) = 3000 \cos(2\pi f t)$ A with a frequency $f = 50$ Hz (see Figure 3.3). Finally, the initial currents in the conductors are $I_{0,1} = 3000$ A and $I_{0,2} = -3000$ A, respectively. These initial conditions allow us to obtain the steady state current $\vec{I}(t)$ from the beginning of the simulation.

We solve the problem in a source cycle (that is, in the time interval $[0, T] = [0, 0.02]$ seconds) with several successively refined meshes and time steps, starting from the mesh shown in Figure 3.4 and a step size $\Delta t = \frac{T}{40}$. We have computed the errors by comparing the numerical solutions with the analytical one given by $\vec{I}(t) = \big(I(t), -I(t) \big)^{\mathrm{T}}$. Specifically, we have com-

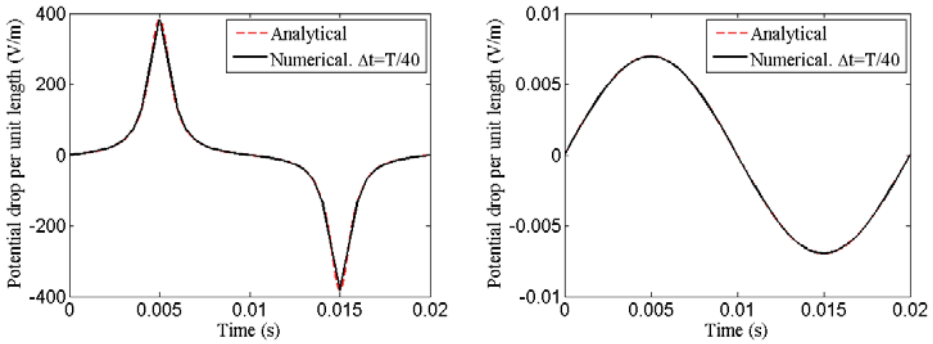

Figure 3.3: Potential drops vs. time in Ω_1 (left) and Ω_2 (right).

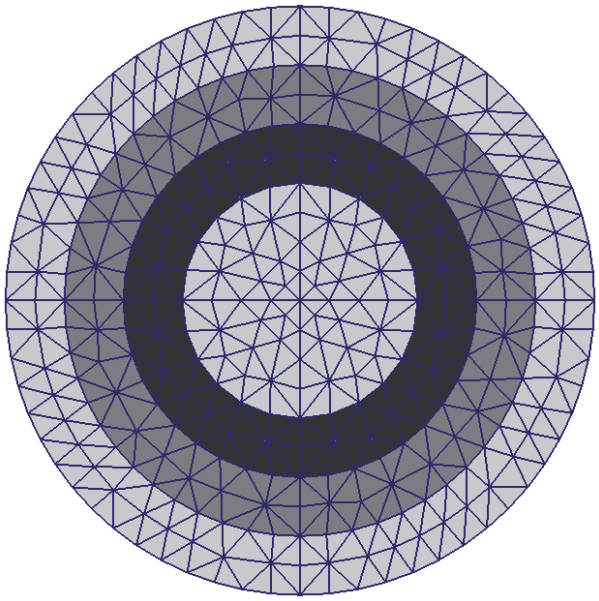

Figure 3.4: Coarsest mesh.

puted the relative error for currents $\left\{\vec{I}_h^m\right\}_{m=1}^M$ in the $\mathrm{L}^2(0,T)$-norm, that is,

$$\mathcal{E}_h^{\Delta t} := \frac{\left(\sum_{m=1}^M \Delta t \left|\vec{I}(t_m) - \vec{I}_h^m\right|^2\right)^{1/2}}{\left(\sum_{m=1}^M \Delta t \left|\vec{I}(t_m)\right|^2\right)^{1/2}}.$$

Table 3.1 shows these relative errors at different levels of discretization. We notice that, when we take a time step small enough, an $O(h^2)$ error decay can be observed (see last row in Table 3.1). On the other hand, considering a mesh size small enough allows us to show the expected convergence order in time $O(\Delta t)$ (see highlighted values in the last column in Table 3.1). We notice that the continuous solution is such that $A(t)|_{\Omega_n} \in \mathrm{H}^2(\Omega_n)$, $n = 1, 2$, for every $t \in [0, T]$. Thus, the corresponding part of the convergence order proved in Theorem 3.25 is $O(h)$, which is less than the one numerically obtained. The improvement of this order is due to the fact that the norm used in (3.23) is $||\cdot||_{\mathrm{H}^1(\cup_{n=1}^{N_c}\Omega_n)}$, while the $\mathrm{L}^2\left(\cup_{n=1}^{N_c}\Omega_n\right)$-norm could have been used. In the

	h	$\frac{h}{2}$	$\frac{h}{4}$	$\frac{h}{8}$	$\frac{h}{16}$
Δt	0.1138	0.0806	0.0774	0.0772	0.0771
$\frac{\Delta t}{2}$	0.0895	0.0438	0.0390	0.0388	0.0388
$\frac{\Delta t}{4}$	0.0831	0.0279	0.0199	0.0195	0.0195
$\frac{\Delta t}{8}$	0.0815	0.0222	0.0105	0.0098	0.0098
$\frac{\Delta t}{16}$	0.0812	0.0206	0.0062	0.0050	0.0049
$\frac{\Delta t}{32}$	0.0811	0.0201	0.0045	0.0027	0.0025
$\frac{\Delta t}{64}$	0.0811	0.0200	0.0040	0.0016	0.0012
$\frac{\Delta t}{128}$	0.0811	0.0200	0.0039	0.0012	0.0006
$\frac{\Delta t}{256}$	0.0811	0.0200	0.0038	0.0011	0.0004
$\frac{\Delta t}{512}$	0.0811	0.0200	0.0038	0.0011	0.0003

Table 3.1: Relative errors $\mathcal{E}_h^{\Delta t}$.

$\mathrm{L}^2\left(\cup_{n=1}^{N_c}\Omega_n\right)$-norm, the magnetostatic problem converges with order $O(h^2)$ for this particular example.

Once the convergence order is checked, we illustrate in one single figure the simultaneous dependence on h and Δt of the error for current $\vec{I}$ in the $\mathrm{L}^2(0,T)$-norm by choosing initial coarse values for both discretization step-sizes and, for each successively refined mesh, we take the value of Δt proportional to h^2 (see the framed values in Table 3.1). Figure 3.5 shows a log-log plot of the corresponding relative errors $\mathcal{E}_h^{\Delta t}$ versus the number of degrees of freedom (d.o.f.). The slope of the curve shows again the convergence order $O(h^2+\Delta t)$.

3.6.2 Conductor within a Ferromagnetic Core

We have also solved a more realistic problem having the same geometry as one presented in [33], considering separately a sinusoidal and a PWM voltage drop, and using nonlinear materials.

Thus, we consider a two-dimensional problem inspired by the one introduced in [33]. In Fig-

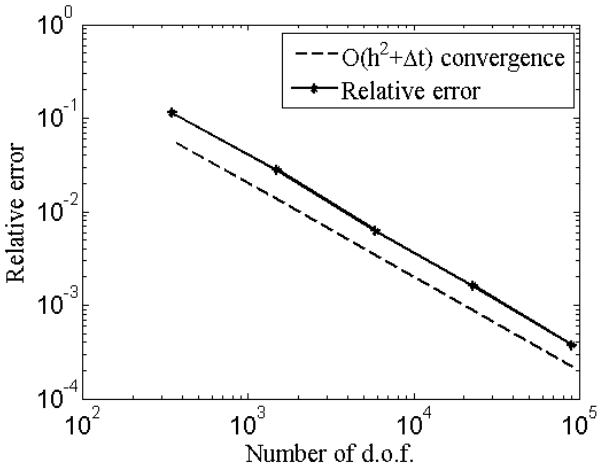

Figure 3.5: $\mathcal{E}_h^{\Delta t}$ versus d.o.f. (log-log scale); $\Delta t = Ch^2$.

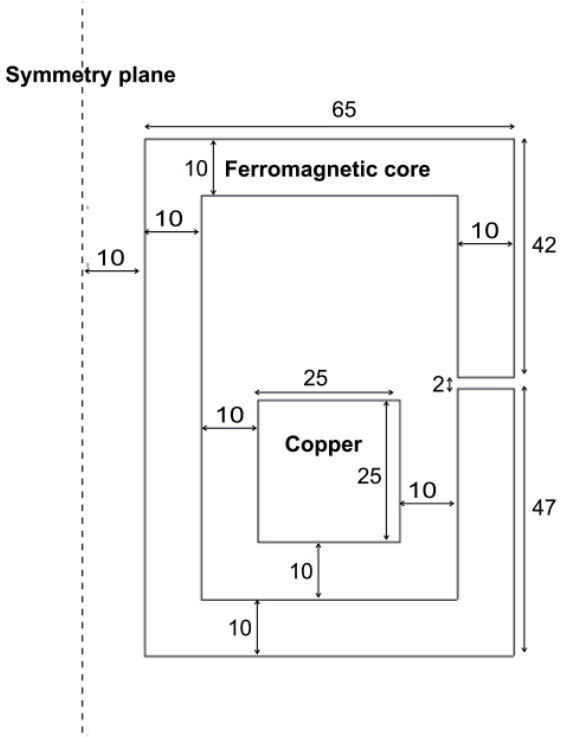

Figure 3.6: Dimensions of the 2D domain cross section (mm).

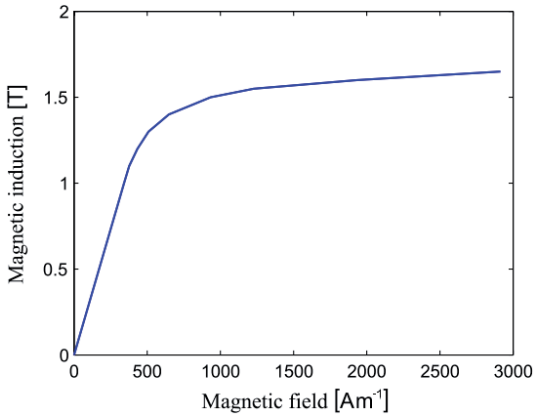

H (A m^{-1})	B (T)
0.00	0.00
342.00	1.00
377.00	1.10
433.00	1.20
509.00	1.30
648.00	1.40
933.00	1.50
1228.00	1.55
1934.00	1.60
2913.00	1.65

Figure 3.7: BH curve of the ferromagnetic core.

ure 3.6, taken from [33], we show the main part of the problem's domain, composed by a copper coil and a ferromagnetic core, which is placed inside a bounding rectangular box. In order to be able to neglect the eddy currents, in opposition to the problem solved in [33], we assume the core to be non-conducting and the copper domain to be the section of a stranded coil. The copper coil material has an electrical conductivity σ equal to 5.7×10^7 (Ohm m)$^{-1}$ and the magnetic permeability of the vacuum, $\mu_0 = 4\pi \times 10^{-7}$ H m^{-1}; the nonlinear BH curve of the ferromagnetic core is shown in Figure 3.7.

In the first part of the test, the source in the coil is given by the potential drop per unit length in the $z-$direction $C(t) = 1.4\sin(100\pi t)$ V m^{-1}, the initial current being $I_0 = 477.45$ A. This initial condition allows us to obtain a current $I(t)$ very close to the steady-state one from the beginning of the simulation, and was computed using the methodology described in [16].

We solved the problem in a source cycle (that is, in the time interval $[0, T] = [0, 0.02]$ seconds) with several successively refined meshes and time steps. Since this problem does not have an analytical solution, we computed the errors by comparing the numerical solutions with a reference one $I(t)$ obtained using a very fine discretization step both in space and time. Specifically, we computed the relative error for the current $\{I_h^m\}_{m=1}^M$ in the $\mathrm{L}^2(0,T)$-norm.

Table 3.1 shows these relative errors at the different levels of discretization. We notice that, when we take a time step small enough, the $O(h)$ error decay proved theoretically can be observed (see the last column in Table 3.1). We notice that this spatial error reduction is one order smaller than the one observed in the previous example. On the other hand, considering a mesh size small enough allows us to show the expected convergence order in time $O(\Delta t)$ (see the last row in Table 3.1).

We also illustrate in one single figure the simultaneous dependence on h and Δt for the current I in the $\mathrm{L}^2(0,T)$-norm by choosing initial coarse values for both discretization steps and, for each successively refined mesh, we take the value of Δt proportional to h (see the framed values in Table 3.2). Figure 3.8 shows a log-log plot of the corresponding relative errors $\mathcal{E}_h^{\Delta t}$ versus the number of degrees of freedom (d.o.f.). The slope of the curve exemplifies again the convergence order $O(h + \Delta t)$.

	$\Delta t = \frac{T}{20}$	$\frac{\Delta t}{2}$	$\frac{\Delta t}{4}$	$\frac{\Delta t}{8}$
h	$\boxed{9.482e10^{-4}}$	$7.883e10^{-4}$	$7.455e10^{-4}$	$7.355e10^{-4}$
$\frac{h}{2}$	$7.271e10^{-4}$	$\boxed{4.968e10^{-4}}$	$4.234e10^{-4}$	$4.044e10^{-4}$
$\frac{h}{4}$	$6.372e10^{-4}$	$3.499e10^{-4}$	$\boxed{2.322e10^{-4}}$	$1.943e10^{-4}$
$\frac{h}{8}$	$6.144e10^{-4}$	$3.055e10^{-4}$	$1.562e10^{-4}$	$\boxed{0.894e10^{-4}}$

Table 3.2: Sinusoidal test. Relative errors $\mathcal{E}_h^{\Delta t}$. Reference solution: $\frac{h}{16}$, $\frac{\Delta t}{64}$.

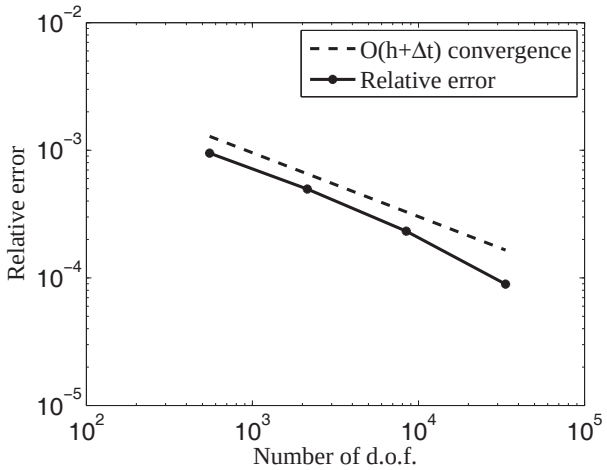

Figure 3.8: Sinusoidal test. $\mathcal{E}_h^{\Delta t}$ versus d.o.f. (log-log scale); $\Delta t = Ch$.

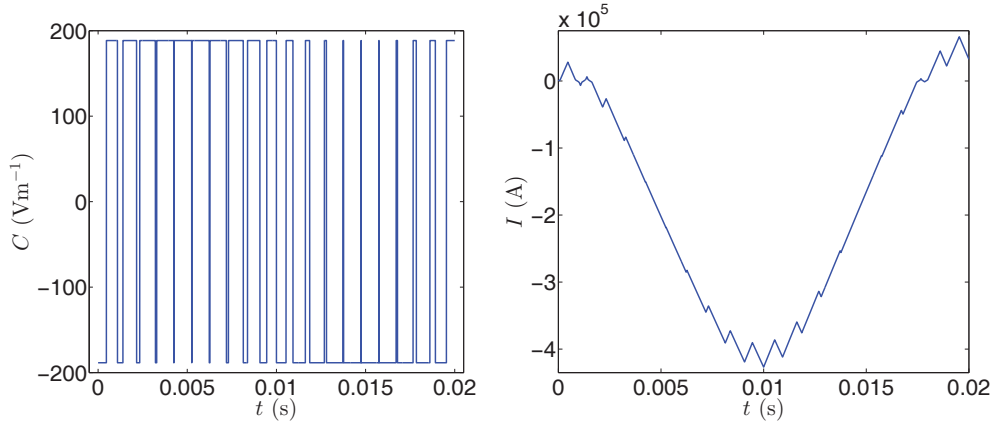

Figure 3.9: PWM test. Voltage drop per unit length over time (left); current over time for the reference solution (right).

On the other hand, we consider the geometry of the previous test supplied with a pulse-width modulation (PWM) voltage drop, a kind of source often used to feed electrical machines. It is a discontinuous function with a great number of discontinuities in each period (see, for instance, [58]). Thus, let us consider the voltage drop per unit length $C(t)$ depicted in Figure 3.9-left, whose period is equal to 0.02 seconds and oscillates between -188.46 V m^{-1} and 188.46 V m^{-1}. All material properties are the same as the ones used in the previous case. We solved the problem in a source cycle, and the initial value taken for the current is equal to $I_0 = 0$ A. In Figure 3.9-right we show the current corresponding to the solution of this test.

We notice that, in this particular case, $C(t) \notin \mathcal{C}([0,T])$, and the theory developed for the error estimate is not applicable. However, the PWM potential drop verifies the regularity conditions in Remark 3.10 and, therefore, Problem 3.5 has a unique solution $I(t) \in AC([0,T])$. In particular, as it can be deduced from Figure 3.9-right, current I is not everywhere differentiable (but it is almost everywhere).

USC
UNIVERSIDADE
DE SANTIAGO
DE COMPOSTELA

Chapter 4

An Optimal Control Problem for a Permanent Magnet Synchronous Motor

4.1 Introduction

Several advances have been made during the last decades in optimization and optimal control of electrical machines (see, for instance, [46, 67]). This has had a great impact on the development of new design methodologies due to the fact that most specifications are contradictory, requiring a systematic approach to reach a compromise between all constraints. Among the typical desired properties we can find high efficiency, low construction and operating costs (with special concern over permanent magnets materials), high torque capacity, low maintenance, etc.

The global design requirements on these devices generally involve different disciplines because they are subject to several physical phenomena: electromagnetics, structural mechanics, manufacturing, vibroacoustics, heat transfer …Therefore, it is interesting to address their study from a multiphysics perspective (see, for instance, [90] and references therein). However, this approach requires the use of modelling methodologies of low computational cost, such as thermal or magnetic networks, usually sacrificing accuracy. For instance, a popular technique for optimization and optimal control consists in evaluating the objectives and constraints by means of analytical models.

In contrast, it is sometimes more adequate to separately study each aspect of the machine design, in order to be able to use more precise but computationally demanding numerical techniques. For this purpose, a very important aspect is the electromagnetic design of the electrical machine (see [31, 112]). In this framework, the finite element method (FEM) is widely used for the study of electrical machines due to its high accuracy, but its associated computational cost may represent a drawback. This is sometimes solved by means of surrogate models, which predict the relation between some design parameters and the desired characteristics with only a few FEM evaluations (see, for instance, [45, 49, 113]).

In this work, we will deal with an optimal control problem related to the electromagnetic design of a permanent magnet synchronous motor (PMSM). Rather than trying to solve an ambitious problem from the engineering perspective, our target is to provide theoretical support, from the mathematical and numerical analysis point of view, to a particular problem appearing in the electric motor field. More precisely, our goal is to minimize the power losses in the machine coils while generating at least a minimum desired torque. This problem is similar to the one presented in [76], but we use finite element techniques to evaluate the torque constraint. Moreover, we refer to [50] for a rigourous theoretical analysis on a PMSM but from the point of view of shape optimization.

From the theoretical perspective, we are going to deal with an optimal control problem having a finite-dimensional control space, that is, a semi-infinite optimal control problem. Finite-dimensional controls appear in many real-life applications because it is sometimes difficult to practically implement control functions that can vary arbitrarily in space (see, for instance, [44, 104]). Besides, this property allows us to simplify some of the mathematical arguments needed in the theoretical results. However, we will work with a state constraint given in terms of the integral of the trace of the derivative of the state on an interior surface, what leads to an adjoint state having a jump discontinuity on this interface.

The outline of this chapter is the following. In Section 4.2 we develop the mathematical model for the PMS motor, that will be the state formulation for the optimal control problem, defined and analyzed in Section 4.3. Then, in Section 4.4 we present the spatial discretization of the model and perform its numerical analysis. Moreover, in Section 4.5 we give some details on the implementation strategy adopted for solving the optimal control problem. Finally, in Section 4.6 we report some numerical results obtained for an academic permanent magnet synchronous motor, which allows us to illustrate the theoretical results.

4.2 Mathematical Model

As mentioned in the introduction, this chapter performs the mathematical and numerical analysis of an optimal control problem defined on the cross-section of a permanent magnet synchronous motor (see Figure 4.1). Similarly to the previous chapter, we are going to start from Problem II.2 to write the model for the motor. In opposition to the preceding chapter, we are going to assume that the data in conductors are given in terms of the currents through them, and thus we will have $N_V = 0$ and $N_c = N_V$. Moreover, in order to reduce the computational cost, as a first step we are going to consider the ferromagnetic core to be a linear material.

In line with the typical structure of a PM synchronous motor, we are going to consider that its cross-section Ω is composed by

- A rotor domain, that rotates at constant speed around the machine axis, and that can be divided in the following parts
  - a permanent magnet region $\Omega^r_{\rm pm}(t)$, (eventually having several connected components),

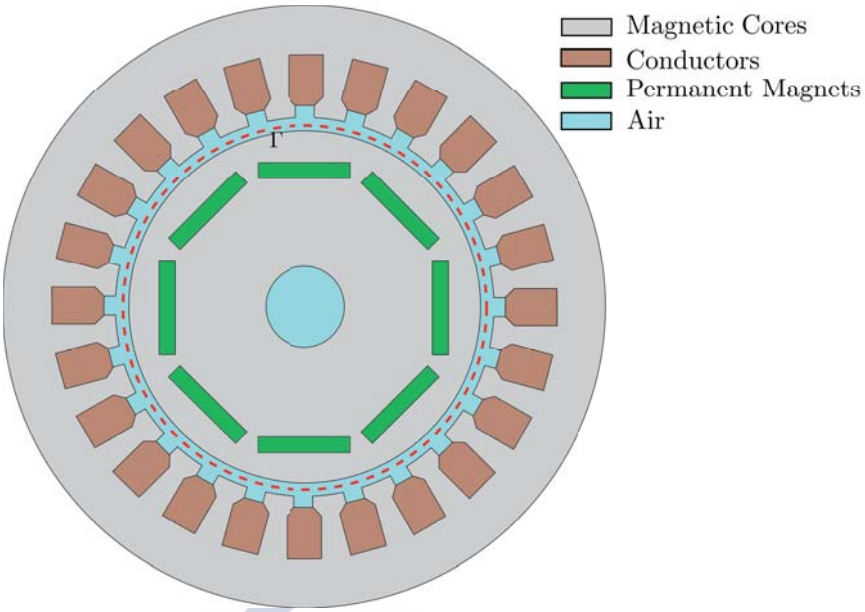

Figure 4.1: Transversal section of a PM synchronous motor.

  - a ferromagnetic non-conducting laminated core $\Omega^r_{\rm mc}(t)$, and
  - the machine shaft.

  Notice that we have taken the rotor motion into account by explicitly writing the subdomain's dependence on time.

- A stator domain, that remains still during normal operation, and that can be divided in the following parts
  - several stranded conductors representing the cross sections of the coils Ω^s_n, $n = 1, \ldots, N_c$,
  - a ferromagnetic non-conducting laminated core $\Omega^s_{\rm mc}$,
- An air-gap between rotor and stator.

We notice that, in this chapter, the machine cores will be denoted by $\Omega^s_{\rm mc}$ and $\Omega^r_{\rm mc}(t)$; we have changed the notation with respect to the other chapters because, here, we assume that the cores are magnetically linear.

We will assume that we can define an artificial interface between rotor and stator, which will be denoted by Γ, being a circle in the air-gap of radius R that does not touch the ferromagnetic cores and does not depend on time (see dashed red line in Figure 4.1). This artificial boundary divides the air-gap into two parts, one adjacent to the rotor core, $\Omega^r_0(t)$, and another one touching the stator core, Ω^s_0. Moreover, we notice that the shaft is usually modeled as a non-conducting, magnetically linear domain, whose material has the vacuum reluctivity, ν_0, and thus it will be considered as if it was air, and therefore contained in $\Omega^r_0(t)$. Similarly, should the motor be surrounded by an artificial air-box for computational purposes, it will be considered as belonging to Ω^s_0. Accordingly, we will denote the rotor and stator domains by

$$\Omega^r(t) := \left(\overline{\Omega^r_0}(t) \cup \overline{\Omega^r_{\rm pm}}(t) \cup \overline{\Omega^r_{\rm mc}}(t)\right)^\circ, \quad \Omega^s := \left(\overline{\Omega^s_0} \cup \left(\cup_{n=1}^{N_c} \overline{\Omega^s_n}\right) \cup \overline{\Omega^s_{\rm pm}}\right)^\circ,$$

respectively. Besides, the global magnetic reluctivity function, $\nu : \Omega \times [0,T] \longrightarrow \mathbb{R}$, is defined as

$$\nu(\boldsymbol{x};t) = \begin{cases} \nu_0 & \text{if } \boldsymbol{x} \in \Omega_0^s \cup \Omega_0^r(t), \\ \nu_0 & \text{if } \boldsymbol{x} \in \Omega_n^s,\ n = 1,\dots,N_c, \\ \nu_{\mathrm{pm}} & \text{if } \boldsymbol{x} \in \Omega_{\mathrm{pm}}^r(t), \\ \nu_{\mathrm{mc}} & \text{if } \boldsymbol{x} \in \Omega_{\mathrm{mc}}^s \cup \Omega_{\mathrm{mc}}^r(t). \end{cases}$$

Furthermore, we call r_t the rotation operator whose angular velocity is the one of the rotor, at time t, and r_{-t} its inverse. Then, $\Omega_0^r(t) = r_t\Omega_0^r(0)$, $\Omega_{\mathrm{pm}}^r(t) = r_t\Omega_{\mathrm{pm}}^r(0)$ and $\Omega_{\mathrm{mc}}^r(t) = r_t\Omega_{\mathrm{mc}}^r(t)$. Notice that the geometric set $\Omega^r(t) \equiv \Omega^r$ is always the same, a circle, but the physical parameters at each point change with time as they are not invariant with respect to rotation r_t. Besides, the remanent flux in the permanent magnets, $\boldsymbol{B}^r = B_x^r((x,y);t)\boldsymbol{e}_x + B_y^r((x,y);t)\boldsymbol{e}_y$, depends on time because the orientation of the permanent magnets changes with the motion of the machine; more precisely, we have that $\boldsymbol{B}^r((x,y);t) = r_t\boldsymbol{B}^r(r_{-t}(x,y);0)$ (see Figure 4.2).

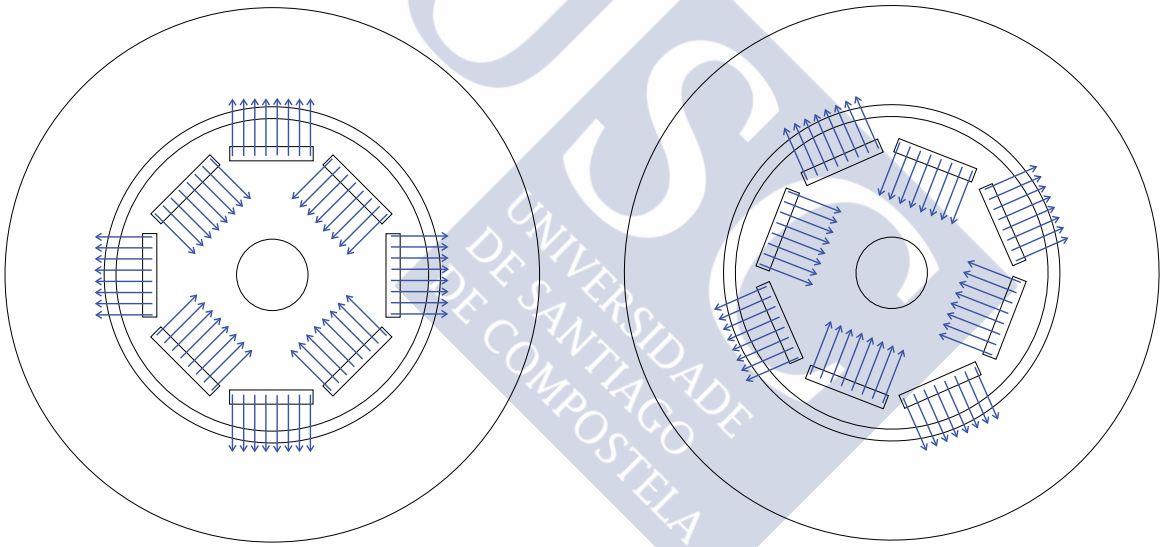

Figure 4.2: Orientation of the PM's remanent magnetization $\boldsymbol{B}^r((x,y);0)$ (left) and $\boldsymbol{B}^r((x,y);t)$ (right).

Since the stator coils are considered to be stranded conductors, the current density in them is assumed to be uniformly distributed, that is,

$$\boldsymbol{J}((x,y);t) = J_{z,n}(t)\boldsymbol{e}_z = \frac{i_n(t)}{\mathrm{meas}(\Omega_n^s)}\boldsymbol{e}_z, \quad \forall\,(x,y) \in \Omega_n^s,$$

$i_n(t)$ being the total intensity across Ω_n^s, $n = 1,\dots,N_c$.

Under the above conditions, Problem II.2 reads:

Problem 4.1. *Given* $(i_1(t),\dots,i_{N_c}(t))^{\mathrm{T}}$ *and* $\boldsymbol{B}^r$*, find* $A(x,y;t)$ *for every* $t\in[0,T]$ *satisfying*

$$-\operatorname{div}(\nu_0\,\mathbf{grad}\,A)=0 \quad \textit{in } \Omega_0^s\cup\Omega_0^r(t), \tag{4.1}$$

$$-\operatorname{div}(\nu_0\,\mathbf{grad}\,A)=\frac{i_n(t)}{\operatorname{meas}(\Omega_n^s)} \quad \textit{in } \Omega_n^s,\quad n=1,\dots,N_c, \tag{4.2}$$

$$-\operatorname{div}(\nu_{\mathrm{pm}}\,\mathbf{grad}\,A)=-\operatorname{div}\left(\nu_{\mathrm{pm}}\,(\boldsymbol{B}^r)^{\perp}\right) \quad \textit{in } \Omega_{\mathrm{pm}}^r(t), \tag{4.3}$$

$$-\operatorname{div}(\nu_{\mathrm{mc}}\,\mathbf{grad}\,A)=0 \quad \textit{in } \Omega_{\mathrm{mc}}^s\cup\Omega_{\mathrm{mc}}^r(t), \tag{4.4}$$

$$[\nu\,\mathbf{grad}\,A\cdot\boldsymbol{n}]_S=\begin{cases}\nu_{\mathrm{pm}}\,(\boldsymbol{B}^r)^{\perp}\cdot\boldsymbol{n}, & \textit{if } S\subset\partial\Omega_{\mathrm{pm}}^r(t),\\ 0, & \textit{otherwise},\end{cases} \tag{4.5}$$

$$A=0 \quad \textit{on } \partial\Omega. \tag{4.6}$$

At each time t, Problem 4.1 is a linear magnetostatic problem; thus, t only plays the role of a parameter in the PDE problem. By formal integration of (4.1)–(4.6), and considering the time discretization

$$\left\{t_m\in\mathbb{R}\,:\,t_m=m\Delta t,\ m=0,\dots,M-1\right\},$$

with $\Delta t:=T/M$, we obtain the variational formulation:

Problem 4.2. *Given* $i_n(t)\in\mathcal{C}^1[0,T]$*,* $n=1,\dots,N_c$*, and* $\boldsymbol{B}^r(\cdot;t)\in\mathrm{L}^2\left(\Omega_{\mathrm{pm}}^r(t)\right)^3$ *for every* $t\in[0,T]$*, find* $A(t_m)\in\mathrm{H}_0^1(\Omega)$ *for every* $m=0,\dots,M-1$ *such that*

$$\int_{\Omega(t_m)}\nu\,\mathbf{grad}\,A(t_m)\cdot\mathbf{grad}\,W=\sum_{n=1}^{N_c}\int_{\Omega_n^s}\frac{i_n(t_m)}{\operatorname{meas}(\Omega_n^s)}W+\int_{\Omega_{\mathrm{pm}}^r(t_m)}\nu_{\mathrm{pm}}(\boldsymbol{B}^r)^{\perp}\cdot\mathbf{grad}\,W$$

for every $W\in\mathrm{H}_0^1(\Omega)$.

Remark 4.3. *Additionally, from Problem 4.2 we define problems* $(SP)_{\boldsymbol{B}^r}$ *and* $(SP)_i$*, the first one with sources given only in terms of the remanent flux in permanent magnets (and thus* $i_n(t)\equiv 0$*,* $n=1,\dots,N_c$*), and the second problem with sources only in the stator conductors (and therefore the permanent magnet region is replaced with a magnetically linear material with permeability* ν_{pm}*). These auxiliary problems will be used for the mathematical analysis of the optimal control problem.*

The proof of the next result follows directly from Lax-Milgram's theorem:

Theorem 4.4. *Problem 4.2 has a unique solution* $A(t_m)\in\mathrm{H}_0^1(\Omega)$ *for every* $m=0,\dots,M-1$*. Moreover, there exist a constant* $C>0$*, not depending on the data, such that*

$$||A(t_m)||_{\mathrm{H}^1(\Omega)}\le C\left(\sum_{n=1}^{N_c}|i_n(t_m)|+\frac{1}{\mu_0}||\boldsymbol{B}^r(0)||_{\mathrm{L}^2\left(\Omega_{\mathrm{pm}}^r(0)\right)^3}\right)$$

for every $m=0,\dots,M-1$.

Remark 4.5. *If the magnetic reluctivity was more regular (for example, $\nu \in \mathcal{C}^{0,1}(\overline{\Omega})$), we would have solutions with higher regularity, $A(t_m) \in \mathrm{H}^2(\Omega)$ for every $m = 0, \dots, M-1$ (see Theorems 2.2.2.3 and 3.1.3.1 in [54]). However, since we are assuming that ν is only piecewise constant, $A(t_m)$ are generally not globally in $\mathrm{H}^2(\Omega)$. Nevertheless, we are still allowed to say that the magnetic vector potential A is regular in open subsets strictly contained in the subdomains. More precisely, it follows from [62] that*

$$||A(t_m)||_{\mathrm{H}^2(\Xi)} \leq C \left(\sum_{n=1}^{N_c} |i_n(t_m)| + \frac{1}{\mu_0} ||\boldsymbol{B}^r(0)||_{\mathrm{L}^2\left(\Omega^r_{\mathrm{pm}}(0)\right)^3} \right)$$

for any $m = 1, \dots, M$, Ξ being any open subset of $\widetilde{\Omega}(t_m) := \left(\Omega^r_0(t_m) \cup \Omega^r_{\mathrm{pm}}(t_m) \cup \Omega^r_{\mathrm{mc}}(t_m)\right) \cup \left(\Omega^s_0 \cup \left(\cup_{n=1}^{N_c} \Omega^s_n\right) \cup \Omega^s_{\mathrm{mc}}\right)$ with $\mathcal{C}^2$ boundary.

4.3 Optimal Control Problem

Now, we are going to formulate an optimal control problem having the state formulation that we have just introduced. For this purpose, we assume that σ is constant in each Ω^s_n, and that the currents through them are given by sinusoidal functions of the same frequency ω, with amplitudes I_n and phases α_n; that is, $i_n(t) = I_n \cos(\omega t + \alpha_n)$, $n = 1, \dots, N_c$. Then, if the final time T is equal to the currents period, the power dissipated in the coils by Joule effect, $\mathcal{P}$, is:

$$\mathcal{P} = \frac{1}{T} \int_0^T \sum_{n=1}^{N_c} \int_{\Omega^s_n} \frac{1}{\sigma} \left| \frac{i_n(t)}{\mathrm{meas}(\Omega^s_n)} \right|^2 = \sum_{n=1}^{N_c} \frac{I_n^2}{2\,\mathrm{meas}(\Omega^s_n)\sigma}.$$

On the other hand, let $\boldsymbol{\tau}(t)$ be the instantaneous torque on Ω^r at time t, which can be computed as

$$\boldsymbol{\tau}(t) = \int_{\Omega^r} \boldsymbol{r} \times \mathrm{div}\, \mathcal{M}(t) = \int_\Gamma \boldsymbol{r} \times \mathcal{M}^{ext}(t)\boldsymbol{n},$$

where $\mathcal{M}^{ext}$ is the limit value of the magnetic part of the classical Maxwell's stress tensor, $\mathcal{M} = \boldsymbol{B} \otimes \boldsymbol{H} - \frac{1}{2}\boldsymbol{B} \cdot \boldsymbol{H}\mathcal{I}$, coming from outside of Ω^r (see [28]). Formal calculations lead us to the following expression for the magnetic torque on Ω^r:

$$\boldsymbol{\tau} = \nu_0 \int_\Gamma (\mathbf{grad}\, A \cdot \boldsymbol{r})\, (\mathbf{grad}\, A \times \boldsymbol{n}) = \left(\nu_0 \int_\Gamma \left(\frac{\partial A}{\partial x} n_y - \frac{\partial A}{\partial y} n_x \right) \left(\frac{\partial A}{\partial x} r_x + \frac{\partial A}{\partial y} r_y \right) \right) \boldsymbol{e}_z.$$

We can formulate an optimal control problem in the following way: we seek amplitudes I_n such that the dissipated power $\mathcal{P}$ is minimum, with the restriction that the approximated mean torque on Ω^r along the axial axis of the machine during one current period is above a certain value $\tau_d > 0$. For this purpose, we notice that if we use the composed trapezoidal rule to approximate the mean torque, we obtain the expression

$$\frac{1}{T} \int_0^T \boldsymbol{\tau}(t) \cdot \boldsymbol{e}_z \approx \frac{1}{T} \sum_{m=0}^{M-1} \frac{\Delta t}{2} (\boldsymbol{\tau}(t_m) + \boldsymbol{\tau}(t_{m+1})) \cdot \boldsymbol{e}_z = \frac{1}{M} \sum_{m=0}^{M-1} \boldsymbol{\tau}(t_m) \cdot \boldsymbol{e}_z,$$

since $A(0) = A(T)$ and thus, in particular, $\boldsymbol{\tau}(0) = \boldsymbol{\tau}(T)$.

Let us denote by $\mathcal{U}_{ad} := [-I_{max}, I_{max}]^{N_c} \subset \mathbb{R}^{N_c}$ the set of admissible controls, with $I_{max} > 0$. Thus, we can formulate an optimal control problem in the following way:

Problem 4.6.

$$\min_{\boldsymbol{I} \in \mathcal{U}_{feas}} \mathcal{J}(\boldsymbol{I}) := \sum_{n=1}^{N_c} \frac{I_n^2}{2\,\mathrm{meas}(\Omega_n^s)\sigma}, \tag{4.7}$$

where

$$\mathcal{U}_{feas} = \left\{ \boldsymbol{I} \in \mathcal{U}_{ad} : \, G(\boldsymbol{I}) \leq 0 \right\},$$

G being integral operator

$$G(\boldsymbol{I}) := \tau_d - \frac{1}{M} \sum_{m=0}^{M-1} \nu_0 \int_\Gamma \left(\frac{\partial A}{\partial x}(t_m) n_y - \frac{\partial A}{\partial y}(t_m) n_x \right) \left(\frac{\partial A}{\partial x}(t_m) r_x + \frac{\partial A}{\partial y}(t_m) r_y \right),$$

with $A(t_m)$ the solutions to Problem 4.2, $m = 0, \ldots, M-1$.

Remark 4.7. *Let us notice that, since $A(t_m) \in \mathrm{H}^2(\Xi)$ for every $m = 0, \ldots, M-1$, Ξ being a $\mathcal{C}^2$ domain strictly contained in the air-gap and such that $\Gamma \subset \Xi$, and since $\boldsymbol{r} = R\boldsymbol{n}$ on Γ, the integrals involved in the torque's expression are well-defined because the following applications are continuous*

$$\begin{aligned} \mathrm{H}^2(\Xi) &\longrightarrow \mathrm{H}^{1/2}(\Gamma) \quad u \mapsto \gamma_n(\mathbf{grad}\, u) := (\mathbf{grad}\, u \cdot \boldsymbol{n})|_\Gamma, \\ \mathrm{H}^2(\Xi) &\longrightarrow \mathrm{H}^{1/2}(\Gamma)^3 \quad u \mapsto \gamma_\tau(\mathbf{grad}\, u) := (\mathbf{grad}\, u \times \boldsymbol{n})|_\Gamma \end{aligned}$$

(see Chapter II of [52]). In particular,

$$(\mathbf{grad}\, A(t_m) \times \boldsymbol{n}) \cdot \boldsymbol{e}_z, \mathbf{grad}\, A(t_m) \cdot \boldsymbol{r} \in \mathrm{H}^{1/2}(\Gamma) \subset \mathrm{L}^2(\Gamma).$$

Moreover, as we mentioned in Remark 4.5,

$$||A(t_m)||_{\mathrm{H}^2(\Xi)} \leq C \left(\sum_{n=1}^{N_c} |I_n(t_m)| + \nu_0 ||\boldsymbol{B}^r(0)||_{\mathrm{L}^2\left(\Omega^r_{\mathrm{pm}}(0)\right)^3} \right).$$

Let $S_{t_m} : \mathbb{R}^{N_c} \longrightarrow \mathrm{H}_0^1(\Omega)$ be the control-to-state operators, with $m = 0, \ldots, M-1$, which are affine functions. Indeed, since Problem 4.2 is linear, thanks to the superposition principle, its solutions at time $t_m \in [0, T]$ can be written as $S_{t_m}(\mathbf{K}) = L_{t_m}(\mathbf{K}) + A_{\boldsymbol{B}^r}(t_m)$, with L_{t_m} the linear control-to-state operators for Problem $(SP)_{\boldsymbol{i}}$ and $A_{\boldsymbol{B}^r}$ the solutions to Problem $(SP)_{\boldsymbol{B}^r}$ (see Remark 4.3). Since L_{t_m} are linear and bounded, L_{t_m} are continuous, and the same is true for the control-to-state operators S_{t_m}.

In the following theorem we state the existence of at least one solution to Problem 4.6:

Theorem 4.8. *If $\mathcal{U}_{feas}$ is nonempty, Problem 4.6 has at least one optimal control $\overline{\boldsymbol{I}}$.*

Proof. Since G is continuous, the set of feasible controls,

$$\mathcal{U}_{feas} = [-I_{max}, I_{max}]^{N_c} \cap \{\mathbf{K} \in \mathbb{R}^{N_c} : G(\mathbf{K}) \leq 0\}$$

is a closed and bounded subset of $\mathbb{R}^{N_c}$, and therefore a compact. Then, since the operator $\mathcal{J} : \mathbb{R}^{N_c} \longrightarrow \mathbb{R}$ defined by

$$\mathcal{J}(\boldsymbol{I}) = \sum_{n=1}^{N_c} \frac{I_n^2}{2\,\mathrm{meas}(\Omega_n^s)\sigma}$$

is continuous, we can deduce the result from Weierstrass' theorem. □

4.3.1 Including Lagrange Multipliers

The Lagrangian function associated to Problem 4.6 is

$$\mathcal{L} : \mathbb{R}^{N_c} \times \mathbb{R} \longrightarrow \mathbb{R}, \quad \mathcal{L}(\boldsymbol{I}; \lambda) := \mathcal{J}(\boldsymbol{I}) + \lambda G(\boldsymbol{I}).$$

Let $\overline{\boldsymbol{I}}$ be a local solution to Problem 4.6. Then, any $\lambda^* \geq 0$ such that

$$\lambda^* G(\overline{\boldsymbol{I}}) = 0, \tag{4.8}$$

$$D_I \mathcal{L}(\overline{\boldsymbol{I}}; \lambda^*)(\boldsymbol{I} - \overline{\boldsymbol{I}}) \geq 0, \quad \forall\, \boldsymbol{I} \in \mathcal{U}_{ad} \tag{4.9}$$

is called a *Lagrange multiplier* associated with $\overline{\boldsymbol{I}}$. We will assume the following constraint qualification for $\overline{\boldsymbol{I}}$:

(CQ) If $G(\overline{\boldsymbol{I}}) = 0$, there exists $\boldsymbol{I}^0 \in \mathbb{R}^{N_c}$ such that $DG(\overline{\boldsymbol{I}})\boldsymbol{I}^0 < 0$, with

$$I_{0,n} \begin{cases} \leq 0 & \text{if } \overline{I}_n = I_{max}, \\ \geq 0 & \text{if } \overline{I}_n = -I_{max}. \end{cases}$$

We have the following result:

Theorem 4.9. *Let $\overline{\boldsymbol{I}}$ be a local solution to the optimal control problem 4.6 satisfying (CQ). Then, there exists a Lagrange multiplier λ^* associated with $\overline{\boldsymbol{I}}$. Moreover, the set of Lagrange multipliers associated with $\overline{\boldsymbol{I}}$ is bounded.*

Proof. Firstly, let us notice that $\mathcal{J}$ is a continuously differentiable operator. Moreover, functional G is also a continuously differentiable operator in an open neighbourhood of $\overline{\boldsymbol{I}}$. Indeed, we know that to proof that G is differentiable it is sufficient to show that all its partial derivatives exist. But since

$$G(\mathbf{K}) = \tau_d - \frac{1}{M} \sum_{m=0}^{M-1} \nu_0 \int_\Gamma \left(\frac{\partial S_{t_m}}{\partial x}(\mathbf{K}) n_y - \frac{\partial S_{t_m}}{\partial y}(\mathbf{K}) n_x \right) \left(\frac{\partial S_{t_m}}{\partial x}(\mathbf{K}) r_x + \frac{\partial S_{t_m}}{\partial y}(\mathbf{K}) r_y \right),$$

and taking into account that $S_{t_m}(\mathbf{K}) = L_{t_m}(\mathbf{K}) + A_{\boldsymbol{B}^r}(t_m)$, with L_{t_m} linear, it is easy to see that, for $n = 1, \dots, N_c$,

$$\begin{aligned}\frac{\partial G}{\partial I_n}(\mathbf{K}) &= \lim_{\delta\to 0}\frac{1}{\delta}(G(\mathbf{K}+\delta\boldsymbol{e}_n) - G(\mathbf{K}))\\ &= -\frac{1}{M}\sum_{m=0}^{M-1}\nu_0\int_\Gamma 2\frac{\partial S_{t_m}}{\partial x}(\mathbf{K})\frac{\partial L_{t_m}}{\partial x}(\boldsymbol{e}_n)n_y r_x - 2\frac{\partial S_{t_m}}{\partial y}(\mathbf{K})\frac{\partial L_{t_m}}{\partial y}(\boldsymbol{e}_n)n_x r_y\\ &\qquad + \left(\frac{\partial S_{t_m}}{\partial x}(\mathbf{K})\frac{\partial L_{t_m}}{\partial y}(\boldsymbol{e}_n) + \frac{\partial L_{t_m}}{\partial x}(\boldsymbol{e}_n)\frac{\partial S_{t_m}}{\partial y}(\mathbf{K})\right)(n_y r_y - n_x r_x)\\ &= -\frac{1}{M}\sum_{m=0}^{M-1}\nu_0\int_\Gamma(\mathbf{grad}\, L_{t_m}(\boldsymbol{e}_n)\cdot\boldsymbol{r})(\mathbf{grad}\, S_{t_m}(\mathbf{K})\times\boldsymbol{n})\cdot\boldsymbol{e}_z\\ &\qquad\qquad + (\mathbf{grad}\, S_{t_m}(\mathbf{K})\cdot\boldsymbol{r})(\mathbf{grad}\, L_{t_m}(\boldsymbol{e}_n)\times\boldsymbol{n})\cdot\boldsymbol{e}_z,\end{aligned}$$

with $\{\boldsymbol{e}_n\}_{n=1}^{N_c}$ the canonical basis of $\mathbb{R}^{N_c}$. Since L_{t_m} are linear and continuous, G is differentiable with

$$\begin{aligned}DG(\mathbf{K})\mathbf{h} = -\frac{1}{M}\sum_{m=0}^{M-1}\nu_0\int_\Gamma&(\mathbf{grad}\, L_{t_m}(\mathbf{h})\cdot\boldsymbol{r})(\mathbf{grad}\, S_{t_m}(\mathbf{K})\times\boldsymbol{n})\cdot\boldsymbol{e}_z\\ &+ (\mathbf{grad}\, S_{t_m}(\mathbf{K})\cdot\boldsymbol{r})(\mathbf{grad}\, L_{t_m}(\mathbf{h})\times\boldsymbol{n})\cdot\boldsymbol{e}_z.\end{aligned}$$

Besides, the derivatives of G are continuous because, since S_{t_m} are affine, we have that

$$\begin{aligned}|(DG(\mathbf{K}_1) - DG(\mathbf{K}_2))\mathbf{h}| = \Bigg|&\frac{1}{M}\sum_{m=0}^{M-1}\frac{1}{\mu_0}\int_\Gamma 2\frac{\partial L_{t_m}}{\partial x}(\mathbf{K}_1-\mathbf{K}_2)\frac{\partial L_{t_m}}{\partial x}(\mathbf{h})n_y r_x\\ &- 2\frac{\partial L_{t_m}}{\partial y}(\mathbf{K}_1-\mathbf{K}_2)\frac{\partial L_{t_m}}{\partial y}(\mathbf{h})n_x r_y + \Bigg(\frac{\partial L_{t_m}}{\partial x}(\mathbf{K}_1-\mathbf{K}_2)\frac{\partial L_{t_m}}{\partial y}(\mathbf{h})\\ &+\frac{\partial L_{t_m}}{\partial x}(\mathbf{h})\frac{\partial L_{t_m}}{\partial y}(\mathbf{K}_1-\mathbf{K}_2)\Bigg)(n_y r_y - n_x r_x)\Bigg| \to 0 \quad \text{as} \quad |\mathbf{K}_1-\mathbf{K}_2|\to 0.\end{aligned}$$

Following Theorem 6.3 from [103], we can conclude the proof by showing that $\overline{\boldsymbol{I}}$ satisfies the Zowe-Kurcyusz constraint qualification, that is, that for every $z \in \mathbb{R}$ there exist $\alpha, \beta, k \geq 0$ and $\boldsymbol{I} \in \mathcal{U}_{ad}$ such that

$$\alpha DG(\overline{\boldsymbol{I}})(\boldsymbol{I}-\overline{\boldsymbol{I}}) + \beta(k + G(\overline{\boldsymbol{I}})) = z.$$

We will study the case in which $G(\overline{\boldsymbol{I}}) = 0$ in the first place. In this case we have assumed that there exists $\boldsymbol{I}^0 \in \mathbb{R}^{N_c}$ such that $DG(\overline{\boldsymbol{I}})\boldsymbol{I}^0 < 0$, with

$$I_{n^0}\begin{cases}\leq 0 & \text{if } \overline{I}_n = I_{max},\\ \geq 0 & \text{if } \overline{I}_n = -I_{max}.\end{cases}$$

If $z < 0$, let $\boldsymbol{I} := \varepsilon\boldsymbol{I}^0 + \overline{\boldsymbol{I}}$, with $\varepsilon > 0$ small enough to ensure that $\boldsymbol{I} \in \mathcal{U}_{ad}$. Then,

$$DG(\overline{\boldsymbol{I}})(\boldsymbol{I}-\overline{\boldsymbol{I}}) = \varepsilon DG(\overline{\boldsymbol{I}})\boldsymbol{I}^0 < 0.$$

Let also $\beta := 0$, $k := 0 \in K$ and

$$\alpha := \frac{z}{DG(\overline{\boldsymbol{I}})(\boldsymbol{I} - \overline{\boldsymbol{I}})} > 0.$$

Then,

$$\alpha DG(\overline{\boldsymbol{I}})(\boldsymbol{I} - \overline{\boldsymbol{I}}) + \beta(k + G(\overline{\boldsymbol{I}})) = z.$$

On the other hand, if $z \geq 0$, we can take $\alpha := 0$, $\boldsymbol{I} := \mathbf{0} \in \mathcal{U}_{ad}$, $\beta := 1$ and $k := z$.

Finally, let us study the case in which $G(\overline{\boldsymbol{I}}) < 0$. Taking $\boldsymbol{I} := \overline{\boldsymbol{I}} \in \mathcal{U}_{ad}$, any $\alpha \geq 0$ and

- $k := 0 \in K$, $\beta := \dfrac{z}{G(\overline{\boldsymbol{I}})} \geq 0$ if $z \leq 0$,
- $\beta := 1$, $k := z - G(\overline{\boldsymbol{I}}) \in K$ if $z > 0$,

we obtain that

$$\alpha DG(\overline{\boldsymbol{I}})(\boldsymbol{I} - \overline{\boldsymbol{I}}) + \beta(k + G(\overline{\boldsymbol{I}})) = z.$$

□

4.3.2 Adjoint State

In this section we are going to define the adjoint problem associated to the state constraint, which will allow us to evaluate the derivative of its Lagrangian function in a more straightforward manner. First, let us notice that the operator $D\mathcal{J} : \mathbb{R}^{N_c} \longrightarrow \mathbb{R}$ is defined in the following way:

$$D\mathcal{J}(\mathbf{K})\mathbf{h} = \sum_{n=1}^{Nc} \frac{K_n h_n}{\text{meas}(\Omega_n^s)\sigma}.$$

Then,

$$\begin{aligned} D_I\mathcal{L}(\overline{\boldsymbol{I}}; \lambda^*)(\boldsymbol{I} - \overline{\boldsymbol{I}}) = &\sum_{n=1}^{Nc} \frac{\overline{I}_n(I_n - \overline{I}_n)}{\text{meas}(\Omega_n^s)\sigma} \\ &- \lambda^* \frac{1}{M} \sum_{m=0}^{M-1} \nu_0 \int_\Gamma (\mathbf{grad}\, L_{t_m}(\boldsymbol{I} - \overline{\boldsymbol{I}}) \cdot \boldsymbol{r})(\mathbf{grad}\, S_{t_m}(\overline{\boldsymbol{I}}) \times \boldsymbol{n}) \cdot \boldsymbol{e}_z \\ &+ (\mathbf{grad}\, S_{t_m}(\overline{\boldsymbol{I}}) \cdot \boldsymbol{r})(\mathbf{grad}\, L_{t_m}(\boldsymbol{I} - \overline{\boldsymbol{I}}) \times \boldsymbol{n}) \cdot \boldsymbol{e}_z. \end{aligned}$$

To simplify the second term in the expression of $D_I\mathcal{L}$, let us introduce the adjoint problem:

Problem 4.10. *Given* $A(t_m) \in \mathrm{H}_0^1(\Omega)$ *such that* $A(t_m)|_\Xi \in \mathrm{H}^2(\Xi)$ *for every* $m = 0, \ldots, M-1$ *and* $\lambda \in \mathbb{R}$*, find* $P(t_m)$ *for every* $m = 0, \ldots, M-1$ *such that*

$$\begin{aligned} -\operatorname{div}(\nu\,\mathbf{grad}\,P(t_m)) &= 0 \quad \textit{in } \Omega^s \cup \Omega^r(t_m), \\ [(\nu\,\mathbf{grad}\,P(t_m))\cdot\boldsymbol{n}] &= -\lambda\,\nu_0(\operatorname{curl}_\Gamma((\mathbf{grad}\,A(t_m)\cdot\boldsymbol{r})\boldsymbol{e}_z) \\ &\qquad - \operatorname{div}((\mathbf{grad}\,A(t_m)\times\boldsymbol{n})\cdot\boldsymbol{e}_z\boldsymbol{r})) \quad \textit{on } \Gamma, \\ [(\nu\,\mathbf{grad}\,P(t_m))\cdot\boldsymbol{n}] &= 0 \quad \textit{on } \partial\widetilde{\Omega}(t_m), \\ P(t_m) &= 0 \quad \textit{on } \partial\Omega. \end{aligned}$$

In the above problem, we recall that

$$\widetilde{\Omega}(t_m) := \left(\Omega_0^r(t_m) \cup \Omega_{\mathrm{pm}}^r(t_m) \cup \Omega_{\mathrm{mc}}^r(t_m)\right) \cup \left(\Omega_0^s \cup \left(\cup_{n=1}^{N_c}\Omega_n^s\right) \cup \Omega_{\mathrm{mc}}^s\right).$$

We can obtain the weak formulation of the above problem in a similar way to the derivation of the weak formulation for the state equation. Concerning the integral of the jump across Γ (see Section 3.4 in [77]):

$$\int_\Gamma -\operatorname{div}((\mathbf{grad}\,A\times\boldsymbol{n})\cdot\boldsymbol{e}_z\boldsymbol{r})\,W = \int_\Gamma (\mathbf{grad}\,W\cdot\boldsymbol{r})(\mathbf{grad}\,A\times\boldsymbol{n})\cdot\boldsymbol{e}_z,$$

$$\begin{aligned} \int_\Gamma \operatorname{curl}_\Gamma((\mathbf{grad}\,A\cdot\boldsymbol{r})\boldsymbol{e}_z)\,W &= \int_\Gamma (\mathbf{curl}_\Gamma\,W\cdot\boldsymbol{e}_z)(\mathbf{grad}\,A\cdot\boldsymbol{r}) \\ &= \int_\Gamma (\mathbf{grad}\,A\cdot\boldsymbol{r})(\mathbf{grad}_\Gamma W\times\boldsymbol{n})\cdot\boldsymbol{e}_z = \int_\Gamma (\mathbf{grad}\,A\cdot\boldsymbol{r})(\mathbf{grad}\,W\times\boldsymbol{n})\cdot\boldsymbol{e}_z. \end{aligned}$$

Notice that the surface operators involved in the above expressions are well-defined since $A|_\Xi \in \mathrm{H}^2(\Xi)$ and $W \in \mathrm{H}^1(\Omega)$, and then, in particular,

$$(\mathbf{grad}\,A\cdot\boldsymbol{r})|_\Gamma \in \mathrm{L}_t^2(\Gamma) \quad \text{and} \quad W|_\Gamma \in \mathrm{L}^2(\Gamma)$$

(see [3], Theorem 4.12). This leads us to:

Problem 4.11. *Given* $A(t_m) \in \mathrm{H}_0^1(\Omega)$ *such that* $A(t_m)|_\Xi \in \mathrm{H}^2(\Xi)$ *for every* $m = 0, \ldots, M-1$ *and* $\lambda \in \mathbb{R}$*, find* $P(t_m) \in \mathrm{H}_0^1(\Omega)$ *for every* $m = 0, \ldots, M-1$ *such that*

$$\begin{aligned} &\int_{\Omega(t_m)} \nu\,\mathbf{grad}\,P(t_m)\cdot\mathbf{grad}\,W \\ &\quad = -\lambda\,\nu_0\int_\Gamma (\mathbf{grad}\,W\cdot\boldsymbol{r})(\mathbf{grad}\,A(t_m)\times\boldsymbol{n})\cdot\boldsymbol{e}_z + (\mathbf{grad}\,A(t_m)\cdot\boldsymbol{r})(\mathbf{grad}\,W\times\boldsymbol{n})\cdot\boldsymbol{e}_z \end{aligned}$$

for every $W \in \mathrm{H}_0^1(\Omega)$.

We have the following result:

Lemma 4.12. *Problem 4.10 has a unique solution $P(t_m) \in \mathrm{H}^1_0(\Omega)$ for every $m = 0, \dots, M-1$, which verifies:*

$$||P(t_m)||_{\mathrm{H}^1(\Omega)} \leq C \left(\sum_{n=1}^{N_c} |i_n(t_m)| + \nu_0 \, ||\boldsymbol{B}^r(0)||_{\mathrm{L}^2\left(\Omega^r_{\mathrm{pm}}(0)\right)^3} \right).$$

Proof. The result follows immediately from Lax-Milgram's theorem. Indeed, the left hand side defines a continuous and $\mathrm{H}^1(\Omega)$-elliptic bilinear function and, if we denote by f_m, $m = 0, \dots, M-1$, the operators on the right hand side,

$$\begin{aligned} \|f_m\|_{\mathrm{H}^{-1}(\Omega)} &= \sup_{W \in \mathrm{H}^1_0(\Omega)), \|W\|_{\mathrm{H}^1(\Omega)}} \left| \langle f_m, W \rangle \right| \\ &\leq C \sup_{W \in \mathrm{H}^1_0(\Omega)), \|W\|_{\mathrm{H}^1(\Omega)}} \Big| \int_\Gamma (\mathbf{grad}\, W \cdot \boldsymbol{r})(\mathbf{grad}\, A(t_m) \times \boldsymbol{n}) \cdot \boldsymbol{e}_z \\ &\qquad + (\mathbf{grad}\, A(t_m) \cdot \boldsymbol{r})(\mathbf{grad}\, W \times \boldsymbol{n}) \cdot \boldsymbol{e}_z \Big| \leq C \|A(t_m)\|_{\mathrm{H}^2(\Xi)}. \end{aligned}$$

□

In the next lemma we show that the second term in the expression of $D_I \mathcal{L}$ can be computed from the solution to the adjoint problem that we have just defined:

Lemma 4.13. *Let $\mathbf{K}, \mathbf{h} \in \mathbb{R}^{N_c}$, and $A^{\mathbf{K}}(t_m), A^{\mathbf{h}}(t_m)$, $m = 0, \dots, M-1$, the associated weak solutions to Problem 4.2 with currents $i_n(t) = K_n \cos(\omega t + \alpha_n)$, $n = 1, \dots, N_c$, and $(SP)_i$ with currents $i_n(t) = h_n \cos(\omega t + \alpha_n)$, $n = 1, \dots, N_c$, respectively. Then, the solutions $P(t_m)$ to Problem 4.10 with data $A^{\mathbf{K}}(t_m)$ and λ are such that:*

$$\begin{aligned} &\frac{1}{M} \sum_{m=0}^{M-1} \sum_{n=1}^{N_c} \int_{\Omega_n^s} \frac{h_n \cos(\omega t_m + \alpha_n)}{\mathrm{meas}(\Omega_n^s)} P(t_m) \\ &\qquad = -\frac{1}{M} \sum_{m=0}^{M-1} \lambda \, \nu_0 \int_\Gamma (\mathbf{grad}\, A^{\mathbf{h}}(t_m) \cdot \boldsymbol{r})(\mathbf{grad}\, A^{\mathbf{K}}(t_m) \times \boldsymbol{n}) \cdot \boldsymbol{e}_z \\ &\qquad\qquad + (\mathbf{grad}\, A^{\mathbf{K}}(t_m) \cdot \boldsymbol{r})(\mathbf{grad}\, A^{\mathbf{h}}(t_m) \times \boldsymbol{n}) \cdot \boldsymbol{e}_z. \end{aligned}$$

Proof. If we take $P(t_m) \in \mathrm{H}^1_0(\Omega)$ as test functions in problem $(SP)_i$ with currents $i_n(t) = h_n \cos(\omega t + \alpha_n)$, $n = 1, \dots, N_c$, we obtain:

$$\int_{\Omega(t_m)} \nu \, \mathbf{grad}\, A^{\mathbf{h}}(t_m) \cdot \mathbf{grad}\, P(t_m) = \sum_{n=1}^{N_c} \int_{\Omega_n^s} \frac{h_n \cos(\omega t_m + \alpha_n)}{\mathrm{meas}(\Omega_n^s)} P(t_m).$$

Analogously, we can take $A^{\mathbf{h}}(t_m)$ as test function in the adjoint equation with $A^{\mathbf{K}}(t_m)$ and λ as data and get:

$$\begin{aligned} &\int_{\Omega(t_m)} \nu \, \mathbf{grad}\, P(t_m) \cdot \mathbf{grad}\, A^{\mathbf{h}}(t_m) = \\ &\qquad - \lambda \, \nu_0 \int_\Gamma (\mathbf{grad}\, A^{\mathbf{h}}(t_m) \cdot \boldsymbol{r})(\mathbf{grad}\, A^{\mathbf{K}}(t_m) \times \boldsymbol{n}) \cdot \boldsymbol{e}_z \\ &\qquad\qquad + (\mathbf{grad}\, A^{\mathbf{K}}(t_m) \cdot \boldsymbol{r})(\mathbf{grad}\, A^{\mathbf{h}}(t_m) \times \boldsymbol{n}) \cdot \boldsymbol{e}_z. \end{aligned}$$

Subtracting the first equation to the second equation above, we deduce, after summing up for $m = 0, \dots, M-1$, and dividing over M we obtain

$$\frac{1}{M}\sum_{m=0}^{M-1}\sum_{n=1}^{N_c}\int_{\Omega_n^s}\frac{h_n\cos(\omega t_m+\alpha_n)}{\operatorname{meas}(\Omega_n^s)}P(t_m)$$
$$= -\frac{1}{M}\sum_{m=0}^{M-1}\lambda\,\nu_0\int_\Gamma(\mathbf{grad}\,A^{\mathbf{h}}(t_m)\cdot\boldsymbol{r})(\mathbf{grad}\,A^{\mathbf{K}}(t_m)\times\boldsymbol{n})\cdot\boldsymbol{e}_z$$
$$+(\mathbf{grad}\,A^{\mathbf{K}}(t_m)\cdot\boldsymbol{r})(\mathbf{grad}\,A^{\mathbf{h}}(t_m)\times\boldsymbol{n})\cdot\boldsymbol{e}_z.$$

□

In the next theorem we present the optimality system for the optimal control problem 4.6. Its proof is a direct consequence of Theorem 4.9 and Lemma 4.13.

Theorem 4.14. *Let $\overline{\boldsymbol{I}}$ be a local solution to the optimal control problem 4.6 satisfying (CQ). Let $\overline{A}(t_m)$ be the states associated to $\overline{\boldsymbol{I}}$. There exists $\lambda^* \geq 0$ associated with $\overline{\boldsymbol{I}}$ satisfying the following optimality system:*

$$\int_{\Omega(t_m)}\nu\,\mathbf{grad}\,\overline{A}(t_m)\cdot\mathbf{grad}\,W=\sum_{n=1}^{N_c}\int_{\Omega_n^s}\frac{\overline{I}_n\cos(\omega t+\alpha_n)}{\operatorname{meas}(\Omega_n^s)}W$$
$$+\int_{\Omega^r_{\mathrm{pm}}(t_m)}\nu_{\mathrm{pm}}(\boldsymbol{B}^r)^\perp\cdot\mathbf{grad}\,W\quad\forall\,W\in\mathrm{H}_0^1(\Omega),$$

$$\int_{\Omega(t_m)}\nu\,\mathbf{grad}\,\overline{P}(t_m)\cdot\mathbf{grad}\,W$$
$$=-\lambda^*\,\nu_0\left(\int_\Gamma(\mathbf{grad}\,W\cdot\boldsymbol{r})(\mathbf{grad}\,\overline{A}(t_m)\times\boldsymbol{n})\cdot\boldsymbol{e}_z\right.$$
$$\left.+\int_\Gamma(\mathbf{grad}\,\overline{A}(t_m)\cdot\boldsymbol{r})(\mathbf{grad}\,W\times\boldsymbol{n})\cdot\boldsymbol{e}_z\right)\quad\forall\,W\in\mathrm{H}_0^1(\Omega),$$

$$\lambda^*\left(\tau_d-\frac{1}{M}\sum_{m=0}^{M-1}\nu_0\int_\Gamma(\mathbf{grad}\,\overline{A}\cdot\boldsymbol{r})\,(\mathbf{grad}\,\overline{A}\times\boldsymbol{n})\cdot\boldsymbol{e}_z\right)=0,$$

$$\sum_{n=1}^{Nc}\frac{\overline{I}_n(I_n-\overline{I}_n)}{\operatorname{meas}(\Omega_n^s)\sigma}+\frac{1}{M}\sum_{m=0}^{M-1}\sum_{n=1}^{N_c}\int_{\Omega_n^s}\frac{(I_n-\overline{I}_n)\cos(\omega t_m+\alpha_n)}{\operatorname{meas}(\Omega_n^s)}\overline{P}(t_m)\geq 0,$$

for every $\boldsymbol{I}\in\mathcal{U}_{ad}$.

4.4 Numerical Analysis

In this section we will present a space discretization of Problem 4.6 and perform its analysis. We will use a conforming approximation for the problem based on the finite element method.

We consider M families of triangulations $\mathcal{T}_h^m$, $m = 0, \ldots, M-1$. With each element $K \in \mathcal{T}_h^m$ we associate two parameters $\rho(K)$ and $\sigma(K)$, where $\rho(K)$ denotes the diameter of the set K and $\sigma(K)$ is the diameter of the largest ball contained in K. We define the mesh size by $h = \max_{m=0,\ldots,M-1} \max_{K\in\mathcal{T}_h^m} \rho(K)$ and assume that the following conditions are satisfied:

1. There exist two positive constants ρ and σ such that

$$\frac{\rho(K)}{\sigma(K)} \leq \sigma, \quad \frac{h}{\rho(K)} \leq \rho$$

for all $K \in \mathcal{T}_h^m$, $m = 0, \ldots, M-1$, and $h > 0$.

2. Let us denote $\overline{\Omega_h}(t_m) := \cup_{K\in\mathcal{T}_h^m} K$, and let $\Omega_h(t_m)$ and $\partial\Omega_h(t_m)$ denote its interior and its boundary, respectively. We assume that $\overline{\Omega_h}(t_m)$ is convex and that the vertices of $\mathcal{T}_h^m$ placed on the boundary $\partial\Omega_h(t_m)$ are points of $\partial\Omega$, for every $m = 0, \ldots, M-1$. From [88], estimate (5.2.19), we know that $|\Omega \setminus \Omega_h(t_m)| \leq Ch^2$. Similar assumptions are made for each subdomain.

3. Since Ω^s does not change in time, for the sake of simplicity we will assume that the sets $\overline{\Omega_h}$ and $\partial\Omega_h$ do not either. Furthermore, we also assume that the vertices of $\mathcal{T}_h^m$ placed on the boundary of $\overline{\Omega_h^r}(t_m) := \bigcup_{\substack{K\in\mathcal{T}_h^m,\\ K\subset\overline{\Omega^r}(t_m)}} K$ are points of Γ.

4.4.1 Discretization of the State Problem

We introduce the following discrete spaces:

$$\mathfrak{X}_h^m := \left\{\psi_h \in \mathcal{C}^0(\overline{\Omega}) \,:\, \psi_h|_K \in \mathbb{P}_1(K) \quad \forall K \in \mathcal{T}_h^m, \psi_h = 0 \text{ in } \overline{\Omega} \setminus \overline{\Omega_h} \text{ and } \psi_h = 0 \text{ on } \partial\Omega_h\right\},$$

$m = 0, \ldots, M-1$.

Then, the discretization of Problem 4.2 reads as follows:

Problem 4.15. *Given $i_n(t) = I_n \cos(\omega t + \alpha_n) \in \mathcal{C}^1([0,T])$, $n = 1, \ldots, N_c$, and $\boldsymbol{B}^r(\cdot;t) \in \mathrm{L}^2\left(\Omega_{\mathrm{pm}}^r(t)\right)^3$ for every $t \in [0,T]$, find $A_h(t_m) \in \mathfrak{X}_h^m$ for every $m = 0, \ldots, M-1$ such that*

$$\int_{\Omega_h(t_m)} \nu\, \mathbf{grad}\, A_h(t_m) \cdot \mathbf{grad}\, W_h^m = \sum_{n=1}^{N_c} \int_{\Omega_{h,n}^s} \frac{i_n(t_m)}{\mathrm{meas}(\Omega_n^s)} W_h^m + \int_{\Omega_{h,\mathrm{pm}}^r(t_m)} \nu_{\mathrm{pm}} (\boldsymbol{B}^r)^\perp \cdot \mathbf{grad}\, W_h^m$$

for every $W_h^m \in \mathfrak{X}_h^m$.

Remark 4.16. *Additionally, from Problem 4.15 we define problems $(SP)_{h,\boldsymbol{B}^r}$ and $(SP)_{h,i}$, the first one with sources given only in terms of the remanent flux in permanent magnets (and thus*

$i_n(t) \equiv 0$, $n = 1, \ldots, N_c$), and the second problem with sources only in the stator coils (and therefore the permanent magnet region is replaced with a magnetically linear material with permeability $\nu_{\rm pm}$). These auxiliar problems will be used for the numerical analysis of the optimal control problem.

The following theorems can be proved:

Theorem 4.17. *Problem 4.15 has a unique solution $A_h(t_m) \in \mathfrak{X}_h^m$ for every $m = 0, \ldots, M-1$. Moreover, there exist a constant $C > 0$, not depending on the data or h, such that, for every $m = 0, \ldots, M-1$,*

$$||A_h(t_m)||_{\mathrm{H}^1(\Omega_h)} \leq C \left(\sum_{n=1}^{N_c} |i_n(t_m)| + \nu_{\rm pm} ||\boldsymbol{B}^r(0)||_{\mathrm{L}^2\left(\Omega^r_{h,\rm pm}(0)\right)^3} \right).$$

Theorem 4.18. *Let $A(t_m) \in \mathrm{H}_0^1(\Omega)$ and $A_h(t_m) \in \mathfrak{X}_h^m$ be the solutions to Problems 4.2 and 4.15, respectively, for $m = 0, \ldots, M-1$. Then,*

$$||A(t_m) - A_h(t_m)||_{\mathrm{H}^1(\Xi_h(t_m))} \leq C(\mu, \Omega) h |A(t_m)|_{\mathrm{H}^2(\Xi)},$$

where $\Xi_h(t_m) := \bigcup_{\substack{K \in \mathcal{T}_h^m, \\ K \subset \overline{\Xi}}} K$ (see [42], Remark 3.2.2).

4.4.2 Discretization of the Optimal Control Problem

Let $S_{t_m,h} : \mathbb{R}^{N_c} \longrightarrow \mathfrak{X}_h^m$ be the discrete control-to-state operator for each $m = 0, \ldots, M-1$, which are affine mappings. In a similar way to the continuous case, since Problem 4.15 is linear, its solutions can be expressed as the linear combinations $S_{t_m,h}(\mathbf{K}) = L_{t_m,h}(\mathbf{K}) + A_{h,\boldsymbol{B}^r}(t_m)$, with $L_{t_m,h}$ the linear discrete control-to-state operators for Problem $(SP)_{h,\boldsymbol{i}}$ and $A_{h,\boldsymbol{B}^r}$ the solutions to Problem $(SP)_{h,\boldsymbol{B}^r}$ (see Remark 4.16). Since $L_{t_m,h}$ are linear and bounded, $L_{t_m,h}$ are continuous, and the same is true for the control-to-state operators $S_{t_m,h}$.

Let G_h be the discrete integral operator

$$G_h(\boldsymbol{I}) := \tau_d - \frac{1}{M} \sum_{m=0}^{M-1} \nu_0 \int_\Gamma (\mathbf{grad}\, A_h(t_m) \cdot \boldsymbol{r}) \, (\mathbf{grad}\, A_h(t_m) \times \boldsymbol{n}) \cdot \boldsymbol{e}_z$$

with $A_h(t_m)$ the solution to Problem 4.15 at time $t_m \in [0, T]$, $m = 0, \ldots, M-1$, with currents $i_n(t) = I_n \cos(\omega t + \alpha_n)$, $n = 1, \ldots, N_c$. Then, the discrete optimal control problem reads:

Problem 4.19.

$$\min_{\boldsymbol{I}_h \in \mathcal{U}_{feas,h}} \mathcal{J}(\boldsymbol{I}_h) := \sum_{n=1}^{N_c} \frac{I_{h,n}^2}{2\,\mathrm{meas}(\Omega_n^s)\sigma},$$

where

$$\mathcal{U}_{feas,h} = \left\{ \boldsymbol{I}_h \in \mathcal{U}_{ad} : G_h(\boldsymbol{I}_h) \leq 0 \right\}.$$

Remark 4.20. *The space $\mathfrak{X}_h^m$ is a subspace of*

$$\mathrm{H}^2(\Omega, \mathcal{T}_h^m) := \left\{ \psi_h \in \mathrm{L}^2(\Omega) \,:\, \psi_h|_K \in \mathrm{H}^2(K) \quad \forall K \in \mathcal{T}_h^m \right\},$$

for $m = 0, \ldots, M-1$ (see Section 4.4 in [88]). Consequently, G_h is well-defined for every $\mathbf{K} \in \mathbb{R}^{N_c}$.

In a similar way to the continuous case, we can proof by the Weierstrass theorem that:

Theorem 4.21. *If $\mathcal{U}_{feas,h}$ is nonempty, Problem 4.19 has at least one optimal control $\overline{\boldsymbol{I}}_h$.*

In order to perform the numerical analysis of the optimal control problem, first we will proof the convergence of the operator associated to the discrete state restriction to the continuous one.

Lemma 4.22. *Given $\mathbf{K} \in \mathbb{R}^{N_c}$, $G_h(\mathbf{K}) \to G(\mathbf{K})$ as $h \to 0$.*

Proof. Given $\mathbf{K} \in \mathbb{R}^{N_c}$, let $A(t_m)$ and $A_h(t_m)$, $m = 0, \ldots, M-1$, be the associated solutions to Problems 4.2 and 4.15, respectively.

$$\begin{aligned}
|G_h(\mathbf{K}) - G(\mathbf{K})| = \Bigg| \frac{\nu_0}{M} \sum_{m=0}^{M-1} \int_\Gamma & (\mathbf{grad}\, A(t_m) \cdot \boldsymbol{r})\, (\mathbf{grad}\, A(t_m) \times \boldsymbol{n}) \cdot \boldsymbol{e}_z \\
& - (\mathbf{grad}\, A_h(t_m) \cdot \boldsymbol{r})\, (\mathbf{grad}\, A_h(t_m) \times \boldsymbol{n}) \cdot \boldsymbol{e}_z \Bigg| \\
\leq C \sum_{m=0}^{M-1} \sum_{\substack{K \in \mathcal{T}_h^m, \\ K \cap \Gamma \neq \emptyset}} & ||A_h(t_m)||_{\mathrm{H}^2(K)} ||A(t_m) - A_h(t_m)||_{\mathrm{H}^1(K)} \\
& + ||A(t_m)||_{\mathrm{H}^2(K)} ||A(t_m) - A_h(t_m)||_{\mathrm{H}^1(K)} \\
\leq Ch \sum_{m=0}^{M-1} & |A(t_m)|_{\mathrm{H}^2(\Xi)} ||A(t_m)||_{\mathrm{H}^2(\Xi)} \to 0 \quad \text{as } h \to 0,
\end{aligned}$$

for every $m = 0, \ldots, M-1$. □

Theorem 4.23. *Let us assume that there exists a solution $\widetilde{\boldsymbol{I}}$ to the optimal control problem 4.6 satisfying (CQ). Let $\{\boldsymbol{I}_h\}_{h>0}$ be a sequence of optimal controls of Problem 4.19. There exists a subsequence of $\{\boldsymbol{I}_h\}_{h>0}$ converging in $\mathbb{R}^{N_c}$ towards an optimal control of Problem 4.6 as $h \to 0$. Every convergent subsequence of $\{\boldsymbol{I}_h\}_{h>0}$ converges in $\mathbb{R}^{N_c}$ towards an optimal control of Problem 4.6 as $h \to 0$.*

Proof. Given $\{\boldsymbol{I}_h\}_{h>0}$ sequence of optimal controls of Problem 4.19, $\boldsymbol{I}_h \in \mathcal{U}_{feas,h}$ for every $h > 0$, and thus $\{\boldsymbol{I}_h\}_{h>0}$ is bounded. Then, $\{\boldsymbol{I}_h\}_{h>0}$ has a convergent subsequence (which will also be denoted by $\{\boldsymbol{I}_h\}_{h>0}$), $\boldsymbol{I}_h \to \boldsymbol{I}$ as $h \to 0$. Since $|I_{n,h}| \leq I_{max}$ and $G_h(\boldsymbol{I}_h) \leq 0$ for every $h > 0$, taking Lemma 4.22 and the fact that G is continuous into account, we conclude that $\boldsymbol{I} \in \mathcal{U}_{feas}$.

- If $G(\widetilde{\boldsymbol{I}}) < 0$, since $G_h(\widetilde{\boldsymbol{I}}) \to G(\widetilde{\boldsymbol{I}})$ as $h \to 0$, there exists an $h_0 > 0$ such that $G_h(\widetilde{\boldsymbol{I}}) < 0$ for every $h \in (0, h_0)$. Then, $\widetilde{\boldsymbol{I}} \in \mathcal{U}_{feas,h}$ for every $h \in (0, h_0)$, and then $\mathcal{J}(\boldsymbol{I}_h) \leq \mathcal{J}(\widetilde{\boldsymbol{I}})$ for every $h \in (0, h_0)$. Thus,

$$\mathcal{J}(\boldsymbol{I}) = \lim_{h\to 0} \mathcal{J}(\boldsymbol{I}_h) \leq \mathcal{J}(\widetilde{\boldsymbol{I}}).$$

- If $G(\widetilde{\boldsymbol{I}}) = 0$, let $\widetilde{\boldsymbol{I}}_h := \widetilde{\boldsymbol{I}} + s(h)\boldsymbol{I}_0$, with $s(h) \geq 0$ to be defined later. Then,

  $$G_h(\widetilde{\boldsymbol{I}}_h) = G_h(\widetilde{\boldsymbol{I}}) + DG_h(\widetilde{\boldsymbol{I}})s(h)\boldsymbol{I}_0 + o(h) = G_h(\widetilde{\boldsymbol{I}}) - G(\widetilde{\boldsymbol{I}}) + s(h)DG_h(\widetilde{\boldsymbol{I}})\boldsymbol{I}_0 + o(h).$$

  Let us denote $\Delta(h) := G_h(\widetilde{\boldsymbol{I}}) - G(\widetilde{\boldsymbol{I}}) + o(h)$, $\delta(h) := DG_h(\widetilde{\boldsymbol{I}})\boldsymbol{I}_0$ and take, for any given $h > 0$,

  $$s(h) := \begin{cases} 0 & \text{if } \Delta(h) \leq 0, \\ -\frac{\Delta(h)}{\delta(h)} & \text{if } \Delta(h) > 0. \end{cases}$$

  Then,
  - Let $\varepsilon < 0$ such that $DG(\widetilde{\boldsymbol{I}})\boldsymbol{I}_0 \leq 2\varepsilon < 0$, there exists $h_0 > 0$ such that $DG_h(\widetilde{\boldsymbol{I}})\boldsymbol{I}_0 \leq \varepsilon < 0$ for every $h \in (0, h_0)$. Therefore,

    $$\left|\frac{1}{\delta(h)}\right| = -\frac{1}{\delta(h)} = -\frac{1}{DG_h(\widetilde{\boldsymbol{I}})\boldsymbol{I}_0} \leq \frac{1}{\varepsilon}$$

    for every $h \in (0, h_0)$. Taking Lemma 4.22 into account, it is clear that $\Delta(h) \to 0$ as $h \to 0$, and then $s(h) \to 0$ as $h \to 0$.
  - Taking the definition of $\boldsymbol{I}_0$ into account, there exists $h_0 > 0$ such that $\widetilde{\boldsymbol{I}}_h \in \mathcal{U}_{ad}$ for every $h \in (0, h_0)$.
  - From the definition of $s(h)$, we have that $G_h(\widetilde{\boldsymbol{I}}_h) = \Delta(h) + s(h)\delta(h) \leq 0$ for every $h > 0$.

  Consequently, $\widetilde{\boldsymbol{I}}_h \to \widetilde{\boldsymbol{I}}$ as $h \to 0$ and $\widetilde{\boldsymbol{I}}_h \in \mathcal{U}_{feas,h}$ for every $h \in (0, h_0)$ (and then $\mathcal{J}(\boldsymbol{I}_h) \leq \mathcal{J}(\widetilde{\boldsymbol{I}}_h)$ for every $h \in (0, h_0)$). Thus,

  $$\mathcal{J}(\boldsymbol{I}) = \lim_{h\to 0} \mathcal{J}(\boldsymbol{I}_h) \leq \lim_{h\to 0} \mathcal{J}(\widetilde{\boldsymbol{I}}_h) = \mathcal{J}(\widetilde{\boldsymbol{I}}).$$

Therefore, in both cases $\boldsymbol{I}$ is an optimal control of Problem 4.6. □

The Lagrangian function associated to Problem 4.19 is

$$\mathcal{L}_h : \mathbb{R}^{N_c} \times \mathbb{R}^J \longrightarrow \mathbb{R}, \quad \mathcal{L}_h(\boldsymbol{I}_h; \lambda_h) := \mathcal{J}(\boldsymbol{I}_h) + \lambda_h \cdot G_h(\boldsymbol{I}_h).$$

In the following theorem we state the conditions for the existence of a discrete Lagrange multiplier associated to the solutions to Problem 4.19 converging to a continuous solution that satisfies the Slater condition. Since the constraint qualification is preserved under perturbation, its proof is analogous to that of the continuous case.

Theorem 4.24. *Let $\{\overline{\boldsymbol{I}}_h\}$ be a sequence of local solutions to the optimal control problem 4.19, $\{\overline{\boldsymbol{I}}_h\} \to \overline{\boldsymbol{I}}$ as $h \to 0$, $\overline{\boldsymbol{I}}$ satisfying (CQ). Then, for h sufficiently small, there exists a Lagrange multiplier λ_h^* associated with $\overline{\boldsymbol{I}}_h$. Moreover, the set of Lagrange multipliers associated with $\overline{\boldsymbol{I}}_h$ is bounded.*

Let us recall that $D\mathcal{J} : \mathbb{R}^{N_c} \longrightarrow \mathbb{R}$,

$$D\mathcal{J}(\mathbf{K})\mathbf{h} = \sum_{n=1}^{Nc} \frac{K_n h_n}{\text{meas}(\Omega_n^s)\sigma}.$$

Then,

$$\begin{aligned} D_I\mathcal{L}_h(\overline{\boldsymbol{I}};\lambda^*)(\boldsymbol{I}-\overline{\boldsymbol{I}}) = &\sum_{n=1}^{Nc} \frac{\overline{I}_n(I_n-\overline{I}_n)}{\text{meas}(\Omega_n^s)\sigma} \\ &- \lambda^* \frac{1}{M} \sum_{m=0}^{M-1} \nu_0 \int_\Gamma (\mathbf{grad}\, L_{t_m,h}(\boldsymbol{I}-\overline{\boldsymbol{I}})\cdot\boldsymbol{r})(\mathbf{grad}\, S_{t_m,h}(\overline{\boldsymbol{I}})\times\boldsymbol{n})\cdot\boldsymbol{e}_z \\ &+ (\mathbf{grad}\, S_{t_m,h}(\overline{\boldsymbol{I}})\cdot\boldsymbol{r})(\mathbf{grad}\, L_{t_m,h}(\boldsymbol{I}-\overline{\boldsymbol{I}})\times\boldsymbol{n})\cdot\boldsymbol{e}_z. \end{aligned}$$

To simplify the second term in $D_I\mathcal{L}_h$, let us introduce the discrete adjoint problem:

Problem 4.25. *Given $A_h(t_m) \in \mathfrak{X}_h^m$ for every $m = 0,\dots,M-1$ and $\lambda \in \mathbb{R}$, find $P_h(t_m) \in \mathfrak{X}_h^m$ for every $m = 0,\dots,M-1$ such that*

$$\begin{aligned} \int_{\Omega_h(t_m)} &\nu\, \mathbf{grad}\, P_h(t_m)\cdot\mathbf{grad}\, W_h^m \\ &= -\lambda\frac{1}{M}\sum_{m=0}^{M-1}\nu_0\int_\Gamma(\mathbf{grad}\, W_h\cdot\boldsymbol{r})(\mathbf{grad}\, A_h(t_m)\times\boldsymbol{n})\cdot\boldsymbol{e}_z \\ &\quad + (\mathbf{grad}\, A_h(t_m)\cdot\boldsymbol{r})(\mathbf{grad}\, W_h\times\boldsymbol{n})\cdot\boldsymbol{e}_z \end{aligned}$$

for every $W_h^m \in \mathfrak{X}_h^m$.

Using the usual finite element method techniques, the following result can be proved:

Lemma 4.26. *Problem 4.25 has a unique solution $P_h(t_m) \in \mathfrak{X}_h^m$, $m = 0,\dots,M-1$, which satisfies*

$$\lim_{h\to 0} ||P(t_m) - P_h(t_m)||_{\mathrm{H}^1(\Omega)} = 0$$

for every $m = 0,\dots,M-1$. Moreover, if $P(t_m) \in \mathrm{H}^2(\Omega_n^s)$, $n = 1,\dots,N_c$, $m = 0,\dots,M-1$,

$$||P(t_m) - P_h(t_m)||_{\mathrm{H}^1(\Omega_n^s)} \le Ch|P(t_m)|_{\mathrm{H}^2(\Omega_n^s)}.$$

In the following lemma, whose proof is similar to the corresponding one in the continuous case, we state that the second term in $D_I\mathcal{L}_h$ can be expressed in terms of the adjoint state.

Lemma 4.27. *Let* $\mathbf{K}, \mathbf{h} \in \mathbb{R}^{N_c}$*, and* $A_h^{\mathbf{K}}(t_m), A_h^{\mathbf{h}}(t_m)$, $m = 0, \ldots, M-1$*, the associated weak solutions to Problem 4.15 with currents* $i_n(t) = K_n \cos(\omega t + \alpha_n)$, $n = 1, \ldots, N_c$*, and* $(SP)_{h,\boldsymbol{i}}$ *with currents* $i_n(t) = h_n \cos(\omega t + \alpha_n)$, $n = 1, \ldots, N_c$*, respectively. Then, the solutions* $P_h(t_m)$, $m = 0, \ldots, M-1$*, to Problem 4.25 with data* $A_h^{\mathbf{K}}(t_m)$ *and* λ *are such that:*

$$\frac{1}{M}\sum_{m=0}^{M-1}\sum_{n=1}^{N_c}\int_{\Omega_n^s}\frac{h_n\cos(\omega t_m+\alpha_n)}{\operatorname{meas}(\Omega_n^s)}P_h(t_m)$$
$$= -\lambda\frac{1}{M}\sum_{m=0}^{M-1}\int_{\Gamma}(\mathbf{grad}\, A_h^{\mathbf{h}}(t_m)\cdot\boldsymbol{r})(\mathbf{grad}\, A_h^{\mathbf{K}}(t_m)\times\boldsymbol{n})\cdot\boldsymbol{e}_z$$
$$+(\mathbf{grad}\, A_h^{\mathbf{K}}(t_m)\cdot\boldsymbol{r})(\mathbf{grad}\, A_h^{\mathbf{h}}(t_m)\times\boldsymbol{n})\cdot\boldsymbol{e}_z.$$

Remark 4.28. *As we will show in Section 4.6, we have numerically checked that the discrete controls converge with order 1 to the continuous one. Although we have not obtained this result theoretically, it seems that under appropriate assumptions on the continuous locally optimal control* $\overline{\boldsymbol{I}}$*, the approximation order of the state and the adjoint state should transfer to the approximated currents* $\{\overline{\boldsymbol{I}}_h\}_{h>0}$.

4.5 Implementation Issues

In order to solve the optimality system, we have implemented a MATLAB code that solves the control problem by means of an *Augmented Lagrangian Technique* (also known as *Multiplier Penalty Method*) similar to the one described in Section 5.4.2 in [51] (see also Section 17.3 in [81]). Firstly, we have replaced the inequality state constraint with an equality constraint in the following way:

Problem 4.29.

$$\min \mathcal{J}(\boldsymbol{I}) \quad \textit{subject to} \quad G_h(\boldsymbol{I}) + s^2 = 0,\ \boldsymbol{I} \in \mathcal{U}_{ad}, s \in \mathbb{R}.$$

Consequently, the Multiplier-Penalty-function associated to this problem is:

$$\overline{\mathcal{L}}_h(\boldsymbol{I}, s, \lambda; \alpha) := \mathcal{J}(\boldsymbol{I}) + \lambda\left(G_h(\boldsymbol{I}) + s^2\right) + \frac{\alpha}{2}\left(G_h(\boldsymbol{I}) + s^2\right)^2.$$

If the minimization with respect to variable s is carried out exactly, we finally obtain the following function:

$$\widehat{\mathcal{L}}_h(\boldsymbol{I}, \lambda; \alpha) := \mathcal{J}(\boldsymbol{I}) + \frac{1}{2\alpha}\left(\max\left\{0, \lambda + \alpha G_h(\boldsymbol{I})\right\}^2 - \lambda^2\right). \tag{4.10}$$

Therefore, we are going to solve a series of box-constrained problems with objective function $\widehat{\mathcal{L}}_h$, each of them having α and λ fixed. In order to do this, a conjugate gradient method was used, with search direction $\overline{\psi}_k$ computed with the Hestenes-Stiefel formula (see Remark 4.30)

and a step length r_k computed as described in [78]; in particular, the step length fulfills the strong Wolfe-Powell conditions. Therefore, $\overline{\psi}_k$ is computed as

$$\overline{\psi}_k = -\mathbf{grad}_{\boldsymbol{I}}\widehat{\mathcal{L}}_h(\boldsymbol{I}_k, \lambda_k; \alpha_k) + \beta_k \overline{\psi}_{k-1},$$
$$\text{with } \beta_k = \frac{\mathbf{grad}_{\boldsymbol{I}}\widehat{\mathcal{L}}_h(\boldsymbol{I}_k, \lambda_k; \alpha_k)^\top \left(\mathbf{grad}_{\boldsymbol{I}}\widehat{\mathcal{L}}_h(\boldsymbol{I}_k, \lambda_k; \alpha_k) - \mathbf{grad}_{\boldsymbol{I}}\widehat{\mathcal{L}}_h(\boldsymbol{I}_{k-1}, \lambda_k; \alpha_k)\right)}{||\mathbf{grad}_{\boldsymbol{I}}\widehat{\mathcal{L}}_h(\boldsymbol{I}_k, \lambda_k; \alpha_k)||^2},$$

and r_k is such that

$$\widehat{\mathcal{L}}_h(\boldsymbol{I}_k + r_k\overline{\psi}_k, \lambda_k; \alpha_k) \leq \widehat{\mathcal{L}}_h(\boldsymbol{I}_k, \lambda_k; \alpha_k) + C_1 r_k \mathbf{grad}_{\boldsymbol{I}}\widehat{\mathcal{L}}_h(\boldsymbol{I}_k, \lambda_k; \alpha_k)^\top \overline{\psi}_k,$$
$$\left\|\mathbf{grad}_{\boldsymbol{I}}\widehat{\mathcal{L}}_h(\boldsymbol{I}_k + r_k\overline{\psi}_k, \lambda_k; \alpha_k)^\top \overline{\psi}_k\right\| \leq C_2 \left\|\mathbf{grad}_{\boldsymbol{I}}\widehat{\mathcal{L}}_h(\boldsymbol{I}_k, \lambda_k; \alpha_k)^\top \overline{\psi}_k\right\|,$$

for some constants $C_1, C_2 \in (0, 1)$. The implementation of the algorithm in [78] was retrieved from `www.cs.umd.edu/users/oleary/software/`. We notice that, concerning the search direction $\overline{\psi}_k$, if the current iterant $\boldsymbol{I}_k$ is at the boundary of the box-constrained admissible set, the corresponding search direction component is set to zero if it points outwards. Moreover, as initial conditions we have considered $\beta_0 = 0$ and

$$r_0 = r_{k-1}\frac{\mathbf{grad}_{\boldsymbol{I}}\widehat{\mathcal{L}}_h(\boldsymbol{I}_{k-1}, \lambda_{k-1}; \alpha_k)^\top \overline{\psi}_{k-1}}{\mathbf{grad}_{\boldsymbol{I}}\widehat{\mathcal{L}}_h(\boldsymbol{I}_k, \lambda_k; \alpha_k)^\top \overline{\psi}_k}.$$

After each minimization, the parameter α is increased if there is not a sufficient decrease in the state constraint violation. The corresponding minimization algorithm is described in Algorithm 1, where $\{\boldsymbol{e}_i,\ i = 1, \ldots, N\}$, is the canonical basis of $\mathbb{R}^N$.

Remark 4.30. *In order to choose the method to perform the minimization of $\widehat{\mathcal{L}}_h(\boldsymbol{I}, \lambda; \alpha)$ with respect to $\boldsymbol{I}$, we decided to follow a line-search strategy. The main idea under this family of methods is to choose, at each inner iteration k, a direction $\boldsymbol{p}_k$ and search along this direction from the current iterate $\boldsymbol{I}_k$ for a new iterate with a lower value of the function to minimize. The distance s_k to move along $\boldsymbol{p}_k$, known as step-length, can be found by solving the one-dimensional problem*

$$\min_{s>0} \widehat{\mathcal{L}}_h(\boldsymbol{I}_k + s\boldsymbol{p}_k, \lambda; \alpha)$$

either exactly or approximately; we recall that both λ and α are fixed at each outer iteration of the Augmented Lagrangian algorithm. Therefore, to specify a particular line-search method we need to set the procedure to select directions $\mathbf{p}_k$ and step-lengths s_k.
For the search direction, we compared some of the common choices appearing in the related literature, in order to asses which one was more suitable for our particular problem. Specifically, we studied the performance of the steepest descent method, the nonlinear conjugate gradient direction computed with Hestenes-Stiefel formula and the quasi-newton direction $\boldsymbol{p}_k = -H_k \mathbf{grad}_{\boldsymbol{I}}\widehat{\mathcal{L}}_h$, with H_k computed with a BFGS modified method that ensures that these matrices are positive definite (see [83]). In Table 4.1 we compare the performance in terms of iterations and computation time of these three algorithms in a simple case with only two controls, for which the conjugate gradient techniques performs better.

Algorithm 1: Optimization Algorithm

Data: $\boldsymbol{I}_0 \in \mathbb{R}^{N_c}$, $\lambda_0, I_{max} \in \mathbb{R}$, $\alpha_0 > 0$, $c \in (0,1)$
Result: $\boldsymbol{I}_{k+1}, \lambda_{k+1}$

```
while isOptimal (I_k, λ_k, I_max) == false do
    I_{k+1} ⟵ minimizeMultiplierPenaltyFunction (I_k, λ_k, α_k, I_max);
    λ_{k+1} ⟵ max{0, λ_k + α_k G_h(I_{k+1})};
    if enoughConstraintDecrease (I_{k+1}, I_k, λ_{k+1}, λ_k, α_k, c) == false then
        α_{k+1} = 10 α_k;
    end
end
```

Function isOptimal($\boldsymbol{I}_k$,λ_k, I_{max})

Data: $\boldsymbol{I}_k$, λ_k, I_{max}
Result: $flag$

```
if |λ_k G_h(I_k)| > 0 then
    flag ⟵ false;
else if λ_k < 0 then
    flag ⟵ false;
else if isStationary (L_h, I_k, λ_k, I_max) == false then
    flag ⟵ false;
else
    flag ⟵ true;
end
```

Function isStationary(F, $\boldsymbol{I}_k$, λ_k, I_{max})

Data: F, $\boldsymbol{I}_k$, λ_k, I_{max}
Result: $flag$

if $\boldsymbol{I}_k \in (-I_{max}, I_{max})^{N_c} \wedge |\nabla_{\boldsymbol{I}} F(\boldsymbol{I}_k, \lambda_k)| > 0$ **then**
  $flag \longleftarrow$ `false`;
else if $\boldsymbol{I}_k \in \partial[-I_{max}, I_{max}]^{N_c}$ **then**
  $flag \longleftarrow$ `true`;
  for $i = 1$ **to** N_c **do**
    if $(\boldsymbol{I}_k(i) = I_{max}) \wedge (\nabla_{\boldsymbol{I}} F(\boldsymbol{I}_k, \lambda_k)\boldsymbol{e}_i > 0)$ **then**
      $flag \longleftarrow$ `false`;
      break;
    else if $(\boldsymbol{I}_k(i) = -I_{max}) \wedge (\nabla_{\boldsymbol{I}} F(\boldsymbol{I}_k, \lambda_k)\boldsymbol{e}_i < 0)$ **then**
      $flag \longleftarrow$ `false`;
      break;
    else if $|\nabla_{\boldsymbol{I}} F(\boldsymbol{I}_k, \lambda_k)\boldsymbol{e}_i| > 0$ **then**
      $flag \longleftarrow$ `false`;
      break;
  end
else
  $flag \longleftarrow$ `true`;
end

Function enoughConstraintDecrease($\boldsymbol{I}_{k+1}$, $\boldsymbol{I}_k$, λ_{k+1}, λ_k, α_k, c)

Data: $\boldsymbol{I}_{k+1}$, $\boldsymbol{I}_k$, λ_{k+1}, λ_k, α_k, c
Result: $flag$

$h_k \longleftarrow \max\{G_h(\boldsymbol{I}_k), -\lambda_k/\alpha_k\}$;
$h_{k+1} \longleftarrow \max\{G_h(\boldsymbol{I}_{k+1}), -\lambda_{k+1}/\alpha_k\}$;
if $|h_{k+1}| \geq c|h_k|$ **then**
  $flag \longleftarrow$ `false`;
else
  $flag \longleftarrow$ `true`;
end

	Steepest Descent	Modified BFGS	Conjugate Gradient
Outer Iterations	6	5	6
Inner Iterations (sum)	83	49	31
CPU Time (s)	1473	1129	614

Table 4.1: Performance of different line-search methods.

Function minimizeMultiplierPenaltyFunction($\boldsymbol{I}_k$, λ_k, α_k, I_{max})

Data: $\boldsymbol{I}_k$, λ_k, α_k, I_{max}
Result: $\boldsymbol{I}_{k+1}$

$\boldsymbol{I}_0 \longleftarrow \boldsymbol{I}_k$;
$\overline{\psi}_0 \longleftarrow -\nabla_{\boldsymbol{I}} \widehat{\mathcal{L}}_h(\boldsymbol{I}_0, \lambda_k; \alpha_k)$;
$\ell_0 \longleftarrow \nabla_{\boldsymbol{I}} \widehat{\mathcal{L}}_h(\boldsymbol{I}_0, \lambda_k; \alpha_k)$;
while `isStationary` ($\widehat{\mathcal{L}}_h$, $\boldsymbol{I}_k$, λ_k, I_{max}) == `false` **do**
  for $i = 1$ **to** N_c **do**
    if $\boldsymbol{I}_j(i) = I_{max} \wedge \overline{\psi}_j(i) > 0$ **then**
      $\overline{\psi}_j(i) \longleftarrow 0$;
    else if $\boldsymbol{I}_j(i) = -I_{max} \wedge \overline{\psi}_j(i) < 0$ **then**
      $\overline{\psi}_j(i) \longleftarrow 0$;
  end
  $s_{j+1} \longleftarrow$ `lineSearch`$(\boldsymbol{I}_j, \lambda_k, \alpha_k, \overline{\psi}_k)$;
  $\boldsymbol{I}_{j+1} \longleftarrow \boldsymbol{I}_j + s_{j+1}\overline{\psi}_j$;
  $\ell_{j+1} \longleftarrow \nabla_{\boldsymbol{I}} \widehat{\mathcal{L}}_h(\boldsymbol{I}_{j+1}, \lambda_k; \alpha_k)$;
  $\beta_{j+1} \longleftarrow \left(\ell_{j+1}^{\top}(\ell_{j+1} - \ell_j)\right) / ||\ell_{j+1}||^2$;
  $\overline{\psi}_{j+1} \longleftarrow -\nabla_{\boldsymbol{I}} \widehat{\mathcal{L}}_h(\boldsymbol{I}_{j+1}, \lambda_k; \alpha_k) + \beta_{j+1}\overline{\psi}_j$;
end

4.6 Numerical Results

In this section we report the numerical results obtained for an academic permanent magnet synchronous motor (see Figure 4.3).

The stator consists of $N_c = 6$ rectangular coils and a linear magnetic core with relative magnetic permeability $\mu_r = 100$. Each coil supports a uniformly distributed current $i_n(t) = I_n \cos(\omega t + \alpha_n)$ A, $n = 1, \ldots, 6$, has the magnetic permeability of the vacuum, $\mu = \mu_0 = 4\pi \times 10^{-7}\ H/m$, and an electrical conductivity equal to $5.96 \times 10^7\ (\Omega \cdot m)^{-1}$. On the other hand, the rotor consists of two permanent magnets with relative magnetic permeability $\mu_r = 1.096$ and remanent fluxes with modulus $|\boldsymbol{B}^r| = 1.26\ T$ and oriented parallel to $-\boldsymbol{e}_y$ at time $t = 0$ seconds. Moreover, the material of the rotor's magnetic core is the same as that of the stator. Finally, the shaft of the machine, the air-gap between rotor and stator, and the air surrounding the machine will have a

magnetic permeability $\mu = \mu_0$. Moreover, the angular frequency of the current is $\omega = 2\pi f$ with $f = 50\ Hz$, and therefore the rotor speed is 3000 rpm.

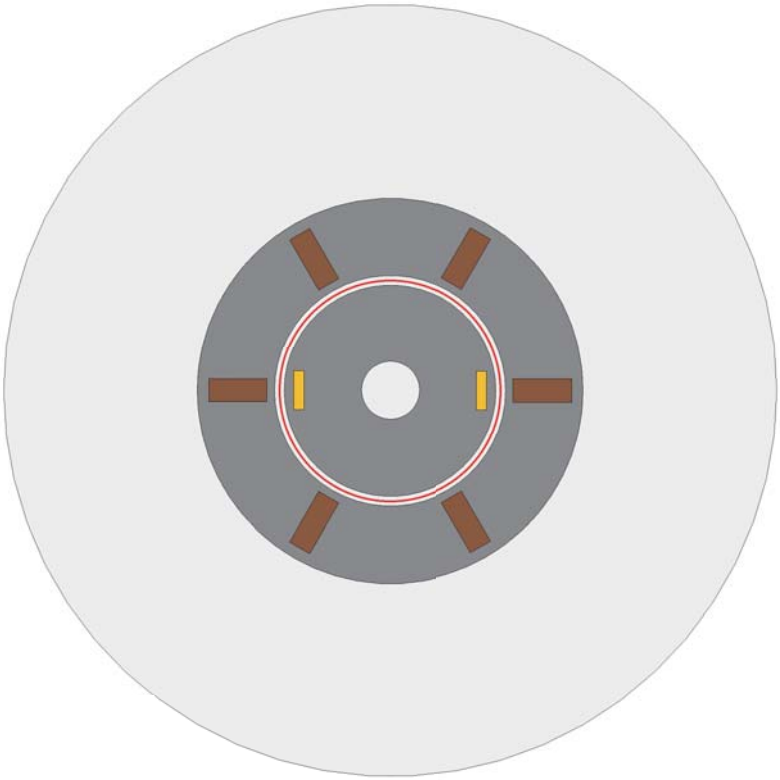

Figure 4.3: Geometrical setting for the numerical results.

We will impose the torque on the rotor to be above a certain threshold τ_d:

$$G(\boldsymbol{I}) := \tau_d - \frac{1}{M}\sum_{m=0}^{M-1} \nu_0 \int_\Gamma (\mathbf{grad}\, A(t_m) \cdot \boldsymbol{r})\, (\mathbf{grad}\, A(t_m) \times \boldsymbol{n}),$$

with $A(t_m)$ the solutions to Problem 4.2 (see Remark 4.7).

To the authors' knowledge, the presented problem has no analytical solution. Therefore, the solution computed in a mesh with a very high number of degrees of freedom has been used as an *approximate exact solution* to show the convergence orders. In Figure 4.4 – left we show the $O(h^2)$ convergence rate for the solution to the state problem at time $t = 0$ seconds in Ξ, which is one order above the $O(h)$ rate proved in the theoretical results. Moreover, in Figure 4.4 – right we show that an order $O(h)$ is attained in this particular example for the state constraint (that is, a mean average of the magnetic torque over the rotor).

Finally, in Figure 4.5 we show that the optimal control $\boldsymbol{I}_h$ and the associated lagrange multiplier λ_h converge with order $O(h)$.

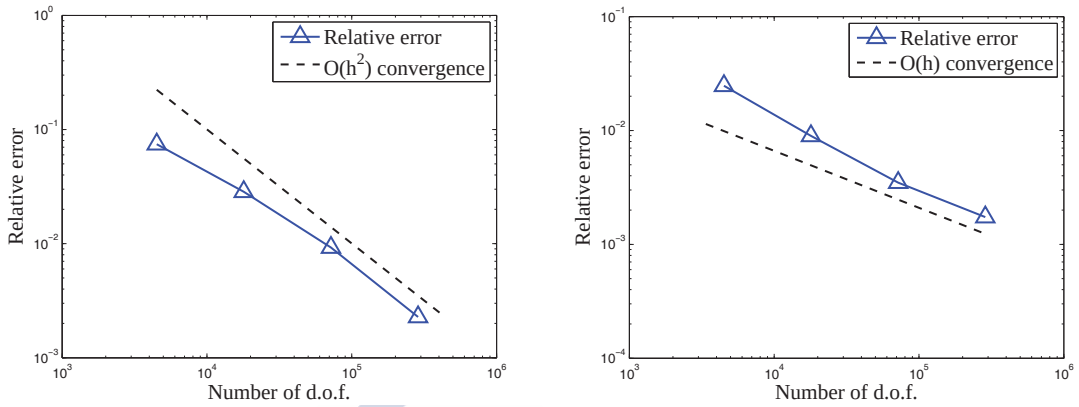

Figure 4.4: Convergence order for $A_h(0)$ in $\mathrm{H}^1(\Xi)$ (left). Convergence order for G_h (right).

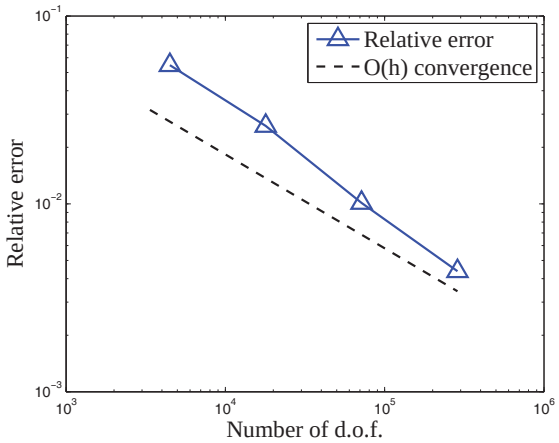

Figure 4.5: Convergence order for $\boldsymbol{I}_h + \lambda_h$.

USC
UNIVERSIDADE
DE SANTIAGO
DE COMPOSTELA

Chapter 5

A Numerical Method for Accelerating the Computation of the Steady-State in Induction Machines

5.1 Introduction

This chapter deals with the finite element approximation of the steady-state behaviour of squirrel cage induction machines by using a fast numerical procedure. For this purpose, a numerical method to compute periodic solutions by determining suitable initial currents in the rotor bars is developed, shortening the transient part of the solution considerably, so that the steady-state is reached in a reduced number of cycles.

Generally, the numerical simulation of induction electrical machines by using finite element methods requires solving a nonlinear system of partial differential equations derived from Maxwell equations, coupled with electrical circuits and mechanical equations; see, for instance, [86, 93] and references therein. The resulting mathematical model is a transient problem that needs to be provided with initial conditions which are neither known a priori, nor easy to obtain.. When unappropriate values are prescribed for these conditions (for instance, when they are set to zero), a very long CPU time is needed to reach the steady-state solution. Considering that, in most cases, the transient part of the solution is not meaningful, techniques allowing us to compute the steady solution in the shortest possible time are in high demand, and, in particular, those determining suitable initial conditions.

In the literature, we can find different approaches to the problem of reducing the computational cost to reach the steady-state in the numerical simulation of induction motors. The worst case scenario would be what is known as *brute-force method*, which consists in starting with zero initial conditions and letting the simulation advance in time until the steady-state is reached. In this case, several days of simulation may be needed, even with the performance of modern computers. In recent years, different approaches have been developed to address the problem we

are considering. For example, the so-called *Time Periodic Finite Element Methods* (TPFEM) are based on writing the discretized problem in a time-interval in which its solution is periodic, and solving all time steps at the simultaneously (see [57, 79]). Even though this technique avoids the step-by-step simulation, it requires solving nonlinear systems with very large non-symmetric matrices. Therefore, parallelization techniques, which can be applied in space or time (see [98, 99]). Alternatively, in the *Time Periodic - Explicit Error Correction Methods* (TP-EEC), (see [61, 101]), and the *Time Differential Correction* (TDC), (see [75, 100]), convergence of the transient model is accelerated by incorporating error correction techniques already present in more general iterative methods, along with some properties of TPFEM. Finally, we highlight the methodology consisting in prescribing as initial conditions the ones obtained as the solution to a nonlinear eddy current problem in the frequency domain. The harmonic approximation is based on the hypothesis that the time variation of the fields can be written in terms of a complex exponential function, the nonlinear effects are taken into account by means of an *effective magnetization curve* and the rotor motion with an adjustment in the electrical conductivity of the rotor bars (see [96]).

A common obstacle for TPFEM, TP-EEC and TDC methods is choosing a suitable time interval in which the solution is assumed to be periodic. This is due to the fact that the magnetic fields in rotor and stator oscillate at different frequencies, and the common time at which both are periodic (the so-called *effective period*) is generally quite large. However, at the same time, the periodicity condition has to be defined in a small enough time interval for the method to be useful. In TPFEM methods, there are several strategies to deal with this restriction, most of them based on the spatio-temporal symmetries of the problem (see again [98, 99]). On the other hand, TP-EEC and TDC methods handle it by accelerating the convergence in both domains separately, or even only in one of them (see again [61]). In this regard, our methodology has the advantage of making use of the periodicity condition only in the rotor bars, so this limitation does not apply to our case. Moreover, the computational cost of our approach does not depend on the size of this period, and the number of unknowns is very small in comparison with the mentioned methods.

Thus, the main objective of this chapter will be to reduce the simulation time, so that the steady regime is reached in the shortest time possible by pre-computing suitable initial conditions. For this purpose, we will restrict ourselves to the case of an induction machine with squirrel cage rotor. The proposed methodology is inspired in the techniques introduced in [16] for a 2D transient magnetic model with sources given in terms of currents and voltage drops. In the present paper, we will extend some of the ideas proposed there to a case including motion of some parts of the domain and conductors in which neither currents nor voltage drops are known. Moreover, initial currents are sought in these conductors, what represents an additional difficulty.

This chapter is organized as follows. In Section 5.2 we state the problem to be solved, that consists of a transient 2D nonlinear distributed model coupled with a lumped one for the electrical circuit of the squirrel cage. Then, in Section 5.3 we will formally rewrite the problem as an implicit system of ODE in terms of the current in the rotor bars of the squirrel cage. Section 5.4 is devoted to the approximation of the initial condition corresponding to a periodic steady solution. For this purpose, we perform twice a time-integration of the reduced problem, neglect

some terms and approximate the currents in the rotor bars by their respective main harmonics. In Section 5.5 we validate the method with some numerical results that illustrate its performance. Moreover, in Section 5.6 we generalize the methodology to cover the multiharmonic case. Finally, in Appendix A we detail the computation of a Jacobian matrix that is useful for applying the presented methodology.

5.2 Mathematical Modeling

Let us consider the 2D bounded domain Ω, corresponding to the cross-section of a squirrel cage induction motor configuration at initial time (see Figures 5.1 and 5.2). Hence, domain Ω consists of N_c connected conductors (stator coil sides and rotor bars), the ferromagnetic core (in rotor and stator), the air between rotor and stator (air-gap), and the rotor shaft. We notice that the shaft is usually modeled as a non-conducting, magnetically linear domain, whose material has the vacuum reluctivity, ν_0, and thus it will be considered as if it was air. Moreover, we notice that we have considered that the domain boundary is the outer boundary of the stator, but the same methodology applies with no change to the case in which the motor is surrounded by an artificial box filled with air. Thus, we have

- Ω_0: domain occupied by air (white color in Figure 5.2).
- Ω_n, $n = 1, \ldots, N_c$: linear conductors representing the cross-sections of the rotor bars ($n = 1, \ldots, N_b$; grey color in Figure 5.2) and of the stator coil sides ($n = N_b + 1, \ldots, N_c$; blue, yellow and red colors in Figure 5.2).
- Ω_{nl}: non-conducting nonlinear magnetic cores (brown color in Figure 5.2).

In the methodology developed in this chapter, we will make a simplification based on assuming that the bars are stranded conductors, that is, conductors where the induced currents are distributed in an uniform way. In a similar way, we will also treat the stator coil sides as stranded

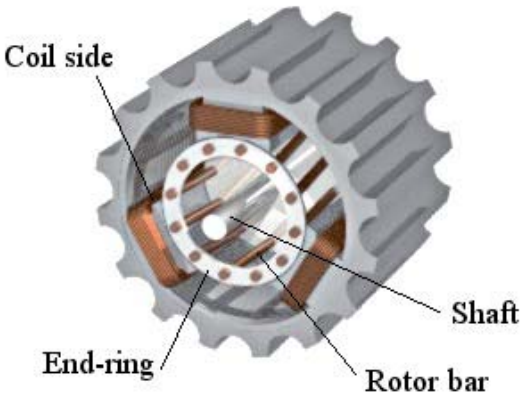

Figure 5.1: Main parts integrating an induction motor. From Wikimedia Commons by Mtodorov 69 under license CC-BY-SA-3.0.

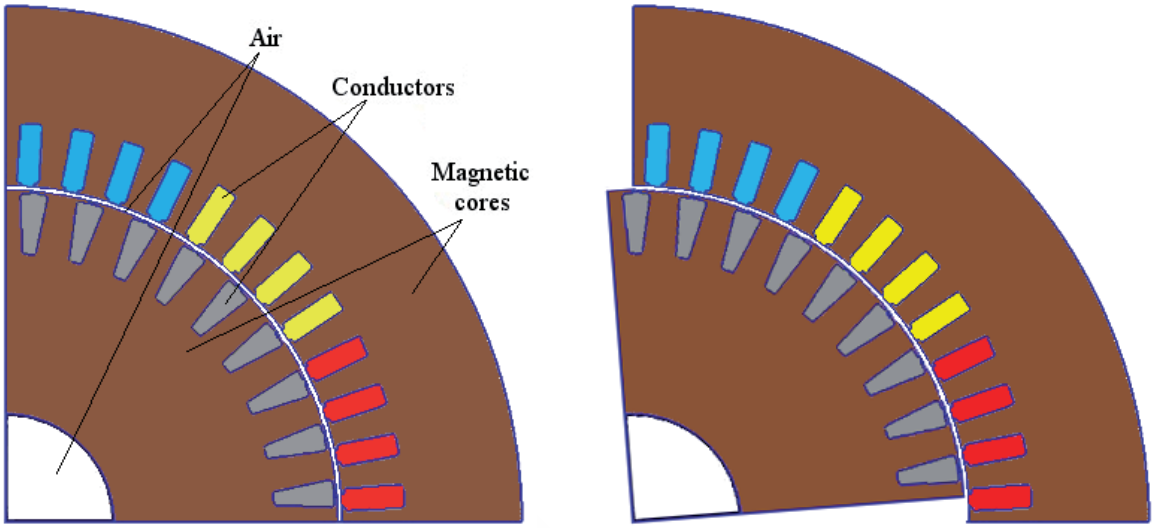

Figure 5.2: A quarter of the geometric domain at time $t = 0$ (left) and $t > 0$ (right). Modification of a picture provided by Robert Bosch GmbH.

conductors. These assumptions make it possible to say that the current density is uniformly distributed in all conducting subdomains Ω_n and given by

$$J_{z,n}(t) = \begin{cases} \dfrac{y_n(t)}{\text{meas}(\Omega_n)}, & n = 1, \ldots, N_b, \\ \dfrac{I_n(t)}{\text{meas}(\Omega_n)}, & n = N_b + 1, \ldots, N_c, \end{cases}$$

where we have denoted $y_n(t)$, $n = 1, \ldots, N_b$, the currents through the cross-section of each rotor bar at time t, and $I_n(t)$, $n = N_b + 1, \ldots, N_c$, the currents through the cross-section of each stator coil side at time t. Moreover, we consider a balanced three-phase electrical supply for the induction machine. Thus, currents $I_n(t)$, $n = N_b + 1, \ldots, N_c$, can be computed a priori from the currents in the three phases A, B and C.

We notice that, in the simulation of induction machines, the bars of the squirrel cage are usually modeled as solid conductors, where, in opposition to stranded conductors, the induced currents are not uniformly distributed (see, for instance, the classical model presented in [93]). Nevertheless, we advance that assuming the rotor bars as stranded conductors will not constitute a limitation to the applicability of the methodology (see Remark 5.10 in Section 5.5).

Therefore, we start by considering the formulation in Problem II.2, modelling the laminated core as a homogeneous non-conducting medium and neglecting the effects of eddy currents in the z space direction except along the rotor bars (since the ferromagnetic core is laminated in this direction). However, we have to extend the formulation to take into account the motion of the machine. Then, for numerical purposes, we split Ω_{nl} and Ω_0 into two parts using a circle Γ strictly contained in the air-gap: $\Omega_{\text{nl}} = \Omega_{\text{nl}}^{\text{rot}} \cup \Omega_{\text{nl}}^{\text{sta}}$, $\Omega_0 = \Omega_0^{\text{rot}} \cup \Omega_0^{\text{sta}}$, where $\Omega_{\text{nl}}^{\text{rot}} \cup \Omega_0^{\text{rot}}$ corresponds to the rotor and $\Omega_{\text{nl}}^{\text{sta}} \cup \Omega_0^{\text{sta}}$ to the stator. Let us notice that circle Γ also divides the whole domain Ω into two parts to be called Ω^{rot} and Ω^{sta}, which correspond to the initial

position of the rotor and to the stator, respectively. More precisely,

$$\Omega^{\mathrm{rot}} = \left(\overline{\Omega_0^{\mathrm{rot}}} \cup \left(\bigcup_{n=1}^{N_b} \overline{\Omega_n} \right) \cup \overline{\Omega_{\mathrm{nl}}^{\mathrm{rot}}} \right)^{\circ}, \quad \Omega^{\mathrm{sta}} = \left(\overline{\Omega_0^{\mathrm{sta}}} \cup \left(\bigcup_{n=N_b+1}^{N_c} \overline{\Omega_n} \right) \cup \overline{\Omega_{\mathrm{nl}}^{\mathrm{sta}}} \right)^{\circ}.$$

In the case of moving bodies, Ohm's law (II.8) changes accordingly to the movement law (see [64] for a short presentation). However, we consider a reference frame moving with the rotor, and thus Ω^{rot} is fixed and Ω^{sta} is moving. As a consequence, equations (II.11) remain valid. We notice that, in the framework of induction machines, a usual solution is working with Lagrangian coordinates in both rotor and stator (see, for instance, [39, 93]). However, in our case, it is enough to consider a unique reference system moving with the rotor as the conductors present in the stator are stranded conductors where the currents are known. Therefore, in the stator, nor Ohm's law (II.8) neither Faraday's law (II.5) are needed to state the problem.

If we call r_t the rotation whose angular velocity is the opposite to the one of the rotor, at time $t > 0$, the stator has a different configuration with respect to the initial time, given by

$$r_t\left(\Omega_0^{\mathrm{sta}}\right) \cup \left(\bigcup_{n=N_b+1}^{N_c} r_t\left(\Omega_n\right) \right) \cup r_t\left(\Omega_{\mathrm{nl}}^{\mathrm{sta}}\right).$$

It is important to notice that both the rotor and stator geometric sets, Ω^{rot} and Ω^{sta}, are always the same, but the physical parameters at each point may change along the time as they are not invariant with respect to rotation r_t.

Finally, we notice that neither the currents nor the voltage drops are known in the rotor bars, and thus we will need to add new equations to be able to compute them in terms of the problem data.

5.2.1 The Transient Magnetic Model

The 2D problem that we have described up to now has known sources only in the stator coil sides, which are given in terms of the current through them. Therefore, in this case, the formulation in Problem II.2 with moving geometry reduces to

$$-\operatorname{div}(\nu_0 \mathbf{grad}\, A) = 0 \quad \text{in } \Omega_0^{\mathrm{rot}} \cup r_t\left(\Omega_0^{\mathrm{sta}}\right), \tag{5.1}$$

$$-\operatorname{div}(\nu_0 \mathbf{grad}\, A) = \frac{y_n(t)}{\operatorname{meas}(\Omega_n)} \quad \text{in } \Omega_n,\ n = 1, \ldots, N_b, \tag{5.2}$$

$$-\operatorname{div}(\nu_0 \mathbf{grad}\, A) = \frac{I_n(t)}{\operatorname{meas}(\Omega_n)} \quad \text{in } r_t(\Omega_n),\ n = N_b + 1, \ldots, N_c, \tag{5.3}$$

$$-\operatorname{div}(\nu(\cdot, |\mathbf{grad}\, A|) \mathbf{grad}\, A) = 0 \quad \text{in } \Omega_{\mathrm{nl}}^{\mathrm{rot}} \cup r_t\left(\Omega_{\mathrm{nl}}^{\mathrm{sta}}\right), \tag{5.4}$$

$$A = 0 \quad \text{on } \partial\Omega. \tag{5.5}$$

However, the current in the squirrel cage is induced by the one in the stator, and therefore currents $y_n(t)$, $n = 1, \ldots, N_b$, are not known in advance. To be able to compute them, we have to take

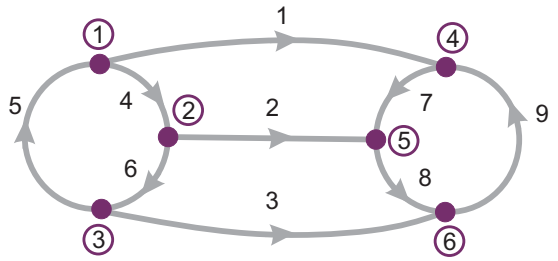

$$\mathcal{A} = \begin{pmatrix} -1 & 0 & 0 & -1 & 1 & 0 & 0 & 0 & 0 \\ 0 & -1 & 0 & 1 & 0 & -1 & 0 & 0 & 0 \\ 0 & 0 & -1 & 0 & -1 & 1 & 0 & 0 & 0 \\ 1 & 0 & 0 & 0 & 0 & 0 & -1 & 0 & 1 \\ 0 & 1 & 0 & 0 & 0 & 0 & 1 & -1 & 0 \\ 0 & 0 & 1 & 0 & 0 & 0 & 0 & 1 & -1 \end{pmatrix}$$

Figure 5.3: Example of graph topology and associated incidence matrix

into account that all bars are connected to each other through the end-rings (see Figure 5.1). Considering that we cannot include these end-rings in the 2D model of cross-section of the motor, we will write a lumped model for the squirrel cage electrical circuit, and couple it with the distributed one. The topology of this circuit is modeled as a directed graph. Let us recall that the incidence matrix of a directed graph is a $nod \times edg$ (nodes by edges) matrix $\mathcal{A} = (a_{ij})$ defined by

$$a_{ij} = \begin{cases} -1 & \text{if } i = m(1,j), \\ 1 & \text{if } i = m(2,j), \\ 0 & \text{otherwise,} \end{cases}$$

for $i \in \{1, \dots, nod\}$, $j \in \{1, \dots, edg\}$, and $m(1,j)$, $m(2,j)$ denote the first and second nodes of the j-th edge, respectively. A simple example is shown in Figure 5.3 where the number of nodes is $nod = 2N_b = 6$ and the number of edges $edg = 3N_b = 9$.

By using the incidence matrix, the first Kirchhoff's law, which states that the charge is conserved at the nodes of the circuit, can be written as follows:

$$\mathcal{A}\vec{y}(t) = \vec{0}, \tag{5.6}$$

where $\vec{y}(t) \in \mathbb{R}^{edg}$ denotes the vector of currents along the edges of the graph. Moreover, let us introduce the vector of nodal electric potentials at time t, denoted by $\vec{v}(t) \in \mathbb{R}^{nod}$, and the resistance of the n-th bar per unit length in the z-direction, denoted by $\alpha_n := (\sigma \operatorname{meas}(\Omega_n))^{-1}$, $n = 1, \dots, N_b$. Then, the constitutive equations for the circuit elements can be written as

$$\mathcal{D}\vec{y}(t) + \mathcal{A}^{\mathrm{T}}\vec{v}(t) = \vec{0}, \tag{5.7}$$

where $\mathcal{D}$ denotes the diagonal operator given by $\left(\mathcal{D}\vec{y}(t)\right)_n = \mathcal{D}_n\left(y_n(t)\right)$, with

$$\mathcal{D}_n\left(y_n(t)\right) = \begin{cases} R_n \dfrac{d}{dt} \displaystyle\int_{\Omega_n} \sigma A(t) \; + R_n y_n(t) & n = 1, \dots, N_b, \\ R_n y_n(t) & n = N_b + 1, \dots, edg, \end{cases}$$

R_n, $n = N_b + 1, \dots, edg$, being the resistance of the n-th edge of the graph, and $R_n = \ell_n \alpha_n$, $n = 1, \dots, N_b$, the resistance of the n-th rotor bar, with ℓ_n its length. We notice that expressions of $\mathcal{D}_n\left(y_n(t)\right)$ for $n = 1, \dots, N_b$ are obtained similarly to (II.11).

Thus, the problem to be solved is the following:

Problem 5.1. *Given the currents along the coil sides $I_n(t)$, $n = N_b + 1, \dots, N_c$, and initial currents along the bars y_n^0, $n = 1, \dots, N_b$, find, for every $t \in [0, T]$, a field $A(x, y; t)$, currents*

$y_n(t)$, $n = 1, \ldots, edg$, *along the edges of the graph and voltages* $v_n(t)$, $n = 1, \ldots, nod$, *at the nodes of the graph such that* $y_n(0) = y_n^0$, $n = 1, \ldots, N_b$, *and*

$$
\begin{aligned}
-\operatorname{div}(\nu_0 \, \mathbf{grad}\, A) &= 0 && \text{in } \Omega_0^{\mathrm{rot}} \cup r_t\left(\Omega_0^{\mathrm{sta}}\right), && (5.8)\\
-\operatorname{div}(\nu_0 \, \mathbf{grad}\, A) &= \frac{y_n(t)}{\operatorname{meas}(\Omega_n)} && \text{in } \Omega_n,\ n = 1, \ldots, N_b, && (5.9)\\
-\operatorname{div}(\nu_0 \, \mathbf{grad}\, A) &= \frac{I_n(t)}{\operatorname{meas}(\Omega_n)} && \text{in } r_t(\Omega_n),\ n = N_b + 1, \ldots, N_c, && (5.10)\\
-\operatorname{div}(\nu(\cdot, |\mathbf{grad}\, A|) \, \mathbf{grad}\, A) &= 0 && \text{in } \Omega_{\mathrm{nl}}^{\mathrm{rot}} \cup r_t\left(\Omega_{\mathrm{nl}}^{\mathrm{sta}}\right), && (5.11)\\
A &= 0 && \text{on } \partial\Omega, && (5.12)\\
\mathcal{D}\vec{y}(t) + \mathcal{A}^{\mathrm{T}}\vec{v}(t) &= \vec{0}, && && (5.13)\\
\mathcal{A}\vec{y}(t) &= \vec{0}. && && (5.14)
\end{aligned}
$$

5.3 A Reduced Problem

The goal of this section is to obtain an equivalent formulation to Problem 5.1 having the currents along the rotor bars as the only unknowns. For this purpose, let us first introduce some notations that will allow us to write Problem 5.1 in a more compact form. Let $\vec{\mathcal{F}} : [0, T] \times \mathbb{R}^{N_b} \longrightarrow \mathbb{R}^{N_b}$ be the nonlinear operator defined as

$$
\vec{\mathcal{F}}(t, \vec{w}) := \left(\int_{\Omega_1} \sigma A(x, y, t) \, dx \, dy, \ldots, \int_{\Omega_{N_b}} \sigma A(x, y, t) \, dx \, dy \right)^{\mathrm{T}} \in \mathbb{R}^{N_b}, \quad t \in [0, T], \vec{w} \in \mathbb{R}^{N_b},
$$

with $A(x, y, t)$ the solution to the following nonlinear magnetostatic problem:

Problem 5.2. *Given a fixed* $t \in [0, T]$, *currents along the coil sides* $I_n(t)$, $n = N_b + 1, \ldots, N_c$, *and* $\vec{w} \in \mathbb{R}^{N_b}$, *find a field* $A(x, y, t)$ *such that*

$$
\begin{aligned}
-\operatorname{div}(\nu_0 \, \mathbf{grad}\, A) &= 0 && \text{in } \Omega_0^{\mathrm{rot}} \cup r_t\left(\Omega_0^{\mathrm{sta}}\right), && (5.15)\\
-\operatorname{div}(\nu_0 \, \mathbf{grad}\, A) &= \frac{w_n}{\operatorname{meas}(\Omega_n)} && \text{in } \Omega_n,\ n = 1, \ldots, N_b, && (5.16)\\
-\operatorname{div}(\nu_0 \, \mathbf{grad}\, A) &= \frac{I_n(t)}{\operatorname{meas}(\Omega_n)} && \text{in } r_t(\Omega_n),\ n = N_b + 1, \ldots, N_c, && (5.17)\\
-\operatorname{div}(\nu(\cdot, |\mathbf{grad}\, A|) \, \mathbf{grad}\, A) &= 0 && \text{in } \Omega_{\mathrm{nl}}^{\mathrm{rot}} \cup r_t\left(\Omega_{\mathrm{nl}}^{\mathrm{sta}}\right), && (5.18)\\
A &= 0 && \text{on } \partial\Omega. && (5.19)
\end{aligned}
$$

On the other hand, two blocks can be distinguished in equation (5.13), one corresponding to the rotor bars and another one corresponding to the remaining edges of the squirrel cage, namely, those of the end-rings. Let us denote the incidence matrices of their respective subgraphs by $\mathcal{A}^b$ and $\mathcal{A}^r$. Thus, we have $\mathcal{A} = \left(\mathcal{A}^b \mid \mathcal{A}^r\right)$, and, accordingly, the vector of currents $\vec{y}$ is decomposed as

$$
\vec{y} = \begin{pmatrix} \vec{y}^{\,b} \\ \vec{y}^{\,r} \end{pmatrix}.
$$

Then, equation (5.13) can be rewritten as

$$\mathcal{R}^b \frac{d}{dt}\vec{\mathcal{F}}\left(t, \vec{y}^b(t)\right) + \mathcal{R}^b \vec{y}^b(t) + \left(\mathcal{A}^b\right)^{\mathrm{T}} \vec{v}(t) = \vec{0},$$
$$\mathcal{R}^r \vec{y}^r(t) + \left(\mathcal{A}^r\right)^{\mathrm{T}} \vec{v}(t) = \vec{0},$$

where $\mathcal{R}^b$ and $\mathcal{R}^r$ are the diagonal matrices defined by

$$\left(\mathcal{R}^b\right)_{ij} = R_i \delta_{ij}, \qquad i,j = 1,\ldots,N_b,$$
$$\left(\mathcal{R}^r\right)_{ij} = R_{i+N_b} \delta_{ij}, \quad i,j = 1,\ldots,edg - N_b.$$

with δ_{ij} the Kronecker delta, that is,

$$\delta_{ij} = \begin{cases} 0 & \text{if } i \neq j, \\ 1 & \text{if } i = j. \end{cases}$$

Thus, equations (5.8)–(5.14) can be rewritten in the more compact manner,

$$\mathcal{R}^b \frac{d}{dt}\vec{\mathcal{F}}\left(t, \vec{y}^b(t)\right) + \mathcal{R}^b \vec{y}^b(t) + \left(\mathcal{A}^b\right)^{\mathrm{T}} \vec{v}(t) = \vec{0}, \tag{5.20}$$
$$\mathcal{R}^r \vec{y}^r(t) + \left(\mathcal{A}^r\right)^{\mathrm{T}} \vec{v}(t) = \vec{0}, \tag{5.21}$$
$$\mathcal{A}^b \vec{y}^b(t) + \mathcal{A}^r \vec{y}^r(t) = \vec{0}. \tag{5.22}$$

Moreover, since $\mathcal{R}^r$ is a non-singular matrix, from (5.21) we get

$$\vec{y}^r(t) = -\left(\mathcal{R}^r\right)^{-1} \left(\mathcal{A}^r\right)^{\mathrm{T}} \vec{v}(t).$$

Therefore, Problem 5.1 is equivalent to the following one,

Problem 5.3. *Given the currents along the coil sides $I_n(t)$, $n = N_b+1,\ldots,N_c$, and the initial currents along the bars y_n^0, $n = 1,\ldots,N_b$, find, for every $t \in [0,T]$, currents $y_n(t)$, $n = 1,\ldots,N_b$, along the bars and voltages $v_n(t)$, $n = 1,\ldots,nod$, at the nodes of the graph such that $y_n(0) = y_n^0$, $n = 1,\ldots,N_b$, and*

$$\mathcal{R}^b \frac{d}{dt}\vec{\mathcal{F}}\left(t, \vec{y}^b(t)\right) + \mathcal{R}^b \vec{y}^b(t) + \left(\mathcal{A}^b\right)^{\mathrm{T}} \vec{v}(t) = \vec{0}, \tag{5.23}$$
$$\mathcal{A}^b \vec{y}^b(t) - \mathcal{A}^r \left(\mathcal{R}^r\right)^{-1} \left(\mathcal{A}^r\right)^{\mathrm{T}} \vec{v}(t) = \vec{0}. \tag{5.24}$$

where operator $\vec{\mathcal{F}}$ is defined in terms of $I_n(t)$, $n = N_b+1,\ldots,N_c$, through the solution to Problem 5.2.

Next, we show that $\vec{v}(t)$ can be eliminated from system (5.23)–(5.24).

Lemma 5.4. *If the currents along the bars, $y_n(t)$, $n = 1,\ldots,N_b$, are such that*

$$\mathcal{A}^b \vec{y}^b(t) \cdot \begin{pmatrix} \vec{0} \\ \vec{e} \end{pmatrix} = 0,$$

where $\vec{e} = (1,\ldots,1)^{\mathrm{T}} \in \mathbb{R}^{N_b}$, there exist a matrix $\mathcal{B}^{-1}$ and a scalar function $\lambda(t)$ such that

$$\vec{v}(t) = \mathcal{B}^{-1}\mathcal{A}^b \vec{y}^b(t) + \lambda(t) \begin{pmatrix} \vec{0} \\ \vec{e} \end{pmatrix}.$$

Proof. Firstly, let us analyse the nullspace of matrix $(\mathcal{A}^r)^{\mathrm{T}}$. Since the subgraph obtained by removing the bars has two connected components (the two end-rings), each of them having N_b nodes, the rank of matrix $\mathcal{A}^r$ is $2N_b - 2$ (see Theorem 7.2 in [43]). Therefore, we conclude that the dimension of the nullspace of $(\mathcal{A}^r)^{\mathrm{T}}$ is two. If we number the nodes belonging to one of the rings first and then the ones of the other ring, this nullspace is given by

$$\mathrm{N}\left((\mathcal{A}^r)^{\mathrm{T}}\right) =< \begin{pmatrix} \vec{e} \\ \vec{0} \end{pmatrix}, \begin{pmatrix} \vec{0} \\ \vec{e} \end{pmatrix} > .$$

Moreover, it is easy to prove that

$$\mathrm{N}\left(\mathcal{A}^r \left(\mathcal{R}^r\right)^{-1} \left(\mathcal{A}^r\right)^{\mathrm{T}}\right) = \mathrm{N}\left((\mathcal{A}^r)^{\mathrm{T}}\right).$$

Indeed, it is obvious that $\mathrm{N}\left((\mathcal{A}^r)^{\mathrm{T}}\right) \subset \mathrm{N}\left(\mathcal{A}^r \left(\mathcal{R}^r\right)^{-1} \left(\mathcal{A}^r\right)^{\mathrm{T}}\right)$. Conversely, given

$$\vec{z} \in \mathrm{N}\left(\mathcal{A}^r \left(\mathcal{R}^r\right)^{-1} \left(\mathcal{A}^r\right)^{\mathrm{T}}\right),$$

we have,

$$\mathcal{A}^r \left(\mathcal{R}^r\right)^{-1} \left(\mathcal{A}^r\right)^{\mathrm{T}} \vec{z} \cdot \vec{z} = 0 = \left(\mathcal{R}^r\right)^{-1} \left(\mathcal{A}^r\right)^{\mathrm{T}} \vec{z} \cdot \left(\mathcal{A}^r\right)^{\mathrm{T}} \vec{z}$$

and, since the linear transformation associated to $\left(\mathcal{R}^r\right)^{-1}$ is bijective, we conclude that $\vec{z}$ also belongs to $\mathrm{N}\left((\mathcal{A}^r)^{\mathrm{T}}\right)$.

Now, we are going to see how we can obtain $\vec{v}(t)$ in terms of $\mathcal{A}^b\vec{y}^b(t)$. Let us denote by $\mathcal{E}$ the matrix of order $2N_b \times (2N_b - 2)$ whose columns span the space $\mathrm{N}\left((\mathcal{A}^r)^{\mathrm{T}}\right)^{\perp}$. Since $\mathrm{N}\left((\mathcal{A}^r)^{\mathrm{T}}\right)^{\perp} = \mathrm{Im}\left(\mathcal{A}^r\right)$, matrix $\mathcal{E}$ can be obtained from matrix $\mathcal{A}^r$ by eliminating two columns, each corresponding to an edge of each end-ring.

Moreover, $\mathcal{E}^{\mathrm{T}}\mathcal{A}^r(\mathcal{R}^r)^{-1}\left(\mathcal{A}^r\right)^{\mathrm{T}}\mathcal{E}$ is an invertible matrix of order $(2N_b-2)\times(2N_b-2)$. Indeed, since $\mathcal{R}^r$ is a non-singular diagonal matrix, $\mathcal{E}^{\mathrm{T}}\mathcal{A}^r(\mathcal{R}^r)^{-1}\left(\mathcal{A}^r\right)^{\mathrm{T}}\mathcal{E}$ is invertible if and only if $\mathcal{E}^{\mathrm{T}}\mathcal{A}^r\left(\mathcal{A}^r\right)^{\mathrm{T}}\mathcal{E}$ is also invertible. Besides, since $\mathrm{rank}(P) = \mathrm{rank}(P^{\mathrm{T}}P)$ for any matrix P, the result follows from the definition of matrix $\mathcal{E}$. This can be easily seen by rearranging the columns in $\mathcal{A}^r$ such that the first $2N_b - 2$ columns are linearly independent.

Additionally, if

$$\vec{y}^b \perp \left(\mathcal{A}^b\right)^{\mathrm{T}} \begin{pmatrix} \vec{e} \\ \vec{0} \end{pmatrix} \quad \text{and} \quad \vec{y}^b \perp \left(\mathcal{A}^b\right)^{\mathrm{T}} \begin{pmatrix} \vec{0} \\ \vec{e} \end{pmatrix}, \tag{5.25}$$

then

$$\vec{v}_1(t) = \mathcal{E}(\mathcal{E}^{\mathrm{T}}\mathcal{A}^r(\mathcal{R}^r)^{-1}\left(\mathcal{A}^r\right)^{\mathrm{T}}\mathcal{E})^{-1}\mathcal{E}^{\mathrm{T}}\mathcal{A}^b\vec{y}^b(t)$$

is a solution to (5.24). Indeed, on the one hand, we have

$$\begin{aligned} &\mathcal{E}^{\mathrm{T}}\mathcal{A}^r(\mathcal{R}^r)^{-1}\left(\mathcal{A}^r\right)^{\mathrm{T}}\vec{v}_1(t) \\ &\quad = \mathcal{E}^{\mathrm{T}}\mathcal{A}^r(\mathcal{R}^r)^{-1}\left(\mathcal{A}^r\right)^{\mathrm{T}}\mathcal{E}(\mathcal{E}^{\mathrm{T}}\mathcal{A}^r(\mathcal{R}^r)^{-1}\left(\mathcal{A}^r\right)^{\mathrm{T}}\mathcal{E})^{-1}\mathcal{E}^{\mathrm{T}}\mathcal{A}^b\vec{y}^b(t) = \mathcal{E}^{\mathrm{T}}\mathcal{A}^b\vec{y}^b(t). \end{aligned} \tag{5.26}$$

On the other hand, as the columns of $\mathcal{E}$ form a basis of $\mathrm{N}\left(\mathcal{A}^r(\mathcal{R}^r)^{-1}\left(\mathcal{A}^r\right)^{\mathrm{T}}\right)^{\perp}$, then $\vec{v}_1(t)$ belongs to this subspace. Also, conditions (5.25) imply that $\mathcal{A}^b\vec{y}^b(t)$ belongs to $\mathrm{N}\left(\mathcal{A}^r(\mathcal{R}^r)^{-1}\left(\mathcal{A}^r\right)^{\mathrm{T}}\right)^{\perp}$. Then, since $\mathcal{E}^{\mathrm{T}}$ is one-to-one on $\mathrm{Im}\left(\mathcal{A}^r(\mathcal{R}^r)^{-1}\left(\mathcal{A}^r\right)^{\mathrm{T}}\right)$, (5.26) implies

$$\mathcal{A}^r(\mathcal{R}^r)^{-1}\left(\mathcal{A}^r\right)^{\mathrm{T}}\vec{v}_1(t) = \mathcal{A}^b\vec{y}^b(t).$$

Hence, the general solution to (5.24) is

$$\vec{v}(t) = \mathcal{E}(\mathcal{E}^{\mathrm{T}}\mathcal{A}^r(\mathcal{R}^r)^{-1}\left(\mathcal{A}^r\right)^{\mathrm{T}}\mathcal{E})^{-1}\mathcal{E}^{\mathrm{T}}\mathcal{A}^b\vec{y}^b(t) + \phi(t)\begin{pmatrix}\vec{e}\\ \vec{0}\end{pmatrix} + \lambda(t)\begin{pmatrix}\vec{0}\\ \vec{e}\end{pmatrix},$$

for any choice of $\phi(t)$ and $\lambda(t)$. Therefore, we can take

$$\mathcal{B}^{-1} = \mathcal{E}(\mathcal{E}^{\mathrm{T}}\mathcal{A}^r(\mathcal{R}^r)^{-1}\left(\mathcal{A}^r\right)^{\mathrm{T}}\mathcal{E})^{-1}\mathcal{E}^{\mathrm{T}}.$$

Since the potential is defined up to a constant, we can arbitrarily choose either $\phi(t)$ or $\lambda(t)$. For instance, if we take $\phi(t) = 0$, $\lambda(t)$ is an unknown of the problem that is determined by the second condition in (5.25). □

Finally, the problem to be solved can be written in terms of $\vec{y}^b(t)$ and $\lambda(t)$ as follows:

Problem 5.5. *Given the currents along the coil sides $I_n(t)$, $n = N_b+1,\dots,N_c$, and the initial currents along the bars y_n^0, $n = 1,\dots,N_b$, find, for every $t \in [0,T]$, currents $y_n(t)$, $n = 1,\dots,N_b$, along the bars such that $y_n(0) = y_n^0$, $n = 1,\dots,N_b$, and*

$$\mathcal{R}^b\frac{d}{dt}\vec{\mathcal{F}}\left(t,\vec{y}^b(t)\right) + \left(\mathcal{R}^b + \left(\mathcal{A}^b\right)^{\mathrm{T}}\mathcal{B}^{-1}\left(\mathcal{A}^b\right)\right)\vec{y}^b(t) + \lambda(t)\left(\mathcal{A}^b\right)^{\mathrm{T}}\begin{pmatrix}\vec{0}\\ \vec{e}\end{pmatrix} = \vec{0}, \qquad (5.27)$$

$$\mathcal{A}^b\vec{y}^b(t)\cdot\begin{pmatrix}\vec{0}\\ \vec{e}\end{pmatrix} = 0, \qquad (5.28)$$

where operator $\vec{\mathcal{F}}$ is defined in terms of $I_n(t)$, $n = N_b+1,\dots,N_c$, through the solution to Problem 5.2.

5.4 An Approximate Method to Compute Appropriate Initial Currents

In this section, we propose a method to compute an approximation of the initial condition of Problem 5.5 corresponding to a periodic steady solution. If the currents along the stator coil sides are periodic functions of the same frequency f_c (in Hz) and the rotor is moving at a constant angular velocity n_r (in rpm), the full problem has also a steady periodic solution to period T_e, the so-called effective period. If we denote by T_c the electrical period of stator coil sides (in s), $\left(\text{i.e., } T_c = \frac{1}{f_c}\right)$, and by T_r the mechanical period of the rotor motion (in s), $\left(\text{i.e., } T_r = \frac{60}{n_r}\right)$, then

$$T_e = N\,T_c = M\,T_r,$$

where M and N are integers such that

$$\frac{T_c}{T_r} = \frac{M}{N}$$

and the greatest common divisor between M and N is equal to 1. Actually, the effective period guarantees the periodicity of all the magnitudes involved in the induction machine problem, because one can prove that T_e is an integer multiple of T_c, T_r and T_b, the period of the current in the bars (to be defined below).

In order to compute the steady periodic solution, we could take any initial conditions $y_1^0, \ldots, y_{N_b}^0$, (null, for instance), and integrate the algebraic-differential system of equations given above until convergence. However, this procedure can be very costly from the computational point of view if the initial currents are far from the ones corresponding to the periodic solution we are looking for. The goal of this section is to propose a method to determine these initial currents, in such a way that the periodic steady solution can be obtained by integrating the problem along a time-interval as small as possible.

Let n_s be the so-called synchronous speed (that is, the rotation rate of the magnetic field in the stator), which is given by $n_s = (60 f_c)/p$ (in rpm), p being the number of pole-pairs of the machine. Furthermore, let s be the slip, that is, the difference between synchronous and operating speed, relative to the synchronous speed, $s = (n_s - n_r)/n_s$. Then, one can prove that the period of the current in the bars, T_b (in s), is such that $T_b = T_c/s$ (see, for instance, [35]).

Firstly, let us successively integrate (5.27), first in $[0, t]$ and then $[0, T_b]$, obtaining

$$\begin{aligned}\mathcal{R}^b \left(\int_0^{T_b} \vec{\mathcal{F}}\left(t, \vec{y}^b(t)\right)\, dt - T_b \vec{\mathcal{F}}\left(0, \vec{y}^{b,0}\right) \right) \\ + \left(\mathcal{R}^b + (\mathcal{A}^b)^{\mathrm{T}} \mathcal{B}^{-1} (\mathcal{A}^b)\right) \int_0^{T_b} \left(\int_0^t \vec{y}^b(s)\, ds \right) dt \\ + \left(\int_0^{T_b} \left(\int_0^t \lambda(s)\, ds \right) dt \right) (\mathcal{A}^b)^{\mathrm{T}} \begin{pmatrix} \vec{0} \\ \vec{e} \end{pmatrix} = \vec{0}, \quad (5.29)\end{aligned}$$

where we have used the notation $\vec{y}^{b,0} := \left(y_1^0, \ldots, y_{N_b}^0\right)^{\mathrm{T}}$, from which it easily follows that

$$\begin{aligned}\mathcal{R}^b \left(\int_0^{T_b} \vec{\mathcal{F}}\left(t, \vec{y}^b(t)\right)\, dt - T_b \vec{\mathcal{F}}\left(0, \vec{y}^{b,0}\right) \right) \\ + \left(\mathcal{R}^b + (\mathcal{A}^b)^{\mathrm{T}} \mathcal{B}^{-1} (\mathcal{A}^b)\right) \int_0^{T_b} (T_b - t) \vec{y}^b(t)\, dt \\ + \left(\int_0^{T_b} (T_b - t) \lambda(t)\, dt \right) (\mathcal{A}^b)^{\mathrm{T}} \begin{pmatrix} \vec{0} \\ \vec{e} \end{pmatrix} = \vec{0}. \quad (5.30)\end{aligned}$$

Notice that we have changed the order of integration with respect to t and s in the planar region depicted in Figure 5.4 to obtain the identity

$$\int_0^{T_b} \left(\int_0^t \vec{y}^b(s)\, ds \right) dt = \int_0^{T_b} \left(\int_s^{T_b} dt \right) \vec{y}^b(s)\, ds = \int_0^{T_b} (T_b - t) \vec{y}^b(t)\, dt,$$

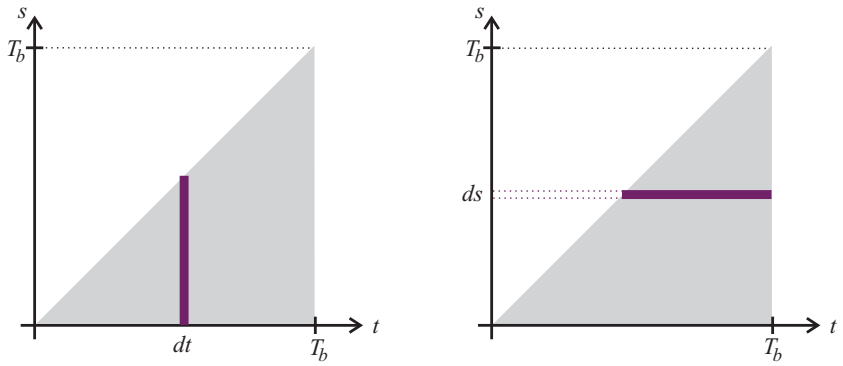

Figure 5.4: Sketch of the domains of integration $\{(s,t), s \in [0,t],\ t \in [0,T_b]\}$ (left) and $\{(s,t), t \in [s,T_b],\ s \in [0,T_b]\}$ (right).

and a similar one for the term involving λ.

Equations (5.28) and (5.30) are exact for any initial condition and time T_b. They allow us to compute the initial currents $\vec{y}^{b,0}$ leading to a periodic solution from the initial time. This computation can be done by using iterative methods which require solving problem (5.8)–(5.14) in $[0,T_b]$ at each iteration, what would be very costly. In what follows we propose a much simpler alternative method, which is obtained by approximating equation (5.30) in a way to be specified below.

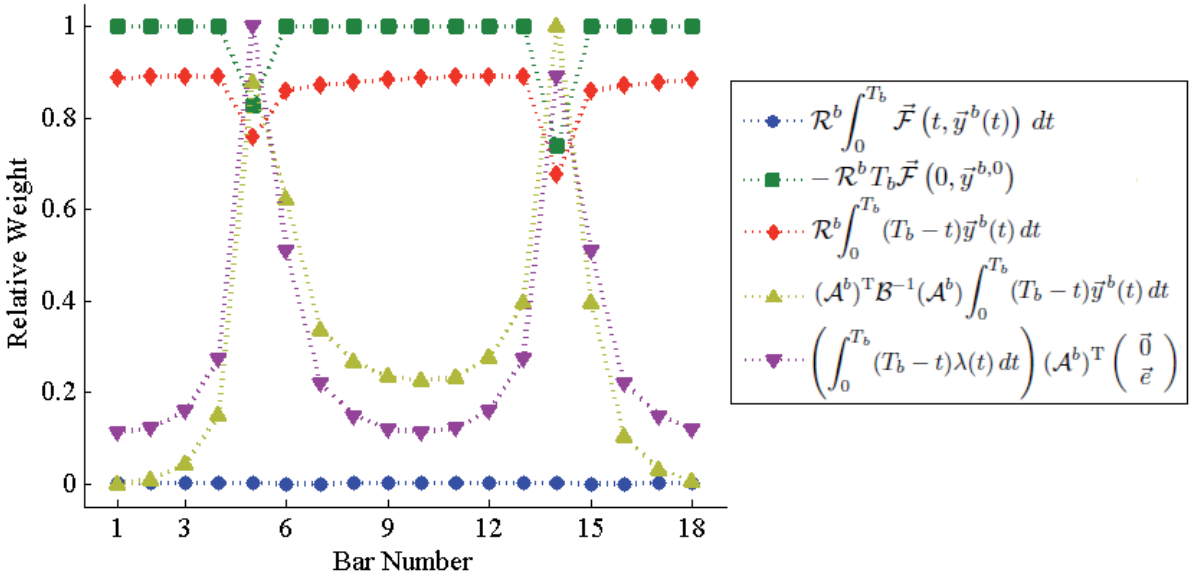

Figure 5.5: Relative value of the different terms in equation (5.30) versus the bar number.

Thus, on the one hand, we conjecture that the first term on the left-hand side in (5.30), namely,

$$\mathcal{R}^b \int_0^{T_b} \vec{\mathcal{F}}\left(t, \vec{y}^b(t)\right)\, dt$$

can be neglected because, in real situations, it seems to be much smaller than the other terms. This can be seen for the particular example shown in Figure 5.5. From a physical point of view,

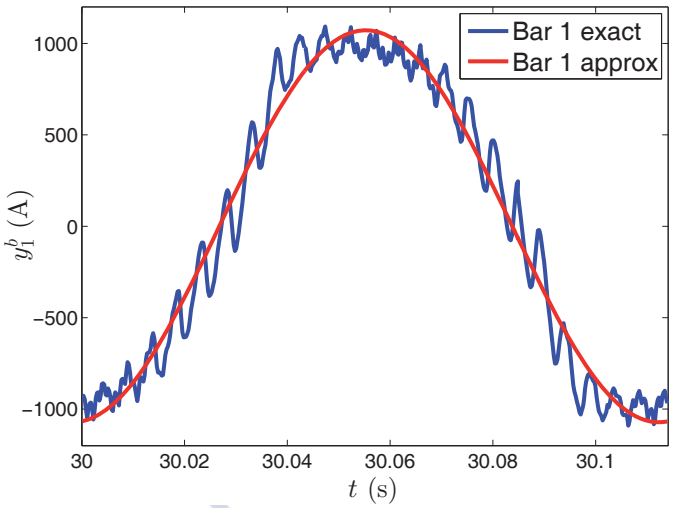

Figure 5.6: Comparison between $y_1^b(t)$ and the approximation given in (5.32)

this assumption means that the flux linkages of the rotor bars have approximately zero mean over one period of the fundamental frequency of currents in the rotor bars. Let us notice, however, that the term involving the resistances, namely,

$$\left(\mathcal{R}^b + (\mathcal{A}^b)^{\mathrm{T}}\mathcal{B}^{-1}\mathcal{A}^b\right)\int_0^{T_b}(T_b - t)\vec{y}^b(t)\,dt$$

cannot be neglected (see again Figure 5.5). Therefore, we should consider the equation

$$-T_b\mathcal{R}^b\vec{\mathcal{F}}\left(0,\vec{y}^{b,0}\right) + \left(\mathcal{R}^b + (\mathcal{A}^b)^{\mathrm{T}}\mathcal{B}^{-1}\mathcal{A}^b\right)\int_0^{T_b}(T_b - t)\vec{y}^b(t)\,dt + \left(\int_0^{T_b}(T_b - t)\lambda(t)\,dt\right)(\mathcal{A}^b)^{\mathrm{T}}\begin{pmatrix}\vec{0}\\ \vec{e}\end{pmatrix} = \vec{0}. \tag{5.31}$$

On the other hand, we would also like to avoid the calculation of $\vec{y}^b(t)$ because it is very expensive. Indeed, notice that at each iteration of any iterative algorithm solving (5.28)–(5.31), the computation of $\vec{y}^b(t)$ starting from $\vec{y}^{b,0}$ would involve the solution to the full model along the interval $[0, T_b]$. In order to avoid such a drawback, we notice that the currents along the rotor bars can be approximated by a harmonic function of frequency $f_b := 1/T_b$ (see Figure 5.6). This is a key point in the proposed technique because it allows us to approximate the original problem with a time-independent one. Moreover, for symmetry reasons, we will assume the amplitudes of the approximations of the currents in the rotor bars to be the same in all of them, which will be denoted by Y. Then, the idea is to approximate the vector of rotor bar currents, $\vec{y}^b(t)$, as follows:

$$y_n^b(t) \simeq \left[(\mathcal{A}^b)^{\mathrm{T}}\begin{pmatrix}\vec{0}\\ \vec{e}\end{pmatrix}\right]_n Y\cos(2\pi f_b t + \beta_n), \tag{5.32}$$

where β_n is the phase-shift between phase A of the current source in the coil sides and the current of the n-th bar. Accordingly, the initial currents are given by,

$$y_n^{b,0} = Y\left[(\mathcal{A}^b)^{\mathrm{T}}\begin{pmatrix}\vec{0}\\ \vec{e}\end{pmatrix}\right]_n \cos\beta_n. \tag{5.33}$$

On the other hand, from periodicity arguments one can show that the phase angles are

$$\beta_n = \beta_1 + (n-1)\gamma, \quad n = 1, \ldots, N_b, \tag{5.34}$$

with $\gamma = (2\pi p)/N_b$, and then only two unknowns remain: Y and β_1. In order to compute them we will construct a system of N_b nonlinear equations that will be solved in the least-square sense.

Let us introduce the column vectors $\vec{u}$ and $\vec{w}$, whose respective n-th components are

$$u_n := \left[(\mathcal{A}^b)^{\mathrm{T}} \begin{pmatrix} \vec{0} \\ \vec{e} \end{pmatrix}\right]_n \cos\beta_n \quad \text{and} \quad w_n := \left[(\mathcal{A}^b)^{\mathrm{T}} \begin{pmatrix} \vec{0} \\ \vec{e} \end{pmatrix}\right]_n \sin\beta_n,$$

$n = 1, \ldots, N_b$. Then, $\vec{y}^{\,b,0} = Y\vec{u}$. We also observe that

$$\vec{u} = \frac{\partial \vec{w}}{\partial \beta_1} \quad \text{and} \quad \vec{w} = -\frac{\partial \vec{u}}{\partial \beta_1}. \tag{5.35}$$

The approximate currents introduced in (5.32) trivially satisfy

$$\int_0^{T_b} \vec{y}^{\,b}(t)\, dt \approx \vec{0}.$$

Additionally, they also satisfy constraint (5.28), as we state in the following lemma:

Lemma 5.6. *The approximate currents introduced in (5.32) satisfy constraint (5.28) for any values of Y and β_1.*

Proof. Taking into account that

$$\left[(\mathcal{A}^b)^{\mathrm{T}} \begin{pmatrix} \vec{0} \\ \vec{e} \end{pmatrix}\right]_n = \pm 1$$

for $n = 1, \ldots, N_b$, depending on the orientation of the n-the edge, we have

$$\begin{aligned}
\vec{y}^{\,b}(t) \cdot (\mathcal{A}^b)^{\mathrm{T}} \begin{pmatrix} \vec{0} \\ \vec{e} \end{pmatrix} &\approx \sum_{n=1}^{N_b} \left[(\mathcal{A}^b)^{\mathrm{T}} \begin{pmatrix} \vec{0} \\ \vec{e} \end{pmatrix}\right]_n^2 Y \cos(2\pi f_b t + \beta_n) \\
&= Y \sum_{n=1}^{N_b} \cos(2\pi f_b t + \beta_n) = Y \mathrm{Re}\left(\sum_{n=1}^{N_b} \mathrm{e}^{\,i(2\pi f_b t + \beta_1 + (n-1)\gamma)} \right) \\
&= Y \mathrm{Re}\left(\mathrm{e}^{\,i(2\pi f_b t + \beta_1)} \sum_{n=1}^{N_b} \mathrm{e}^{\,i((n-1)\gamma)} \right) = Y \mathrm{Re}\left(\mathrm{e}^{\,i(2\pi f_b t + \beta_1)} \frac{\mathrm{e}^{\,iN_b\gamma} - 1}{\mathrm{e}^{\,i\gamma} - 1} \right) \\
&= Y \mathrm{Re}\left(\mathrm{e}^{\,i(2\pi f_b t + \beta_1)} \frac{\mathrm{e}^{\,i2\pi p} - 1}{\mathrm{e}^{\,i\gamma} - 1} \right) = 0,
\end{aligned} \tag{5.36}$$

as long as γ is not an integer multiple of 2π (which would mean that p is a multiple of N_b), because $\mathrm{e}^{\,i2\pi p} = 1$ for all integer p. □

Remark 5.7. *We also notice that, from the calculation in the proof of the above lemma, we deduce that*

$$\sum_{n=1}^{N_b} \cos\beta_n = 0 \quad \textit{and} \quad \sum_{n=1}^{N_b} \sin\beta_n = 0.$$

Now, let us compute the integrals $\int_0^{T_b}(T_b-t)y_n^b(t)\,dt$ by using the approximation introduced in (5.32). We have

$$\int_0^{T_b}(T_b-t)y_n^b(t)\,dt \approx \left[(\mathcal{A}^b)^{\mathrm{T}}\begin{pmatrix}\vec{0}\\ \vec{e}\end{pmatrix}\right]_n \int_0^{T_b}(T_b-t)Y\cos\left(\frac{2\pi}{T_b}t+\beta_n\right)dt$$
$$= -\left[(\mathcal{A}^b)^{\mathrm{T}}\begin{pmatrix}\vec{0}\\ \vec{e}\end{pmatrix}\right]_n Y\frac{T_b^2}{2\pi}\sin\beta_n$$

and hence,

$$\int_0^{T_b}(T_b-t)\vec{y}^b(t)\,dt \approx -Y\frac{T_b^2}{2\pi}\vec{w}. \tag{5.37}$$

Finally, using the notation $\mu = \int_0^{T_b}(T_b-s)\lambda(s)\,ds$, the problem to be solved reduces to:

Problem 5.8. *Given periodic currents along the coil sides $I_n(t)$, $n = N_b+1,\dots,N_c$, find $Y\in\mathbb{R}$, $\beta_1\in[0,2\pi)$ and $\mu\in\mathbb{R}$ such that*

$$-T_b\mathcal{R}^b\vec{\mathcal{F}}(0,Y\vec{u}) - \frac{T_b^2}{2\pi}Y\left(\mathcal{R}^b+(\mathcal{A}^b)^{\mathrm{T}}\mathcal{B}^{-1}\mathcal{A}^b\right)\vec{w} + \mu(\mathcal{A}^b)^{\mathrm{T}}\begin{pmatrix}\vec{0}\\ \vec{e}\end{pmatrix} = \vec{0}.$$

We notice that β_1 appears in the previous system through $\vec{u}$ and $\vec{w}$. Similarly, $\vec{\mathcal{F}}(0,Y\vec{u})$ is defined in terms of $I_n(0)$, $n=N_b+1,\dots,N_c$, through the solution to Problem 5.2.

Moreover, in the above system, it is possible to eliminate unknown μ in terms of Y and β_1 (through $\vec{u}$), which is more convenient from the computational point of view. Indeed, it is easy to see that

$$\mu = \frac{\left(\mathcal{R}^b+(\mathcal{A}^b)^{\mathrm{T}}\,\mathcal{B}^{-1}\,\mathcal{A}^b\right)^{-1}T_b\mathcal{R}^b\vec{\mathcal{F}}(0,Y\vec{u})\cdot(\mathcal{A}^b)^{\mathrm{T}}\begin{pmatrix}\vec{0}\\ \vec{e}\end{pmatrix}}{(\mathcal{R}^b+(\mathcal{A}^b)^{\mathrm{T}}\,\mathcal{B}^{-1}\,\mathcal{A}^b)^{-1}(\mathcal{A}^b)^{\mathrm{T}}\begin{pmatrix}\vec{0}\\ \vec{e}\end{pmatrix}\cdot(\mathcal{A}^b)^{\mathrm{T}}\begin{pmatrix}\vec{0}\\ \vec{e}\end{pmatrix}}.$$

By replacing this expression for μ we get

$$-T_b\mathcal{R}^b\vec{\mathcal{F}}(0,Y\vec{u}) - Y\frac{T_b^2}{2\pi}\left(\mathcal{R}^b+(\mathcal{A}^b)^{\mathrm{T}}\mathcal{B}^{-1}\mathcal{A}^b\right)\vec{w}$$
$$+\frac{1}{a}\left[\left(\mathcal{R}^b+(\mathcal{A}^b)^{\mathrm{T}}\,\mathcal{B}^{-1}\,\mathcal{A}^b\right)^{-1}T_b\mathcal{R}^b\vec{\mathcal{F}}(0,Y\vec{u})\cdot(\mathcal{A}^b)^{\mathrm{T}}\begin{pmatrix}\vec{0}\\ \vec{e}\end{pmatrix}\right](\mathcal{A}^b)^{\mathrm{T}}\begin{pmatrix}\vec{0}\\ \vec{e}\end{pmatrix} = \vec{0}, \tag{5.38}$$

where

$$a := \left(\mathcal{R}^b+(\mathcal{A}^b)^{\mathrm{T}}\,\mathcal{B}^{-1}\,\mathcal{A}^b\right)^{-1}(\mathcal{A}^b)^{\mathrm{T}}\begin{pmatrix}\vec{0}\\ \vec{e}\end{pmatrix}\cdot(\mathcal{A}^b)^{\mathrm{T}}\begin{pmatrix}\vec{0}\\ \vec{e}\end{pmatrix}.$$

In this way, Problem 5.8 can also be written as

Problem 5.9. *Given periodic currents along the coil sides* $I_n(t)$, $n = N_b + 1, \ldots, N_c$, *find* $Y \in \mathbb{R}$ *and* $\beta_1 \in [0, 2\pi)$ *such that*

$$T_b \left[\frac{1}{a} (\mathcal{A}^b)^{\mathrm{T}} \begin{pmatrix} \vec{0} \\ \vec{e} \end{pmatrix} \otimes \left(\left(\mathcal{R}^b + (\mathcal{A}^b)^{\mathrm{T}} \, \mathcal{B}^{-1} \, \mathcal{A}^b \right)^{-\mathrm{T}} (\mathcal{A}^b)^{\mathrm{T}} \begin{pmatrix} \vec{0} \\ \vec{e} \end{pmatrix} \right) - \mathcal{I} \right] \mathcal{R}^b \vec{\mathcal{F}}(0, Y\vec{u}) - Y \frac{T_b^2}{2\pi} (\mathcal{R}^b + (\mathcal{A}^b)^{\mathrm{T}} \mathcal{B}^{-1} \mathcal{A}^b) \vec{w} = \vec{0}. \quad (5.39)$$

In the above expression, where $\mathcal{I}$ denotes the identity matrix. This is an overdetermined system that can be solved, for instance, in the least-square sense. With this aim, let us define

$$\vec{f}(Y, \beta_1) := -Y \frac{T_b^2}{2\pi} (\mathcal{R}^b + (\mathcal{A}^b)^{\mathrm{T}} \mathcal{B}^{-1} \mathcal{A}^b) \vec{w} + T_b \left[\frac{1}{a} (\mathcal{A}^b)^{\mathrm{T}} \begin{pmatrix} \vec{0} \\ \vec{e} \end{pmatrix} \otimes \left(\left(\mathcal{R}^b + (\mathcal{A}^b)^{\mathrm{T}} \, \mathcal{B}^{-1} \, \mathcal{A}^b \right)^{-\mathrm{T}} (\mathcal{A}^b)^{\mathrm{T}} \begin{pmatrix} \vec{0} \\ \vec{e} \end{pmatrix} \right) - \mathcal{I} \right] \mathcal{R}^b \vec{\mathcal{F}}(0, Y\vec{u}). \quad (5.40)$$

Then,

$$(Y, \beta_1) = \arg\min_{Z, \xi} \left\{ \left\| \vec{f}(Z, \xi) \right\|_2^2 : \; Y_{min} \leq Z \leq Y_{max}, \; 0 \leq \xi < 2\pi \right\}.$$

This minimization can be performed with different algorithms, for which, in general, the Jacobian matrix of function $\vec{f}$ with respect to (Y, β_1) should be computed. This can be done using (5.39), by means of the chain rule. Let us notice that the calculation of the Jacobian matrix of mapping $\vec{\mathcal{F}}(0, \cdot)$ involves the solution to the magnetostatic problem (5.15)–(5.19) for time $t = 0$. In Appendix A we detail the computation of both matrices.

5.5 Numerical Results

In this section we present the numerical results obtained for a particular induction machine with squirrel cage rotor, which allow us to validate the methodology proposed in this chapter. In particular, we will use the numerical method proposed in last section to estimates suitable initial currents in the bars of the induction motor, assuming that these currents are purely harmonic functions of time. Next, we solve a transient eddy current formulation using the obtained currents as initial condition, and compare the time needed to reach the steady-state with the one needed by taking null initial currents. We notice that, unlike the formulation used for the approximation of suitable initial currents, in this second step we use a more realistic transient simulation, with rotor bars modelled as solid conductors. These numerical results allow us to illustrate the reduction of the time needed to achieve the steady state with respect to the null initial condition.

In what follows, we describe some of the characteristics of the machine and then we show the numerical results for the described methodology. The characteristics of the machine have been provided to us for this research by Robert Bosch GmbH, and the initial currents are computed for different operating points.

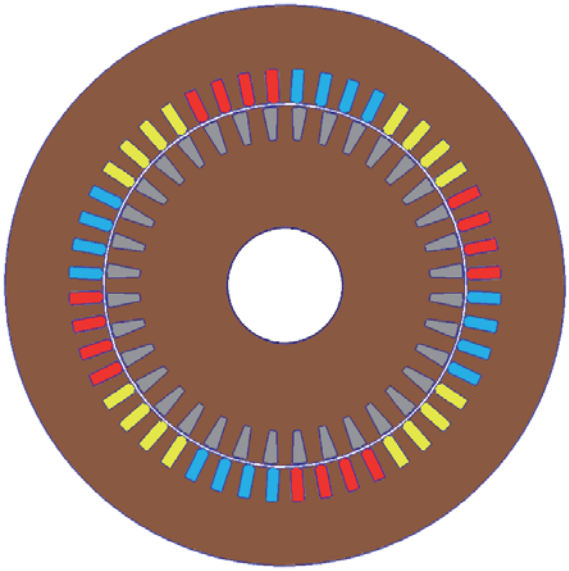

Figure 5.7: Geometric domain. Modification of a picture provided by Robert Bosch GmbH.

5.5.1 Description of the Machine

A cross-section of the induction machine is sketched in Figure 5.7. It is composed by $N_b = 36$ slots in the rotor and $N_c - N_b = 48$ slots in the stator.

This induction motor is a three-phase machine having 2 pole pairs with 12 slots per pole. Figure 5.7 also shows the winding distribution in the stator: red, yellow and blue slots correspond to phases A, B and C, respectively. These source currents are characterized by an electrical frequency f_c and a RMS current I_c through each slot. The currents corresponding to each phase of the stator are defined as

$$
\begin{aligned}
I_A(t) &= \sqrt{2}\, I_c \cos\left(2\pi f_c t\right), \\
I_B(t) &= \sqrt{2}\, I_c \cos\left(2\pi f_c t + \frac{2\pi}{3}\right), \\
I_C(t) &= \sqrt{2}\, I_c \cos\left(2\pi f_c t - \frac{2\pi}{3}\right).
\end{aligned}
$$

Finally, concerning the materials, the rings of the squirrel cage are characterized by a resistance R and the stator coil sides are made of copper. Moreover, the laminated nonlinear material is the electrical steel M330_35A (see [14]).

5.5.2 Initial Currents for Different Operating Points

We recall that if the currents along the rotor bars are approximated by harmonic functions of frequency f_b, the only unknowns to be determined for computing their initial values are Y and

	f_c (Hz)	n_r (rpm)	I_c (A_{RMS})	T_b (s)
Op. Point 1	42.1	1000	675	0.114
Op. Point 2	171.2	5000	314	0.221
Op. Point 3	417.5	12000	675	0.057
Op. Point 4	632.0	18000	531	0.031

Table 5.1: Characteristics of the different operating points.

	Y (A)	β_1 (rad)	$\|\vec{f}(Y,\beta_1)\|^2$	$Y^{(0)}$ (A)	$\beta_1^{(0)}$ (rad)	NL solutions
Op. Point 1	1073.25	3.20	$8.12e-09$	900.00	1.50	14
Op. Point 2	477.78	3.34	$1.12e-08$	400.00	2.00	6
Op. Point 3	1186.80	2.95	$1.75e-09$	1200.00	2.00	8
Op. Point 4	942.20	2.87	$3.80e-10$	1000.00	2.00	5

Table 5.2: Optimal values for the different operating points and computational effort.

β_1. We have proposed to approximate these values by

$$(Y,\beta_1) = \arg\min_{Z,\xi} \left\{ \left\|\vec{f}(Z,\xi)\right\|_2^2 : \; Y_{min} \leq Z \leq Y_{max}, \; 0 \leq \xi < 2\pi \right\},$$

where function $\vec{f}$ is defined by (5.40). In order to validate this methodology, we have considered four operating points corresponding to different electrical sources in the stator and rotor velocities; see Table 5.1. In particular, we notice that the period of the current in the rotor bars, T_b, one order of magnitude smaller in the second operating point 2 with respect to the first one. However, as we have already mentioned, the methodology to compute the initial currents is time-independent, and therefore its computational cost does not depend on these sizes.

For each operating point, we have found the minimum value of function $\left\|\vec{f}(Y,\beta_1)\right\|_2^2$ by using the Matlab function `lsqnonlin`. Table 5.2 shows the optimal values obtained for Y and β_1 and the residual at each operating point. Moreover, in order to measure the computational effort of the `lsqnonlin` function, we have included the initial values, $\left(Y^{(0)} \text{ and } \beta_1^{(0)}\right)$, and the number of nonlinear magnetostatic solutions (NL solutions). The initial values were selected by using a multistart strategy.

Next, we will analyze the consequence of using these optimal values to define the initial currents along the bars in the transient magnetic simulation.

5.5.2.1 Sensitivity Analysis of Steady-State in Terms of Initial Currents

In this section, we will show that the time needed to reach the steady-state in a transient simulation strongly depends on the choice of the initial currents in the rotor bars of the machine. To attain this goal, we will perform a transient simulation starting with initial currents defined from

	Op. Point 1	Op. Point 2	Op. Point 3	Op. Point 4
Bar 1	−1071.40	−468.41	−1165.10	−907.66
Bar 2	−985.38	−407.95	−1172.10	−939.37
Bar 3	−780.48	−298.29	−1037.80	−857.78
Bar 4	−481.45	−152.65	−778.26	−672.73
Bar 5	−124.35	11.40	−424.87	−406.53
Bar 6	247.75	174.08	−20.25	−91.31
Bar 7	589.97	315.76	386.83	234.94
Bar 8	861.03	419.35	747.24	532.84
Bar 9	1028.20	472.37	1017.50	766.48

Table 5.3: Initial currents (in A) defined from Y and β_1 for the different operating points.

the values of Y and β_1 found in the previous section, and we will compare the results with those where the initial currents are equal to zero. The initial current intensities for the four operating points are detailed in Table 5.3. Due to the machine periodicity, we only specify the values for bars 1 to 9.

To analyze if the solution of the transient eddy current model has reached the steady-state, it is usual to study the torque in the rotor and the currents in the bars of the squirrel cage. Therefore, Figures 5.9 to 5.12 show the electromagnetic torque in rotor (left) and the current along the first bar (right) versus time for the different operating points, where τ denotes the electromagnetic torque. In all of these figures, the red curve corresponds to null initial values for the current along the bars, while the blue ones have been obtained by using the values provided by the method introduced in this chapter.

Remark 5.10. *We emphasize that one of the hypothesis of the methodology for computing suitable initial currents in the rotor bars consists in assuming that these currents are uniformly distributed. This assumption has allowed us to write an electromagnetic model for the induction machine having time derivatives only in the equation linking currents and voltage drops, and avoiding, in particular, having a parabolic equation in the bars. In opposition, the transient simulations presented in this section have been performed by considering the bars as solid conductors (see Figure 5.8), and therefore solving a classical eddy current model coupled with circuit equations, like the one presented, for instance, in [93].*

Notice that, in all cases, when starting from the optimal values, the currents reach the steady-state very quickly. However, the time to reach the steady-state in the electromagnetic torque can be very large starting from null currents. In order to assess the potential computational saving of the proposed methodology, we will introduce in the next section a mathematical criterion to determine the steady-state, what allows us to specify the number of time steps needed to reach that state.

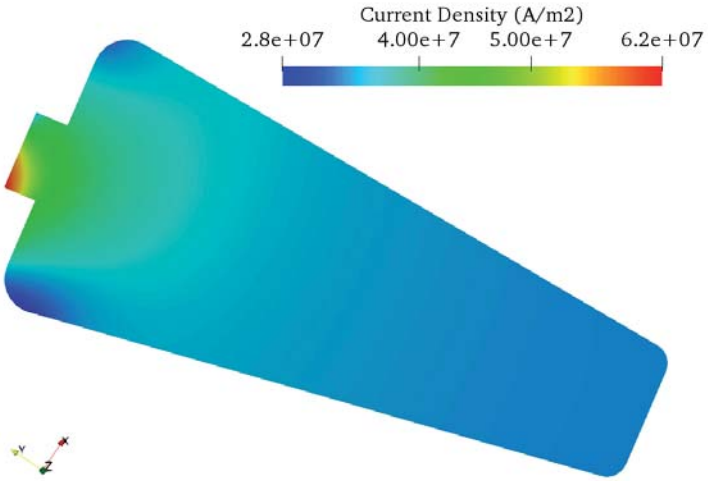

Figure 5.8: Current density distribution in a rotor bar.

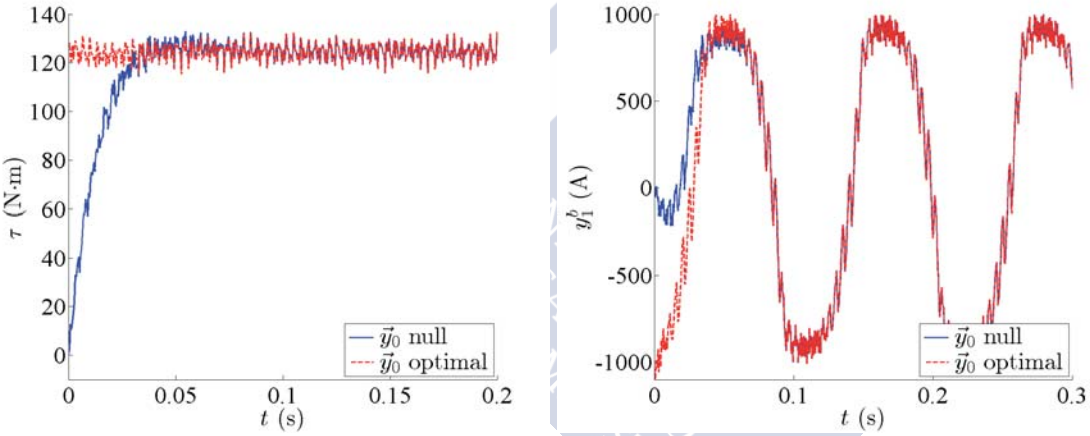

Figure 5.9: Op. Point 1. Torque vs. time (left). Current in bar 1 vs. time (right).

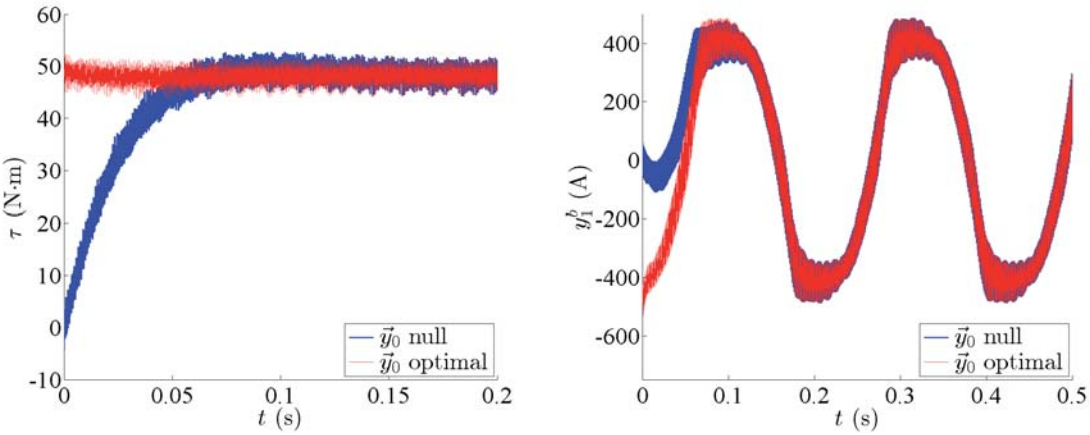

Figure 5.10: Op. Point 2. Torque vs. time (left). Current in bar 1 vs. time (right).

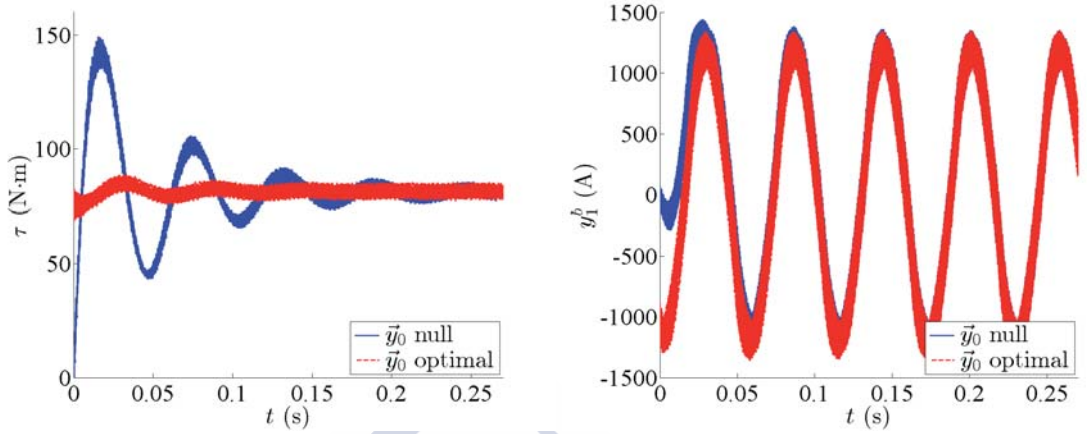

Figure 5.11: Op. Point 3. Torque vs. time (left). Current in bar 1 vs. time (right).

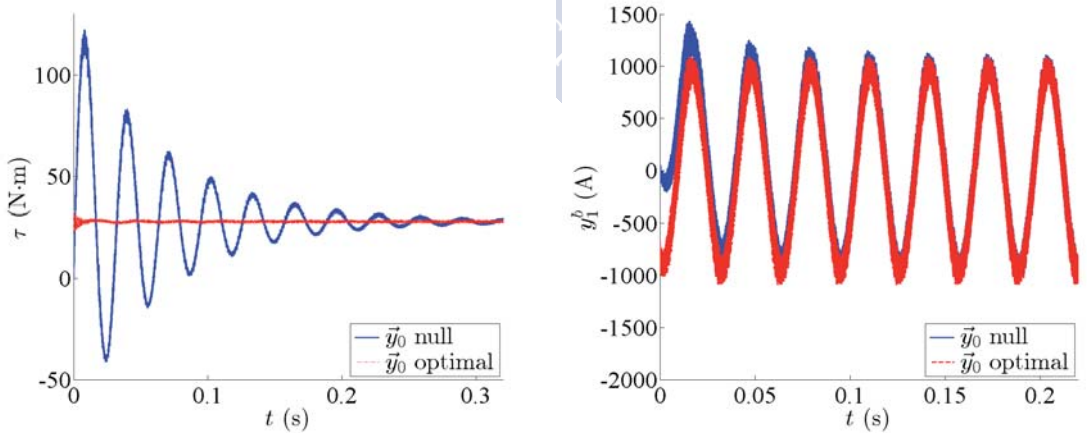

Figure 5.12: Op. Point 4. Torque vs. time (left). Current in bar 1 vs. time (right).

5.5.2.2 Analysis of the Computational Savings

Let us introduce T_{steady} as the time of the transient FEM simulation for which the steady-state is reached. To define this value, let us recall some notation already introduced in Section 5.4. Let n_r be the constant angular velocity at which the rotor is moving (in rpm) and T_r the mechanical period of the rotor motion (in s), that is, $T_r = 60/n_r$.

For each revolution of the machine, $D_n := [nT_r, (n+1)T_r]$, $n = 0, 1, 2, \ldots$, let us consider its uniform time discretization with time step Δt, which is given by:

$$\{nT_r + j\Delta t, j = 1, \ldots, N\} \subset D_n.$$

Then, the mean torque can be defined as:

$$\tau_n := \frac{1}{N}\sum_{j=1}^{N} \tau\left(nT_r + j\Delta t\right),$$

where $\tau : \mathbb{R}^+ \longrightarrow \mathbb{R}$ is a scalar function that expresses the electromagnetic torque as a function of time.

Thus, T_{steady} will be defined as $T_{\text{steady}} = (m+1)T_r$, with m the first natural number for which the relative error between the mean torque in the m-th revolution and the five subsequent ones is less than 2 %. In other words, m is the first natural number for which the following property holds:

$$\frac{|\tau_m - \tau_{m+j}|}{|\tau_m|} < 2\%, \quad j = 1, \ldots, 5.$$

The above criterion has been employed to compute time to the steady-state for the different operating points under study, with the two different initial conditions. The results have been summarised in Table 5.4, both in terms of T_{steady} and the number of revolutions needed to achieve convergence. Notice that the savings are described with respect to the machine revolutions and they are quite remarkable, specially in operating point 4.

Figures 5.13 to 5.20 show the torque over time for the considered operating points. In each case, the time needed to reach the steady-state has been indicated with vertical lines: in red color for initial conditions $\vec{y}^b(0) = \vec{0}$ and in blue color for initial conditions defined through the methodology introduced in this chapter. We remark that, in comparison with the case of null initial currents, starting with the initial currents computed with the proposed methodology leads to a very important computational saving.

	Initial condition	T_{steady} (s)	Number of Revolutions m	Saving (%)
Op. Point 1	$\vec{y}^b(0) = \vec{0}$	0.1200	2	50
	$\vec{y}^b(0) = Y\vec{u}$	0.0600	1	
Op. Point 2	$\vec{y}^b(0) = \vec{0}$	0.0840	7	86
	$\vec{y}^b(0) = Y\vec{u}$	0.0120	1	
Op. Point 3	$\vec{y}^b(0) = \vec{0}$	0.2100	42	74
	$\vec{y}^b(0) = Y\vec{u}$	0.0550	11	
Op. Point 4	$\vec{y}^b(0) = \vec{0}$	0.3467	104	96
	$\vec{y}^b(0) = Y\vec{u}$	0.0133	4	

Table 5.4: Time to reach the steady state for different operating points.

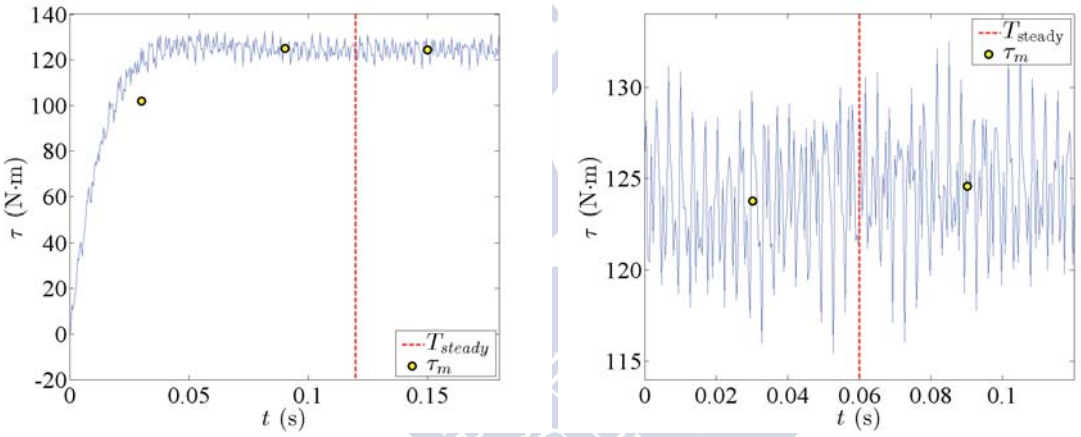

Figure 5.13: Op. Point 1. Torque vs. time. $\vec{y}^b(0) = \vec{0}$ (left) and $\vec{y}^b(0) = Y\vec{u}$ (right).

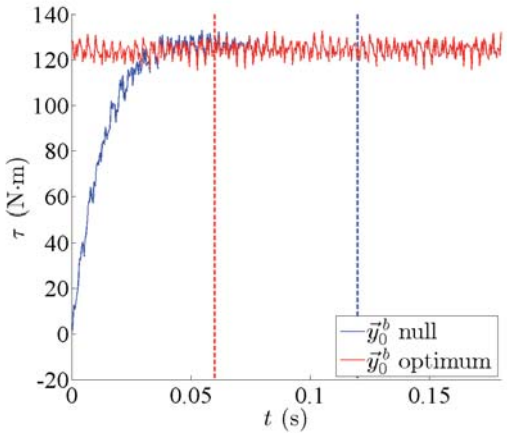

Figure 5.14: Op. Point 1. Time to steady state comparison.

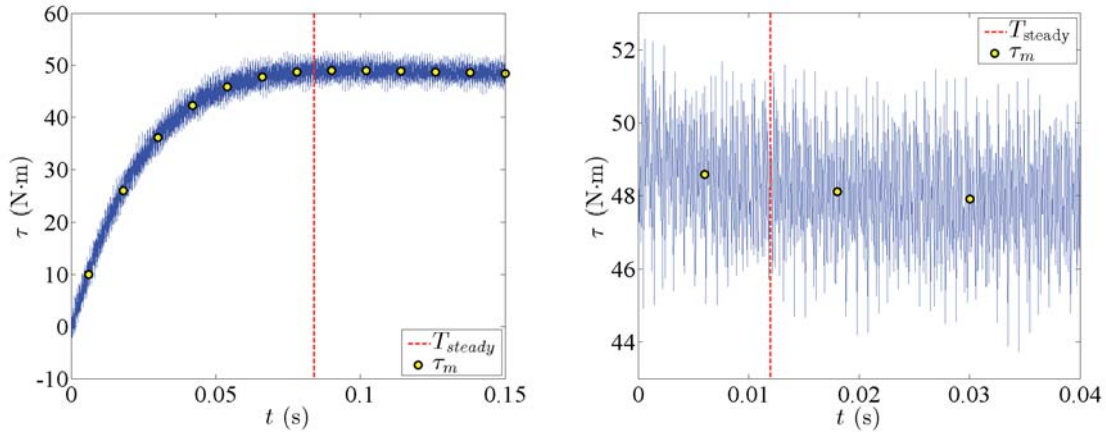

Figure 5.15: Op. Point 2. Torque vs. time. $\vec{y}^b(0) = \vec{0}$ (left) and $\vec{y}^b(0) = Y\vec{u}$ (right).

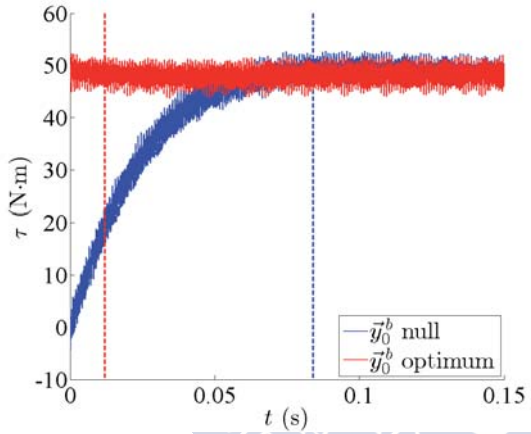

Figure 5.16: Op. Point 2. Time to steady state comparison.

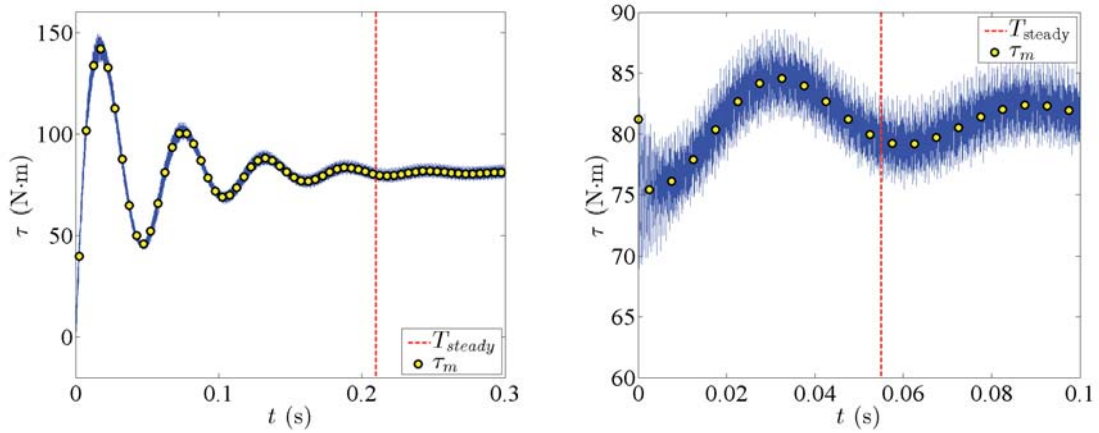

Figure 5.17: Op. Point 3. Torque vs. time. $\vec{y}^b(0) = \vec{0}$ (left) and $\vec{y}^b(0) = Y\vec{u}$ (right).

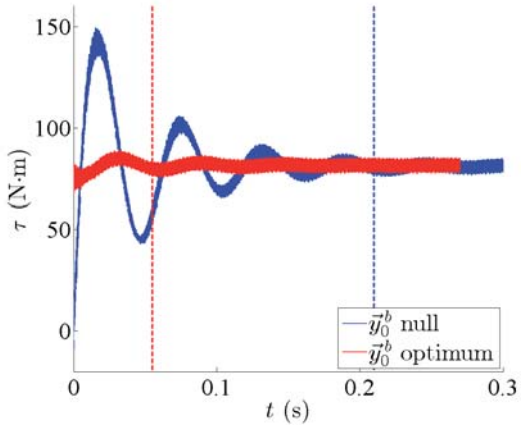

Figure 5.18: Op. Point 3. Time to steady state comparison.

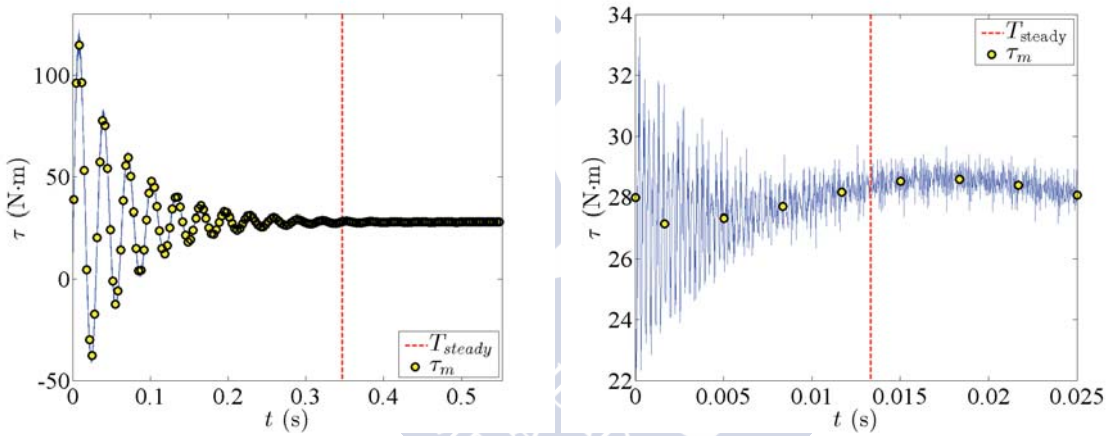

Figure 5.19: Operating point 4. Torque vs. time. $\vec{y}^b(0) = \vec{0}$ (left) and $\vec{y}^b(0) = Y\vec{u}$ (right).

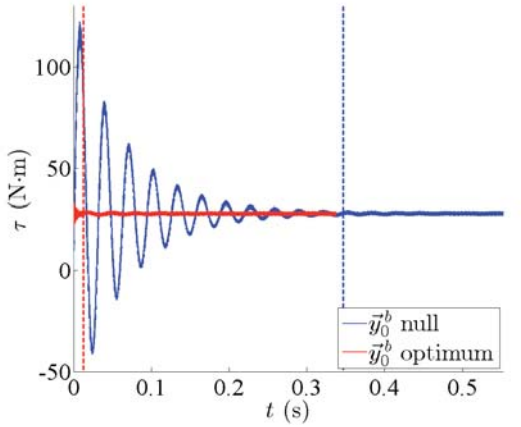

Figure 5.20: Op. Point 4. Time to steady state comparison.

5.6 Generalization of the Method

One of the key points of the methodology proposed in Section 5.4 is approximating the currents along the rotor bars by their fundamental harmonics. A generalization of this step, intended to improve the approximation of these currents, (and thereby the associated initial conditions), can be easily derived. Mainly, the difference with respect to the method appearing in the previous sections consists in using a finite number of sinusoidal terms for the approximation of the rotor bar currents instead of solely its main harmonic. At the end of this section, we will make a few comments on how the additional frequencies could be chosen.

Firstly, for symmetry reasons, we are going to assume that all bars have the same behaviour in the sense that currents $y_n^b(t)$ are the same up to a phase shift. In particular, we will consider that the same frequency components appear in all rotor bar currents with similar importance and that the amplitude of each of these harmonic components is the same for all bars. Therefore, we approximate the vector of rotor bar currents $\vec{y}^b$ by a multiharmonic function with M terms:

$$y_n^b(t) \simeq \left[(\mathcal{A}^b)^{\mathrm{T}} \begin{pmatrix} \vec{0} \\ \vec{e} \end{pmatrix} \right]_n \sum_{m=1}^{M} Y_m \cos(2\pi f_m t + \beta_{m,n}), \tag{5.41}$$

where f_m are the frequencies we are taking into account and, similarly to the previous case, $\beta_{m,n}$ are the phase-shifts between phase A of the current source in the stator and the m-th harmonic of the current along the n-th bar. Accordingly, the initial currents are given by

$$y_n^{b,0} = \left[(\mathcal{A}^b)^{\mathrm{T}} \begin{pmatrix} \vec{0} \\ \vec{e} \end{pmatrix} \right]_n \sum_{m=1}^{M} Y_m \cos \beta_{m,n}. \tag{5.42}$$

Lemma 5.11. *A sufficient condition for the approximated currents introduced in (5.41) to satisfy constraint (5.28) for any values of Y_m and f_m, $m = 1, \ldots, M$, is that the phase-shifts $\beta_{m,n}$, $m = 1, \ldots, M$, $n = 1, \ldots, N_b$, satisfy*

$$\beta_{m,n} = \beta_{m,1} + \frac{z}{p}(n-1)\gamma, \tag{5.43}$$

for any $\beta_{m,1} \in \mathbb{R}$ and $z \in \mathbb{Z}$.

Proof. The proof is very similar to that of Lemma 5.6. If we substitute expressions (5.41) for

$\vec{y}^{\,b}$ in (5.28) and take into account (5.43) we get

$$\begin{aligned}
\vec{y}^{\,b}(t)\cdot(\mathcal{A}^b)^{\mathrm{T}}\begin{pmatrix}\vec{0}\\ \vec{e}\end{pmatrix} &\approx \sum_{n=1}^{N_b}\left[(\mathcal{A}^b)^{\mathrm{T}}\begin{pmatrix}\vec{0}\\ \vec{e}\end{pmatrix}\right]_n^2 \sum_{m=1}^{M} Y_m\cos(2\pi f_m t+\beta_{m,n})\\
&= \sum_{m=1}^{M} Y_m \mathrm{Re}\left(\sum_{n=1}^{N_b}\mathrm{e}^{\,i(2\pi f_m t+\beta_{m,n})}\right)\\
&= \sum_{m=1}^{M} Y_m \mathrm{Re}\left(\mathrm{e}^{\,i(2\pi f_m t+\beta_{m,1})}\sum_{n=1}^{N_b}\mathrm{e}^{\,i\frac{z}{p}(n-1)\gamma}\right)\\
&= \sum_{m=1}^{M} Y_m \mathrm{Re}\left(\mathrm{e}^{\,i(2\pi f_m t+\beta_{m,1})}\frac{\mathrm{e}^{\,i\frac{z}{p}N_b\gamma}-1}{\mathrm{e}^{\,i\gamma}-1}\right)\\
&= \sum_{m=1}^{M} Y_m \mathrm{Re}\left(\mathrm{e}^{\,i(2\pi f_m t+\beta_{m,1})}\frac{\mathrm{e}^{\,i2\pi z}-1}{\mathrm{e}^{\,i\gamma}-1}\right).
\end{aligned}\tag{5.44}$$

Since $\gamma = 2\pi p/N_b$ is not an integer multiple of 2π (as it would mean that p is a multiple of N_b), if $z\in\mathbb{Z}$, then (5.44) is null for any values of Y_m, f_m and $\beta_{m,1}$, $m=1,\ldots,M$. □

Therefore, we will assume in the sequel that phase-shifts $\beta_{m,n}$ satisfy (5.43). Notice that, in Section 5.4, where $M=1$ and $f_1=f_b$, we took $z=p$ in (5.43).

Let us introduce the column vectors $\vec{u}^{\,m}$ and $\vec{w}^{\,m}$, $m=1,\ldots,M$, whose respective n-th components are

$$u_n^m := \left[(\mathcal{A}^b)^{\mathrm{T}}\begin{pmatrix}\vec{0}\\ \vec{e}\end{pmatrix}\right]_n \cos\beta_{m,n} \quad\text{and}\quad w_n^m := \left[(\mathcal{A}^b)^{\mathrm{T}}\begin{pmatrix}\vec{0}\\ \vec{e}\end{pmatrix}\right]_n \sin\beta_{m,n},$$

$n=1,\ldots,N_b$. Then, $\vec{y}^{\,b,0}=\sum_{m=1}^{M} Y_m\vec{u}^{\,m}$. Also, we observe that

$$\vec{u}^{\,m}=\frac{\partial\vec{w}^{\,m}}{\partial\beta_{m,1}} \quad\text{and}\quad \vec{w}^{\,m}=-\frac{\partial\vec{u}^{\,m}}{\partial\beta_{m,1}}.\tag{5.45}$$

Now, let us compute the integrals $\displaystyle\int_0^{T_b}(T_b-t)y_n^b(t)\,dt$ by using the approximation introduced in (5.41). We have

$$\begin{aligned}
\int_0^{T_b}(T_b-t)y_n^b(t)\,dt &\approx \left[(\mathcal{A}^b)^{\mathrm{T}}\begin{pmatrix}\vec{0}\\ \vec{e}\end{pmatrix}\right]_n \int_0^{T_b}(T_b-t)\sum_{m=1}^{M} Y_m\cos(2\pi f_m t+\beta_{m,n})\,dt\\
&= \left[(\mathcal{A}^b)^{\mathrm{T}}\begin{pmatrix}\vec{0}\\ \vec{e}\end{pmatrix}\right]_n \sum_{m=1}^{M}\frac{Y_m}{4\pi^2 f_m^2}\left(\cos\beta_{m,n}-\cos(2\pi f_m T_b+\beta_{m,n})-2\pi f_m T_b\sin\beta_{m,n}\right),
\end{aligned}$$

and hence,

$$\int_0^{T_b}(T_b-t)\vec{y}^{\,b}(t)\,dt \approx \sum_{m=1}^{M}\frac{Y_m}{4\pi^2 f_m^2}\left(\left(1-\cos(2\pi f_m T_b)\right)\vec{u}^{\,m}+\left(\sin(2\pi f_m T_b)-2\pi f_m T_b\right)\vec{w}^{\,m}\right).\tag{5.46}$$

Therefore, the problem to be solved is:

Problem 5.12. *Find Y_m, $\beta_{m,1}$, $m = 1, \dots, M$, and μ^M such that,*

$$- T_b \mathcal{R}^b \vec{\mathcal{F}} \left(0, \sum_{m=1}^{M} Y_m \vec{u}^m \right) + \sum_{m=1}^{M} \frac{Y_m}{4\pi^2 f_m^2} \left((1 - \cos(2\pi f_m T_b)) \left(\mathcal{R}^b + (\mathcal{A}^b)^{\mathrm{T}} \mathcal{B}^{-1} \mathcal{A}^b \right) \vec{u}^m \right.$$
$$\left. + (\sin(2\pi f_m T_b) - 2\pi f_m T_b) \left(\mathcal{R}^b + (\mathcal{A}^b)^{\mathrm{T}} \mathcal{B}^{-1} \mathcal{A}^b \right) \vec{w}^m \right) + \mu^M (\mathcal{A}^b)^{\mathrm{T}} \begin{pmatrix} \vec{0} \\ \vec{e} \end{pmatrix} = \vec{0}.$$

As for the case $M = 1$ and $f_m = f_b$, we can eliminate μ^M in the above system and then solve for Y_m and $\beta_{m,1}$, $m = 1, \dots, M$, by using a nonlinear least-square method. We have

$$\mu^M = \frac{\left(\mathcal{R}^b + (\mathcal{A}^b)^{\mathrm{T}} \, \mathcal{B}^{-1} \, \mathcal{A}^b \right)^{-1} \, T_b \mathcal{R}^b \vec{\mathcal{F}} \left(0, \sum_{m=1}^{M} Y_m \vec{u}^m \right) \cdot (\mathcal{A}^b)^{\mathrm{T}} \begin{pmatrix} \vec{0} \\ \vec{e} \end{pmatrix}}{\left(\mathcal{R}^b + (\mathcal{A}^b)^{\mathrm{T}} \, \mathcal{B}^{-1} \, \mathcal{A}^b \right)^{-1} (\mathcal{A}^b)^{\mathrm{T}} \begin{pmatrix} \vec{0} \\ \vec{e} \end{pmatrix} \cdot (\mathcal{A}^b)^{\mathrm{T}} \begin{pmatrix} \vec{0} \\ \vec{e} \end{pmatrix}}.$$

By replacing this expression we get

$$- T_b \mathcal{R}^b \vec{\mathcal{F}} \left(0, \sum_{m=1}^{M} Y_m \vec{u}^m \right) + \sum_{m=1}^{M} \frac{Y_m}{4\pi^2 f_m^2} \left((1 - \cos(2\pi f_m T_b)) \left(\mathcal{R}^b + (\mathcal{A}^b)^{\mathrm{T}} \mathcal{B}^{-1} \mathcal{A}^b \right) \vec{u}^m \right.$$
$$\left. + (\sin(2\pi f_m T_b) - 2\pi f_m T_b) \left(\mathcal{R}^b + (\mathcal{A}^b)^{\mathrm{T}} \mathcal{B}^{-1} \mathcal{A}^b \right) \vec{w}^m \right)$$
$$+ \frac{1}{a} \left[\left(\mathcal{R}^b + (\mathcal{A}^b)^{\mathrm{T}} \, \mathcal{B}^{-1} \, \mathcal{A}^b \right)^{-1} \, T_b \mathcal{R}^b \vec{\mathcal{F}} \left(0, \sum_{m=1}^{M} Y_m \vec{u}^m \right) \cdot (\mathcal{A}^b)^{\mathrm{T}} \begin{pmatrix} \vec{0} \\ \vec{e} \end{pmatrix} \right] (\mathcal{A}^b)^{\mathrm{T}} \begin{pmatrix} \vec{0} \\ \vec{e} \end{pmatrix} = \vec{0},$$

which can also be written as

$$T_b \left[\frac{1}{a} (\mathcal{A}^b)^{\mathrm{T}} \begin{pmatrix} \vec{0} \\ \vec{e} \end{pmatrix} \otimes \left(\left(\mathcal{R}^b + (\mathcal{A}^b)^{\mathrm{T}} \, \mathcal{B}^{-1} \, \mathcal{A}^b \right)^{-\mathrm{T}} (\mathcal{A}^b)^{\mathrm{T}} \begin{pmatrix} \vec{0} \\ \vec{e} \end{pmatrix} \right) - I \right] \mathcal{R}^b \vec{\mathcal{F}} \left(0, \sum_{m=1}^{M} Y_m \vec{u}^m \right)$$
$$+ \sum_{m=1}^{M} \frac{Y_m}{4\pi^2 f_m^2} \left((1 - \cos(2\pi f_m T_b)) \left(\mathcal{R}^b + (\mathcal{A}^b)^{\mathrm{T}} \mathcal{B}^{-1} \mathcal{A}^b \right) \vec{u}^m \right.$$
$$\left. + (\sin(2\pi f_m T_b) - 2\pi f_m T_b) \left(\mathcal{R}^b + (\mathcal{A}^b)^{\mathrm{T}} \mathcal{B}^{-1} \mathcal{A}^b \right) \vec{w}^m \right) = \vec{0}. \quad (5.47)$$

It is important to notice that one can add harmonic terms selectively according to their importance. One way to address this choice is to compute the so-called *energy spectral density* of the steady-state current in the rotor bars, $S_{\vec{y}^b}(f)$, $f \in \mathbb{R}$, which describes the distribution of energy into frequency components f of $\vec{y}^b$ (see, for instance, [87]). This provides possible frequencies to include in the analysis.

Let us denote by $\widehat{y}_n^b(f)$ the Fourier transform of the current in the n-th rotor bar, which is defined in the following way:

$$\widehat{y}_n^b(f) = \int_{-\infty}^{\infty} y_n^b(t) \mathrm{e}^{-i2\pi f t} \, dt.$$

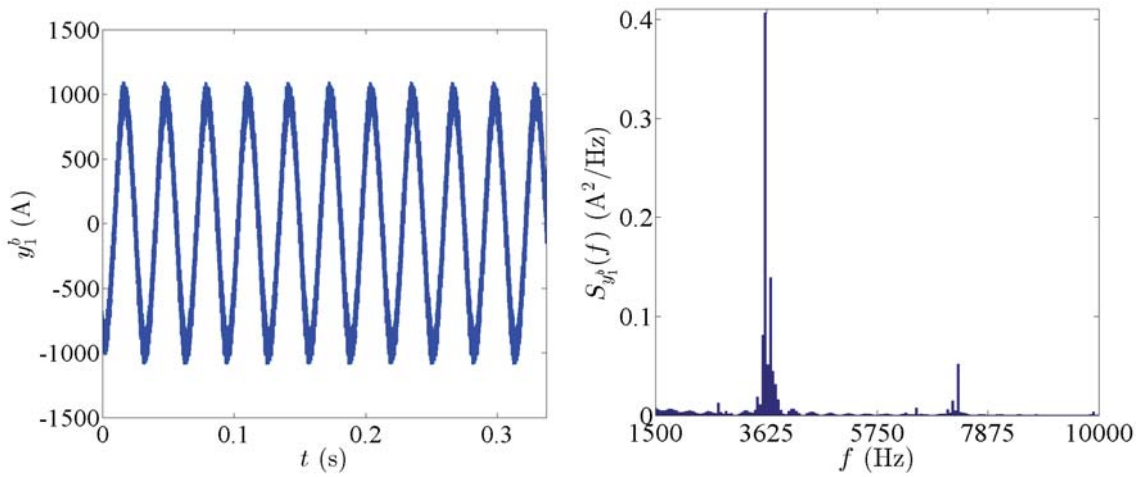

Figure 5.21: Current $\vec{y}^b(t)$ (left) and $S_{\vec{y}^b}(f)$ (right).

Then, the energy spectral density of $y_n^b(t)$ is defined as $S_{y_n^b}(f) = \left|\widehat{y}_n^b(f)\right|^2$, $f \in \mathbb{R}$. For instance, in Figure 5.21–right we show an approximation for the energy spectral density corresponding to the steady-state current in the first bar for operating point 4 (see Section 5.5), shown in Figure 5.21–left. To perform this approximation, we have used the discrete Fourier transform instead of the continuous one as we only had access to the rotor currents sampled at discrete times. Moreover, we notice that only positive frequencies are shown because, since the rotor currents are real-valued functions of time, $S_{\vec{y}^b}(-f) = S_{\vec{y}^b}(f)$.

Finally, we highlight that the above procedure needs the pre-computation of the current in the rotor bars, which is not suitable for the purpose of our methodology. However, according to the literature, there exist frequency components that tend to appear in the rotor bar currents, which can be computed *a priori*, only in terms of the machine specifications. A particular type of these harmonic components, of special interest in electrical engineering, are the so-called *spatial harmonics*. These components of the rotor bar currents are induced by the spatial periodicities present in the magnetic flux density at the machine air-gap, which are caused by the unsymmetrical physical structure of both stator and rotor. According to [109], these frequencies can be expressed in terms of the frequency of the current in the stator coil-sides, f_c, and the slip of the machine, s, in the following way:

$$f_\nu = f_c(1 - (1 + 6\nu)(1 - s)), \quad \nu \in \mathbb{Z}. \tag{5.48}$$

In what follows, we are going to illustrate the use of the generalized methodology in the case of operating point 4 from Section 5.5, solving problem (5.47) considering the fundamental current f_b and some other spatial harmonics of the steady-state currents in the rotor bars. In Table 5.5 we specify the frequencies that we have used in the simulations. In particular, we notice that, for $M = 5$, these frequencies are precisely the ones with higher energy spectral density in Figure 5.21–right.

If we define the phase-shifts corresponding to a spatial harmonic of order ν as:

$$\beta_{n,\nu} = \beta_{1,\nu} + (1 + 6\nu)(n - 1)\gamma, \quad n = 1, \ldots, N_b,$$

ν	$M=5$ f_ν (Hz)	$M=7$ f_ν (Hz)	$M=9$ f_ν (Hz)
0	32	32	32
1	−3568	−3568	−3568
−1	3632	3632	3632
2	−7168	−7168	−7168
−2	7232	7232	7232
3		−10768	−10768
−3		10832	10832
4			−14368
−4			14432

Table 5.5: First spatial frequencies for Op. Point 4.

we can solve problem (5.47) in the least-square sense, obtaining approximations for Y_ν and $\beta_{1,\nu}$. More precisely, if we call $\vec{f}$ the expression appearing in the left-hand side of (5.47), we have found the minimum value of $\left\|\vec{f}(Y_\nu, \beta_{1,\nu})\right\|_2^2$ by using the Matlab function `lsqnonlin`.

In Table 5.6 we show, for the case $M = 7$, the optimal values obtained when solving the minimization problem with different starting points. For each of these optimal values, we have specified the norm of the residual at the optimal point (that is, the norm of the function to minimize). We notice that several local minima were found with similar residual, but in Figure 5.22 we observe that they lead to very different approximations of the exact initial currents.

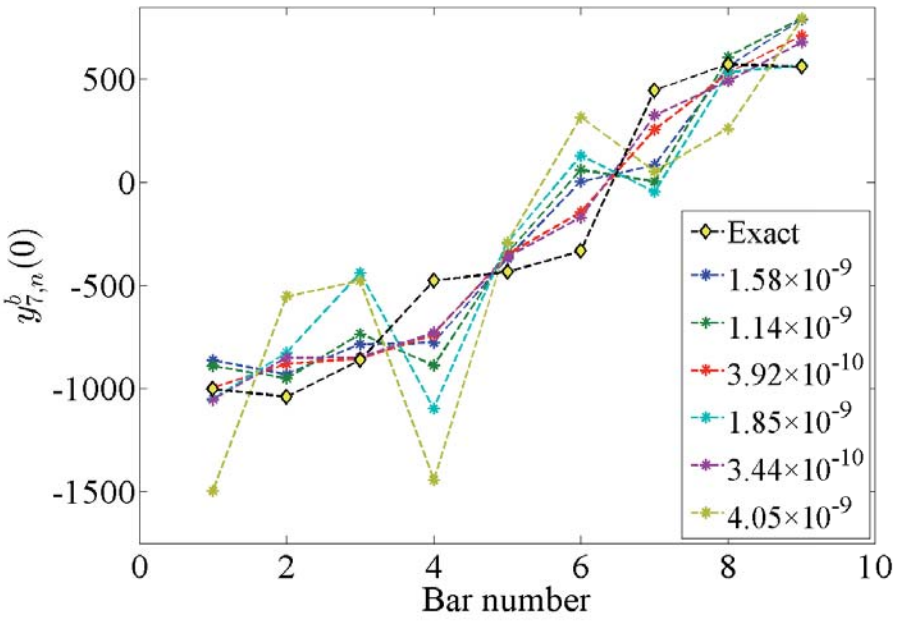

Figure 5.22: Comparative of initial currents $y^b_{7,n}(0)$ with the exact value $y^b_n(0)$, $n = 1, \ldots, 9$.

ν	0	1	-1	2	-2	3	-3	$\|\vec{f}(Y_\nu, \beta_{1,\nu})\|^2$
$Y_\nu^{(0)}$ (A)	700.0	7.0	7.0	7.0	7.0	7.0	7.0	
Y_ν (A)	829.9	50.9	33.9	34.5	32.3	49.0	48.9	1.6×10^{-9}
$\beta_{1,\nu}^{(0)}$ (rad)	2.0	2.0	2.0	2.0	2.0	2.0	2.0	
$\beta_{1,\nu}$ (rad)	2.9	1.2	1.5	1.8	1.2	3.0	3.0	
$Y_\nu^{(0)}$ (A)	700.0	10.0	10.0	10.0	10.0	10.0	10.0	
Y_ν (A)	838.5	74.4	53.1	54.2	72.0	53.1	53.1	1.1×10^{-9}
$\beta_{1,\nu}^{(0)}$ (rad)	2.0	2.0	2.0	2.0	2.0	2.0	2.0	
$\beta_{1,\nu}$ (rad)	2.8	1.4	1.7	1.8	1.2	3.1	3.1	
$Y_\nu^{(0)}$ (A)	900.0	40.0	40.0	40.0	40.0	40.0	40.0	
Y_ν (A)	841.4	35.2	16.4	15.3	37.2	51.2	51.6	3.9×10^{-10}
$\beta_{1,\nu}^{(0)}$ (rad)	2.0	2.0	2.0	2.0	2.0	2.0	2.0	
$\beta_{1,\nu}$ (rad)	2.9	3.2	1.7	3.5	2.9	2.7	2.7	
$Y_\nu^{(0)}$ (A)	1000.0	70.0	70.0	70.0	70.0	70.0	70.0	
Y_ν (A)	664.6	136.3	106.2	106.6	136.6	100.6	102.9	1.9×10^{-8}
$\beta_{1,\nu}^{(0)}$ (rad)	2.0	2.0	2.0	2.0	2.0	2.0	2.0	
$\beta_{1,\nu}$ (rad)	2.8	1.9	2.5	2.5	1.8	3.0	3.0	
$Y_\nu^{(0)}$ (A)	1200.0	100.0	100.0	100.0	100.0	100.0	100.0	
Y_ν (A)	903.3	128.3	24.1	22.6	103.8	18.0	22.5	3.4×10^{-10}
$\beta_{1,\nu}^{(0)}$ (rad)	2.0	2.0	2.0	2.0	2.0	2.0	2.0	
$\beta_{1,\nu}$ (rad)	2.9	4.2	3.1	3.5	2.0	3.2	3.2	
$Y_\nu^{(0)}$ (A)	2000.0	300.0	300.0	300.0	300.0	300.0	300.0	
Y_ν (A)	720.6	0.0	300.0	300.0	253.8	241.1	241.1	4.1×10^{-9}
$\beta_{1,\nu}^{(0)}$ (rad)	2.0	2.0	2.0	2.0	2.0	2.0	2.0	
$\beta_{1,\nu}$ (rad)	2.4	2.7	2.0	3.0	2.3	3.7	3.7	

Table 5.6: Optimal values corresponding with different starting iteration (case $M = 7$).

ν	$M=5$		$M=7$		$M=9$	
	Y_ν (A)	$\beta_{1,\nu}$ (rad)	Y_ν (A)	$\beta_{1,\nu}$ (rad)	Y_ν (A)	$\beta_{1,\nu}$ (rad)
0	942.73	2.87	903.31	2.85	904.30	2.90
1	16.90	2.72	128.33	4.21	29.69	3.67
−1	82.02	4.82	24.11	3.12	180.00	4.88
2	82.66	4.90	22.62	3.53	6.52	2.40
−2	16.15	1.18	103.78	1.98	18.05	3.92
3			17.97	3.17	24.68	2.12
−3			22.50	3.17	24.55	2.12
4					32.60	3.80
−4					4.60	1.75

Table 5.7: Optimal points corresponding to different values of M.

Moreover, in Table 5.7 we show the optimal points obtained for different values of M and the frequencies appearing in Table 5.5. For each case, we used a multistart strategy and, from the obtained optimal points, we selected the best one in terms of the average of the relative error in the initial current in the rotor bars with respect to the exact values $\vec{y}^b$:

$$\overline{\mathcal{E}\left(\vec{y}_M^{b,0}\right)} := \frac{1}{9}\sum_{n=1}^{9}\mathcal{E}\left(y_{M,n}^{b,0}\right) = \frac{1}{9}\sum_{n=1}^{9}\frac{\left|y_n^b(0)-y_{M,n}^b(0)\right|}{|y_n^b(0)|}, \quad M\geq 1,$$

with

$$y_{1,n}^b(0) = \left[(\mathcal{A}^b)^{\mathrm{T}}\begin{pmatrix}\vec{0}\\ \vec{e}\end{pmatrix}\right]_n Y\cos(\beta_1+(n-1)\gamma),$$

$$y_{M,n}^b(0) = \left[(\mathcal{A}^b)^{\mathrm{T}}\begin{pmatrix}\vec{0}\\ \vec{e}\end{pmatrix}\right]_n \sum_{\nu=-(M-1)/2}^{(M-1)/2} Y_\nu\cos(\beta_{1,\nu}+(1+6\nu)(n-1)\gamma), \quad M>1,$$

and Y, β_1 taken from Table 5.2. In Table 5.8 we compare the relative difference between the numerical steady-state currents $\vec{y}^b$ and the harmonic approximations $\vec{y}_M^b$ at $t=0$ computed from the optimal values in Table 5.7. We deduce that adding more harmonic component does not necessarily lead to a better approximation of the initial currents. Additionally, in Figure 5.23 we show the approximation of these initial currents for each bar and compare them with the exact initial currents.

Finally, Figure 5.24 shows the torque over time in the eddy current simulation of the induction motor taking as initial currents the ones computed from the values appearing in the last column of Table 5.8, comparing it with the torque when these initial currents are computed using the method explained in Section 5.4. We notice that, even though the error with respect to the exact initial currents is much lower in the first case, $4.06\ \%$ for $M=9$ versus $25.63\ \%$ for $M=1$, the transient part of the solution is greater in this case.

	$\mathcal{E}(\vec{y}_1^b)$ (%)	$\mathcal{E}(\vec{y}_5^b)$ (%)	$\mathcal{E}(\vec{y}_7^b)$ (%)	$\mathcal{E}(\vec{y}_9^b)$ (%)
Bar 1	9.45	11.00	5.09	5.79
Bar 2	9.67	6.89	18.27	1.15
Bar 3	0.58	6.46	1.55	2.11
Bar 4	41.05	14.36	52.76	6.41
Bar 5	6.24	10.39	16.79	5.18
Bar 6	72.53	34.17	48.82	9.86
Bar 7	47.42	22.41	27.31	2.23
Bar 8	6.83	10.66	14.48	0.00
Bar 9	36.89	5.05	21.31	3.82
Average	25.63	13.49	22.93	4.06

Table 5.8: Relative difference between $\vec{y}^b(0)$ and the harmonic/multi-harmonic approximation.

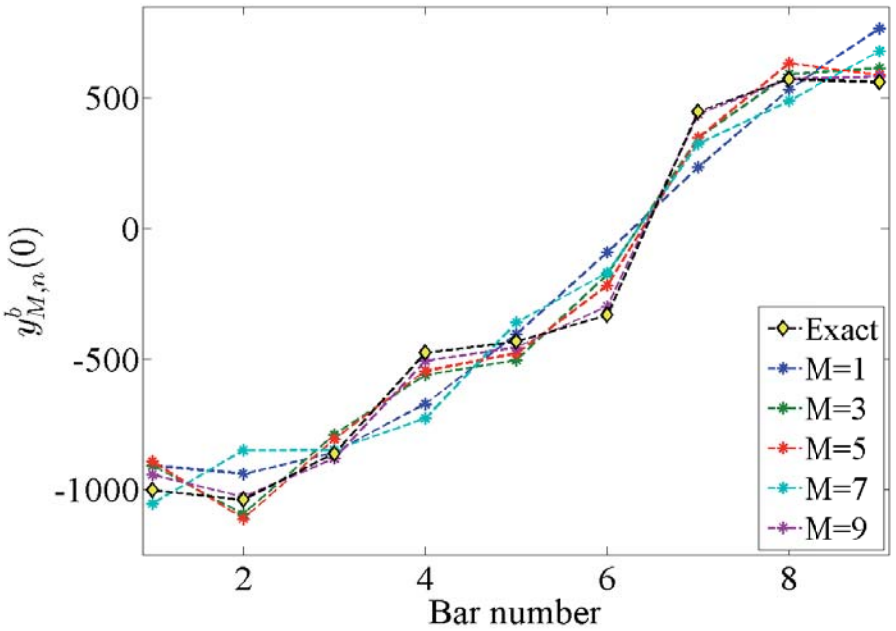

Figure 5.23: Comparative of initial currents $y^b_{M,n}(0)$ with the exact value $y^b_n(0)$, $n = 1, \ldots, 9$.

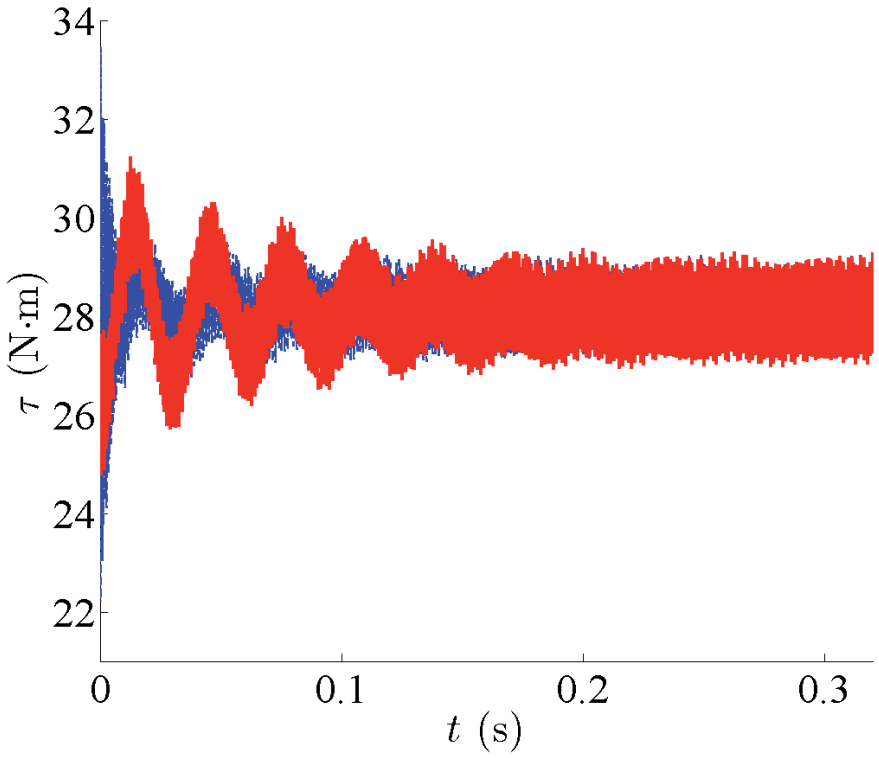

Figure 5.24: Torque vs time. Initial currents $\vec{y}_1^b(0)$ (blue) and $\vec{y}_9^b(0)$ (red).

USC
UNIVERSIDADE
DE SANTIAGO
DE COMPOSTELA

USC
UNIVERSIDADE
DE SANTIAGO
DE COMPOSTELA

Conclusions and Future Research

In this part of the memoir we present a brief description of the main contributions of this thesis and we detail the related work to develop in the future.

Conclusions

This thesis deals with the study of several problems appearing in the context of low-frequency electromagnetics, and it is divided into two parts. In the first part, we have considered two eddy current problems, the first one from the point of view of the mathematical and numerical analysis, and the second one for the purpose of developing a numerical tool that simulates magnetization and demagnetization processes of axisymmetric ferromagnetic pieces. In the second part of the memoir, we have focused on the mathematical modeling and numerical simulation of electrical machines. For this purpose, we have firstly presented a two-dimensional transient magnetic model, written in terms of the magnetic vector potential, coupled with circuit equations that has allowed us to consider sources in conductors given in terms of voltage drops. Then, starting from this formulation, we have proceeded to consider three different problems. In the two first ones, we perform the mathematical and numerical analysis of the previous formulation, with sources in conductors given in terms of voltage sources, and of an optimal control problem with a state being the solution to a problem closely related to this formulation. Then, in the final chapter, we have enhanced the mathematical model by taking more general circuit equations and motion into account, in order to develop a novel methodology to reduce the transient-state in the simulation of induction motors.

In the sequel, we detail the results obtained within each chapter of the memoir:

Chpt. 1. In this chapter we have studied the so-called $\boldsymbol{T}$,ϕ–ϕ formulation for the harmonic eddy current problem with electric ports, that is, with sources given in terms of currents and/or voltage drops through the boundary of some conductors. Moreover, we have considered two possibilities, depending on wether we apply or not a gauge condition to field $\boldsymbol{T}$ in order to get a unique decomposition of the magnetic field $\boldsymbol{H}$. For the ungauged problem, we have proved that it has a solution and that, even though it is not unique, every solution leads to the same magnetic field. To derive the result, we

have shown the equivalence, in terms of $\boldsymbol{H}$, between the $\boldsymbol{T}$,ϕ–ϕ formulation and another formulation for the same problem, written in terms of $\boldsymbol{H}$, whose well-posedness is immediate from results appearing in the literature. Then, we have applied the same technique to obtain existence and uniqueness of solution to the gauged problem. Additionally, we have performed a finite element discretization for both formulations, with first-order Nédélec elements for $\boldsymbol{T}$ and first-order Lagrange elements for potential ϕ. Again, we have obtained analogous results concerning the well-posedness of the discrete formulations, and we have shown an a-priori error estimate of order $O(h)$ under typical regularity assumptions. The obtained results provide theoretical support to this well-known formulation, often implemented in commercial software.

Chpt. 2. The goal of this chapter is to describe a finite element method for the numerical simulation of magnetization and demagnetization processes in materials with hysteresis. It was motivated by a non-destructive test known as magnetic particle inspection (MPI), intended to detect subsurface cracks in ferromagnetic pieces. In particular, we have restricted ourselves to cylindrical specimens and we have considered processes subjected to sources having different directions, known as circular and longitudinal magnetization. In each case, we have detailed the mathematical model allowing us to obtain the final remanent flux in the piece, and the numerical techniques exploited for its discretization. The inclusion of hysteresis in the MPI simulation, along with the inclusion of the demagnetization stage, are relevant contributions with respect to the results found in the literature related to this topic.

Chpt. 3. This chapter deals with the mathematical and numerical analysis of a nonlinear 2D transient magnetic model with sources given in terms of the voltage drop excitations in conductors and remanent magnetic fluxes within permanent magnets. The formulation consists of a distributed nonlinear magnetostatic model, with time playing the role of a parameter, and a circuit equation linking currents and voltage drops. This last equation has been used to write the problem as an implicit ODE system, whose operator involves the resolution of the distributed model. The model was spatially discretized using a finite element method and an implicit Euler scheme was employed for time discretization. We have performed the mathematical analysis of the problem at both the continuous and discrete levels, and we have obtained an $O(h + \Delta t)$ error estimate under suitable regularity assumptions. The proved results represent a first contribution to the theoretical study of the genuine problem arising in the modeling of permanent magnet electrical machines with voltage drop excitations.

Chpt. 4. In this chapter we have addressed the optimal control of a permanent magnet synchronous motor, with the intention of giving rigourous mathematical support to a particular problem concerning the electromagnetic behaviour of the machine. In particular, we sought to control the currents in the stator coils that minimize the power losses in these conductors, subject to the restriction that the resulting motor generates a minimum torque, along with the typical box-constraints on the controls. In this part of the thesis we have shown the existence of local optimal controls and the associated lagrange multipliers, at both the continuous and discrete levels, and we have derived an adjoint problem allowing us to simplify the computation of the derivatives of the Lagrangian. The latter is very useful in the implementation, for which we have

chosen an Augmented Lagrangian Technique. Moreover, under certain regularity assumptions, we have proved that the discrete controls converge to the continuous ones. The main contribution of this chapter is the rigourous theoretical analysis of a particular optimal control problem, inspired in the ones appearing in the literature for the electromagnetic behaviour of a permanent magnet synchronous motor.

Chpt. 5. In this chapter, we have presented a novel methodology to accelerate the computation of the steady-state solution to a problem that models the electromagnetic behaviour of induction motors with squirrel-cage rotor, when the source in the stator coil sides is given in terms of the currents. Essentially, the procedure consists in computing appropriate initial conditions for the currents in the rotor bars, allowing us to obtain the steady-state fields by solving the transient magnetic model in just a few machine revolutions. Firstly, we have enhanced the mathematical previous formulation in order to get a more realistic model of the induction model. Specifically, we have considered more general circuit equations to incorporate the squirrel-cage end-rings into the model, and we have taken the motion of the machine into account. Then, we have developed an approximation of this model that provides us with suitable initial currents by computing the solution, in the least-square sense, to an overdetermined problem with only two unknowns. One of the key points of the approximation consists in simplify the current in the rotor bars to time-harmonic functions. Finally, we have briefly introduced a possible generalization to the methodology, that considers the current approximation as the sum of several harmonics. We highlight that the proposed methodology has been applied to several realistic examples provided by Robert Bosch GmbH, leading to important savings from a computational point of view.

For most numerical methods appearing in the thesis, we implemented the corresponding source codes (either in Fortran or Matlab), which have allowed us to asses their performance by means of academic and realistic examples.

Future Research

Finally, we consider that there are still many open problems related to the ones discussed in the thesis. We describe here some of the further work we would like to develop in the future:

Chpt. 1.

- We plan to perform the mathematical and numerical analysis of the transient $\boldsymbol{T}, \phi - \phi$ formulation in three-dimensional bounded domains with electric ports. Similarly to the study performed in this chapter for the harmonic case, we will try to establish an equivalence between the weak formulation of this problem and the one appearing in [22], in terms of the magnetic field constructed from its potentials, $\boldsymbol{H} = \widetilde{\boldsymbol{T}} + \boldsymbol{T}_0 - \mathbf{grad}\,\phi$. Moreover, we will try to extend the transient formulation to the nonlinear case, in which the magnetic permeability depends nonlinearly on the modulus of the magnetic field $\boldsymbol{H}$.

- As a second step, we will study coupling of the above problem with lumped equations modelling electrical circuits, using equation (1.22) as the constitutive law of the components of the circuit corresponding to conductors appearing in the distributed model.

Chpt. 2.

- We have the intention of performing the mathematical and numerical analysis of the problem describing the longitudinal magnetization appearing in this chapter. This is a nonlinear one-dimensional problem characterised by a degenerate parabolic partial differential equations, with a Dirac measure in the right-hand side of its weak formulation. For this purpose, we will try to take advantage of some results already present in the literature for problems with a similar PDE structure (see [2]). Moreover, the nonlinearity involves a hysteresis operator, which will be assumed to be causal, strongly continuous and piecewise monotone for the mathematical analysis, in order to be able to adapt the techniques appearing in [107] for an eddy current problem involving hysteresis.
- On the other hand, we will try to change the longitudinal model in order to be able to simulate magnetization and demagnetization processes with general axisymmetrical pieces and without approximating the source in the coils with a surface current density. For this purpose, we will write the mathematical model in terms of the magnetic vector potential, obtaining an scalar formulation. However, under these settings, this scalar potential leads to a magnetic flux density having components in the piece meridional section, requiring the use of a vector hysteresis law.

Chpt. 3.

- We have the intention of exploring the possibility of incorporating motion to the mathematical and numerical analysis of Problem II.2. This would allow us to approximate the genuine problem arising in the modeling of permanent magnets machines.
- Additionally, we would like to adapt the study developed for the problem appearing in this chapter, combining voltage with current sources in conductors; that is, perform the mathematical and numerical analysis of Problem II.2. The consideration of this new source type leads to a dependence in time of operator $\vec{\mathcal{F}}$, what affects the analysis.

Chpt. 4.

- Firstly, we are currently working on the error estimate of the discrete controls and lagrange multipliers to the continuous ones. Moreover, a publication describing the results obtained in this chapter, in which we will consider a more general setting with several state constraints.
- As a second step, we would like to extend the optimal control problem to a case with voltage drop sources. In this way, we would exploit the analysis developed in Chapter 3 for the state problem analysis.
- On the other hand, we will try to analyze a similar control problem involving a three-dimensional formulation written in terms of scalar magnetic potentials (see, for instance, [30]). This would allow us to consider more general electrical machines, such as axial or transversal flux motors.

Chpt. 5.

- We plan to exploit the methodology for other induction motor cases, such as induction motors with squirrel-cage rotor in which the inductance of the end-rings cannot be neglected, or induction motors with windings in the rotor (as substitutes for the squirrel-cage).
- Concerning the transient nonlinear eddy current model coupled with circuit equations that describes the electromagnetic behaviour of the induction machine, we would like to perform its mathematical and numerical analysis. For this purpose, we would start with the study performed in [39], in which the authors consider a linear eddy current problem with moving geometries, adding the nonlinearity of the cores and the circuit equations for the squirrel-cage.
- Furthermore, we would like to consider the extension of the methodology developed in this chapter to fit under more general ODE problems with periodic solution.

USC
UNIVERSIDADE
DE SANTIAGO
DE COMPOSTELA

Acknowledgements

First and foremost, I wish to express my deep gratitude to my supervisor Prof. Pilar Salgado, who wisely and patiently guided my steps through my research, and helped me to grow as a scientist. I could not have imagined a better advisor for my study.

Besides, I want to thank Prof. Alfredo Bermúdez and Prof. Dolores Gómez, who gave me the opportunity to join their research team, introducing me to the field of Applied Mathematics at an early stage of my career. Both of them contributed in time and ideas to much of this work. Also, I want to thank all professors in the Department of Applied Mathematics of the University of Santiago de Compostela, since all of them participated in this work to a greater or lesser extent.

I am indebted to Prof. Rodolfo Rodriguez and Prof. Pablo Venegas for their feedback and dedicated involvement, both during their stays in Santiago and in the distance.

I also want to thank Prof. Fredi Tröltzsch for the many hints and insightful comments he gave me during the total of six months I spent at the Technical University of Berlin learning about Optimal Control. Along with Esther, Christopher and Mathieu, he made Berlin a home away from home for me. Vielen Dank!

I want to express my gratitude to Prof. Ana Alonso Rodríguez and Prof. Alberto Valli for fruitful discussions that helped me with different topics, in particular with the theory of loop fields.

Moreover, I would like to acknowledge Dr. Marcus Alexander and Dr. Stefan Kurz from Robert Bosch GmbH for useful insights about induction machines and for providing the data for the numerical results appearing in Chapter 5.

Finally, I want to thank my family for their support during these years, along with all the fellow students that accompanied me all along the way.

This work was supported by FEDER and Xunta de Galicia (Spain) under grants GRC2013–014, R2016/051 and ED431C 2017/60, by FEDER and Ministerio de Economía y Competitividad (Spain) under the research projects 2013–CE330 and ENE2013–47867–C2–1–R, by Ministerio de Economía, Industria y Competitividad (Spain) under grant MTM2017–86459–R, by Robert Bosch GmbH under contracts ITMATI–C31–2015 and ITMATI–C45–2017 and by Ministerio de Educación, Cultura y Deporte (Spain) under grant FPU13/03409.

USC
UNIVERSIDADE
DE SANTIAGO
DE COMPOSTELA

Appendices

USC
UNIVERSIDADE
DE SANTIAGO
DE COMPOSTELA

Appendix A

In this appendix we detail the computation of the Jacobian matrix of $\vec{f}$ appearing in (5.40). Let us denote by $\mathcal{C}$ the matrix

$$\mathcal{C} := \left[\frac{1}{a}(\mathcal{A}^b)^{\mathrm{T}} \begin{pmatrix} \vec{0} \\ \vec{e} \end{pmatrix} \otimes \left(\left(\mathcal{R}^b + (\mathcal{A}^b)^{\mathrm{T}}\, \mathcal{B}^{-1}\, \mathcal{A}^b\right)^{-\mathrm{T}} (\mathcal{A}^b)^{\mathrm{T}} \begin{pmatrix} \vec{0} \\ \vec{e} \end{pmatrix} \right) - \mathcal{I} \right] \mathcal{R}^b$$

and by $D_{\vec{y}}\vec{\mathcal{F}}(0,\vec{x})$ the Jacobian matrix of mapping $\vec{\mathcal{F}}$ with respect to $\vec{y}$ at point $(0,\vec{x})$. By using (5.35) we get

$$\frac{\partial \vec{f}}{\partial Y}(Y,\beta_1) = T_b\, \mathcal{C}\, D_{\vec{y}}\vec{\mathcal{F}}(0, Y\vec{u})\vec{u} - \frac{T_b^2}{2\pi}\left(\mathcal{R}^b + (\mathcal{A}^b)^{\mathrm{T}}\mathcal{B}^{-1}\mathcal{A}^b\right)\vec{w},$$

$$\frac{\partial \vec{f}}{\partial \beta_1}(Y,\beta_1) = -T_b\, Y\, \mathcal{C}\, D_{\vec{y}}\vec{\mathcal{F}}(0, Y\vec{u})\vec{w} - Y\frac{T_b^2}{2\pi}\left(\mathcal{R}^b + (\mathcal{A}^b)^{\mathrm{T}}\mathcal{B}^{-1}\mathcal{A}^b\right)\vec{u}.$$

The computation of $D_{\vec{y}}\vec{\mathcal{F}}(0,\vec{x})$ is detailed in the sequel, and it requires to solve N_b magnetostatic linear problems.

Let us introduce the nonlinear operator $\Psi : \mathbb{R}^{N_b} \longrightarrow \mathrm{H}_0^1(\Omega)$ and the linear operator $\vec{\mathcal{L}} : \mathrm{H}_0^1(\Omega) \longrightarrow \mathbb{R}^{N_b}$, defined by,

$$\Psi(\vec{w}) := A(0),$$
$$\left(\vec{\mathcal{L}}(A)\right)_n := \int_{\Omega_n} \sigma A, \quad n = 1, \ldots, N_b,$$

where $A(0)$ is the solution to Problem 5.2 for $t = 0$. It is clear that $\vec{\mathcal{F}}(0,\cdot)$ can be expressed as composition of mappings Ψ and $\vec{\mathcal{L}}$ defined above: $\vec{\mathcal{F}}(0,\vec{y}) = (\vec{\mathcal{L}} \circ \Psi)(\vec{y})$. As a consequence, by using the chain rule and the linearity of operator $\vec{\mathcal{L}}$, we deduce

$$D_{\vec{y}}\vec{\mathcal{F}}(0,\vec{y})\delta\vec{y} = \vec{\mathcal{L}}\left(D\Psi(\vec{y})(\delta\vec{y})\right) \quad \forall\, \delta\vec{y} \in \mathbb{R}^{N_b}, \tag{B.1}$$

where $D\Psi(\vec{y}) : \mathbb{R}^{N_b} \longrightarrow H_0^1(\Omega)$ denotes the Fréchet-differential of mapping Ψ at point $\vec{y}$. Therefore, computing $D_{\vec{y}}\vec{\mathcal{F}}(0,\vec{w})$ amounts to compute $D\Psi(\vec{y})$. In order to build this differential, we introduce a weak formulation of the magnetostatic problem defining $\vec{\mathcal{F}}(0,\vec{y})$, namely,

$$\begin{cases} \text{Given } \vec{y} \in \mathbb{R}^{N_b} \text{ and } I_n(0) \in \mathbb{R},\ n = N_b+1, \dots, N_c, \text{ find } A \in \mathrm{H}_0^1(\Omega) \text{ such that} \\ \displaystyle\int_\Omega \nu(\cdot, |\mathbf{grad}\, A|)\mathbf{grad}\, A \cdot \mathbf{grad}\, W \\ \qquad = \displaystyle\sum_{n=1}^{N_b} \int_{\Omega_n} \frac{y_n}{\mathrm{meas}(\Omega_n)} W + \sum_{n=N_b+1}^{N} \int_{\Omega_n} \frac{I_n(0)}{\mathrm{meas}(\Omega_n)} W \quad \forall\, W \in \mathrm{H}_0^1(\Omega), \end{cases} \tag{B.2}$$

and operator $\mathcal{P} : \mathrm{H}_0^1(\Omega) \longrightarrow \mathrm{H}^{-1}(\Omega)$ defined by

$$\langle \mathcal{P}(A), W \rangle = \int_\Omega \nu(\cdot; |\mathbf{grad}\, A|)\, \mathbf{grad}\, A \cdot \mathbf{grad}\, W$$

for every $W \in \mathrm{H}_0^1(\Omega)$. Let us emphasize that $I_n(0)$, $n = N_b+1, \dots, N_c$, are the initial intensities along the stator coils, which are known.

Firstly, we try to compute the Gâteaux derivative of $\mathcal{P}$ with respect to A in a direction Z:

$$\begin{aligned} \langle D\mathcal{P}(A)(Z), W \rangle = \lim_{h\to 0} \frac{1}{h} \left(\langle \mathcal{P}(A+hZ), W \rangle - \langle \mathcal{P}(A), W \rangle \right) = \int_{\Omega \setminus \Omega_{\mathrm{nl}}} \nu_0\, \mathbf{grad}\, Z \cdot \mathbf{grad}\, W \\ + \int_{\Omega_{\mathrm{nl}}} \Big(\lim_{h\to 0} \frac{1}{h} \left(\widetilde{\nu}(|\mathbf{grad}\, A + h\mathbf{grad}\, Z|) \right) (\mathbf{grad}\, A + h\mathbf{grad}\, Z) \\ - \widetilde{\nu}(|\mathbf{grad}\, A|)\, \mathbf{grad}\, A) \Big) \cdot \mathbf{grad}\, W. \end{aligned}$$

We notice that, even though the norm application is not differentiable at the null vector, the application $\vec{p} \in \mathbb{R}^2 \mapsto \widetilde{\nu}(|\vec{p}\,|)\, \vec{p} \in \mathbb{R}^2$ is in $\mathcal{C}^1(\mathbb{R}^2)$. Indeed, if $\vec{p} \neq \vec{0}$

$$\lim_{h\to 0} \frac{1}{h} \left(\widetilde{\nu}(|\vec{p} + h\vec{q}\,|) \right) (\vec{p} + h\vec{q}\,) - \widetilde{\nu}(|\vec{p}\,|)\, \vec{p}\,) = \widetilde{\nu}(|\vec{p}\,|)\vec{q} + \frac{\widetilde{\nu}\,'(|\vec{p}\,|)}{|\vec{p}\,|} (\vec{p} \cdot \vec{q}\,)\vec{p}.$$

Moreover, if $\vec{p} = \vec{0}$,

$$\lim_{h\to 0} \frac{1}{h} \left(\widetilde{\nu}(|h\vec{q}\,|) \right) (h\vec{q}\,) - \widetilde{\nu}(0)\, \mathbf{0}) = \widetilde{\nu}(0)\vec{q}.$$

Therefore, if we denote

$$D_0 := \{ \boldsymbol{x} \in \Omega_{\mathrm{nl}} \,:\, |\mathbf{grad}\, A(\boldsymbol{x})| = 0 \},$$

we have

$$\begin{aligned} \langle D\mathcal{P}(A)(Z), W \rangle = \int_\Omega \nu(\cdot, |\mathbf{grad}\, A|)\, \mathbf{grad}\, Z \cdot \mathbf{grad}\, W \\ + \int_{\Omega_{\mathrm{nl}} \setminus D_0} \frac{\widetilde{\nu}\,'(|\mathbf{grad}\, A|)}{|\mathbf{grad}\, A|} (\mathbf{grad}\, A \cdot \mathbf{grad}\, Z)(\mathbf{grad}\, A \cdot \mathbf{grad}\, W). \end{aligned} \tag{B.3}$$

By applying the implicit function theorem, we can deduce that for any $\delta\vec{y} \in \mathbb{R}^{N_b}$, the field $\delta A := D\Psi(\vec{y})(\delta\vec{y})$ is the solution to the following linear magnetostatic problem:

$$\begin{cases} \text{Given } \delta\vec{y} \in \mathbb{R}^{N_b}, \text{ find } \delta A \in \mathrm{H}^1_0(\Omega) \text{ such that} \\ \\ \langle D\mathcal{P}(A)(\delta A), W\rangle = \displaystyle\sum_{n=1}^{N_b} \int_{\Omega_n} \frac{\delta y_n}{\mathrm{meas}(\Omega_n)} W \quad \forall\, W \in \mathrm{H}^1_0(\Omega), \\ \\ \text{with } A \text{ the solution to (B.2).} \end{cases} \tag{B.4}$$

Therefore, by using (B.1),

$$D_{\vec{y}}\vec{\mathcal{F}}(0,\vec{y})\delta\vec{y} = \left(\int_{\Omega_1} \sigma\, \delta A, \ldots, \int_{\Omega_{N_b}} \sigma\, \delta A\right)^{\mathrm{T}},$$

δA being the solution to (B.4). Then, in order to obtain the order $N_b \times N_b$ matrix $D_{\vec{y}}\vec{\mathcal{F}}(0,\vec{y})$, it is enough to solve (B.4) for $\delta\vec{y} = \vec{e}_j$, $j = 1, \ldots, N_b$, where $\vec{e}_j$ is the j-th vector of the canonical basis in $\mathbb{R}^{N_b}$. Indeed, for this choice, vector $\vec{\mathcal{L}}(\delta A_j)$ is just the j-th column of the Jacobian matrix $D_{\vec{y}}\vec{\mathcal{F}}(0,\vec{y})$.

Remark 5.13. *According to the previous calculations, obtaining the partial derivatives of function at the n-th iteration of the minimization algorithm amounts to solve N_b linear magnetostatics problems with the same matrix. It is worth mentioning that the coefficient matrix of the finite element approximation of problem (B.4) does not depend on index j, so it can be computed and factorized only once per iteration. Summarizing, per search step of the minimization algorithm we need to solve one nonlinear magnetostatic problem, and then N_b linear magnetostatic problems, with unit currents in one of the rotor bars.*

USC
UNIVERSIDADE
DE SANTIAGO
DE COMPOSTELA

Resumo

O obxectivo central da tese doutoral é o estudo e resolución numérica de problemas que xorden no ámbito do electromagnetismo a baixa frecuencia e a súa aplicación á simulación de procesos industriais. Máis concretamente, abórdanse tanto modelos de correntes inducidas (tamén chamados modelos de *eddy currents*) como de magnetostática. Esta liña de investigación está motivada pola necesidade de coñecer, mediante o uso de modelos matemáticos e simulación por computador, os fenómenos que teñen lugar en distintos procesos industriais, como poden ser a magnetización e desmagnetización de pezas forxadas, o quecemento de pezas por indución ou a utilización de distintos tipos de máquinas eléctricas, para proceder posteriormente á súa optimización e control automático.

A tese estrutúrase en dúas partes. Na primeira delas estúdanse dous problemas de correntes inducidas, un deles linear e proposto no dominio da frecuencia, e outro fortemente non linear, no que ademais se inclúe o fenómeno da histérese magnética. O primeiro destes problemas estúdase dende o punto de vista da análise matemática e numérica, mentres que o segundo analízase dende a perspectiva do desenvolvemento dunha ferramenta numérica para a simulación de procesos de magnetización e desmagnetización de pezas ferromagnéticas. Doutra banda, na segunda parte da tese realízanse diversas contribucións ao modelado de máquinas eléctricas, estudando problemas magnéticos en réxime transitorio dende diferentes perspectivas. En particular, en primeiro lugar preséntase un modelo bidimensional, escrito en termos do vector potencial magnético, acoplado con ecuacións de circuítos que permiten considerar fontes eléctricas nos condutores dadas tanto en termos de correntes como de caídas de potencial. A continuación, partindo desta formulación, procédese a considerar tres problemas de diferente índole: dous eminentemente teóricos e outro máis centrado na utilidade práctica. Deste xeito, os dous primeiros capítulos desta parte tratan sobre a análise matemática e numérica da formulación previamente introducida con fontes voltaxe e dun problema de control óptimo no que o sistema de estado está fortemente relacionado con esta formulación. Finalmente, no último capítulo amplíase o modelo para ter en conta o caso en que unha parte do dominio está en movemento, xunto con ecuacións de circuítos máis xerais, para así desenvolver unha nova metodoloxía que permite acelerar o cálculo do estado estacionario na simulación electromagnética de motores de indución.

Parte I. Análise de problemas de correntes inducidas

O modelo de correntes inducidas ou *eddy currents* obtense a partir do sistema de ecuacións de Maxwell ao desprezar o termo de correntes de desprazamento na lei de Ampère. Este modelo aparece con frecuencia na simulación numérica de procesos industriais, co que foi obxecto de

numerosos estudos dende o punto de vista matemático e numérico nas últimas décadas, especialmente no caso linear. Así mesmo, houbo tamén avances relevantes no estudo dos modelos transitorios non lineares, algúns deles incorporando ademais o fenómeno da histérese magnética.

Os materiais magneticamente lineares caracterízanse porque a densidade de fluxo magnético e a intensidade de campo magnético son colineares en todo punto, co que os problemas con fontes sinusoidais pódense estudar en réxime harmónico. En efecto, nestas condicións as ecuacións de Maxwell preservan a dependencia temporal dos campos, e polo tanto todos eles serán funcións do tempo de tipo sinusoidal. A pesar da súa aparente sinxeleza, o modelo harmónico de *eddy currents* en dominios tridimensionaies limitados deu lugar a numerosas formulacións. Un caso particular, que atraeu a atención da comunidade científica nos últimos anos, é aquel no que os condutores non están estritamente contidos no dominio computacional. Este modelo proporciona a posibilidade de acoplar o modelo distribuído de correntes inducidas cun de parámetros concentrados que permita considerar o circuíto eléctrico asociado á fonte de corrente, aproximándose así máis fielmente á configuración industrial.

Así pois, dentro do estudo de problemas de correntes inducidas, no Capítulo 1 empézase co estudo da formulación $\boldsymbol{T}$,ϕ–ϕ dende o punto de vista da análise matemática e numérica. Esta formulación está caracterizada por descompoñer a intensidade de campo magnético como suma dun potencial vectorial $\boldsymbol{T}$, definido soamente en condutores, o gradiente dun potencial escalar ϕ, definido en todo o dominio, e o chamado potencial vectorial impreso $\boldsymbol{T}_0$, definido en todo o dominio e directamente relacionado coas fontes do problema. En particular, cinguímonos ao caso harmónico con fontes dadas en termos da corrente ou a caída de potencial a través de superficies situadas na fronteira do dominio tridimensional limitado. Ademais, estudamos dúas versións desta formulación, nas que impoñeremos ou non unha restrición adicional (ou *condición gauge*) sobre o vector potencial eléctrico $\boldsymbol{T}$ para garantir a súa unicidade. Deste xeito, a versión sen *gauge* non proporciona unicidade de solución, aínda que o campo magnético construído a partir dos potenciais $\boldsymbol{T}$ e ϕ é único. Ademais, en ambos os casos realízase unha discretización espacial mediante o método de elementos finitos, con elementos finitos de Nédélec de primeira orde para $\boldsymbol{T}$ e elementos finitos de Lagrange, tamén de primeira orde, para o potencial ϕ. Para desenvolver o estudo de existencia e unicidade de solución destes problemas, tanto a nivel continuo como discreto, próbase a equivalencia, en termos do campo magnético, entre as formulacións presentadas e outra formulación presente na literatura, cuxas boas propiedades son coñecidas. Finalmente, mostramos tres exemplos numéricos, un deles con solución analítica coñecida, a cal nos permite ilustrar a orde de erro obtido na análise teórica. Os resultados obtidos proporcionan soporte teórico a esta formulación, comunmente implementada nos paquetes de software comercial máis populares.

Os resultados da versión sen *gauge* da formulación $\boldsymbol{T}$,ϕ–ϕ foron publicados en:

[26] A. Bermúdez, M. Piñeiro, R. Rodríguez, and P. Salgado. Analysis of an ungauged T, ϕ–ϕ formulation of the eddy current problem with currents and voltage excitations. *ESAIM: Math. Model. Numer. Anal.*, 51(6):2487–2509, 2017.

Por outra banda, a presenza de fontes non harmónicas ou materiais magneticamente non lineares require o uso de modelos de *eddy currents* xenuinamente transitorios. Ademais, a inclusión de efectos histeréticos resulta inevitable en certas aplicacións industriais, como a desmagnetización

de pezas ferromagnéticas. Este feito engade unha dificultade adicional, debido a que nestas condicións o fluxo magnético nestes materiais non só depende da intensidade de campo magnético nun momento dado, senón tamén da historia magnética. Dentro dos métodos que modelan a histérese magnética, escollemos o de Preisach, asumindo que os procesos son independentes da taxa de cambio da intensidade de campo magnético con respecto ao tempo.

No Capítulo 2 tratamos o modelado e simulación numérica de problemas de magnetización e/ou desmagnetización. O estudo efectuado neste capítulo iniciouse durante o traballo fin de máster e foi motivado por un proxecto INTERCONNECTA desenvolvido para a empresa CIE-Galfor. No marco da tese, a atención céntrase na creación dunha ferramenta de simulación que nos permita calcular os campos magnéticos durante o proceso de inspección por partículas magnéticas (MPI polas súas siglas en inglés) para a detección de gretas en pezas ferromagnéticas. Neste contexto, desenvolveuse e implementouse un modelo de correntes inducidas unidimensional con histérese para o modelado da chamada magnetización lonxitudinal de pezas cilíndricas, e púxose en marcha un software para simular o proceso completo que se realiza durante este test non destrutivo, que consta de tres etapas: magnetización circular, lonxitudinal e posterior desmagnetización. Ademais de presentar os modelos matemáticos e detallar diversos aspectos da implementación numérica, móstranse resultados relativos ao campo magnético remanente en pezas cilíndricas baixo diferentes condicións de operación, de forma que se poida predicir en que situacións se obterá unha desmagnetización efectiva.

Os principais resultados contidos neste capítulo foron publicados en:

[20] A. Bermúdez, D. Gómez, M. Piñeiro, P. Salgado, and P. Venegas. Numerical simulation of magnetization and demagnetization processes. *IEEE Trans. Magn.*, 53(12):1–6, 2017.

Parte II. Contribucións ao modelado de máquinas eléctricas

Nas últimas décadas, en paralelo co rápido desenvolvemento das capacidades computacionais, realizáronse grandes esforzos para obter modelos numéricos realistas para numerosos procesos industriais. A resolución destes modelos proporciona información importante acerca dos fenómenos físicos involucrados nos devanditos procesos, o que leva á súa mellor comprensión e mesmo ao seu perfeccionamento. En particular, os avances máis recentes derivaron en algoritmos numericamente eficientes para modelos que caracterizan o comportamento electromagnético de máquinas eléctricas, que van máis aló dos clásicos modelos analíticos. Cabe sinalar que estes modelos analíticos están en xeral limitados a materiais lineares e homoxéneos en réxime estático debido ao enfoque mediante circuítos magnéticos. Desta forma, a simulación numérica xoga un papel importante na optimización do deseño e as condicións de operación das máquinas eléctricas, evitando a construción de prototipos innecesarios e reducindo significativamente os custos e o tempo precisos para obter novos deseños.

Na segunda parte da memoria centrámonos en máquinas de corrente alterna (AC polas súas siglas en inglés) de fluxo radial, caracterizadas porque a densidade de corrente ten unha dependencia de tipo sinusoidal con respecto ao tempo e é espacialmente paralela á dirección do eixo de rotación da máquina. Este tipo de máquinas poden ser clasificadas de moi diversas formas, sendo unha das máis comúns a consideración de dúas categorías: síncronas e de indución. O primeiro grupo

está formado por aquelas máquinas cuxa velocidade de rotación está relacionada coa frecuencia angular da corrente de entrada en termos do número de polos da máquina. En cambio, nos motores de indución o campo magnético no rotor é inducido polo do estátor (ou viceversa), que contén as bobinas a través das cales circula a corrente fornecida a través da rede eléctrica. Neste tipo de máquinas a velocidade de rotación é menor que a velocidade síncrona, e chamamos *slip* á cantidade que define a diferenza entre as devanditas velocidades.

Na Parte II, realizamos en primeiro lugar a dedución dunha formulación dun modelo magnético transitorio non linear. Grazas a que neste tipo de dispositivos a corrente no estátor discorre a través de condutores multifilares dirixidos de forma paralela ao eixo de rotación da máquina e a que os núcleos tanto do rotor como do estátor están construídos con material laminado nesta mesma dirección, é razoable asumir que os campos electromagnéticos poden ser aproximados mediante un modelo bidimensional definido nunha sección transversal do dispositivo. Por outra banda, as fontes do problema están dadas en termos das correntes ou as caídas de potencial por unidade de lonxitude nos condutores e a densidade de fluxo remanente nos imáns permanentes. Así, a formulación consiste nun modelo distribuído de magnetostática acoplado con ecuacións de circuítos que vinculan os datos dados en termos de caídas de potencial coas correspondentes correntes que discorren a través dos condutores. Esta formulación constitúe a base para os modelos presentados nos tres capítulos restantes, coas modificacións e/ou restricións pertinentes en cada caso.

Deste xeito, no Capítulo 3 estúdase, dende o punto de vista da análise matemática e numérica, a formulación magnética transitoria, no caso en que as fontes nos condutores son dadas soamente en termos da caída de potencial por unidade de lonxitude. Para iso, a través das ecuacións de circuítos, expresamos o problema como un sistema implícito de ecuacións diferenciais ordinarias, cuxo operador involucra a resolución dun modelo distribuído de magnetostática. O modelo discretízase espacialmente usando un método de elementos finitos, xunto cun esquema de tipo Euler implícito para a discretización temporal. Unha vez máis, realízase unha análise matemática deste problema, tanto a nivel continuo como discreto, obtendo unha estimación de erro para as correntes nos condutores que se ilustra con diversos resultados numéricos.

Os resultados que aparecen neste capítulo foron enviados para a súa publicación

[27] A. Bermúdez, M. Piñeiro, and P. Salgado. Mathematical and Numerical Analysis of a Transient Magnetic Model with Voltage Drop Excitations. (Submitted).

A optimización e o control óptimo de procesos industriais que involucran fenómenos electromagnéticos foron estudados en numerosas publicacións durante os últimos anos e, en particular, para o deseño de máquinas eléctricas. En efecto, este campo de estudo ofrece grandes oportunidades en canto ao deseño de procesos industriais, debido a que conduce automaticamente á mellor opción en termos dos obxectivos escollidos e baixo as restricións dadas. Como consecuencia, desenvolvéronse estudos de optimización para unha ampla gama de aplicacións que involucran máquinas eléctricas, con obxectivos tales como a optimización de custos, a minimización de perdas, o control de variables de circuíto para unha mellora do rendemento, o control óptimo da velocidade, etc.

Neste contexto, no Capítulo 4 estúdase un problema de control óptimo dun motor síncrono de

fluxo radial de imáns permanentes, onde o funcional custo a minimizar é a potencia disipada por efecto Joule nas bobinas do estátor. Ademais, impóñense dous tipos de restricións: restricións de cota sobre as amplitudes das compoñentes do vector de correntes nas bobinas e unha restrición de desigualdade para garantir que a máquina obtida xere un par superior a un determinado valor. Debido ao alto custo computacional que supón a realización de simulacións de máquinas con materiais non lineares, aproxímase a lei constitutiva magnética dos núcleos do motor mediante unha relación linear. Por tanto, partimos do modelo presentado ao comezo desta parte da tese, no caso linear e con fonte nos condutores dada en termos da corrente que os atravesa. Suponse ademais que a dependencia das correntes con respecto ao tempo é harmónica cun período común a todas elas, o que permite expresar a potencia disipada como función cuadrática das amplitudes das devanditas correntes. Por outra banda, utilizando o tensor de Maxwell para calcular o momento de forza sobre o rotor, pódese comprobar que baixo as hipóteses anteriormente mencionadas a media temporal do momento nun período da corrente ten unha única compoñente non nula, que se pode calcular realizando unha integral dos campos electromagnéticos sobre calquera fronteira artificial situada no entreferro da máquina.

En resumo, a nivel continuo atopámonos cun problema de control óptimo cun control nun espazo vectorial finito-dimensional (con dimensión igual ao número de bobinas do estátor), con funcional custo cuadrático e conxunto de controis admisibles definido a partir dunha restrición non linear sobre o estado e restricións de cota sobre o control. Os principais resultados obtidos para este problema son a existencia tanto de controis óptimos como de multiplicadores de Lagrange asociados á restrición sobre o estado, tanto a nivel continuo como discreto, así como a converxencia sen orde dos controis discretos. Para a discretización espacial óptase por un método de elementos finitos e para a resolución do problema de optimización asociado ao problema de control utilízase a técnica do Lagranxiano aumentado.

Este estudo foi desenvolvido en colaboración co profesor Fredi Tröltzsch ao longo de dúas estadías de investigación realizadas na Technische Universität Berlin.

Doutra banda, no caso das máquinas de indución, cinguímonos ao caso en que estas teñen un rotor de tipo gaiola de esquío. Neste tipo de motores, o rotor contén unha serie de barras condutoras inseridas no laminado, conectadas entre si nos extremos do motor mediante os chamados aneis e a fonte de corrente é coñecida no bobinado do estátor. Nas barras condutoras xéranse correntes inducidas, polo que para modelar o dispositivo é necesario ter en conta o devandito fenómeno, ao contrario que no caso dos motores síncronos. Isto realízase considerando un circuíto máis complicado que teña en conta a gaiola de esquío, de forma que as ecuacións en derivadas parciais poidan seguir considerándose nunha sección transversal do motor. Deste xeito, a simulación numérica involucra a resolución dun sistema non linear de ecuacións en derivadas parciais acopladas con ecuacións de circuítos. Esta resolución require xeralmente impoñer certas condicións iniciais que, se non son escollidas de forma adecuada, obrigan a integrar o sistema en tempo durante moitas revolucións ata alcanzar o estado estacionario.

Así, no Capítulo 5 preséntase un método numérico para acelerar o cálculo do estado estacionario en máquinas de indución con rotor de tipo gaiola de esquío. Fundamentalmente, o procedemento consiste en calcular boas aproximacións da corrente inicial nas barras da gaiola de esquío que nos permitan alcanzar o estado estacionario nunha simulación transitoria de correntes inducidas

do motor nunha cantidade reducida de ciclos. Para iso, pártese do modelo de magnetostática transitorio presentado ao comezo da segunda parte da tese, con fontes dadas exclusivamente en termos de correntes nos condutores. A este modelo engádeselle o movemento do rotor, xunto con ecuacións de circuítos máis xerais que nos permiten modelar a gaiola de esquío. A partir de devandito modelo realízanse unha serie de manipulacións e aproximacións que nos permiten obter un problema sobredeterminado que, ao resolverse no sentido de mínimos cadrados, proporciona unha aproximación das correntes iniciais buscadas. Ao aplicar o método para un motor de indución particular e baixo distintas condicións de operación, vemos que a redución no tempo necesario para chegar ao estado estacionario redúcese ata nun 96% en comparación co caso no que se impoñen correntes iniciais nulas.

Os resultados deste capítulo foron enviados para a súa publicación

[18] A. Bermúdez, D. Gómez, M. Piñeiro, and P. Salgado. Numerical Method for Accelerating the Steady State in an Induction Machine. (Submitted).

Ademais, realizouse unha solicitude para a obtención dunha patente sobre o método

[19] A. Bermúdez, D. Gómez, M. Piñeiro, and P. Salgado. Procedimiento y producto de programa informático para acelerar el cálculo del estado estacionario de un motor de inducción de jaula de ardilla, Spanish Patent (request number P201830228).

USC
UNIVERSIDADE
DE SANTIAGO
DE COMPOSTELA

USC
UNIVERSIDADE
DE SANTIAGO
DE COMPOSTELA

Bibliography

[1] A. Abdulle and M. E. Huber. Error estimates for finite element approximations of nonlinear monotone elliptic problems with application to numerical homogenization. *Numer. Meth. Part. D. E.*, 32(3):955–969, 2016.

[2] R. Acevedo. *Métodos de elementos finitos para problemas de corrientes inducidas*. PhD thesis, Universidad de Concepción, 2008.

[3] R. A. Adams. *Sobolev Spaces*. Academic Press, New York, 1975.

[4] A. Alonso Rodríguez. Formulation via vector potentials of eddy-current problems with voltage or current excitation. *Communications in Applied and Industrial Mathematics*, 1(2), 2011.

[5] A. Alonso Rodríguez, E. Bertolazzi, R. Ghiloni, and A. Valli. Construction of a finite element basis of the first de rham cohomology group and numerical solution of 3D magnetostatic problems. *SIAM J. Numer. Anal.*, 51(4):2380–2402, 2013.

[6] A. Alonso Rodríguez, E. Bertolazzi, R. Ghiloni, and A. Valli. Finite element simulation of eddy current problems using magnetic scalar potentials. *J. Comput. Phys.*, 294(1):503–523, 2015.

[7] A. Alonso Rodríguez and A. Valli. *Eddy Current Approximation of Maxwell Equations: Theory, Algorithms and Applications*. Springer, 2010.

[8] H. Ammari, A. Buffa, and J.-C. Nédélec. A justification of eddy currents model for the maxwell equations. *SIAM J. Appl. Math.*, 60(5):1805–1823, 2000.

[9] C. Amrouche, C. Bernardi, M. Dauge, and V. Girault. Vector potentials in three-dimensional non-smooth domains. *Math. Method. Appl. Sci.*, 21(9):823–864, 1998.

[10] Z. Arai. A rigorous numerical algorithm for computing the linking number of links. *Nonlinear Theory and its Applications, IEICE*, 4(1):104–110, 2013.

[11] M. Augustyniak and Z. Usarek. Finite element method applied in electromagnetic NDTE: A review. *J. Nondestruct. Eval.*, 35(39):1–15, 2016.

[12] F. Bagagiolo. Ordinary differential equations. `www.science.unitn.it/~bagagiol/noteODE.pdf`. Accessed: 2018-03-18.

[13] S. Baumanns. *Coupled Electromagnetic Field/Circuit Simulation: Modeling and Numerical Analysis*. PhD thesis, Mathematisch-Naturwissenschaftlichen Fakultät, Universität zu Köln, Germany, 2012.

[14] P. Beckley. *Electrical Steels for Rotating Machines*. Institution of Electrical Engineers, London, UK, 2002.

[15] G. Benderskaya. *Numerical Methods for Transient Field-Circuit Coupled Simulations Based on the Finite Integration Technique and a Mixed Circuit Formulation*. PhD thesis, Fachbereich Elektrotechnik und Informationstechnik, Technische Universität Darmstadt, Germany, 2007.

[16] A. Bermúdez, O. Domínguez, D. Gómez, and P. Salgado. Finite element approximation of nonlinear transient magnetic problems involving periodic potential drop excitations. *Comput. Math. Appl.*, 65:1200–1219, 2013.

[17] A. Bermúdez, L. Dupré, D. Gómez, and P. Venegas. Electromagnetic computations with preisach hysteresis model. *Finite Elem. Anal. Des.*, 126:65–74, 2017.

[18] A. Bermúdez, D. Gómez, M. Piñeiro, and P. Salgado. Numerical method for accelerating the steady state in an induction machine. (Submitted).

[19] A. Bermúdez, D. Gómez, M. Piñeiro, and P. Salgado. Procedimiento y producto de programa informático para acelerar el cálculo del estado estacionario de un motor de inducción de jaula de ardilla, Spanish Patent (request number P201830228).

[20] A. Bermúdez, D. Gómez, M. Piñeiro, P. Salgado, and P. Venegas. Numerical simulation of magnetization and demagnetization processes. *IEEE Trans. Magn.*, 53(12):1–6, 2017.

[21] A. Bermúdez, D. Gómez, and P. Salgado. *Mathematical Models and Numerical Simulation in Electromagnetism*. New York: Springer, 2014.

[22] A. Bermúdez, B. López-Rodríguez, R. Rodríguez, and P. Salgado. Numerical solution of eddy current problems in bounded domains using realistic boundary conditions. *Comput. Methods Appl. Mech. Eng.*, 194(2):411–426, 2005.

[23] A. Bermúdez, B. López-Rodríguez, R. Rodríguez, and P. Salgado. Equivalence between two finite element methods for the eddy current problem. *C. R. Acad. Sci. Paris*, 348:769–774, 2010.

[24] A. Bermúdez, B. López-Rodríguez, R. Rodríguez, and P. Salgado. Numerical solution of transient eddy current problems with input current intensities as boundary data. *IMA J. Numer. Anal.*, 32(3):1001–1029, 2012.

[25] A. Bermúdez and C. Moreno. Duality methods for solving variational inequalities. *Comput. Math. Appl.*, 7:43–58, 1981.

[26] A. Bermúdez, M. Piñeiro, R. Rodríguez, and P. Salgado. Analysis of an ungauged T,ϕ-ϕ formulation of the eddy current problem with currents and voltage excitations. *ESAIM: Math. Model. Numer. Anal.*, 51(6):2487–2509, 2017.

[27] A. Bermúdez, M. Piñeiro, and P. Salgado. Mathematical and numerical analysis of a transient magnetic model with voltage drop excitations. (Submitted).

[28] A. Bermúdez, A. Rodríguez, and I. Villar. Extended formulas to compute resultant and contact electromagnetic force and torque from maxwell stress tensors. *IEEE Trans. Magn.*, 53(4):1–9, 2017.

[29] A. Bermúdez, R. Rodríguez, and P. Salgado. A finite element method with lagrange multipliers for low-frequency harmonic maxwell equations. *SIAM J. Numer. Anal.*, 40(5):1823–1849, 2002.

[30] A. Bermúdez, R. Rodríguez, and P. Salgado. A finite element method for the magnetostatic problem in terms of scalar potentials. *SIAM J. Numer. Anal.*, 46(3):1338–1363, 2008.

[31] N. Bianchi and S. Bolognani. Design optimisation of electric motors by genetic algorithms. *IEE P. Elect. Pow. Appl.*, 145(5):475–483, 1998.

[32] O. Bíró, P. Böhm, K. Preis, and G. Wachutka. Edge finite element analysis of transient skin effect problems. *IEEE Trans. Magn.*, 36(4):835–838, 2000.

[33] O. Bíró and K. Preis. An efficient time domain method for nonlinear periodic eddy current problems. *IEEE Trans. Magn.*, 42(4):695—698, 2006.

[34] O. Bíró and K. Preis. Generating source field functions with limited support for edge finite-element eddy current analysis. *IEEE Trans. Magn.*, 43(4):1165–1168, 2007.

[35] I. Boldea and S. A. Nasar. *The Induction Machine Handbook*. CRC Press, 2002.

[36] A. Bossavit. Eddy currents in dimension 2: voltage drops. In *Int. Symp. on Theoret. Electrical Engineering (Proc. ISTET'99, W. Mathis, T. Schindler, eds)*, pages 103–107. University Otto-von-Guericke (Magdeburg, Germany), 1999.

[37] A. Bossavit. Most general "non-local" boundary conditions for the maxwell equation in a bounded region. *COMPEL*, 19(2):239–245, 2000.

[38] H. Brézis. *Functional Analysis, Sobolev Spaces and Partial Differential Equations*. Springer, 2011.

[39] A. Buffa, Y. Maday, and F. Rapetti. A sliding mesh-mortar method for a two dimensional eddy current model of electric engines. *ESAIM: Math. Model. Num. Anal.*, 35(2):191–228, 2001.

[40] F. C. Campbell. *Inspection of Metals: Understanding the Basics*. ASM International, 2013.

[41] T. Chen, T. Kang, G. Lu, and L. Wu. $\boldsymbol{t} - \psi - \psi_e$ decoupled scheme for a time-dependent multiply-connected eddy current problem. *Math. Meth. Appl. Sci.*, 37:343—359, 2014.

[42] P. G. Ciarlet. *The Finite Element Method for Elliptic Problems*. North-Holland, Amsterdam, 1978.

[43] N. Deo. *Graph Theory with Applications to Engineering and Computer Science*. Prentice Hall, 1974.

[44] P. Deuflhard, M. Seebass, D. Stalling, R. Beck, and H.-C. Hege. Hyperthermia treatment planning in clinical cancer therapy: Modelling, simulation, and visualization. In A. Sydow, editor, *Computational Physics, Chemistry and Biology*, pages 9–17. Wissenschaft und Technik Verlag, 1997.

[45] N. Digă, C. Ghită, D. Popescu, S.-M. Digă, and M. Brojboiu. Use of finite element method software packages for functional-constructive optimization of a permanent magnet synchronous motor with low speed. In *2014 International Conference on Applied and Theoretical Electricity (ICATE)*, 2014.

[46] Y. Duan and D. M. Ionel. A review of recent developments in electrical machine design optimization models with a permanent-magnet synchronous motor benchmark study. *IEEE Trans. Ind. Appl.*, 49(3):1268–1275, 2013.

[47] P. Fernandes and G. Gilardi. Magnetostatic and electrostatic problems in inhomogeneous anisotropic media with irregular boundary and mixed boundary conditions. *IMA J. Appl. Math.*, 66(3):293–318, 2001.

[48] P. Fernandes and I. Perugia. Vector potential formulation for magnetostatics and modelling of permanent magnets. *Math. Models Methods Appl. Sci.*, 7(7):957–991, 1997.

[49] Y. Fijishima, S. Wakao, A. Yamashita, T. Katsuta, K. Matsuoka, and M. Kondo. Design optimization of a permanent magnet synchronous motor by the response surface methodology. *J. Appl. Phys.*, 91(10):8305–8307, 2002.

[50] P. Gangl. *Sensitivity-Based Topology and Shape Optimization with Applications to Electrical Machines*. PhD thesis, Johannes Kepler Universität Linz, Austria, 2016.

[51] C. Geiger and C. Kanzow. *Theorie und Numerik restringierter Optimierungsaufgaben*. Springer-Verlag, Berlin Heidelberg, 2002.

[52] V. Girault and P. A. Raviart. *Finite Element Methods for Navier-Stokes Equations*. Springer, Berlin, 1986.

[53] D. J. Griffiths. *Introduction to Electrodynamics*. Pearson, 2013.

[54] P. Grisvard. *Elliptic Problems in Nonsmooth Domains*. Pitman, Boston, 1985.

[55] D. C. Hanselman. *Brushless Permanent Magnet Motor Design*. Magna Physics Publishing, 1994.

[56] J. D. Hanson and S. P. Hirshman. Compact expressions for the biot-savart fields of a filamentary segment. *Phys. Plasmas*, 9(10):4410–4412, 2002.

[57] T. Hara, T. Naito, and J. Umoto. Time-periodic finite element method for nonlinear diffusion equations. *IEEE Trans. Magn.*, 21(6):2261–2264, 1985.

[58] D. W. Hart. *Power Electronics*. McGraw-Hill, 2011.

[59] B. Heise. Analysis of a fully discrete finite element method for a nonlinear magnetic field problem. *SIAM J. Numer. Anal.*, 31(3):745–759, 1994.

[60] T. Kang, T. Chen, H. Zhang, and K. I. Kim. Improved $\boldsymbol{t}-\psi$ nodal finite element schemes for eddy current problems. *Appl. Math. Comput.*, 218:287—302, 2011.

[61] H. Katagiri, Y. Kawase, T. Yamaguchi, T. Tsuji, and Y. Shibayama. Improvement of convergence characteristics for steady-state analysis of motors with simplified singularity decomposition-explicit error correction method. *IEEE Trans. Magn.*, 47(6):1786–1789, 2011.

[62] R. B. Kellogg. Singularities in interface problems. In *Numerical Solution of Partial Differential Equations–II*, pages 351–400. Academic Press, New York and London, 1972.

[63] R. Krishnan. *Permanent magnet synchronous and brushless DC motor drives*. CRC press, 2017.

[64] S. Kurz, J. Petzer, G. Lehenr, and W. Rucker. A novel formulation for 3D eddy current problems with moving bodies using a lagrangian description and bem-fem coupling. *IEEE Trans. Magn.*, 34:3068–3073, 1998.

[65] J. Y. Lee. *Development of Modeling and Simulation for Magnetic Particle Inspection using Finite Elements*. Master thesis, Dept. Elect. Comput. Eng., Iowa State University, 2003.

[66] J. Y. Lee, S. J. Lee, D. C. Jiles, M. Garton, R. López, and L. Brasche. Sensitivity analysis of simulations for magnetic particle inspection using the finite-element method. *IEEE Trans. Magn.*, 36(9):3604–3606, 2003.

[67] G. Lei, J. Zhu, Y. Guo, C. Liu, and B. Ma. A review of design optimization methods for electrical machies. *Energies*, 10(12):1962–1992, 2017.

[68] F. Liorzou, B. Phelps, and D. L. Atherton. Macroscopic models of magnetization. *IEEE Trans. Magn.*, 36(2):418–428, 2000.

[69] B. López-Rodríguez. *Solución numérica del problema de conformado electromagnético*. PhD thesis, Universidad de Concepción, Chile, 2012.

[70] D. A. Lovejoy. *Magnetic Particle Inspection: A Practical Guide*. London: Chapman & Hall, 1993.

[71] C. Ma. The finite element analysis of a decoupled $\boldsymbol{t}-\psi$ scheme for solving eddy-current problems. *Appl. Math. Comput.*, 205:352—361, 2008.

[72] M. Matthes. *Numerical Analysis of Nonlinear Partial Differential-Algebraic Equations: A Coupled and an Abstract Systems Approach*. PhD thesis, Mathematisch-Naturwissenschaftlichen Fakultät, Universität zu Köln, Germany, 2012.

[73] I. D. Mayergoyz. *Mathematical Models of Hysteresis*. New York: Springer-Verlag, 1991.

[74] G. Meunier, Y. L. Floch, and C. Guérin. A nonlinear circuit coupled $\boldsymbol{t}-\boldsymbol{t}_0-\phi$ formulation for solid conductors. *IEEE Trans. Magn.*, 39:1729—1732, 2003.

[75] K. Miyata. Fast analysis method of time-periodic nonlinear fields. *J. Math-for-Ind.*, 3:131–140, 2011.

[76] N. Moehle and S. Boyd. Optimal current waveforms for brushless permanent magnet motors. *Int. J. Control*, 88(7):1389–1399, 2015.

[77] P. Monk. *Finite element methods for Maxwell's equations*. Oxford University Press, 2003.

[78] J. J. Moré and D. J. Thuente. Line search algorithms with guaranteed sufficient decrease. *ACM Trans. Math. Softw.*, 20:286–307, 1994.

[79] T. Nakata, N. Takahashi, K. Fujiwara, K. Muramatsu, H. Ohashi, and H. L. Zhu. Practical analysis of 3-D dynamic nonlinear magnetic field using time-periodic finite element method. *IEEE Trans. Magn.*, 31(3):1416–1419, 1995.

[80] S. Nicaise and F. Tröltzsch. A coupled maxwell integrodifferential model for magnetization processes. *Math. Nachr.*, 287(4):432–452, 2013.

[81] J. Nocedal and S. J. Wright. *Numerical Optimization*. Springer-Verlag, Berlin New York, 2006.

[82] C. Pechstein. *Multigrid-Newton-Methods for Nonlinear Magnetostatic Problems*. PhD thesis, Johannes Kepler Universität Linz, Austria, 2004.

[83] M. J. Powell. A fast algorithm for nonlinearly constrained optimization calculations. In *Numerical Analysis*, pages 144–157. Springer, 1978.

[84] F. Preisach. Über die magnetische Nachwirkung. *Z. Phys.*, 94:277–302, 1935.

[85] A. Quarteroni and A. Valli. *Numerical Approximation of Partial Differential Equations*. Springer Verlag, 1994.

[86] M. Rachek and T. Merzouki. Finite element method applied to the modelling and analysis of induction motors. In D. P. Miidla, editor, *Numerical Modelling*. InTech, 2012.

[87] R. B. Randall. *Frequency Analysis*. Brüel & Kjaer, 1987.

[88] P. A. Raviart and J. M. Thomas. *Introduction à l'Analyse Numérique des Équations aux Dérivées Partielles*. Masson, 1992.

[89] R. T. Rockafellar and R. J. Wets. *Variational Analysis*. Springer, 1997.

[90] A. L. Rodríguez. *Development of a multidisciplinary and optimized design methodology for surface permanent magnet synchronous machines*. PhD thesis, Universidade de Santiago de Compostela, 2016.

[91] D. Rolfsen. *Knots and Links*, volume 346. American Mathematical Soc., 1976.

[92] M. Rosu, P. Zhou, D. Lin, D. Ionel, M. Popescu, F. Blaabjerg, V. Rallabandi, and D. Staton. *Multiphysics simulation by design for electrical machines, power electronics and drives*. John Wiley & Sons, 2017.

[93] V. N. Savov, Z. D. Georgiev, and E. S. Bogdanov. Analysis of cage induction motor by means of the finite element method and coupled of field, circuit and motion equations. *Electrical Engineering*, 80(1):21–28, 1997.

[94] E. Schmidt. Finite element analysis of electrical machines and transformers: State of the art and future trends. *COMPEL*, 30(6):1899–1913, 2011.

[95] M. Slodička and V. Vrábel'. Existence and uniqueness of a solution for a field/circuit coupled problem. *ESAIM: Math. Model. Num. Anal.*, 51(3):1045–1061, 2017.

[96] A. Stermecki, O. Bíró, K. Preis, S. Rainer, and G. Ofner. Numerical analysis of steady-state operation of three-phase induction machines by an approximate frequency domain technique. *Elektrotech. Inf. Tech.*, 128(3):81–85, 2011.

[97] J. K. Sykulski. Field simulation as an aid to machine design: the state of the art. In *12th International Power Electronics and Motion Control Conference, EPE-PEMC*, pages 1937–1942, 2006.

[98] Y. Takahashi, T. Iwashita, H. Nakashima, T. Tokumasu, M. Fujita, S. Wakao, K. Fujiwara, and Y. Ishihara. Parallel time-periodic finite-element method for steady-state analysis of rotating machines. *IEEE Trans. Magn.*, 48(2):1019–1022, 2012.

[99] Y. Takahashi, T. Tokumasu, M. Fujita, T. Iwashita, H. Nakashima, S. Wakao, and K. Fujiwara. Time-domain parallel finite-element method for fast magnetic field analysis of induction motors. *IEEE Trans. Magn.*, 49(5):2413–2416, 2013.

[100] Y. Takahashi, T. Tokumasu, M. Fujita, S. Wakao, K. Fujiwara, and Y. Ishihara. Comparison between fast steady-state analysis methods for time-periodic nonlinear magnetic field problems. *IEEE Trans. Magn.*, 48(2):235–238, 2012.

[101] Y. Takahashi, T. Tokumasu, K. Fujiwara, T. Iwashita, and H. Nakashima. Parallel TP-EEC method based on phase conversion for time-periodic nonlinear magnetic field problems. *IEEE Trans. Magn.*, 51(3):1–5, 2015.

[102] R. Touzani and J. Rappaz. *Mathematical Models for Eddy Currents and Magnetostatics with Selected Applications*. Springer, 2013.

[103] F. Tröltzsch. *Optimal Control of Partial Differential Equations - Theory, Methods and Applications*. American Mathematical Society, Providence, Rhode Island, 2010.

[104] F. Tröltzsch and A. Unger. Fast solution of optimal control problems in the selective cooling of steel. *ZAAM*, 81:447–456, 2001.

[105] G. Ugalde, G. Almandoz, J. Poza, and A. González. Computation of iron losses in permanent magnet machines by multi-domain simulations. In *13th European Conference on Power Electronics and Applications*, pages 1–10. IEEE, 2009.

[106] L. K. Urankar. Vector potential and magnetic field of current-carrying finite arc segment in analytial form, part I: filament approximation. *IEEE Trans. Magn.*, 16(5):1283–1288, 1980.

[107] P. Venegas. *Contribución al análisis matemático y numérico de algunos problemas de electromagnetismo*. PhD thesis, Universidad de Concepción, 2013.

[108] J. P. Webb and B. Forghani. The low-frequency performance of $\mathbf{h} - \phi$ and $\boldsymbol{t} - \omega$ methods using edge elements for 3d eddy current problems. *IEEE Trans. Magn.*, 29(6):2461–2463, 1993.

[109] B. M. Wilamowski and J. D. Irwin. *Power Electronics and Motor Drives: The Industrial Electronics Handbook*. CRC Press, 2011.

[110] B. S. Wong, Y. G. Low, X. Wang, J.-H. Ho, C.-S. Tan, and J. B. Ooi. 3D finite element simulation of magnetic particle inspection. In *Proceedings of the 2010 IEEE Conference on Sustainable Utilization and Development in Engineering and Technology*, pages 50–55, Nov. 2010.

[111] J. Xu. Two-grid discretization techniques for linear and nonlinear pdes. *SIAM J. Numer. Anal.*, 33(5):1759–1777, 1996.

[112] Y.-P. Yang, J.-P. Wang, S.-W. Wu, and Y.-P. Luh. Design and control of axial-flux brushless dc wheel motors for electric vehicles-part II: optimal current waveforms and performance test. *IEEE Trans. Magn.*, 40(4):1883–1891, 2004.

[113] D. Zarko, S. Stipetic, M. Martinovic, M. Kovacic, T. Jercic, and Z. Hanic. Reduction of computational efforts in finite element-based permanent magnet traction motor optimization. *IEEE Trans. Ind. Electron.*, 65(2):1799–1807, 2018.

[114] E. Zeidler. *Nonlinear Functional Analysis and its Applications II/B. Nonlinear Monotone Operators*. Springer-Verlag, New York, 1990.

[115] A. Ženíšek. The finite element method for nonlinear elliptic equations with discontinuous coefficients. *Numer. Math.*, 58(1):51–77, 1990.

[116] K. Zhou. *Computationally-Efficient Finite-Element-Based Thermal and Electromagnetic Models of Electric Machines*. PhD thesis, Electrical Engineering Systems Department, University of Michigan, 2015.

[117] Z. Zhu, K. Ng, N. Schofield, and D. Howe. Improved analytical modelling of rotor eddy current loss in brushless machines equipped with surface-mounted permanent magnets. *IEE Proceedings - Electric Power Applications*, 151(6):641–650, 2004.

USC
UNIVERSIDADE
DE SANTIAGO
DE COMPOSTELA

USC
UNIVERSIDADE
DE SANTIAGO
DE COMPOSTELA